ΠΑΝΕΠΙΣΤΗΜΙΟ
ΠΕΛΟΠΟΝΝΗΣΟΥ
UNIVERSITY *of the* PELOPONNESE

Ph.D. Thesis

Data analytics on graphs

Author:
Konstantinos Theocharidis

Supervisor:
Professor Spiros Skiadopoulos

July 31, 2022

Ανάλυση σε δεδομένα γράφων

Διδακτορική Διατριβή
του
Κωνσταντίνου Θεοχαρίδη

Διπλωματούχου Ηλεκτρολόγων Μηχανικών και Μηχανικών Υπολογιστών Πολυτεχνείου Θεσσαλίας (2012) και MSc Πολυτεχνείου Θεσσαλίας (2013)

Συμβουλευτική Επιτροπή: Σπύρος Σκιαδόπουλος Επιβλέπων καθηγητής
Παναγιώτης Καρράς
Μανώλης Τερροβίτης

Εγκρίθηκε από την επταμελή εξεταστική επιτροπή την 18/07/2022

Όνομα	Βαθμίδα	Ίδρυμα
Σπύρος Σκιαδόπουλος	Καθηγητής	Παν. Πελοποννήσου
Παναγιώτης Καρράς	Αν. Καθηγητής	Παν. Άαρχους
Μανώλης Τερροβίτης	Ερευνητής Β	ΙΠΣΥ / Ε.Κ. ΑΘΗΝΑ
Κώστας Βασιλάκης	Καθηγητής	Παν. Πελοποννήσου
Χρήστος Τρυφωνόπουλος	Αν. Καθηγητής	Παν. Πελοποννήσου
Θοδωρής Δαλαμάγκας	Ερευνητής Α	ΙΠΣΥ / Ε.Κ. ΑΘΗΝΑ
Ειρήνη Φουντουλάκη	Ερευνήτρια Β	Ίδρυμα Τεχνολογίας & Έρευνας

Ευχαριστίες

Αρχικά, θα ήθελα να ευχαριστήσω τον επιβλέποντα καθηγητή μου, Δρ. Σπύρο Σκιαδόπουλο, για την πολύτιμη βοήθεια του καθ'όλη τη διάρκεια της διδακτορικής διατριβής μου. Ιδιαίτερα, επίσης, ευχαριστώ τον Δρ. Μανώλη Τερροβίτη από το Ινστιτούτο Πληροφοριακών Συστημάτων του Ερευνητικού Κέντρου Αθηνά, τον Δρ. Παναγιώτη Καρρά από το Πανεπιστήμιο του Άαρχους, και τον Δρ. Γιάννη Λιαγούρη από το Πανεπιστήμιο της Βοστώνης, για την συνεργασία μου μαζί τους στο περιεχόμενο της διατριβής μου. Τέλος, πάνω απ'όλα ευχαριστώ θερμά την οικογένεια μου για την αδιάκοπη στήριξη.

Abstract

Nowadays, there is an increasing need for brands (stakeholders) to effectively and efficiently connect with their customers in both spatial and social domains so as to grow their revenues. In the spatial field, there are a variety of location-based services (e.g., Google Maps, Uber, Foursquare) for utilization by brands, whereas in social area, there are several social networks (e.g., Facebook, Instagram, VK) in which brands can maintain their own social network pages for advertising. In this thesis, we analyze and study fundamental spatial and social data operations on graphs that can significantly contribute to the successful connection among brands and customers.

In the spatial domain, our contribution is the development of a spatial RDF system named SRX that extends the popular RDF-3X store to provide spatial RDF data operations. RDF-3X itself does not support spatial RDF data. In particular, SRX supports three types of *spatial queries*: range selections (e.g., find entities within a given polygon), distance joins (e.g., find pairs of entities whose locations are close to each other), and k nearest neighbors (e.g., find the three closest entities from a given location). Further, SRX supports *spatial updates* (e.g., deletions, insertions, and modifications of spatial RDF triples). SRX relies its good performance on a grid-scheme that approximates the geometries of the spatial entities inside their integer IDs. We extensively evaluate the performance of SRX for both queries and updates by comparing it with the systems RDF-3X, Virtuoso, GraphDB, and Strabon on LGD and YAGO datasets. Our results show that SRX outperforms other systems for queries and updates, while it incurs just a little overhead to RDF-3X for updates.

In the social domain, we contribute by studying three novel *content-aware recommendation* problems relative to the *Influence Maximization* (IM) problem. IM seeks for the k users who can maximize the influence of a *given* post in a social network.

The first problem we study, named *Content-Aware Influence Maximization* (CAIM), is the inverse variant of IM and seeks for the k features that can form the content of a *non-given* post so as to make it popular in a social network. The diffusion of the post starts from a *given* set of initial adopters (*subscribers* of brand's social network page). We prove that CAIM does not have influence guarantees, and for that we deploy heuristic methods to solve it. Our experimental results on Gnutella and VK

datasets show that our advanced heuristic algorithm is more influential than simple heuristics and it is also much faster than a conventional greedy approach.

The second problem we study is an adaptive (online) version of CAIM, named *Adaptive Content-Aware Influence Maximization* (ACAIM), and aims to maximize the *cumulative* influence achieved in a social network over a number of rounds. In each round, the content of a post is sought (comprising k features) and the influence feedback of posts in the previous rounds is utilized for the content decision of posts in the next rounds. To solve ACAIM, we integrate *Online Learning to Rank* (OLR) techniques to our *machine learning* IM framework. To achieve that, we deploy a propagation model, a simulator that runs the model to generate realistic feedback, and three ACAIM learners. Our thorough experimental study on various VK datasets for several brands shows that ACAIM is solvable in big social networks.

Finally, the third problem we study relates with how brands can maximize their *subscription* (instead of *influence* as happens in CAIM and ACAIM) in social networks. Specifically, we propose a *content recommendation policy* to brands for *Gaining Subscribers by Messaging* (GSM). The goal of the GSM problem is to maximize the *cumulative* subscription gain in a social network over a series of rounds. In each round, GSM recommends to brands what content (consisting of k features) to publish in their social network pages and which m users to notify of that content. We develop three GSM solvers, and by conducting a rich experimental evaluation on different VK datasets, we ascertain the importance and practical value of GSM.

Περίληψη

Στις μέρες μας, υπάρχει ολοένα και μεγαλύτερη ανάγκη να συνδέονται οι εταιρείες αποτελεσματικά και αποδοτικά με τους πελάτες τους, σε χωρικό αλλά και σε κοινωνικό επίπεδο, για να αυξήσουν τα έσοδα τους. Στο χωρικό πεδίο, υπάρχουν διάφορες εφαρμογές που χρησιμοποιούν τοποθεσία (π.χ., Google Maps, Uber, Foursquare) από τις οποίες μπορούν να επωφεληθούν οι εταιρείες. Αντίστοιχα στο κοινωνικό πεδίο, υπάρχουν αρκετά κοινωνικά δίκτυα (π.χ., Facebook, Instagram, VK) στα οποία οι εταιρείες μπορούν να διατηρούν τις κοινωνικές σελίδες τους για διαφημιστικούς λόγους. Στη διατριβή αυτή, παρουσιάζουμε χρήσιμες χωρικές και κοινωνικές λειτουργίες γράφων που μπορούν να συνεισφέρουν σημαντικά στην επιτυχή σύνδεση των εταιρειών με τους πελάτες τους.

Στο χωρικό πεδίο, η συνεισφορά μας έγκειται στην ανάπτυξη ενός χωρικού RDF συστήματος, με όνομα SRX, που επεκτείνει το δημοφιλές σύστημα RDF-3X για να μπορέσει να παρέχει λειτουργίες χωρικών RDF δεδομένων. Το RDF-3X από μόνο του δεν υποστηρίζει χωρικά RDF δεδομένα. Συγκεκριμένα, το SRX υποστηρίζει τρία είδη *χωρικών ερωτημάτων*: επιλογές εμβέλειας (π.χ., βρείτε τις οντότητες εντός ενός πολυγώνου), ενώσεις με βάση την απόσταση (π.χ., βρείτε ζευγάρια οντοτήτων που έχουν κοντινές τοποθεσίες), και k κοντινότερων γειτόνων (π.χ., βρείτε τις τρεις πλησιέστερες οντότητες σε μια τοποθεσία). Επιπλέον, το SRX υποστηρίζει *χωρικές ενημερώσεις* (π.χ., διαγραφές, εισαγωγές, και τροποποιήσεις χωρικών RDF τριπλέτων). Η καλή απόδοση του SRX οφείλεται σε ένα σχήμα πλέγματος που προσεγγίζει τις γεωμετρίες των χωρικών οντοτήτων μέσα στα ακέραια αναγνωριστικά τους. Αξιολογούμε εκτενώς την απόδοση του SRX και στα ερωτήματα και στις ενημερώσεις, συγκρίνοντας το με τα συστήματα RDF-3X, Virtuoso, GraphDB, και Strabon στα σύνολα δεδομένων LGD και YAGO. Τα αποτελέσματα δείχνουν ότι το SRX υπερτερεί των άλλων συστημάτων στην ταχύτητα διαχείρισης των ερωτημάτων και των ενημερώσων, ενώ επιφέρει μόλις μια μικρή επιβάρυνση στο RDF-3X στις ενημερώσεις.

Στο κοινωνικό πεδίο, μελετούμε τρία καινοτόμα προβλήματα *σύστασης βάσει περιεχομένου* που σχετίζονται με το πρόβλημα της *Μεγιστοποίησης Επιρροής* (ΜΕ). Το πρόβλημα ΜΕ ψάχνει τους k χρήστες που μπορούν να μεγιστοποιήσουν την επιρροή μιας *δεδομένης* ανάρτησης σε ένα κοινωνικό δίκτυο.

Το πρώτο πρόβλημα που εξετάζουμε, ονομάζεται *Μεγιστοποίηση Επιρροής Βάσει*

Περιεχομένου (ΜΕΒΠ), και αποτελεί την αντίστροφη παραλλαγή του ΜΕ. Το πρόβλημα ΜΕΒΠ ψάχνει τα k χαρακτηριστικά που μπορούν να σχηματίσουν το περιεχόμενο μιας *μη-δεδομένης* ανάρτησης έτσι ώστε αυτή να μπορεί να γίνει δημοφιλής σε ένα κοινωνικό δίκτυο. Η διάδοση της ανάρτησης ξεκινάει από ένα *δεδομένο* σύνολο *συνδρομητών* της κοινωνικής σελίδας της εκάστοτε εταιρείας. Αποδεικνύουμε ότι το ΜΕΒΠ δεν έχει εγγυήσεις επιρροής, οπότε υλοποιήσαμε ευρετικές μεθόδους για να το λύσουμε. Τα πειραματικά μας αποτελέσματα στα σύνολα δεδομένων Gnutella και VK δείχνουν ότι ο ενισχυμένος ευρετικός αλγόριθμος μας σημειώνει μεγαλύτερη επιρροή από απλές ευρετικές λύσεις και είναι πολύ πιο γρήγορος από συμβατικές άπληστες προσεγγίσεις.

Το δεύτερο πρόβλημα που εξετάζουμε είναι μια προσαρμοστική σε πραγματικό χρόνο εκδοχή του ΜΕΒΠ, ονομάζεται *Προσαρμοστική Μεγιστοποίηση Επιρροής Βάσει Περιεχομένου* (ΠΜΕΒΠ), και στοχεύει να μεγιστοποιήσει την *συνολική* επιρροή σε ένα κοινωνικό δίκτυο που επιτυγχάνεται σε πολλούς γύρους. Σε κάθε γύρο, αναζητείται το περιεχόμενο μιας ανάρτησης που αποτελείται από k χαρακτηριστικά, ενώ η ανάδραση επιρροής των αναρτήσεων σε προηγούμενους γύρους αξιοποιείται στη δημιουργία περιεχομένου για τις αναρτήσεις των επόμενων γύρων. Για να λύσουμε το ΠΜΕΒΠ, ενσωματώνουμε τεχνικές *Πραγματικού Χρόνου Μάθησης Βάσει Κατάταξης* στο *μηχανικής μάθησης* πλαίσιο εργασίας μας που σχεδιάσαμε για μεγιστοποίηση επιρροής. Για να το πετύχουμε αυτό, υλοποιήσαμε ένα μοντέλο διάδοσης, έναν προσομοιωτή που τρέχει το εν λόγω μοντέλο για την παραγωγή ρεαλιστικής ανάδρασης, και τρεις αλγορίθμους μάθησης. Η εξονυχιστική πειραματική μελέτη μας σε ποικίλα σύνολα δεδομένων VK για αρκετές εταιρείες δείχνει ότι το ΠΜΕΒΠ είναι επιλύσιμο σε μεγάλα κοινωνικά δίκτυα.

Τέλος, το τρίτο πρόβλημα που εξετάζουμε σχετίζεται με το πως οι εταιρείες μπορούν να μεγιστοποιήσουν την *συνδρομή* τους (αντί για την *επιρροή* τους όπως συμβαίνει στα ΜΕΒΠ και ΠΜΕΒΠ) στα κοινωνικά δίκτυα. Συγκεκριμένα, προτείνουμε μια *πολιτική σύστασης περιεχομένου* στις εταιρείες για την *Απόκτηση Συνδρομητών μέσω Μηνυμάτων* (ΑΣΜ). Ο στόχος του προβλήματος ΑΣΜ είναι η μεγιστοποίηση της *συνολικής* απόκτησης συνδρομητών σε ένα κοινωνικό δίκτυο θεωρώντας πολλούς γύρους. Σε κάθε γύρο, το ΑΣΜ συστήνει στις εταιρείες το περιεχόμενο (αποτελούμενο από k χαρακτηριστικά) που πρέπει να δημοσιεύσουν στις κοινωνικές σελίδες τους και τους m χρήστες που πρέπει να ειδοποιήσουν για το εν λόγω περιεχόμενο. Για να λύσουμε το ΑΣΜ, υλοποιήσαμε τρεις αλγορίθμους, ενώ πραγματοποιώντας μια εκτενή πειραματική αξιολόγηση σε διάφορα σύνολα δεδομένων VK, διαπιστώνουμε την σημαντική αξία του ΑΣΜ.

Contents

List of Figures

Chapter 1

Introduction

A constant aim of *brands* (stakeholders) is to effectively and efficiently connect with their *customers* (simple users) in order to increase their revenues. Customers also want to easily and instantly consume the services/products of brands. Nowadays, with the prevalence of smartphones and social networks, such a *connection* can be really fruitful for both sides in the *spatial* and *social* fields. Specifically, in the previous years (without smartphones and social networks) the typical way for a brand to advertise itself is first to build a website. Then, the owners of brand contact the brand's website to their close friends to gain the initial subscribers to that site. Last, the owners send informative or promotional emails to subscribed users to keep them engaged. By doing that, they also hope these users to advertise the brand further to their friends, and so on. However, these days things are much more simplified for brands to become further known to the public. Namely, users now have already installed *mobile-applications* (in brief, *apps*) to theirs smartphones that can be leveraged by brands to engage the attention of users. Further, each app is also provided as a complete software program for main computers (desktops, laptops, etc.). For instance, a user now can quickly find in a *spatial* platform like Google Maps (exists also as an app) the stores of various brands that located at a specific region (coastal, central, etc.). As well, a brand can easily integrate its website to a *social* network of users such as Facebook (is also provided as an app) to boost its visibility. The *spatial* field offers the chances for the physical stores of brands to effectively be explored by users, while the *social* field significantly enhances the presence of brands on the internet. Therefore, the overall goal of this thesis is to empower brands with *spatial* and *social* graph operations to connect with their customers in a meaningful, practical, and beneficial way.

In the spatial domain, data can be modeled as graphs that consist of directed edges. The source node of an edge is a brand and the destination node of the edge contains a piece of information (non-spatial or spatial) for that brand. The edge itself contains a property that connects the nodes. Let depict by `a b c` an edge from node `a` to

node c with a property b. For example, the edge Starbucks hasCoffee "Americano" provides non-spatial information denoting that Starbucks serves a kind of coffee named "Americano". Yet, the edge Starbucks hasGeometry "POINT(19.9, 39.6)" depicts spatial information that mentions to a Starbucks store located in Corfu. The combination of non-spatial and spatial information enables a *connector* to execute useful spatial queries relative to brands having a geometry. A connector is a spatial data management system that connects brands with customers. Such a spatial system benefits both sides when it provides *efficient spatial query operations as also dynamic support of spatial updates*. As a complete example, assume that a customer uses the Uber application (connector) in her mobile to get a nearby taxi to her location and wants to book such a taxi instantly without waiting. To achieve that, Uber has utilized beforehand a kind of *range* and *nearby* spatial queries to satisfy any customer along with a variety of other data analytics, such as user preferences, traffic estimation, etc. Yet, even all such analytics are available, when a customer searches for a taxi in real time, all the respective queries should be executed as fast as possible. Since Uber provides such kind of real-time operations, Uber successfully connects customers with taxi drivers who play the role of brands in this example. Note that Uber is also a brand and as connector it benefits from both sides. Additionally, spatial *distance join* queries such as "find the pairs of hotels and restaurants in the city that are not further to each other than a given distance" are also leveraged by Uber for a variety of cases. A possible case could be the arrangement of a number of taxis to be ready to service tourists in the city that often move from their hotels to visit some good restaurants located out of the city center. Last, spatial updates are also an inherent component of the system since data analysts of Uber constantly add more venues, remove others that proved not useful, or modify existing ones by enhancing their spatial accuracy. In our work, we deploy a spatial graph system that efficiently covers all mentioned cases of a system like Uber that supports *spatial queries* and *spatial updates*.

In the social domain, data are inherently modeled as graphs in which the nodes represent the social network users and the edges among them depict their friendships. In these networks, when a user finds a post interesting and marks it as liked (in short, a user likes the post) then that post propagates to the friends of user. Brands want to exploit this diffusion mechanism to make their services/products further known to the public. For that, brands tend to maintain their own social network pages in social networks and share in these pages appealing *content* with their subscribers (the social network users who selected to follow the brand's page). This content is either created by a brand or recommended to that brand. In the former case, the brand can search for a set of influential users to maximize the promotion of its own content to a network. In the latter case, the brand can use a content-aware recommendation service to find a set of engaging features to form its content for

optimal advertising to that network. Commonly, the brand's subscribers participate in both cases; some of them are contacted to initialize the influence process of a given content or the content itself defines which of them will be the initial adopters, respectively. Further, a brand may decide to propagate content *once*, *many times*, or adjust the content to repetitively influence *certain users* such as they opt at some time to follow the brand's page (become subscribers of brand). In our work, we focus on the case where the content is sought (not created by the brand) and we handle all the mentioned influence scenarios. Namely, we devise *content-aware recommendation services* that enable brands to maximize influence in *one round*, *many rounds*, or repetitively personalize such influence to *specific users* to gain their subscription. The content we recommend via our services comprises features corresponding to social network pages. We contend that these pages can inspire the advertiser of a brand to create influential content in each case. When we consider that features have weights then the content is ranked, meaning the higher the rank of a feature the higher its portion degree within content. Else, when we treat all features the same then the content can be seen as a simple set of equal features that occupy the same amount of space in it. For instance, suppose that the features *Rafael Nadal*, *Paris*, *Artistic photography*, and *Street city life* are recommended in that specific ranked order to form the content of a new post for the brand GoPro. The advertiser of GoPro can take a look at the recent content published in these pages so as to obtain knowledge and inspiration for the content creation. For instance, a possible post could be a GoPro campaign that depicts Rafael Nadal (wearing a GoPro camera) exercising for a tennis tournament by running in the central streets of Paris located in artistic background areas. This post will give more focus to GoPro, then to Rafael Nadal, thereafter to Paris, afterwards to artistic pics, and finally to the city life on streets.

In the following, we present more specific details about the spatial and social data operations deployed in our work. Then, we conclude this introductory chapter with the contributions and the organization structure of the thesis.

1.1 Spatial Data

Spatial data consist of tuples related with entities that have a geometry. When this geometry is just a point, we call it a *location* geometry, while any other kind of geometry (e.g., polygon, line, multipoint) is mentioned as *extent* geometry. Users can execute several queries on spatial data management systems. The most popular spatial queries are the *range selections*, the *distance joins*, and the k *nearest neighbors*. For example, a user can type an address at Google Maps and have a look at a concrete area (associated with various points of interest having a geometry) in the vicinity of

the location specified by the address. Then, the user may zoom in (e.g, by using a mouse) to that area to view the venues that exist in a smaller piece of the initial area. Also, the user can enlarge the current area to see a bigger set of venues by selecting to zoom out the respective area. Each time that the user zooms in to decrease an area or zooms out to increase an area, the user implicitly runs a *range selection* query to the area derived from zooming. In addition, a *distance join* query takes as input two collections of objects (e.g., roads and rivers) and a spatial relationship (e.g., intersects) and finds the pairs of objects from the two sets that satisfy the condition (e.g., pairs or road segments and river segments that cross each other). Moreover, a k *nearest neighbor* query requests for the set of closest objects to a reference location. For instance, mobile users often use location-based services to browse the closest points of interest to their current location (e.g., k nearest banks, k nearest restaurants, etc.). The value of spatial queries is that they are also related with non-spatial components in them. When a user searches for a restaurant, the user often interested for a specific cuisine (e.g., Italian, Chinese) that exists in that restaurant. So, that query applies a non-spatial selection (i.e., cuisine = Italian) before ranking the restaurants with respect to their distance to the user location. Finally, we stress that updates also occur for spatial data for two main reasons. First, there are platforms that enable simple users to contribute to the collection of spatial data, and that is an efficient process but error-prone too. Second, the complexity of several geometries is refined over time by the system administrators to improve further their accuracy.

Two popular categories of spatial data management systems are the relational databases and the RDF databases. The former store tuples in tables that have a specific schema and these tables connect among each other via relations also represented by tables. Instead, RDF databases do not have any schema restrictions and they simply store tuples in triples. Each triple has the form <subject, property, object> where a subject is connected to an object via a property. Spatial RDF data comprise subjects having as object the geometry of such subjects with the respective property to be *hasGeometry*. Non-spatial RDF data consist of subjects that do not have a geometry. For instance, Prague hasGeometry "POINT(14.3, 50)" is a spatial RDF triple, while Wagner performedIn Prague is a non-spatial RDF triple. The subjects of spatial RDF triples are called *spatial entities*. In our work, we study spatial RDF data stores, queries and updates on them. Since spatial entities can be related with other non-spatial entities (e.g., Prague connects with Wagner), the previous discussion on spatial queries and updates also applies to spatial entities. Consider that the RDF data of a database form a graph where nodes are subjects or objects and edges are their properties. As a result, each RDF query can be seen as a specific subgraph pattern match to the database graph. Further, RDF updates can be *deletions*, *insertions*, or *modifications* of existing triples, as also they can convert a non-spatial entity to a

spatial one and vice versa. For example, if we remove the geometry of Prague then Prague is not anymore a spatial entity. Also, if we find that Wagner did not performed in Prague, but Leipzig instead, then we have a modification of Wagner triple; yet, if Wagner also performed in Leipzig besides Prague, then we have a insertion of a new triple for Wagner. Similar updates can be done for any kind of triples.

In this thesis, we implement a spatial RDF system that provides efficient management of *range selections*, *distance joins*, and k *nearest neighbors* queries as also updates (*deletions*, *insertions*, and *modifications*) on spatial RDF data.

1.2 Social Data

Social data pertain to social networks such as Facebook, Instagram, VKontakte (in brief, VK), etc. Each social network represents a graph in which the nodes denote the social network users and the edges depict the friendships or followerships of users in the network. When a user v_a is a friend of another user v_b, then when v_a finds appealing the content of a post and likes the post then v_a contributes that post to be visible to v_b. As v_b is also friend of v_a, the same propagation effect happens from v_b to v_a in case v_b likes a post. Yet, if v_b is not a friend but a follower of v_a, then only v_a can propagate a post to v_b. Besides the connections among users, we also have connections among users and brands in these networks. Specifically, brands maintain their own social network pages for advertising purposes and the users can select to follow these pages in order to stay tuned with the latest news of respective brands. All the pages that a user follows constitute the preference set of user; each preference maps to a specific page. Such preference set can be modeled as binary or weighted. In the former case, a page is either included or not in the user preferences. In the latter case, all pages of the network are included in the preference set of user in different weights; even the pages that are not followed by users take a dummy weight value. The assignment of weights usually depends on topic modeling techniques and past activity responses of users in regards to the posts published by brands. For instance, assume that Nike is the only brand of network. If v_a liked 10 posts of Nike and v_b liked 5 posts of Nike, then the weight of v_a for Nike is double the weight of v_b. In our work, we call such preferences as *attributes* or *features*, and we stress that each feature corresponds to a specific social network page. In other words, whatever entity has a social network page is treated as a brand and represents a feature in our case. Moreover, the *subscribers* of a brand are all the users who follow its page and denote the users that have instant access to the published posts of brand.

Due to the popularity of social networks, an increasing number of brands build their pages in them. The brand agent or advertiser is the person or a team that

is responsible for the posts (*content*) published in the page of a brand. The aim is to share content with the brand's subscribers that can collect many *likes* as via this mechanism posts propagate further in the network and make more known the brand to the public. When a user likes a post then that post influences the user; the maximum the post propagates in the network the maximum the number of users that post influences. Generally, there are two types of posts; the campaign of the month and the daily content. The advertiser should make a campaign popular (viral) in the network and also share daily content that gradually gains more and more *likes* over time. So, the advertiser looks for *content recommendation services* that can help her in the creation of the proper content to achieve her *influence maximization* purposes. In this thesis, we devise such kind of *content-aware services*. On the contrary, when the brand agent wants to make known her own created content and does not look for it, there are other ways to maximize influence in a network. The most classic and popular method to do that is to search for a set of influential users (have many friends) in the network such as they share that content with their friends. Besides, the agent can also send messages to specific users to invite them to see her content, may contact with brand agents of other pages to help her by sharing that content in their pages, or she can also utilize the promotion services provided by the respective social network; given a content, such services use advanced data analytics to effectively advertise it. We stress that in all previous cases, the advertiser needs to spend a budget to succeed her goals; the difference is where the budget goes in each case. When the content is sought then the budget goes to the content recommendation services, while when the users are sought then the budget goes to them based on what kind of users they are. As mentioned, they can be simple users but influential ones, brand advertisers of other pages, or data analysts of the social network company. Note that messaging is free but it has strict restrictions on how many users one can invite per day (e.g., 20 users per 12 hours in the social network VK).

For simplicity, let focus on two main categories (inverse of each other) from the aforementioned ones. Namely, given a set of users (subscribers) the advertiser searches for influential content, whereas given a content the advertiser seeks for influential users. The content can consist of tags, abstract themes, general topics, public entities, or inspired by specific social network pages. For brevity, we mention to all these content aspects as *features*. The type of content affects the influence maximization strategy that is selected for its diffusion. In particular, a big campaign often includes many features and as a result it has a high budget. So, a brand opts to maximize its campaign in one or few rounds in order to pay once either for the participated features (when content is sought) or for a big set of influential users (when content is given). This *one-round* procedure constitutes the *classic influence maximization* setting. Yet, in contrast to a campaign, the daily content usually depicts a small number of posts

published per day with each post comprising a low set of features. For this type of content, brands follow a different strategy. They everyday share content in the network (diffusion takes place in rounds, one post per round) and aim to utilize the influence feedback of posts in the previous rounds to form more influential posts for the next rounds. The budget is divided per post and goes either to a small set of influential users or to few content features depending on whether the content is given or not. This *multi-round* process defines the *adaptive influence maximization* setting. A crucial difference among the two mentioned settings of influence maximization is that the *classic* version of the problem is solved offline, while its *adaptive* version is solved online as it leverages influence feedback in real time to take decisions. Hence, brands request both offline and online solutions to maximize influence in a network.

Apart from maximizing influence in a social network, another important goal of brands is how to maximize subscription in that network. The *subscription maximization* setting pertains to how a brand can maximize the increase of its subscribers, namely the gain of the maximum number of new subscribers to its social network page. Under this setting, a brand can utilize personalized techniques to diffuse the content to *certain users* that it is more feasible (or the brand wants) to become its next subscribers. The logic here is that if a user repetitively likes the posts of a brand, at some time the user will opt to follow the brand's page. Also, some users tend to have very specific preferences or are interested much more to some content features than others, so the brands select the mechanism to repetitively influence those users. As happens for influence maximization, this mechanism still relies on either finding the proper content features or searching for the most suitable set of influential users, since the intuition is that the consecutive influence of a user will yield the subscription of user. The choice of which user to target for subscription relates with several factors, such as the number and the profile characteristics of the user friends, how close the interests of user are with those of brand, the age of user, and so on. Inherently, the subscription setting depends on adaptive influence maximization solutions as repetitive influence entails many propagation rounds. Yet, the relative decisions for these rounds can be taken either offline (beforehand for all rounds) or online (in real time). In this thesis, we devise an offline *content recommendation service* to help brands to maximize their subscribers, even when they have no subscribers at all.

1.3 Contributions

In what follows, we summarize the main contributions of this thesis.

Spatial Data Management. Spatial data management systems operate as *connectors* among brands and customers. As mentioned, such systems store spatial entities

(have a geometry) that correspond to brands and at the same time these systems enable customers to execute useful queries on them relative to brands. A special case of brand is the connector system itself (i.e., the company that provides the system) that has access to the location of both brands and customers. The location of a customer can be obtained on demand when the customer runs a query on the system. A beneficial connection among brands and customers is feasible only when those systems efficiently support fundamental *spatial queries* and dynamic *spatial updates*. Moreover, RDF knowledge bases have also spatially enriched due to the popularity of their simple storage schema; data just stored in triples. Yet, the current spatial extensions of RDF stores (e.g., Virtuoso [Vir], GraphDB [Gra], Strabon [KKK12]) focus mainly on simply supporting spatial operations, and less on performance optimization. We fill this gap by deploying SRX (Spatial RDF-3X), a system built on top of the open-source RDF-3X store [NW08] to efficiently support spatial queries and spatial updates; RDF-3X does not provide support for spatial RDF data. In more detail, the main contributions of SRX over RDF-3X are the following:

- SRX supports three types of spatial queries: *range selections*, *distance joins*, and *k nearest neighbors*. Also, it manages three kinds of spatial updates: *deletions*, *insertions*, and *modifications* of triples.
- SRX uses an R-tree index to store the geometries of spatial entities so as to help the efficient evaluation of queries with very selective spatial components.
- SRX uses a grid-based index to encode the geometries of spatial entities inside their IDs. This encoding acts as a cheap filter to unqualified entities of spatial queries since it avoids the I/O overhead of accessing the entities' geometries. Any sorting of triples is retained in queries and updates are effectively handled.
- SRX includes *spatial merge join* and *spatial hash join* algorithms based on the encoding scheme. Other *hash joins* are also implemented to use R-tree.
- SRX includes two *k nearest neighbor* algorithms that make use of the encoding scheme. The first algorithm is designed for *unordered* input whereas the second one for *ordered* input.
- SRX enhances the query optimizer to consider the spatially encoded entities.
- SRX provides a dynamic re-encoding technique that leverages the grid index to handle updates with a low overhead in performance.
- SRX is extensively compared for both queries and updates with the systems RDF-3X, Virtuoso, GraphDB, and Strabon on the real datasets LGD [LGD] and

YAGO [YAG]. To evaluate updates, we generated a realistic update benchmark based on the deltas we collected between different versions of LGD and YAGO. Results show that SRX outperforms other systems for queries and updates. SRX also incurs a little overhead to RDF-3X for updates.

Classic Influence Maximization. The *Classic Influence Maximization* (IM) problem [KKT03] asks for the k users that can maximize the influence of a given post in a social network. In our work, we analyze and study the inverse variant of IM where the users (brand's subscribers) are given and the content of post, comprising k features[1] (or attributes), is sought; we name this problem as *Content-Aware Influence Maximization* (CAIM). In brief, we mention the contributions of this work as follows:

- We study the CAIM problem that is the *first* inverse variant of IM problem in which the users are given and the content is sought.
- We devise a *content-aware* propagation model, whereby the probability of influence across edges depends on content. Based on this model, we prove that CAIM is NP-hard and it is also NP-hard to approximate its optimal solution.
- We implement a heuristic algorithm to solve CAIM, named Explore-Update, which uses maximum influence paths along with a threshold to skip the examination of several users and features.
- We compare Explore-Update with two baselines and a standard Greedy approach on Gnutella[2] and VK[3] datasets. Results show that it is remarkably more effective than baselines and more efficient than Greedy with competitive efficacy.

Adaptive Influence Maximization. The *Adaptive Influence Maximization* (AIM) problem aims to maximize the *cumulative* influence achieved in a social network over a number of rounds. Particularly, AIM pertains to a setting where brands publish one post per round and in each round they search for a set of influential users (when content is given) or for a set of influential content features (when content is not given). In both cases, the influence feedback in the previous rounds (the number of users who liked the propagated posts) is utilized for more influential decisions to be taken in the next rounds. In this thesis, we examine and study the *Adaptive Content-Aware Influence Maximization* (ACAIM) problem that depicts an *adaptive* version of the CAIM problem tailored for online (real-time) applicability to social networks.

[1] We consider that each *feature* corresponds to a specific social network page.
[2] https://snap.stanford.edu/data/p2p-Gnutella04.html
[3] https://vk.com/

Namely, ACAIM seeks in each round k content features to form an influential post in order to maximize the cumulative influence of created posts over all rounds. In addition, ACAIM includes the *first* integration of *Online Learning to Rank* (OLR) techniques to maximize influence in a network. In summary, we make the following contributions in the field of adaptive influence maximization:

- We study the ACAIM problem that is the *first* work that searches for influential content features under adaptive (multi-round) settings to maximize the cumulative influence in a social network.
- We propose the CATRID propagation model that enables for *first* time the utilization of an OLR framework for influence maximization purposes.
- We deploy a *simulator* (named SimCATRID) that runs the CATRID model to represent a realistic feedback environment for ACAIM. To do that, the simulator follows a *machine learning* scheme that is based on real VK posts.
- We develop three *learners* to solve the ACAIM problem. The best of them eliminates content features over rounds by using a *transitive* structure and also ranks the survived ones by using a *participation* structure.
- We present a plethora of experiments that examines the ACAIM performance of learners for multiple brands on several VK datasets under the metrics of *reliability* and *scalability*. We also provide a *business applicability* study that demonstrates the ACAIM results of worldwide known brands. Results show that the performance of our best learner is impressive in all cases, making it suitable for utilization in the social network industry.

Subscription Maximization. The *Subscription Maximization* (SM) problem targets to maximize the *cumulative* number of gained subscribers in a social network over a series of rounds. Specifically, SM adopts a similar to AIM setting with the difference that the propagated posts intend to influence certain users. The repetitive influence achieved on them can naturally yield their subscription. In our work, we study a relative problem named *Gaining Subscribers by Messaging* (GSM) that enables brands to earn new subscribers to their social network pages. The goal of GSM is to maximize the subscription gain over all rounds. In more detail, GSM applies to many rounds and in each round it guides the brand advertiser to invite some users to visit the last published content in brand's page such as they really find appealing that content and subscribe to the page. Our overall contributions in the domain of subscription maximization can be summarized as follows:

- We are the *first* that study the GSM problem. In each round, GSM recommends to brands what content to publish (comprising k features) and which m users to notify of that content so as to maximize their subscription gain over all rounds.

- We deploy three GSM solvers, named Random, Scan, and Substitute. Random opts to notify users uniformly at random. Scan finds the best pair of users and features by examining all the possible pair combinations. Substitute importantly reduces the exhaustive search burden of Scan by using fast retrieval techniques based on sorting of users in regards to their achieved subscription gains.

- We evaluate the performance of deployed GSM solvers on VK data by considering different user and feature sets. Results show that Substitute provides the best solution, as it is significantly more efficient than Scan with a minor loss of efficacy and clearly more effective than Random with competitive efficiency.

1.4 Organization

The rest of this thesis is structured as follows:

Chapter 2. This chapter discusses related work about RDF stores and their spatial extensions. Following, we consider *Influence Maximization* (IM) and its variants. In more detail, the *Classic Influence Maximization* (IM) problem seeks for the k users who can maximize the influence of a given post in a social network. The *Topic-Aware Influence Maximization* (TIM) problem extends IM to maximize topic-aware (content-aware) influence in a network by considering the topics that accompany the propagated post. The *Influence Maximization with Viral Product Design* (VPD) problem limits the topic selection to a specific set of functional features that can be attached to a certain product. Still, the purpose is the influence maximization of that product in a network. The *Adaptive Influence Maximization* (AIM) problem intends to maximize the cumulative influence in a social network over a number of rounds. One post is assigned per round, and the influence feedback of posts in the previous rounds is utilized for the finding of influential decisions in the next rounds. Finally, the *Personalized Influence Maximization* (PIM) problem focus to maximize the influence of propagated posts on a certain subset of social network users. It can be executed in one or more rounds depending on the respective setting. Complementary to the IM research, we also include the *Online Learning to Rank* (OLR) literature as it is part of our content-aware AIM work we present in this thesis. The OLR problem seeks for a set of clickable items per round to maximize the cumulative satisfaction (measured in number of clicks) of users over a series of rounds.

Chapter 3. In this chapter, we present the SRX system that extends the RDF-3X store for spatial data management. SRX supports WITHIN, DISTANCE, and kNN spatial queries, as also spatial updates. For both queries and updates, we compare SRX with the systems RDF-3X, Virtuoso, GraphDB, and Strabon on LGD and YAGO datasets. Results show the clear superiority of SRX over other systems for queries and updates. Also, the overhead for updates of SRX over RDF-3X is minor.

Chapter 4. This chapter presents the *Content-Aware Influence Maximization* (CAIM) problem that constitutes the inverse variant of the classic IM problem. IM seeks for influential users to promote a given content in a social network, while CAIM considers known the initial adopters and searches for engaging features to form an influential content. We prove that CAIM does not have influence guarantees, and so we deploy heuristic methods to solve it. Experimental results are provided on Gnutella and VK datasets. Results show that our advanced heuristic algorithm is more influential than simple heuristics and it is also much faster than a standard greedy approach.

Chapter 5. This chapter presents the *Adaptive Content-Aware Influence Maximization* (ACAIM) problem that aims to maximize the cumulative influence in a social network over a number of rounds. ACAIM constitutes an online version of CAIM. To solve ACAIM, we follow a machine learning approach based on the years 2010-2019 of the social network VK and we show how an OLR framework can be utilized for IM purposes. For that, we deploy a propagation model, a simulator that runs the model to generate realistic feedback, and three ACAIM learners. Our thorough experimental study on various VK datasets for several brands shows that ACAIM is solvable in big social networks. This fact highlights its suitability to the social network industry.

Chapter 6. In this chapter, we present the *Gaining Subscribers by Messaging* (GSM) problem that pertains to a content recommendation policy for brands to effectively increase their subscribers. We present three GSM solvers and evaluate their performance by issuing a rich experimental process on different VK datasets. Results demonstrate the important and practical value of GSM to real social networks.

Chapter 7. In this chapter, we summarize the contributions of this thesis. We also provide interesting directions for future social and spatio-social research problems.

Chapter 8. This chapter provides the Appendix of this thesis. It contains information for the queries, updates, and datasets we used for the experiments of SRX system.

Chapter 2

Related Work

In this chapter, we present the related work of this thesis. We start the discussion from the spatial domain and afterwards proceed to the social field. Our work relative to spatial data management (presented in Chapter 3) compares with similar works about storing and indexing of RDF data and executing RDF queries on them, as also with spatial extensions of those RDF systems. On the other hand, our works relative to social data mining (presented in Chapters 4, 5, and 6) mainly depend on works that study the *Influence Maximization* (IM) problem that searches for the k users who can maximize the influence of a given post in a social network. We also discuss related work of *Online Learning to Rank* (OLR) problem that seeks for the k most clickable items to satisfy users, since we utilize OLR in Chapter 5 for IM purposes.

2.1 RDF Indexing, Querying, and Spatial Support

RDF Storage and Query Engines. There have been many efforts toward the efficient storage and indexing of RDF data. The most intuitive method is to store all ⟨*subject*, *property*, *object*⟩(SPO) statements in a single, very large *triples* table. The RDF-3X system [NW08] is based on this simple architecture. RDF-3X (following an idea from previous work) uses a *dictionary* to encode URIs and literals as IDs. Indexing is then applied on the ID-encoded SPO triples. Figure 2.1 illustrates a dictionary and the ID-encoded triples for the RDF base of Figure 3.1a. RDF-3X creates a clustered B^+-tree index for each of the six SPO permutations (i.e., SPO, SOP, PSO, POS, OSP, OPS). A SPARQL query is transformed to a multi-way self-join query on the triples table; the query engine binds the query variables to SPO values and joins them (if the query contains literals or filter conditions, these are included as selection conditions). A query is first translated by replacing URIs or literals by the respective IDs and then evaluated using the six indices; finally, the query results (in the form of ID-triples) are translated back to their original form. The

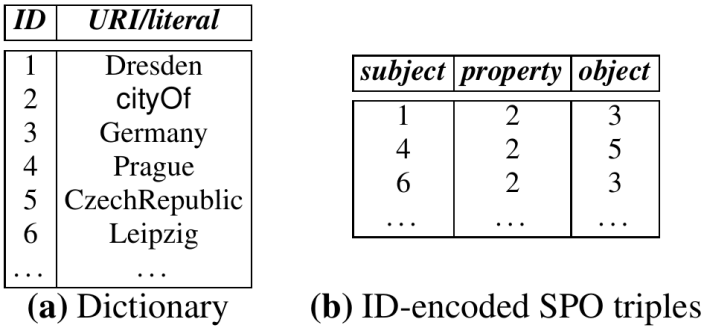

Figure 2.1: Use of Dictiorary.

six indices offer different ways for accessing and joining the triples; RDF-3X includes a query optimizer to identify a good query evaluation plan. The system favors plans that produce *interesting orders*, where merge joins are pipelined without intermediate sorts. In addition, a run-time *sideways information passing* (SIP) mechanism [NW09] reduces the cost of long join chains. RDF-3X maintains nine additional aggregate indices, corresponding to the nine projections of the SPO table (i.e., SP, SO, PS, PO, OS, OP, S, P, O), which provide statistics to the query optimizer and are also useful for evaluating specialized queries. The query optimizer was extended in [NM11] to use more accurate statistics for star-pattern queries. RDF-3X employs a compression scheme to reduce the size of the indices by differential storage of consecutive triples in them. Hexastore [WKB08] is a contemporary to RDF-3X proposal, which also indexes SPO permutations on top of a triples table. An earlier implementation of a triples table by Oracle [CDES05] uses materialized join views to improve performance.

An alternative storage scheme is to decompose the RDF data into *property* tables: one binary table is defined per distinct property, storing the SO pairs that are linked via this property. To avoid the case of having a huge number of property tables, this extreme approach was refined to a *clustered-property* tables approach (used by early RDF stores, like Jena [WSKR03] and Sesame [BKvH01]), where correlated tables are clustered into the same table and triples with infrequent properties are placed into a *left-over* table. Abadi et al.[AMMH07] use a column-store database engine to manage one SO table for each property, sorted by subject and optionally indexed on object.

A common drawback of the column-store approach and RDF-3X is the potentially large number of joins that have to be evaluated, together with the potentially large intermediate results they generate. Atre et al. [ACZH10] alleviate this problem by introducing a 3D compressed bitmap index, which reduces the intermediate results before joining them. A similar idea was recently proposed in [YLW+13]; the participation of subjects and objects in property tables is represented as a sparse 3D matrix, which is compressed. Yet, another storage architecture was proposed in [BDK+13]. The idea is to first cluster the triples by subject and then combine multiple triples

about the same subject into a single row. Thus, the system saves join cost for star-pattern queries, but it may suffer from redundancy due to repetitions and null values.

Trinity [ZYW+13] is a distributed memory-based RDF data store, which focuses on graph query operations such as random walk distance, reachability, etc. RDF data are represented as a huge (distributed) graph and query evaluation is done in an exploration-based manner; starting from the most selective predicates, query variables are bound progressively, while the RDF graph is browsed. Trinity's power lies on the fact that memory storage eliminates the otherwise very high random access cost for graph exploration. More information on distributed RDF systems can be found in [Ö16]. gStore [ZMC+11] is an earlier, graph-based approach, which models SPARQL queries as graph pattern matching queries on the RDF graph. gStore owes its efficiency to a signature generation scheme for the RDF (non-literal) graph nodes. The signature of a vertex is determined by its neighboring edges (i.e., properties) and nodes (i.e., entities or literals). The same encoding scheme is used for query patterns and can be used to effectively filter nodes that do not match with a query. The signatures of all nodes are hierarchically indexed by a search tree, which can help to find query pattern results. The index is also appropriate for *wildcard* queries where variables are bound to literals with wildcards via filter conditions. A similar, but simpler graph-partitioning approach for RDF data was proposed in [YWZ+09]. More recently, EmptyHeaded [ATOR, ATOR16] employed novel worst-case optimal join algorithms to accelerate pattern matching queries on RDF graphs.

Spatial Extensions of RDF Stores. Although the efficient management of RDF data has been a hot research topic for almost two decades, there have been only a few recent efforts toward extending RDF stores to support spatial data. The Parliament [BK12], built on top of Jena [WSKR03], implements most of the features of GeoSPARQL. Strabon [KKK12], developed contemporarily with Parliament, extends Sesame [BKvH01] to manage spatial RDF data stored in PostGIS. Strabon adopts a column-store approach, implementing two SO and OS indices for each property table. Spatial literals (e.g., points, polygons) are given an identifier and are stored in a separate table, which is indexed by an R-tree [Gut84]. Strabon extends the query optimizer of Sesame to consider spatial predicates and indices. The optimizer applies simple heuristics to push down (spatial) filters or literal binding expressions in order to minimize intermediate results. Strabon is shown to outperform Parliament, however, both systems suffer from the poor performance of the RDF stores they are based on (i.e., Jena and Sesame) compared to faster engines (e.g., RDF-3X [NW08]). For that reason, Strabon and Parliament lack sophisticated query evaluation and optimization techniques.

Brodt et al. [BNM10] extend RDF-3X [NW08] to support spatial data. The ex-

tension is limited, since range selection is the only supported spatial operation. Furthermore, query evaluation is restricted to either processing the non-spatial query components first and then verifying the spatial ones or the other way around. Finally, the opportunity of producing an interesting order from a spatial index (in order to facilitate subsequent joins) is not explored.

Geo-Store [WKC12] is another spatial extension of RDF-3X. Geo-Store divides the space by a grid and orders the cells using a *Hilbert* space-filling curve. Each geometry literal g (e.g. "POINT (...)") is approximated by the Hilbert order g.ID of the cell that includes it. Then, for all triples of the form s hasGeometry g, a triple s hasPos g.ID is added to the data. During query evaluation, an extra join with the hasPos triples is applied to perform the filter step of spatial queries. Geo-Store supports only spatial range and k nearest neighbor queries, but not spatial joins. In addition, it does not extend the query optimizer of RDF-3X to consider spatial query components. Finally, besides increasing the size of the original database with the introduction of hasPos triples, it is not clear how its encoding can handle complex spatial literals, such as "POLYGON (...)", which may span multiple cells of the grid.

S-Store [WZF+13] is a spatial extension of gStore [ZMC+11], which appends to the signatures of spatial entities their minimum bounding rectangles (MBRs). The hierarchical index of gStore is then adapted to consider both non-spatial and spatial signatures. Although S-Store was shown to outperform gStore for spatial queries, it handles spatial information only at a high level (i.e., the data are primarily indexed based on their structure) and there is no study on how spatial statistics can be used to improve query evaluation. Spatial RDF queries are also supported by many commercial systems, such as Oracle, Virtuoso [Vir], and GraphDB [Gra], however, details about their internal design are not public.

Finally, [NVDV18] recently introduced DiStRDF that adapts the encoding scheme of [LMBT14] to support RDF queries with spatio-temporal filters on top of Spark.

In this thesis (Chapter 3), we present the first system, named SRX, which efficiently handles a variety of fundamental spatial RDF queries (*range selections*, *distance joins*, and k *nearest neighbors*) as also updates (*deletions*, *insertions*, and *modifications*) on spatial RDF data.

2.2 Influence Maximization and Variants

Classic Influence Maximization. The *Influence Maximization* (IM) problem seeks for the k users that can maximize the influence of a given post in a social network. The first solutions to the IM problem were proposed by Domingos and Richardson [DR01, RD02], yet had no guarantees on influence spread. Then, Kempe et al. [KKT03] formulated the problem based on the *Independent Cascade* (IC) and *Linear Threshold*

(LT) propagation models, proved its NP-hardness, and proposed a greedy algorithm with a $(1-1/e-\epsilon)$ approximation guarantee. Subsequent works investigated efficiency and scalability questions, either with heuristics [CWW10, CYZ10, CSH+14] or preserving an approximation guarantee [LKG+07, GBL11, CPL12, BBCL14, TXS14]. IM has been extensively studied the last two decades due to its lucrative commercial value. A well-known application of IM is viral marketing [DR01], where a company may wish to spread the adoption of a new product from some initially selected adopters through the social links between users. Besides viral marketing, IM is also a crucial component in many other important applications such as network monitoring [LKG+07], rumor control [BAA11, HSCJ12], and social recommendation [YLL12].

Despite its immense application potential, IM embraces enormous research challenges. The first challenge is how to model the information diffusion process in a social network, which would heavily affect the influence spread of any seed set in IM. Second, the IM problem is theoretically complex in general. It has been proven that obtaining an optimal solution of IM is NP-hard under most of the diffusion models [CFL+15, KKT03, LCXZ12]. Furthermore, due to the stochastic nature of information diffusion, even the evaluation of influence spread of any individual seed set is computationally complex. These theoretical results have shown that it is very challenging to retrieve a (near) optimal seed set and to scale to massive social graphs at the same time. Third, recently, online social networks are being equipped with novel features, e.g., topical analysis, location-based services, streaming content, etc. This has opened up an opportunity of combining IM with various contexts, such as topics, location, and time in order to improve the effectiveness of IM. Many technical challenges naturally arise in solving such context-aware influence maximization problems. Last, the works [AGR17, LFWT18] provide good survey material for IM.

In this thesis (Chapter 4), instead of looking for k influential users to promote a given post, we address the IM problem by searching for k influential features to form the content of a non-given post so as to make it viral in a social network. The initial adopters for the post promotion are the subscribers of *brand*'s social network page.

Topic-Aware Influence Maximization. The *Topic-Aware Influence Maximization* (TIM) problem extends the generic IM problem by taking the *topics* of the item being propagated into consideration. Given *topics* as a query, TIM aims at finding the optimal set of users that maximizes the topic-aware influence in a social network. Barbieri et al. [BBM12] were the first to look at social influence taking content (comprising characteristics expressed as topics) into consideration. They proposed methods that learn propagation model parameters such as topic-aware influence strength from a query log of past propagation traces, and verified experimentally that a larger influence spread can be engendered when taking content characteristics into consideration

via their *Topic-Aware Influence Maximization* (TIM) models.

Aslay et al. [ABBBY14] studied online TIM queries; the incentive for this online scenario is that many independent advertisers wish to instantly detect the k most influential users for advertising purposes; each advertisement contains a different set of keywords and hence induces a new probabilistic graph creating a separate TIM instance; an offline-online solution, INFLEX, based on an index used to identify similarities among a new and log TIM queries; pre-computed solutions for log queries are aggregated online so as to provide an approximate solution for a TIM query.

The online TIM problem is also studied in [CLY14, CFL+15]. Chen et al. [CLY14] studied topic-aware influence results on two real networks and utilized the derived properties to form three preprocessing-based algorithms, of which MIS is the best; its main difference from INFLEX is that, in MIS, pre-computed seed sets are based on each separate topic rather than on a mixture of topics from different log queries. Chen et al. [CFL+15] utilized the *maximum influence arborescence* (MIA) model [CWW10] to achieve high influence spread with a theoretical guarantee. The core idea is to utilize upper- and lower-bounding techniques, so that an exact marginal influence is computed only for the most promising nodes. This work provides the state-of-the-art solution for the online TIM problem [ABBBY14].

Recently, Li et al. [LZT15] proposed a variation on the online TIM problem, namely the alternative problem of *Keyword-Based Targeted Influence Maximization* (KB-TIM). By KB-TIM, each user is associated with a weighted vector of preferences for distinct keywords, which stand for topics. This vector can be generated by applying topic modeling techniques [HD10] on aggregated user social activities, such as posts, likes, etc. An advertisement then achieves an impact determined by its own topic-oriented keywords. The KB-TIM problem aims to maximize an advertisement's impact, expressed in terms of its spread to target users relevant to its keywords. The solution in [LZT15] draws from previous work in [TXS14], with the main difference being that, while in [TXS14] θ users in a sampled *Reverse Reachable* (RR) set [BBCL14] are counted without prejudice, in [LZT15] these sampled users are accounted in terms of exerted advertisement impact; [LZT15] also employs two indexing methods to precompute RR sets for different keywords, so as to obtain RR sets associated with the query keywords on the fly. Nevertheless, results in [LZT15] are not compared to those in [CFL+15].

Besides selecting content features instead of users to maximize influence in a network, our works in social domain (Chapters 4, 5, and 6) have another important difference with aforementioned topic-aware IM works. Those works do not examine what kind of posts would be most influential given all topics in the network. Also, the topic-aware approach is based on general topical terms, like music, soccer, cars, etc., ignoring the high variation among different specimens within such terms. In contrast,

we search for specific content features (*social network pages*) to form influential posts.

Finally, authors in [KLK20] consider each topic (they call it *feature*) as a specific social network page and propose an alternative version of LT model based on features, named *Content-Aware Linear Threshold* (CALT) model. Particularly, they first learn the influence parameters of CALT associated with activation probabilities on network edges, and then they use that knowledge to find the k most influential features in order to form a viral post that starts its diffusion from a fixed set of initial adopters. Although this work shares the same meaning of features with our social works in this thesis, it utilizes different influence propagation models than the ones used in Chapters 4 and 5, and also it cannot solve the *Adaptive Influence Maximization* problem that we discuss later and we solve it in Chapter 5.

Influence Maximization with Viral Product Design. Aral and Walker [AW11] investigated the problem of *viral product design* (VPD) under randomized trials focusing on product features like *personalized referrals* and *broadcast notifications*. The goal of VPD is to maximize the influence of a product in a network by exploiting specific engaging features that can meaningfully attached to the product. Thereafter, Barbieri and Bonchi [BB14] studied the problem of IM *in conjunction with* that of VPD, aiming to detect a combination of seed nodes and product attributes that maximize influence in a network. The proposed solutions are generic methods named *Local Update* and *Genetic Update*; the former is a greedy algorithm allowing for both addition and removal of attributes at each greedy iteration; the latter is a brute-force method that randomly selects a subset of all attributes. By contrast, our social works in Chapters 4 and 5 study the problem of content selection for a post (not a product) as a stand-alone IM problem pertaining to distinctive characteristics.

Adaptive Influence Maximization. The *Adaptive Influence Maximization* (AIM) problem attracted significant interest lately due to its high applicability to many IM use-cases in real world. The target of AIM is to maximize the cumulative influence achieved in a social network over a number of rounds. We discuss two main factors that can depict the growing popularity of AIM the last period.

First, it is easily verified in [GBL11] that, given a network with *known* activation probabilities on its edges, one-round propagations of classic IM are often less influential than multi-round ones of AIM. This is logical to happen, since in AIM, the influential candidates are gradually selected over rounds based on a network feedback [GK11, CK13, YT17, SHYC18, HTH+20]. Golovin and Krause [GK11] introduced an adaptive optimization framework with approximation guarantees under a *dependent* (incremental) over rounds seed selection setting; only one seed node can be selected in each round and the propagation capabilities of earlier seeds are not reconsidered for later seeds. To do that, they utilize a *full-adoption feedback* model

that notifies the learner of which nodes activated in each round. All the subsequent works are motivated by the adaptive formulation in [GK11]. In particular, under the full-adoption feedback model, Chen and Krause [CK13] study adaptive seed selection by assuming that more than one seed nodes can be selected in each round. Yuan and Tang [YT17] solve AIM under a *partial-feedback* model that allows selecting seeds without time restrictions in the sense that there is no need to wait for total influence results of previous seeds so as to select the next seeds. The state-of-the-art work for AIM, under the dependent seed selection setting, is the recent work in [HTH+20] that uses approximation algorithms which depend on selecting nodes in equal batches. Differently from previous works, Sun et al. [SHYC18] proposed an alternative setting for AIM under which influence propagates in multiple rounds *independently* from possibly different seed sets and the aim is to maximize the expected number of unique activated nodes over all rounds.

The second reason for the popularity of AIM is the *uncertain* factor. In many realistic scenarios, the parameters of activation probabilities in the edges of a network or even the network topology (nodes and their edges), are partially or completely agnostic to the learner. Several approaches have been proposed [LMM+15, CWYW16, VLS16, VKW+17, WKVV17, WLW+19], which given a network, they learn the underlying diffusion parameters while simultaneously running *independent* (i.e., non-incremental) propagation campaigns. To balance between *exploration* steps (of yet uncertain model aspects) and *exploitation* ones (focusing on the most promising seeds), these approaches rely on *multi-armed bandits* techniques similar to [CWY13]. Among these works, only in [LMM+15] authors target the activation of unique nodes across rounds as in [SHYC18], while all the others share the same non-unique node influence objective. Yet, all these multi-armed bandit approaches still focus on the learning aspect of edge probabilities to find influential seeds. Further, regarding the case where the network topology is unknown, there is an interesting line of adaptive works [SS13, HS15, LCCM19] looking for promising seeds to solve AIM under an agnostic network perspective.

Complementary to mentioned works is the research conducted in [TWTD17, WFLT17]. In particular, Tong et al. [TWTD17] consider the propagation probabilities are random variables conforming to certain distributions and propose a simple greedy adaptive seeding strategy to find an effective solution with a provable performance guarantee. Moreover, Wang et al. [TWTD17, WFLT17] study the IM problem over a social action stream. They define the influence between users in the sliding window model and propose the *Stream Influence Maximization* (SIM) query to continuously track a seed set maximizing the influence with regards to the current window.

Differently from previous works, we address the AIM problem in Chapter 5 by searching influential features over node probabilities instead of seeking influential

nodes over edge probabilities; we consider that the network structure is known.

Personalized Influence Maximization. The *Personalized Influence Maximization* (PIM) problem tunes IM for *topic-relevant targets*. PIM considers that nodes (i.e., users) are topic-aware and wants to maximize the influence on a subset of social network users (called *targets*) relevant to the query topics. Some studies on PIM [GZZ+13, LZT15, NDT16] focus on maximizing the influence over the users who are relevant to the query topics, i.e., the *topic-relevant targets*. Formally, these studies introduce a concept of *benefit* to differentiate the users. Then, they compute the influence as the expected summation of benefits of the activated users, which is also known as targeted influence. Based on this, they introduce techniques to find the users that maximize the targeted influence under their benefit computation models.

Li et. al [LZT15] propose to compute a user's benefit by considering how a user matches query topics. More specifically, they associate each user with a profile that consists of the users preferences on different topics. Given this benefit model, Li et. al [LZT15] address targeted IM problem under the traditional IC model. They introduce a weighted sampling technique to find an unbiased estimator for the targeted influence. Moreover, as conducting online sampling cannot meet the real-time processing requirement, they further devise disk-based index structures to push the sampling procedure from online to offline. The idea is to build a sufficient number of Reverse Reachable (RR) sets for each topic (e.g., music and book) offline. Then, given an online query, they select RR sets from the query topics and merge the RR sets to compute the result. Last, they also introduce an incremental index structure to further reduce the I/O cost.

Nguyen et. al [NDT16] generalize the PIM problem by considering any predefined benefit function over users. Similar to [LZT15], they also adopt an RR framework. Under this framework, they propose an algorithm with a sampling strategy applicable for general benefit functions, and an early termination rule that avoids generating too many samples. Furthermore, this work also studies the cost-aware settings where each user is activated using certain costs.

Complementary to the PIM problem, authors in [GZZ+13] aim to find the seed set that maximizes its influence on one given target user, which can be interpreted that only this user is topic-relevant while the others are not. The work in [GZZ+13] studies this problem under the IC model, and proposes two algorithms. The first is called efficient local greedy algorithm, which can be expressed as a simulation-based algorithm, with some pruning rules tailored for the local structure of the target user. Obviously, this algorithm cannot satisfy the online query requirement. The second is an online local cascade algorithm, which is a hop-based approach that only maintains shortest paths from each user to the target one. However, compared

with [LZT15, NDT16] the influence spread cannot be theoretically guaranteed.

The difference of our work in Chapter 6 relative to mentioned research on the PIM problem is that we exploit influence to gain subscribers for a brand. Previous works do not study neither measure how targeted influence on users can lead to the subscription of users. We also achieve influence via selecting appealing content features and not by searching for influential seed nodes.

2.3 Online Learning to Rank

The *Online Learning to Rank* (OLR) problem mentions to a learner that adaptively selects, in each round, a ranked list of k out of L items so as to maximize the *user satisfaction* over all rounds; each round relates with a single user and users are often different among rounds. Most OLR works [KSWA15, CMPL15, KWAS15, ZNS+16, LWZC16, KKSW16, LVC16] measure that user satisfaction in clicks, by utilizing a *click model* (common to all users in all rounds) that is a stochastic model of how a user examines and clicks on a ranked list of items. There is a variety of click models [CMdR15]. Among them, the most popular ones for the OLR problem are the *Position-Based Model* (PBM) [RDR07] and the *Cascade Model* (CM) [CZTR08]. In PBM, the probability that users click on an item of a ranked list depends on the position of item in the list and the inherent attractiveness of item, while CM assumes that users scan the ranked list from top to bottom, clicking on the first item they find attractive. Yet, it has been experimentally observed that no single existing click model captures the behavior of an entire population of users [GCM+15]. To address this problem, Zoghi et al. [ZTG+17] introduced an algorithm that solves OLR in different click models (including PBM and CM) under reasonable click probability assumptions. After that, Lattimore et al. [LKLS18] enhanced the independent click model setting of previous work by relaxing further its click assumptions and proposed a more practical algorithm, named TopRank, to solve OLR in multiple click models under stronger regret guarantees. Recently, Li et al. [LLS19] proposed a learning framework to handle topic-based OLR.

In Chapter 5 we study the *Adaptive Content-Aware Influence Maximization* (ACAIM) problem that integrates OLR techniques for IM purposes. In particular, among previous OLR works we selected TopRank for integration to solve ACAIM due to its general click model and high usefulness as proved in [LKLS18]. Yet, we stress that ACAIM differs from pure OLR for two main reasons. First, ACAIM applies to a social network of connected users rather than a sequence of independent single users. Second, OLR works focus on learning click probability parameters, while we consider such parameters learned by training, and focus on effectively and efficiently address the online computation challenges of ACAIM.

Chapter 3

SRX: Efficient Management of Spatial RDF Data

In this chapter, we present a general encoding scheme for the efficient management of spatial RDF data. The scheme approximates the geometries of the RDF entities inside their integer IDs and can be used, along with several operators and optimizations we introduce, to accelerate queries with spatial predicates and to re-encode entities dynamically in case of updates. We implement our ideas in SRX, a system built on top of the popular RDF-3X system [NW08]. SRX extends RDF-3X with support for three types of spatial queries: range selections (e.g. find entities within a given polygon), spatial joins (e.g. find pairs of entities whose locations are close to each other), and spatial k nearest neighbors (e.g. find the three closest entities from a given location). We evaluate SRX on spatial queries and updates with real RDF data, and we also compare its performance with the latest versions of three popular RDF stores. The results show SRX's superior performance over the competitors; compared to RDF-3X, SRX improves its performance for queries with spatial predicates while incurring little overhead during updates.

3.1 Introduction

The Resource Description Framework (RDF) has become a standard for expressing information that does not conform to a crisp schema. Semantic-Web applications manage large knowledge bases and data ontologies in the form of RDF. RDF is a simple model, where all data are in the form of ⟨*subject*, *property*, *object*⟩ (SPO) triples, also known as *statements*. The subject of a statement models a *resource* (e.g., a Web resource) and the property (a.k.a. *predicate*) denotes the subject's relationship to the object, which can be another resource or a simple value (called *literal*). A resource is specified by a uniform resource identifier (URI) or by a *blank node* (denoting an

unknown resource). An RDF knowledge base can be modeled as a graph, where nodes are resources or literals and edges are properties.

SPARQL is the standard query language for RDF data, used to express *query graph patterns* that have to be matched in the RDF data graph. The GeoSPARQL standard [BK12], defined by the Open Geospatial Consortium (OGC), extends RDF and SPARQL to represent geographic information and support spatial queries. Geospatial filter functions are used to express spatial predicates between entities in SPARQL queries. stSPARQL [KK10] has similar features.

Despite the large volume of work on indexing and querying large RDF knowledge bases [AMMH07, ACZH10, BDK+13, BKvH01, CDES05, NW08, WKB08, WSKR03, YWZ+09, YLW+13, ZYW+13, ZMC+11], only a few works focus on the effective handling of spatial semantics in RDF data. In particular, the current spatial extensions of RDF stores (e.g., Virtuoso [Vir], GraphDB [Gra], Parliament [Par], Strabon [KKK12], and others [BNM10, WKC12, WZF+13]) focus mainly on supporting GeoSPARQL features, and less on performance optimization. The features and weaknesses of these systems are reviewed in Chapter 2. On the other hand, there is a large number of spatial entities (i.e., resources) in RDF knowledge bases (e.g., YAGO [YAG]). Thus, the power of the state-of-the-art RDF stores is limited by the inadequate handling of spatial semantics, given that it is not uncommon for user queries to include spatial predicates. At the same time, spatial data management systems [EM16] can only be used to index and search the spatial semantics of the entities, but do not support graph pattern search.

We fill this gap by presenting SRX (Spatial RDF-3X), a system built on top of the open-source RDF-3X store [NW08] to efficiently support spatial queries and updates. SRX inherits the basic design principles of RDF-3X, which encodes all values that appear in SPO triples by identifiers with a help of a dictionary, and models the RDF knowledge base as a single long table of ID triples. A SPARQL query can then be modeled as a multi-way join on the triples table. The system creates a clustered B^+-tree for each of the six SPO permutations; the query optimizer identifies an appropriate join order, considering all the available permutations and advanced statistics [NM11]. RDF-3X is known to have robust performance in comparison studies on various RDF datasets and query benchmarks [BDK+13, NW08, YLW+13]. Although we have chosen RDF-3X as a basis for SRX, our techniques are also applicable to other RDF stores, e.g. [YLW+13]. In a nutshell, SRX includes the following extensions over RDF-3X.

Index Support for Spatial Queries. Similar to previous spatial extensions of RDF stores (e.g., [BNM10]), SRX includes a spatial index (i.e., an R-tree [Gut84]) for the geometries associated to the spatial entities. This facilitates the efficient evaluation

of queries with very selective spatial components.

Spatial Encoding of Entities. The identifiers given to RDF resources in the dictionary of RDF-3X (and other RDF stores) do not carry any semantics. Taking advantage of this fact, we encode spatial approximations inside the IDs of entities (i.e., resources) associated to spatial locations and geometries. This mechanism has several benefits. First, for queries that include spatial components, the IDs of resources can be used as cheap filters and data can be pruned without having to access the exact geometries of the involved entities. Second, our encoding scheme does not affect the standard ordering (i.e., sorting) of triples used by the RDF-3X evaluation engine, therefore it does not conflict with the RDF-3X query optimizer; in other words, the original system's performance on non-spatial queries is not compromised. Finally, our encoding scheme adopts a flexible hierarchical space decomposition so that it can easily handle spatially skewed datasets and updates without the need to re-assign IDs for all entities.

Spatial Join Algorithms. We design spatial join algorithms tailored to our encoding scheme. Our *Spatial Merge Join* (SMJ) algorithm extends the traditional merge join algorithm to process the filter step of a spatial join at the approximation level of our encoding, while (i) preserving *interesting orders* of the qualifying triples that can be used by succeeding operators, and (ii) not breaking the pipeline within the operator tree. In typical SPARQL queries which usually involve a large number of joins, the last two aspects are crucial for the overall performance of the system. Our *Spatial Hash Join* (SHJ-ID) operates with unordered inputs, using their encodings to identify fast candidate join pairs.

Spatial kNN Algorithms. We design two k nearest neighbors (kNN) algorithms that make use of our encoding scheme. Both are based on previous work on grid-based kNN query evaluation. The first one operates on unordered input whereas the second exploits interesting orders and can be combined with other order-preserving operators to improve performance and further reduce the memory footprint.

Spatial Query Optimization. In addition to including standard selectivity estimation models and techniques for spatial queries, we extend the query optimizer of RDF-3X to consider spatial filtering operations that can be applied on the spatially encoded entities. To do that, we augment the original join query graph of a SPARQL expression to include binding of spatial variables via spatial join conditions.

Dynamic Spatial Re-encoding. Changes in real RDF datasets are the rule rather than the exception. Such changes occur as new triples are added and old ones are removed or updated, and the need for re-encoding spatial entities arises naturally. To tackle this problem with a low overhead in performance, we carefully integrate a dynamic re-encoding technique with the original update mechanism of RDF-3X.

We evaluate SRX by comparing it with the latest versions of two commercial spatial RDF management systems: Virtuoso [Vir] and GraphDB [Gra], and a popular free RDF management system: Strabon [KKK12]. For query evaluation, we use two real datasets: LinkedGeoData (LGD) [LGD] and YAGO [YAG]. To evaluate dynamic re-encoding, we generated a realistic update benchmark — the first one using real data — based on the deltas we collected between different versions of LGD and YAGO. The results demonstrate the superior performance and robustness of SRX over the competitors; SRX improves the performance of the original RDF-3X for queries with spatial predicates, while incurring insignificant overhead when performing updates.

3.2 Preliminaries

The SPARQL queries we consider follow the format:

Select [projection clause]
Where [graph pattern]
Filter [condition]

The Select clause includes a set of variables that should be instantiated from the RDF knowledge base (variables in SPARQL are denoted by a ? prefix). A graph pattern in the Where clause consists of triple patterns in the form of s p o where any of the s, p and o can be either a constant or a variable. Finally, the Filter clause includes one or more *spatial predicates*. For the ease of presentation, in our discussion and examples, we consider only WITHIN range predicates (for spatial selections), DISTANCE predicates (for spatial joins), and kNN predicates (for k nearest neighbors). However, we emphasize that the results of our work are directly applicable to all spatial predicates defined in the GeoSPARQL standard [BK12]. In addition, we use a simplified syntax for expressing queries and not the one of the GeoSPARQL standard because the latter is verbose.

As an example, consider the RDF knowledge base partially listed in Figure 3.1a. Literals and *spatial literals* (i.e., geometries) are in quotes. An exemplary query with a range predicate is:

Select ?s ?o
Where ?s cityOf Germany . ?s hosted ?o .
?s hasGeometry ?g .
Filter WITHIN(?g, "POLYGON(...)");

This query finds the cities of Germany within a specified polygonal range together with the persons they hosted. Note that there are three variables involved (?s, ?o,

subject	*property*	*object*
Dresden	cityOf	Germany
Prague	cityOf	CzechRepublic
Leipzig	cityOf	Germany
Wrocław	cityOf	Poland
Ostrava	cityOf	CzechRepublic
Hannover	cityOf	Germany
Dresden	sisterCityOf	Wrocław
Dresden	sisterCityOf	Ostrava
Leipzig	sisterCityOf	Hannover
Dresden	hosted	Wagner
Leipzig	hosted	Bach
Wagner	hasName	"Richard Wagner"
Wagner	performedIn	Leipzig
Wagner	performedIn	Prague
Wagner	performedIn	Ostrava
Bach	performedIn	Leipzig
Mozart	performedIn	Hannover
Mozart	performedIn	Dresden
Dresden	hasGeometry	"POINT (13.6, 51)"
Prague	hasGeometry	"POINT (14.3, 50)"
Leipzig	hasGeometry	"POINT (12.3, 51.3)"
Wrocław	hasGeometry	"POINT (16.9, 51.1)"
Ostrava	hasGeometry	"POINT (18.2, 49.8)"
Hannover	hasGeometry	"POINT (9.7, 52.4)"
...	...	...

(a) RDF triples

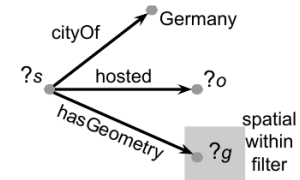

(b) Spatial Within query

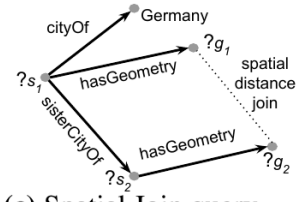

(c) Spatial Join query

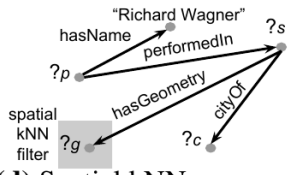

(d) Spatial kNN query

Figure 3.1: Example of RDF data and three spatial queries.

and $?g$) connected via a set of triple patterns which also include constants, i.e., Germany. For example, if POLYGON(...) covers the area of East Germany, (Dresden, Wagner) and (Leipzig, Bach) are results of this query. The query is represented by the pattern graph of Figure 3.1b. In general, queries can be represented as graphs with *chain* (e.g., $?s_1$ hosted $?s_2$. $?s_2$ performedIn $?s_3$.) and *star* (e.g., $?s$ cityOf $?o$. $?s$ hosted Wagner.) components. Another exemplary query, which includes a spatial join predicate, represented by the pattern graph of Figure 3.1c, is:

Select $?s_1$ $?s_2$
Where $?s_1$ cityOf Germany . $?s_1$ sisterCityOf $?s_2$.
$?s_1$ hasGeometry $?g_1$. $?s_2$ hasGeometry $?g_2$.
Filter DISTANCE($?g_1$, $?g_2$) < "300km";

This query asks for pairs of sister cities (i.e., $?s_1$ and $?s_2$) such that the first city (i.e., $?s_1$) is in Germany and the distance between them does not exceed 300km. In the exemplary RDF base of Figure 3.1a, (Dresden, Wroclaw) and (Leipzig, Hannover) are results of this query while (Dresden, Ostrava) is not returned as the distance between Dresden and Ostrava is around 500km. Finally, an examplary query with a kNN predicate, represented by the pattern graph of Figure 3.1d, is the next:

Select $?s$ $?c$
Where $?p$ hasName "Richard Wagner" . $?p$ performedIn $?s$.
$?s$ cityOf $?c$. $?s$ hasGeometry $?g$.
Filter kNN($?g$, "POINT(...)", 2);

This query asks for the two closest to the specified point cities where Richard Wagner has performed, together with their respective countries. E.g., if POINT(...) refers to the city of Chemnitz (12.8, 50.8), then the result of the query in the RDF base of Figure 3.1a consists of the tuples (Leipzig, Germany) and (Prague, CzechRepublic).

Besides queries, we also consider delete, insert, and update operations on RDF data. Updates in SPARQL (and GeoSPARQL) are expressed via DELETE and INSERT statements following the format:

Delete|Insert [triples]

For example, to update the name of the entity Wagner in the RDF base of Figure 3.1a, one can simply apply the following two statements:

Delete Wagner hasName "Richard Wagner";
Insert Wagner hasName "Wilhelm Richard Wagner";

3.3 A Basic Spatial Extension

In the remainder of the chapter, we present the steps of extending a standard query evaluation framework for triple stores (i.e., the framework of RDF-3X) to efficiently handle the spatial components of RDF queries. In RDF-3X, a query evaluation plan is a tree of operators applied on the base data (i.e., the set of RDF-triples). The leaves of the tree are any of the 6 SPO clustered indices. The operators apply either selections or joins. Each operator addresses a triple of the query pattern and instantiates the corresponding variables; the instantiated triples (or query subgraphs) are passed to the next operator, until they reach the root operator, which computes instances for the entire query graph.

This section outlines the basic (but essential) spatial extension to RDF-3X, which improves the spatial RDF-3X extension of Brodt et al. [BNM10] to support spatial join and kNN query evaluation. We also discuss drawbacks of the basic extension that motivated us to design the spatial encoding scheme described in Section 3.4 and the query evaluation algorithms that use it in Section 3.5.

Spatial Indexing. Spatial entities i.e., resources associated to spatial literals like POINT and POLYGON, are indexed by an R-tree [Gut84]. For each entity associated to a polygon, there is an entry at a leaf of the R-tree of the form (mbr, ID), where mbr

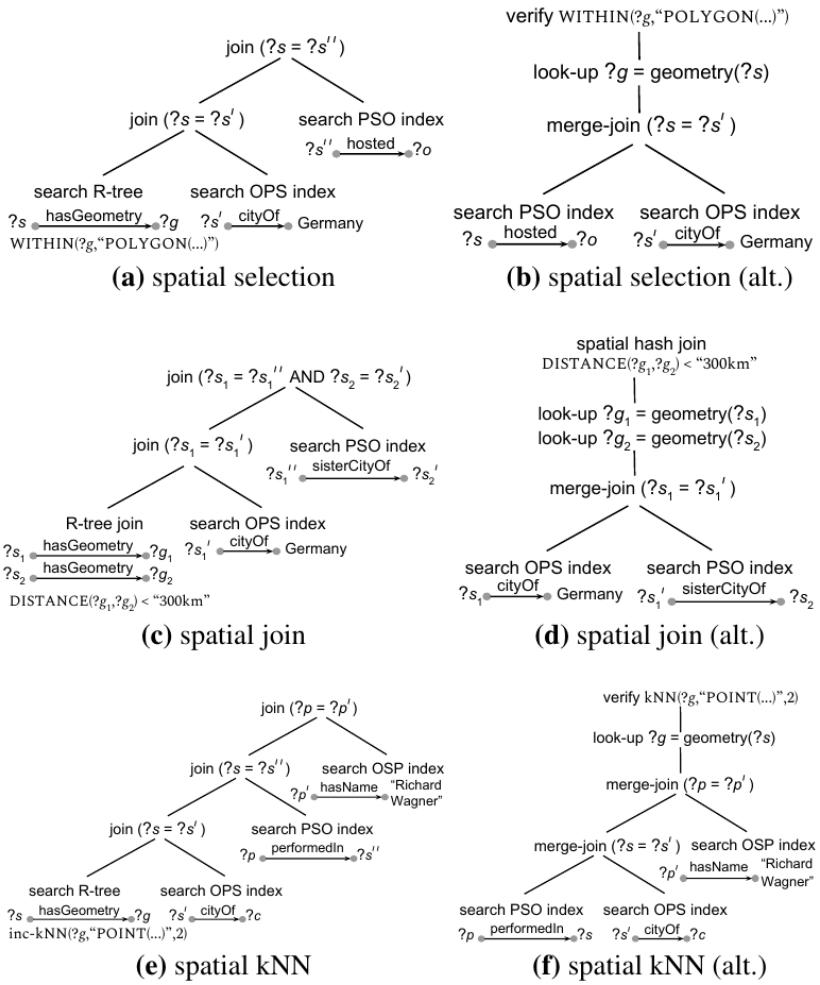

Figure 3.2: Possible query plans in the basic extension.

is the minimum bounding rectangle (MBR) of the polygon. For each entry associated to a point pt, there is a (pt, ID) entry.

Spatial Selections. Given a query with a spatial selection Filter condition, the optimizer may opt to use the R-tree to evaluate this condition first and retrieve the IDs of all entities that satisfy it.[1] However, the output fed to the operators that follow (i.e., those that process non-spatial query components) is in a random order. Thus, query evaluation algorithms that rely on the input being in an *interesting order* (such as merge-join) are inapplicable. On the other hand, if the spatial selection is evaluated after another (i.e., non-spatial) operator, the R-tree cannot be used because the input is no longer indexed. So, in this case, the system must look up the geometries of the entities that qualify the preceding operator at the dictionary, incurring

[1]For entities that have point geometries, the spatial selection can be evaluated using only the R-tree. If the entities have non-point geometries, the R-tree search may result in false positives, thus, the final results of the spatial filter are confirmed by retrieving the exact geometries from the dictionary.

significant cost. Figure 3.2a and Figure 3.2b illustrate two alternative plans for the spatial selection query of Figure 3.1b. The plan of Figure 3.2a uses the R-tree to perform the spatial selection and joins the result with the instances of triple $?s$ cityOf Germany. Finally, the join results are joined with the results of $?s$ hosted $?o$. The plan of Figure 3.2b first evaluates the non-spatial part of the query and then looks up and verifies the geometries of all $?s$ instances in it (i.e., the R-tree is not used here).

Spatial Joins. The R-tree can also be used to evaluate spatial join Filter conditions, by applying join algorithms based on R-trees. We implemented three algorithms for this purpose. First, the R-tree join algorithm [BKS93] can be used in the case where both spatially joined variables involved in the Filter condition are instantiated directly from the base data and do not come as outputs of other query operators. Second, we use the SISJ algorithm [MP03] for the case where the R-tree can be used only for one variable. Finally, we implemented a spatial hash join (SHJ) algorithm [LR96] for the case where both inputs of the spatial join filter condition are output by other operators.[2] As in the case of spatial selections, spatial join algorithms do not produce interesting orders and for spatial join inputs that are instantiated by preceding query operators, the system has to perform dictionary look-ups in order to retrieve the geometries of the entities before the join. Figure 3.2c and Figure 3.2d illustrate two alternative plans for the spatial join query of Figure 3.1c. The plan of Figure 3.2c applies an R-tree self-join [BKS93] to retrieve nearby ($?s_1$, $?s_2$) pairs and then binds $?s_1$ with the result of $?s_1$ cityOf Germany. The output is then joined with the result of $?s_1$ sisterCityOf $?s_2$. The plan of Figure 3.2d first evaluates the non-spatial part of the query and then looks up the geometries of all ($?s_1$, $?s_2$) pairs, and joins them using SHJ. In the following, we briefly describe SISJ and SHJ for completeness.

SISJ joins a spatial input A which is not indexed, with an R-tree B. Assuming that we want to use H hash buckets, SISJ first divides the entries at the uppermost level of B that contains at least H entries into H groups based on their spatial proximity. The i-th group has as spatial extent the MBR of all entries in group i. Bucket B_i contains all objects in the subtrees of B pointed by the entries in the i-th group. The objects from A are hashed to buckets such that bucket A_i contains all objects that intersect the spatial extent of the i-th group. Finally, each A_i is spatially joined in memory with B_i (e.g., using plane sweep). Our SHJ implementation pulls the smallest of the two join inputs (based on the query optimizer's estimation) and constructs from it a spatial hash table in memory. Each hash bucket corresponds to a cell in a 2D grid with side equal to the distance join threshold ϵ. Each entity from the hashed join input is assigned to all buckets (cells) that it spatially overlaps. Then, SHJ pulls the

[2] If the spatial join inputs are very small, we simply fetch the geometries of the input entity sets and do a nested-loops spatial join.

records from the other input one by one and, for each spatial entity e, (i) it retrieves e's geometry from the dictionary, (ii) identifies the cell c whereto e belongs, and (iii) accesses the buckets that correspond to c and its neighboring cells to find candidate entities that can match with e based on their spatial approximations. For each such candidate entity e', the operator computes the exact distance between e and e', and outputs the join pair (e, e') if the distance is at most ϵ.

Spatial kNN. The R-tree can also be used to evaluate a spatial kNN predicate in the Filter clause. In this case, the nearest entities are fetched from the R-tree and fed to the operators that follow. Since some of these entities might be filtered out by subsequent operators, we should use an *incremental NN algorithm* for R-trees [Mam11] (an operation often referred to as *distance browsing*. As in the case of spatial selections, the drawback of using this algorithm is that the IDs of the fetched entities are in random order, preventing the use of efficient operators that rely on interesting orders. On the other hand, when the R-tree is not used, the kNN evaluation needs to perform dictionary lookups to fetch the geometries of all entities that qualify the RDF part of the query and keep track using a heap, the k nearest entities. Figure 3.2e and Figure 3.2f depict two possible plans that correspond to the two options above for the query pattern of Figure 3.1d.

3.4 Encoding the Spatial Dimension

We observe that in most RDF engines, the IDs given to resources or literals at the dictionary mapping do not carry any semantics. Instead of assigning random IDs to resources, we propose to *encode* into the ID of a resource an approximation of the resource's location and geometry that can be used to (i) apply spatial Filter conditions on-the-fly in a query evaluation plan, and (ii) define spatial operators that apply on the approximations.

Figure 3.3b illustrates the *Hilbert* space filling curve, a classic encoding scheme of spatial locations into one-dimensional values. We partition the space using a grid, and order the cells based on the curve. We then divide the ID given to a spatial resource r into two components: (i) the Hilbert order of the cell where r spatially resides occupies the m most significant bits (where $2^{m/2} \times 2^{m/2}$ is the resolution of the grid), and (ii) a *local* identifier which distinguishes r from other resources that reside in the same cell as r. Since the RDF data may also contain resources or literals, which are not spatial, we use a different range of ID values for non-spatial resources with the help of the least significant bit as a flag. In the toy example of Figure 3.3a, the least significant bit (b_0) indicates whether the entity modeled by the ID is spatial ($b_0 = 1$) or non-spatial ($b_0 = 0$), the next 4 bits are used for the local identifier,

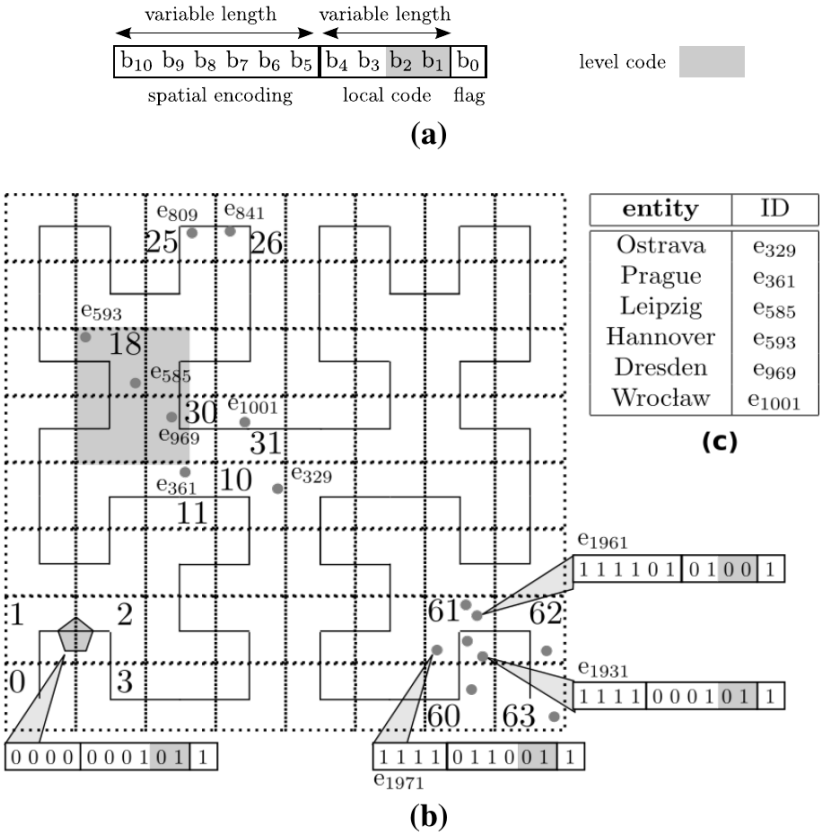

Figure 3.3: Spatial encoding of entity IDs.

and the 6 most significant bits encode the Hilbert order of the cell. For example, in Figure 3.3b, entity e_{1961} is spatial (b_0 is set) and it is located in the cell with Hilbert order 111101 (cell with ID 61), having local code 0100. For a non-spatial resource, bit b_0 would be 0 and the remaining ones would not have any spatial interpretation. Figure 3.3c illustrates which IDs encode the cities of Figure 3.1a.

In the case of a skewed dataset, a cell may overflow, i.e., there could be too many entities falling inside it rendering the available bits for the local codes of entities in it insufficient. In this case, entities that do not fit in a full cell are assigned to the parent of the cell in the hierarchical space decomposition. For instance, consider the data in Figure 3.3b and assume that the cell with ID 61 is full and that the entity e_{1931} cannot be assigned to it. e_{1931} will be assigned to the parent cell, i.e., the square that consists of the cells 60, 61, 62, and 63. This cell's encoding has 4 bits, that is, 2 bits less than its children cells. These 2 bits are now used for the local encoding of entities in it. Intuitively, as we go up in the hierarchy of the grid, each cell can accommodate more entities. An entity that must be assigned to an overflown cell ends in the first non-full ancestor of that cell as we go up in the hierarchy. The $\lceil log_2(m/2) \rceil$ least significant bits of the local code area are reserved to encode the level of the spatially-encoded

cell in the ID (the most detailed level being 0). Here, $m = 6$, hence, 2 bits of the local code are used to denote the level of the cell that approximates each entity.

The encoding we described is also used for arbitrary geometries that may overlap with more than one cells of the bottom level. For example, the polygon at the lower left corner of the grid of Figure 3.3b spans across cells with IDs 1 and 2, thus, it will be assigned to their parent cell, which has a spatial encoding 0000. Due to the variable number of bits given to the spatial approximations, the encoding is also suitable for dynamic data (i.e., inserted entities that fall into overflown cells are given less accurate approximations).

The most important benefit of the spatial encoding is that the (approximate) evaluation of spatial predicates can be seamlessly combined with the evaluation of non-spatial patterns in SPARQL. For example, spatial Filter conditions included in a query which are bound to entity variables (for example, $?s$ hasGeometry $?g$, Filter WITHIN ($?g$, "POLYGON(...)") can be evaluated on-the-fly at any place in the evaluation plan where the entity variable (e.g., $?s$) has been instantiated, by decoding the IDs of the instances. Note that the spatial mapping is only approximate (based on the conservative grid approximation of the spatial locations); by applying a spatial predicate on the approximations (i.e., cells) of the entities, false hits may be included in the results, which need to be verified. Still, for many entities, the spatial approximation suffices to confirm that they are definitely included (or not) in the query result. This way, random accesses for retrieving their exact geometries are avoided.

A side-benefit of using a Hilbert-encoded grid to approximate the object geometries is that by counting the number of resources in each cell (counting is already performed by the mapping scheme), we can have a spatial histogram to be used for selectivity estimation in query optimization (this issue will be discussed in detail in Section 3.6). SRX uses the encoding we described to accelerate queries with spatial predicates as shown in the next section.

3.5 Query Evaluation

We now show how the encoding scheme of SRX further extends the basic framework presented in Section 3.3 to apply efficient spatial filters directly on the entities IDs and reduce the number of dictionary lookups as well as the number of expensive spatial operations on the actual geometries.

All operators we describe in this section evaluate the spatial predicates in two phases: first, by applying the spatial predicate on the IDs of the entities (filtering phase) and, second, by fetching the actual geometries only for the results that could not be verified in the first phase. In general, the sooner we apply the on-the-fly filtering

the better because it does not incur any I/O cost and its CPU cost is negligible[3]. For spatial range and join predicates, the on-the-fly filtering can be done early: after each non-spatial operator that instantiates entity variables, which also appear in a WITHIN or DISTANCE predicate, the condition is applied to the spatially encoded IDs of the entities. In such cases, after applying the filter, we also append a *verification bit* (or vbit) to the tuples that pass the filter. This bit is used in the second phase as follows: if, for a tuple, the verification bit is 1, the tuple is guaranteed to qualify the corresponding spatial predicate (no verification is required). Yet, if the bit is 0, it is unknown at this point whether the exact geometries of the entities in the tuple qualify the spatial predicate and so they cannot be pruned based on their spatial approximations encoded in their IDs. By the end of processing all non-spatial query components, for tuples having their vbits 0, the system fetches the exact geometries of the involved entities and perform verification of the spatial Filter conditions.

3.5.1 Spatial Range Filtering

Spatial range queries bind a pattern variable to geometries that are spatially restricted by a range. As an example, consider again the query depicted in Figure 3.1b. Our encoding sche-me allows the filtering phase of the spatial range query to be performed on-the-fly while scanning the indices, as illustrated by the evaluation plan of Figure 3.4. The plan searches the OPS and PSO indexes in order to fetch and merge-join ($?s = ?s'$) the two lists that qualify patterns $?s$ cityOf Germany, $?s'$ hosted $?o$, i.e., the plan follows the logic of the plan shown in Figure 3.2b. Taking advantage of the spatial encoding, before the merge-join, the plan of Figure 3.4 applies the spatial filter for ($?s$ hasGeometry $?g$, WITHIN($?g$,"POLYGON (...)")) on the instances of $?s$ that arrive from scanning the OPS and PSO indexes; a vbit is appended to each survived tuple, to be used by the next operators. In this example, assume that the spatial entities and the spatial range (i.e., "POLYGON (...)") are the points and the shadowed range, respectively, shown in Figure 3.3b. Entities e_{809} and e_{841} are filtered out from the left scan, because they are not within the cells that intersect the query spatial range. Entity e_{969} survives spatial filtering, but we cannot ensure that it qualifies the spatial range predicate either, because its cell-ID is not completely covered by the spatial query range; therefore the vbit for the tuples that involve e_{969} is 0. On the other hand, the vbit for tuples containing e_{585} or e_{593} is 1 as their cell-ID is completely covered by the spatial range. Therefore, after the merge-join, we only have to fetch and verify the geometry of e_{969}. Range filtering is applied at the bottom of query plans, after each index scan that contains a respective spatial variable.

[3]Most spatial predicates, when translated to the grid-based approximations of the encoding, involve distance computations and/or cheap geometry intersection tests.

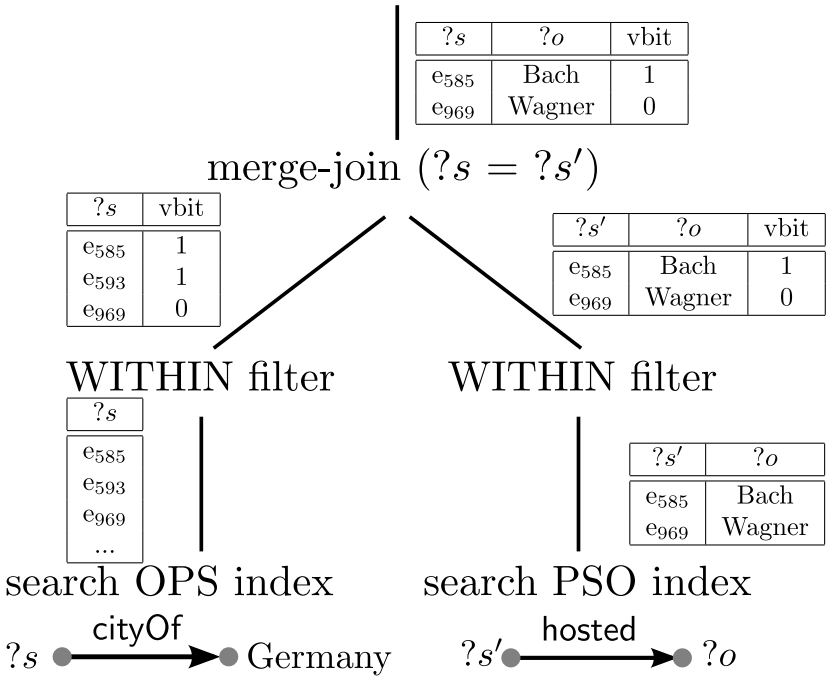

Figure 3.4: Plan for the query of Fig. 3.1b.

3.5.2 Spatial Join Filtering

Similar to spatial range selections, the filtering phase for binary spatial join predicates can also be applied on-the-fly, as soon as the IDs of candidate entity pairs are available. As an example, consider the join query depicted in Figure 3.1c. A possible query evaluation subplan is given in Figure 3.5, which follows the flow of the plan shown in Figure 3.2d; however, the plan of Figure 3.5 applies the spatial join filter (i.e., the distance filter) early. By the time the candidate pairs ($?s'_1$, $?s_2$) are fetched by the index scan on PSO, the filter is applied so that only the pairs of entities that cannot be spatially pruned are passed to the next operator. Assume that the pairs that qualify $?s'_1$ sisterCityOf $?s_2$ are as shown at the right-bottom side of Figure 3.5, above the search PSO index operator. Assume that the distance threshold (i.e., 300km) corresponds to the length of the diagonal of each cell in Figure 3.3. After applying the distance spatial filter on all ($?s'_1$, $?s_2$) pairs produced by the PSO index scan, the pairs that survive are (e_{585}, e_{593}), (e_{969}, e_{1001}) and (e_{969}, e_{329}). However, only entities e_{585} and e_{593} are guaranteed to be within ϵ distance as they belong to same cell; thus, the vbit for pair (e_{585}, e_{593}) is 1. When the pairs are merge-joined ($?s_1 = ?s'_1$) with the results of the OPS index-scan on the left (for $?s_1$ cityOf Germany), the vbits of qualifying tuples are carried forward.

In contrast to the range filter that always appears at the bottom level of the operator tree, distance join filtering can be applied on any intermediate relation that

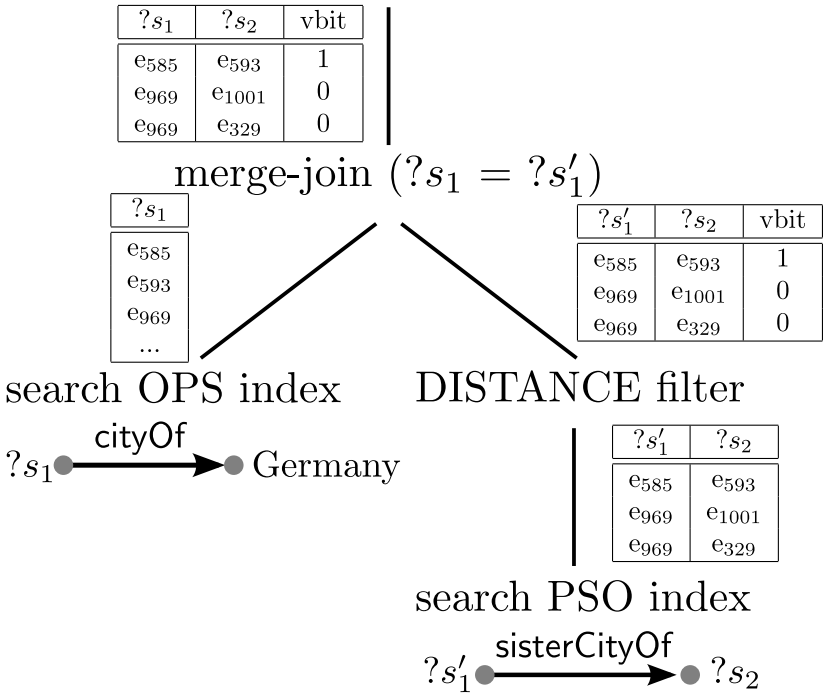

Figure 3.5: Plan for the query of Fig. 3.1c.

contains two joined spatial variables. This case is possible when two relations are first joined on attributes other than the spatial entities. In Section 3.6.1, we show how the query optimizer can identify all pairs of spatially joined variables in a query, for which distance join filtering can be applied; here, we only gave an example with a pair coming from an index scan.

3.5.3 Spatial Merge Join on Encoded Entities

In this section, we propose a *spatial merge join* (SMJ) operator that applies directly on the spatial encodings (i.e., the IDs) of the entities from the two join inputs. SMJ assumes that both its inputs are sorted by the IDs of the spatial entities to be joined. Like the spatial filters discussed above, this algorithm only produces pairs of entities for which the exact geometries are likely to qualify the spatial join predicate (typically, a DISTANCE filter). Again, a verification bit is used to indicate whether the join condition is definitely qualified by a pair. Besides using the spatially encoded IDs of the entities, SMJ takes advantage of and preserves the ID-based sorting of its inputs. Thus, the algorithm does not break the pipeline within the operator tree, as any other spatial join algorithm would. Note that SMJ is a binary join algorithm that takes two inputs, while the filtering technique discussed in Section 3.5.2 takes a single input of candidate join pairs and merely applies the join condition on the entity-ID pairs on-the-fly.

Similarly to a classic merge join algorithm, SMJ uses a buffer B_R to cache the streaming tuples from its right input R. For each entity e_l read from the left input L, SMJ uses the ID of e_l to compute the minimum and maximum cell-IDs that could include entities e_r from R, which could possibly pair with e_l in the join result, based on the given DISTANCE filter. SMJ then keeps reading tuples from input R and buffering them into B_R, as long as they are likely to join with e_l. As soon as B_R is guaranteed to contain all possible entities that may pair with e_l, SMJ computes all join results for e_l and discards e_l (and potentially tuples from B_R).

We now provide the details of SMJ. The algorithm is based on the (on-the-fly and on-demand) computation of four cell IDs for each entity e based on e's ID. First, *minNeighborID* and *maxNeighborID* are the minimum and maximum cell-IDs that could include entities that pair with e in the join result, respectively. To compute these cells, we have to expand e's cell based on the distance join threshold and find the minimum and maximum cell-ID that intersects the resulting range. For example, consider entity e_{841} contained in cell with ID 26 in Figure 3.3b and assume that the join distance threshold equals the diagonal length of a cell. For this entity, *minNeighborID*=18 and *maxNeighborID*=39. Second, *minChildID* and *maxChildID* correspond to the minimum and maximum cell-IDs that have a common non-empty ancestor (in the hierarchical Hilbert space decomposition) with the cell of e. For entity e_{841} which has only empty ancestors, the *minChildID* and *maxChildID* are both 26, that is, the cell ID of e_{841}. For e_{1931}, the *minChildID* and *maxChildID* are 60 and 63 respectively because e_{1931} is assigned to a cell at the first level of the grid.

At each step, the distance join is performed between the current entity e_l from the left input and all entries in B_R. After reading e_l, SMJ reads entries e_r and buffers them into B_R and stops as soon as e_r's *minChildID* is greater than the *maxNeighborID* of e_l; then we know that we can join e_l and all entities in B_R and then discard e_l, because any unseen tuples from R cannot be included within the required distance from e_l.[4] For example, consider the buffered inputs of Figure 3.6 that have to be joined. The *maxNeighborID* of the first entity e_{585} on the left is smaller than the *minChildID* of entry e_{1931}, therefore e_{585} cannot be paired with entries after e_{1931} (that are guaranteed to have *minChildID* greater than the *maxNeighborID* of e_{585}).[5] Thus, for any e_l, we only need to consider all entities in R before the first entity having *minChildID* greater than the *maxNeighborID* of e_l.

After e_l has been joined, it is discarded. At that point we also check if buffered

[4]Recall that the inputs are sorted by ID and that entities may be encoded at different granularities due to data skew or geometry extents. Therefore, using the cell-ID of e_r alone is not sufficient and we have to use the *minChildID* of e_r.

[5]The fact that the entities arrive from the inputs sorted by their IDs guarantees that they are also sorted based on their *minChildID*s.

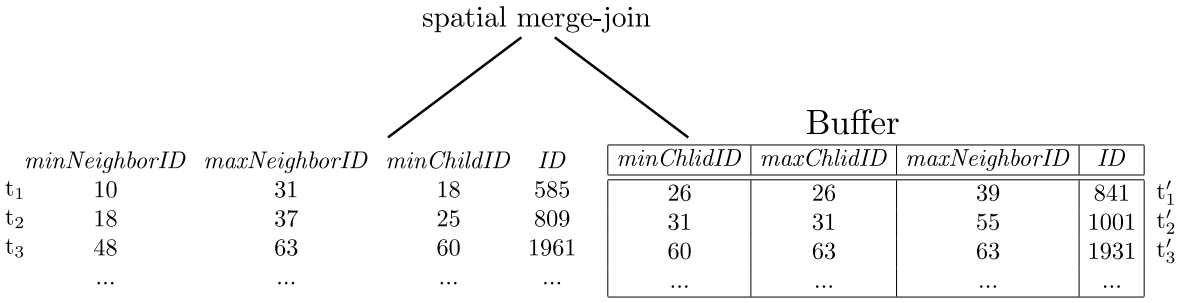

Figure 3.6: Example of SMJ.

tuples in B_R can also be removed. In order to decide this, we use *maxNeighborID* of each entity on the right. In case this is smaller than the *minChildID* of the next entity in L, then the right entry can be safely removed from the buffer without losing any qualifying pairs. Below, we give a pseudocode for SMJ.

Algorithm: SMJ
Input : Two join inputs L and R; a distance threshold ε
Output : Grid-based spatial distance join of L and R

```
1 Initialize (empty) buffer B_R;
2 e_r = R.get_next(); add e_r to B_R;
3 while e_l = L.get_next() do
4     Prune from B_R all tuples e_r such that e_r.maxNeighborID <
      e_l.minChildID;
5     while e_l.maxNeighborID ≥ e_r.maxChildID do
6         e_r = R.get_next(); add e_r to B_R;
7     join e_l with all tuples in B_R and output results to the next
      operator;
```

We now discuss some implementation details. First, the required *min/maxNeighborID* and *min/maxChildID* for the entries are computed fast on-the-fly by simple operations. In particular, *min/maxChildID*s are computed by shifting (or masking) bits to keep only those most significant bits that encode the cell ID at a particular level of the grid (cf. Section3.4). For the neighbor IDs, we rely on the id-to-offset and offset-to-id Hilbert transformations as follows. First, we use e's ID and the (normalized) distance threshold ϵ to identify the offsets of the bottom-level cells that must be examined. Then, we transform the offsets back to the corresponding cell IDs, and we use the latter to compute the minimum and maximum entity IDs by masking bits in the local code (i.e., the least significant bits - cf. Section 3.4). Second, for joining an entity e_l from L, we scan through the qualifying entities of B_R and compute their grid-based distances to e_l, but only for entities whose *minChildID-maxChildID* range overlaps with the *minNeighborID-maxNeighborID* range of e_l; this is a cheap filter

used to avoid grid-based distance computations. Finally, we buffer all tuples that have the same entity ID (in either input). For such a buffer, we perform the join only once but generate all join pairs.

3.5.4 Spatial Hash Join on Encoded Entities

If either of the two inputs of a spatial join is not ordered with respect to the joined entities, SMJ is not applicable. In this case we can still use the IDs of the joined entities to perform the filter step of the spatial join. The idea is to apply a *spatial hash join* (SHJ-ID) algorithm (similar to that proposed in [LR96]) using the approximate geometries of the entities taken from their IDs.[6] SHJ-ID simply uses the existing assignment of the entities to the cells of the grid (as encoded in their IDs) and considers each such cell as a distinct bucket. The only difference from a typical spatial hash join algorithm is that in the bucket-to-bucket join phase, we have to consider all levels of the encoding scheme. So, each bucket from the left input, corresponding to a cell c, is joined with all buckets from the right input which correspond to all cells that satisfy the DISTANCE filter with c. The output of SHJ-ID is verified as soon as the geometries of the candidate pairs are retrieved from disk.

3.5.5 Spatial kNN on Encoded Entities

kNN predicates are evaluated differently from WITHIN and DISTANCE predicates in that no early spatial filtering or verification bits are utilized. We introduce two kNN operators that make use of the encoding: one for handling entities whose IDs come from the previous operator in a random order (Section 3.5.5.1), and a second one that exploits ordering (Section 3.5.5.2) and, thus, can be used efficiently in combination with other order-preserving operators. Both operators are applied in a pipelined fashion at the root of the operator tree (i.e., on the output of the previous operators) and are inspired by the work in [MHP05]. The difference compared to previous kNN operators is the integration with the multi-level encoding scheme of Section 3.4. This integration enables us to (i) compute approximate distances using arithmetic operations on the entity IDs, and (ii) leverage the interesting orders preserved by previous operators in the query plan to reduce random I/Os and improve performance. Random I/Os are common in index-based kNN algorithms from Section 3.3, which we compare with our approach in Section 3.8.2.

[6] Recall that the actual geometries of the entities have not been retrieved yet; otherwise, SHJ [LR96] would be used (see Section 3.3).

3.5.5.1 kNN on Unsorted Entity IDs

The logic of first kNN operator is given in Algorithm KNN-Unsorted-Input. The operator takes as input a point p (the one specified in the Filter clause of the query) along with an iterator I on the tuples coming from the previous operator in the query plan. Let t be a tuple in I and e be the ID of the spatial entity in t that is used in the evaluation of the kNN predicate. The operator uses two priority queues Q_1 and Q_2 to keep tuples ordered in ascending Euclidean distance of e from p's actual geometry: in the former queue, the distance has been calculated based on e's cell whereas in the latter based on e's actual geometry.

Algorithm: KNN-UNSORTED-INPUT
Input : Input I from the previous operator; a point p
Output : k tuples from I that satisfy the kNN predicate
Param. : The number k

let Q_1, Q_2 be two priority queues;
$lastDist = \infty$;
while t = *I.get_next()* **do**
    POPULATE_$Q_1(t, p)$;
while Q_1 *is not empty* **do**
    $(t, minDist) = Q_1$.pop();
    if $minDist \geq lastDist$ **then**
        break;
    POPULATE_$Q_2(t, p, lastDist, k)$;
return all t tuples in Q_2;

Function: POPULATE_Q_1(t: TUPLE, p: POINT)
let e be the ID of the spatial entity in tuple t;
let c be the grid cell e belongs to; `//extracted from e`
if c *is the last-level cell* **then**
    $minDist = 0$;
else if c *is an upper-level cell* **then**
    find the bottom-level child cell of c, let c_b, which is the nearest to the given point p;
    set $minDist$ to the minimum distance of c_b from p;
else
    `//c is a bottom-level cell`
    set $minDist$ to the minimum distance of c from p;
Q_1.push($(t, minDist)$); `//keep in ascending minDist`

Function: POPULATE_Q_2(t: TUPLE, p: POINT, $lastDist$: FLOAT, k: INTEGER)
let e be the ID of the spatial entity in tuple t;
retrieve e's geometry from dictionary and compute the exact distance between e and p, let $exactDist$;
Q_2.push($(t, exactDist)$); `//keep in ascending exactDist`
if $|Q_2| = k$ **then**
    set $lastDist$ equal to $exactDist$ of the k-th entry in Q_2;

The evaluation proceeds in two phases. First, the operator pulls all tuples from the previous operator in the query plan and populates Q_1 (*lines* 3-4). The function Populate-Q_1 uses the multi-level encoding scheme to compute the minimum distance between e's cell and p ($minDist$) and keeps entries in ascending $minDist$. Note that $minDist$ is an approximation of the exact distance between the entity e and the point p; the latter is computed only in the second phase of the algorithm (*lines* 5-9) where the operator starts draining Q_1 to populate Q_2. Specifically, each time an entry is popped from Q_1, the exact geometry of e is retrieved via a dictionary lookup and the tuple t is pushed into Q_2 using now the exact distance between e and p ($exactDist$ in function Populate-Q_2). The draining of Q_1 stops when the algorithm pops an entity e whose minimum possible distance from p is at least equal to the current exact distance of the k-th element in Q_2 (*lines* 7-8 in KNN-Unsorted-Input).

In contrast to Q_2 that holds at most k tuples from the input I, Q_1 is populated with all tuples from I in the first phase of KNN-Unsorted-Input. The intuition behind this strategy is to sort the entities based on their cells and use this ordering to minimize the expensive geometry lookups in the second phase. Since the IDs of the spatial entities come out of order and each next entity may fall anywhere in the grid, Q_1 must store all input tuples from I. This increases the memory footprint (and the latency) of KNN-Unsorted-Input significantly when the RDF part of the query is not selective. When the spatial entities come in order, we can tackle this problem with the kNN operator we describe next.

3.5.5.2 kNN on Sorted Entity IDs

The second kNN operator we introduce uses an adaptation of the CPM technique from [MHP05] and its logic is given in Algorithm KNN-Sorted-Input. The core idea here is to exploit the ordering of entities and avoid draining the iterator I, i.e., pulling the whole output from the pervious operator in the query plan. To do so, the evaluation proceeds in "zones" starting from the (bottom-level) cell of the point p in the Filter condition. Each such zone consists of four rectangles (up, $down$, $left$, $right$), which in turn consist of bottom-level grid cells and form a "circular" area around p's cell, as shown in Figure 3.7a. The operator follows the same steps as in CPM and extends the original technique to (i) work with our multi-level encoding scheme, and (ii) pull tuples from the input gradually, as it examines the zones.

First, the operator identifies the bottom-level cell c_p that contains the given point p (*line* 3). It then computes the maximum ID among all spatial entities that might fall in c_p (*line* 4). This is done in function Compute-Limit, which simply returns the maximum spatially encoded ID that exists in the database and falls either in c_p or in

```
Algorithm: KNN-SORTED-INPUT
Input    : Input I from the previous operator; a point p
Output   : k tuples from I that satisfy the kNN predicate
Param.   : The number k
1  let Q1, Q2 be two priority queues;
2  lastDist = ∞;
3  let c_p be the bottom-level cell that contains p;
4  limit = prevLimit = COMPUTE_LIMIT(c_p);
   //load first round of input data into Q1
5  READ_NEXT(I, limit, p);
6  for each rectangle r in the first zone around c_p do
7      compute the minimum distance of r from p, let minDist;
8      Q1.push((r, minDist));      //keep in ascending minDist
9  while Q1 is not empty do
10     (entry, minDist) = Q1.pop();
11     if minDist ≥ lastDist then
12         break;
13     if entry is a tuple t with a spatial entity then
14         POPULATE_Q2(t, p, lastDist, k);
15     else
           //entry is a rectangle r
16         find the maximum bottom-level cell ID c_m falling in r;
17         limit = COMPUTE_LIMIT(c_m);
18         if limit > prevLimit then
19             prevLimit = limit;
               //load next round of input data
20             READ_NEXT(I, limit, p);
21         let r' be the next zone rectangle in the direction of r;
22         set minDist to the minimum distance of r' from p;
23         Q1.push((r', minDist));      //in ascending minDist
24 return all t tuples in Q2;

Function: READ_NEXT(I: ITERATOR, limit: INTEGER, p:
          POINT)
1  while t = I.peek() do
2      let e be the ID of the spatial entity in tuple t;
3      if e ⩽ limit then
4          t = I.get_next();    //Pull happens at this point
5          POPULATE_Q1(t, p);
6      else break;

Function: COMPUTE_LIMIT(c_id: BOTTOM-LEVEL CELL)
1  let c_i be the parent cell of c_id at the i-th grid level;    //c_0 ≡ c_id
2  let m_i be the maximum encoded spatial entity ID in c_i;
3  return max_{0≤i≤13} m_i;      //14 grid levels with 32-bit IDs
```

a parent cell of c_p[7]. Compute-Limit is a very cheap function that requires only a few lookups in the grid statistics kept in memory. The returned ID serves as an upper *limit* to bound the number of tuples pulled from I when populating Q_1 in function Read-Next. At each step of the algorithm, only the tuples of the current examined zone (initially p's cell) must be pulled from the input. To do so, the operator first peeks into I (*line* 1 in Read-Next) to check the entity ID e of the next tuple and decide if this ID is at most equal to the *limit*; if so, this means that e's actual geometry might fall in the examined zone, thus, the tuple is pulled from I (*line* 4 in Read-Next) and the algorithm continues with peeking the next tuple; otherwise none of the following entities fall in the examined zone, thus, the algorithm exits the loop (*line* 6 in Read-Next), computes the distance of each rectangle in the first zone from p, as in original CPM, and adds the respective entry to Q_1 (*lines* 6-8 in KNN-Sorted-Input).

Then, the operator continues similarly to KNN-Unsorted-Input, i.e. it starts pulling from Q_1 (*line* 9) to populate Q_2 with the exact distances. The termination condition in *lines* 11-12 is the same as in KNN-Unsorted-Input. The only difference here is that, whenever the algorithm encounters a new rectangle r in Q_1, the latter is used to update (i.e. increase) the *limit* and pull the required additional tuples (if any) from the input I (*lines* 16-20). After that, the algorithm also expands the search space to the next zone (*lines* 21-23) by adding to Q_1 the rectangle of the next zone that is in the same direction (*up*, *down*, $left$, $right$) as r with respect to p's cell. This is CPM's actual control flow and the correctness of the computation relies on the correctness of the original method (cf. Lemma 3.1 in [MHP05]). As a final comment, KNN-Sorted-Input is designed to pull as few tuples from I as possible (it exhausts I only in the worst case, i.e. when *limit* is greater than all spatial IDs in I) and, thus, tends to perform much better than KNN-Unsorted-Input, as we show in Section 3.8.

Example 1. *Consider the grid of Figure 3.7 where a_i denotes a spatial entity encoded at the bottom level and b_i denotes a spatial entity encoded at the exact next level. For simplicity, assume that there are no entities at higher levels. Assume also that each bottom-level cell has a side of* 1 *metric unit. Consider a query point p falling in cell* 28 *and let $k = 2$. Algorithm KNN-Sorted-Input first pulls from the input I and inserts into Q_1 all tuples with spatial entities that may fall in p's bottom-level cell, i.e. all tuples from I before a tuple with a spatial entity ID greater than $b_2 = 907$ (recall that tuples in I are in ascending spatial entity ID order). Then, the algorithm proceeds with the insertion of the first zone rectangles L_1, R_1, U_1, D_1 resulting in a priority queue $Q_1 = \{(a_4, 0), (b_1, 0), (b_2, 0), (a_3, 0.1), (U_1, 0.1), (R_1, 0.2), (L_1, 0.8), (D_1, 0.9), (a_2, 2.8), (a_1, 4.9)\}$. Numbers in Q_1 depict the Euclidean distance of the respective entry (grid cell or zone*

[7]In case there are no spatial entities in the database falling in c_p or one of its parent cells, then as *limit* we use the first free (i.e. the minimum) spatial ID for an entity in c_p.

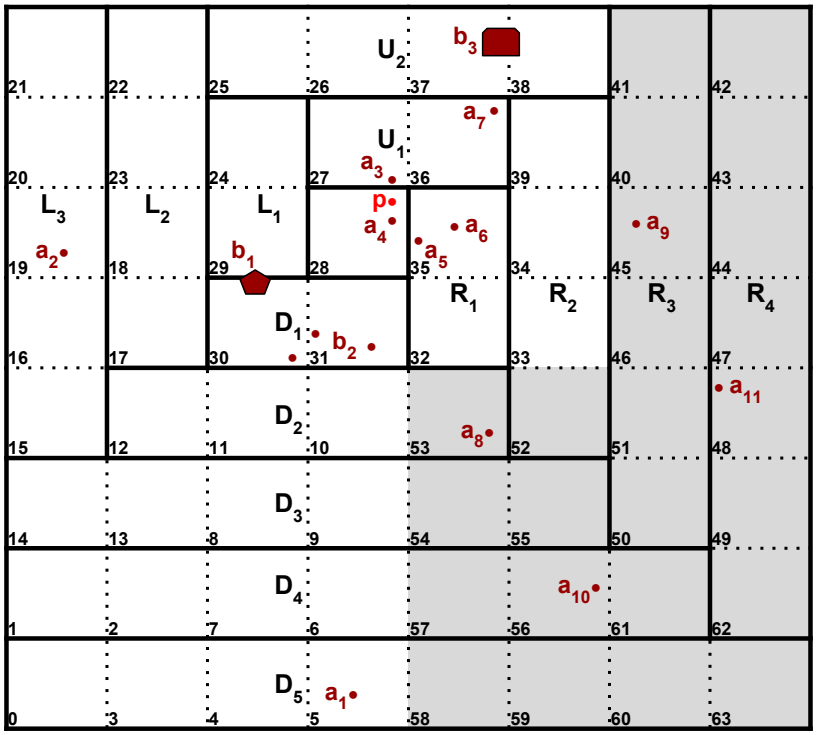

entity	ID (binary) - (decimal)
a_1	000101|0000|1 - 161
a_2	010011|0000|1 - 609
a_3	011011|0000|1 - 865
a_4	011100|0000|1 - 897
a_5	100011|0000|1 - 1121
a_6	100011|0100|1 - 1129
a_7	100100|0000|1 - 1153
b_1	0111|000001|1 - 899
b_2	0111|000101|1 - 907
b_3	1001|000001|1 - 1155

Figure 3.7: An example grid **(a)** with 64 cells at the bottom level (11-bit encoding) ordered according to the Hilbert curve and organized in CPM zones (L_i, R_i, U_i, D_i) around a query point p in cell 28. The entity IDs are shown on the right **(b)** in binary and decimal format.

rectangle) from p's geometry. At the next step, the algorithm starts pulling entries from Q_1 to populate Q_2. When it reaches the first rectangle entry U_1, it computes the new limit $= b_3 = 1155$. At that point, we have $Q_1 = \{(R_1, 0.2), (a_5, 0.2), (a_6, 0.2), (a_7, \sqrt{0.05}), (b_3, \sqrt{0.05}), (L_1, 0.8), (D_1, 0.9), (U_2, 1.1), (a_2, 2.8), (a_1, 4.9)\}$ and $Q_2 = \{(a_3, 0.12), (a_4, 0.21)\}$. Distances in Q_2 have now been computed using the Euclidean distance between the entry's actual geometry and the point p. The algorithm then pops entry R_1, which results in updating Q_1 only with $(R_2, 1.2)$, and terminates when it pops a_7 whose $minDist = \sqrt{0.05}$ is less than the $lastDist = 0.21$ of the previous entry a_4 popped from Q_1. So, $Q_2 = \{(a_3, 0.12), (a_4, 0.21)\}$ and the entries a_3, a_4 are returned.

3.6 Query Optimization

In this section, we describe our extensions to the query optimizer of RDF-3X, so as to take into consideration (i) the R-tree index and the query evaluation plans that involve it (Section 3.3) (ii) the query evaluation techniques described in Section 3.5 for spatial range and join queries. The encoding-based kNN operators (Section 3.5)

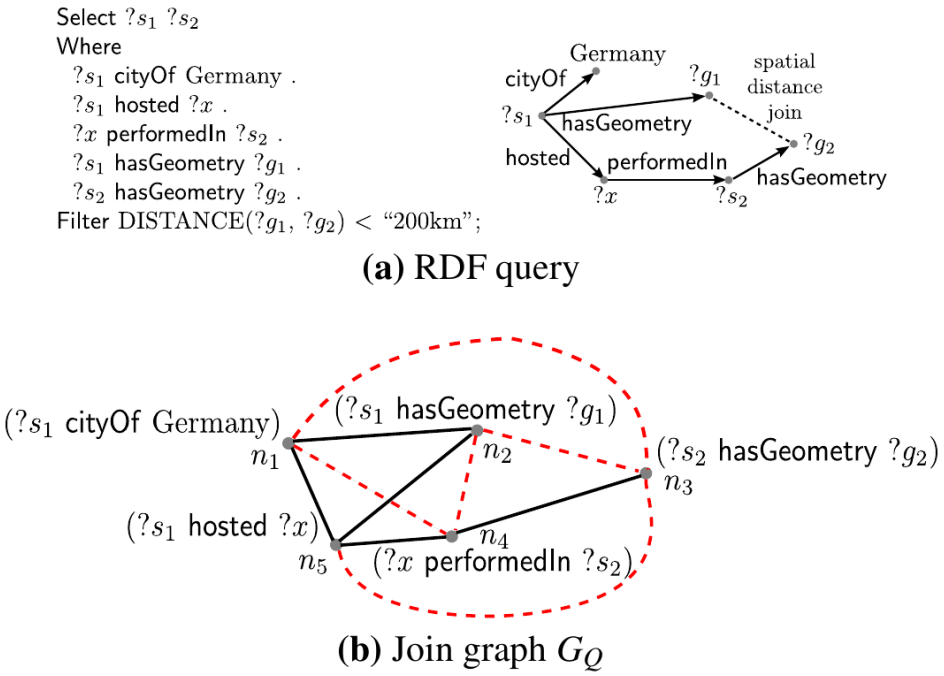

Figure 3.8: Augmenting a query graph.

do not affect query optimization as they are applied after the RDF part.

3.6.1 Augmenting the Query Graph

Consider the query depicted in Figure 3.8a. This query includes a spatial distance join between the geometries ?g_1 and ?g_2. The filtering phase of the spatial distance join can also be applied on the variables ?s_1 and ?s_2, using their IDs, as explained in Section 3.5.3. We call such variables *spatial variables*:

Definition 1. (Spatial Variable) *A variable ?s_i at the subject position of a triple pattern ?s_i hasGeometry ?g_i that appears in the Where clause of a query Q is called a spatial variable. We say that two spatial variables ?s_i, ?s_j $(i \neq j)$ are joined iff ?g_i and ?g_j appear in the same* DISTANCE *predicate in the Filter clause of Q.*

Spatial variables are identified in the beginning of the optimization process and they are used to augment the initial join query graph G_Q with additional join edges that correspond to the filtering step of the spatial operation. For example, the initial G_Q for the RDF query of Figure 3.8a is the graph shown in Figure 3.8b, considering solid lines only as edges; the nodes of G_Q are the triples of the RDF query graph and there is an edge between every pair of nodes that have at least one common variable. An ordering of the edges of G_Q corresponds to a join order evaluation plan.

The procedure of augmenting G_Q is given in Algorithm Augment. First, we identify all spatial variables in the query Q; in our example, ?s_1 and ?s_2. Note that a spatial

variable $?s_i$ may also appear either as subject or object in triple patterns, other than $?s_i$ hasGeometry $?g_i$. The second step is to collect all pairs of nodes in G_Q that include at least one spatial variable. In the example of Figure 3.8b, all nodes include one of $?s_1$ and $?s_2$. Then, for each pair of nodes (n_i, n_j), where $n_i \neq n_j$, such that n_i includes $?s_1$ and n_j includes $?s_2$, we either add a new edge (if no edge exists between n_i and n_j) or we add the spatial join predicate (e.g., DISTANCE($n_i.s_i$, $n_j.s_j$) < "200km") in the set of predicates modeled by the edge between these two nodes (these are equality predicates for their common variables). For instance, n_4 and n_5 in the initial G_Q are connected by an edge with predicate $n_4.x = n_5.x$, but after the augmentation the predicates on this edge are $n_4.x = n_5.x$ *and* DISTANCE($n_4.s_2, n_5.s_1$) < "200km". This implies that the optimizer will consider two possible subplans for joining n_4 with n_5. The first one will first perform the equality join on x and then evaluate the distance predicate whereas the second subplan will first perform the filtering phase of the spatial join on (s_1, s_2) and then apply the equality on x. In the augmented G_Q for our example (Figure 3.8b) the additional edges are denoted with dashed lines.

Algorithm: AUGMENT
Input : A query Q and its initial join query graph G_Q
Output : An augmented query graph G_Q for Q

```
1  Identify all triples in Q that include at least one spatial variable
   in as subject or object. Each such triple corresponds to a node
   of G_Q;
2  for each pair ?s_i, ?s_j of joined spatial variables do
3      for each pair of nodes (n_i, n_j) ∈ G_Q, such that n_i includes
       ?s_i and n_2 includes ?s_j do
4          if there is no edge in G_Q between n_i and n_j then
5              Add a new edge denoting the filtering phase of
               the spatial join of ?s_i and ?s_j;
6          else
7              Add the filtering phase of the spatial join
               predicate of ?s_i and ?s_j in the predicate list of
               edge between n_i and n_j;
8  For each spatial variable ?s appearing in a WITHIN predicate,
   add WITHIN(?s, GEOMETRY) to filtering conditions of Q;
9  For each pair of spatial variables ?s_i, ?s_j (i ≠ j) joined in Q,
   add DISTANCE(?s_i, ?s_j) Op ε to filtering conditions of Q;
10 return G_Q;
```

If a query Q also includes WITHIN predicates, in the end of the augmentation procedure and for each spatial variable $?s$ whose geometry $?g$ participates in a WITHIN predicate, we add a condition of the form WITHIN($?s$, GEOMETRY) to the set of filters of Q, so that this filter can be applied in any (intermediate) relation that

Table 3.1: Spatial join scenarios in optimal plan build.

Case	Algorithm(s) to Consider
L and R sorted on entity IDs	SMJ (Section 3.5.3)
L and R results of ($?s_i$ hasGeometry $?g_i$)	SMJ or R-tree Join [BKS93]
L sorted on entity IDs R result of a pattern ($?s_2$ hasGeometry $?g_2$)	SMJ (Section 3.5.3), SISJ [MP03], or Index Nested Loops
L unsorted R result of a pattern ($?s_2$ hasGeometry $?g_2$)	SHJ-ID (Section 3.5.4), SISJ [MP03] or Index Nested Loops
L and R unsorted	SHJ-ID, SHJ [LR96] or Nested Loops

contains the spatial variable $?s$. Note that this condition differs from the existing spatial condition WITHIN($?g$, GEOMETRY) in that it includes the spatial variable $?s$ and not the geometry variable $?g$. Similarly, for each pair (s_i,s_j) of joined spatial variables, we add the corresponding spatial join condition to Q's existing filters, so that this filter can be applied on every (intermediate) relation that includes both the spatial variables s_i and s_j. Overall, the final augmented G_Q may include more edges than the initial G_Q, additional predicates in the edges, and general spatial filters for variables or pairs of variables that can be applied on intermediate results of subplans.

3.6.2 Spatial Join Operators

Our plan generator can place a spatial join operation at every level of the operator tree. Table 3.1 summarizes all possible cases of the L and R inputs of a spatial join (if L and R are swapped there is no difference because the join is symmetric). The right column includes the join algorithms, which the plan generator of the optimizer considers in each case.

Depending on whether the inputs of the join are indexed, sorted, or unsorted, there are different algorithms to be considered. If both join inputs come ordered by the IDs of the spatial entities to be joined, then SMJ (Section 3.5.3) is the algorithm of choice. In the special case where both inputs are the results of $?s_i$ hasGeometry $?g_i$ patterns applied on the entire set of triples, besides of applying SMJ on the SPO (or SOP) index, we can apply an R-tree self-join [BKS93] on the R-tree index. When just one of the inputs, e.g., R, is a result of a $?s_i$ hasGeometry $?g_i$ pattern, besides SMJ, we can also apply the SISJ algorithm [MP03]. In this case, we also consider Index Nested Loops join using the R-tree, by applying one spatial range query for each tuple of the other input, e.g., L. This should be cheap only when L is very small. Finally, when either L or R are unsorted, SMJ is not applicable and we can use SHJ-ID on the entity IDs (Section 3.5.4), or either SISJ or SHJ depending on whether one of the inputs is a direct result of a $?s_i$ hasGeometry $?g_i$ pattern or not. We also consider Index Nested Loops or Nested Loops, if one of the inputs is too small.

3.6.3 Spatial Query Optimization

We extend the query optimizer of RDF-3X to consider all possible spatial join cases and algorithms outlined in Section 3.6.2. In addition, the optimizer considers the case of performing a spatial selection Filter using the R-tree (see Section 3.3). The optimizer also considers any spatial selection and join filter conditions that are applied on-the-fly; i.e., in plans where the non-spatial query pattern components are evaluated first, our optimizer uses spatial query selectivity statistics to estimate the output size of these components *after* the spatial filter is applied on them. Consider for example, the plan of Figure 3.4. The estimated output of the $?s$ hosted $?o$ pattern is further refined to consider the spatial WITHIN filter that follows. In other words, the cardinality of the right input to the merge-join algorithm that follows is estimated using both RDF-3X statistics on the selectivity of $?s$ hosted $?o$ and spatial statistics for the selectivity of WITHIN($?g$,"POLYGON (...)").

3.6.4 Selectivity Estimation

For estimating the selectivity of spatial query components, we use grid-based statistics, similar to previous work on spatial query optimization (e.g., see [MP03]). Specifically, we take advantage of statistics that are obtained by the spatial encoding phase of the entity IDs. For each cell of the grid, defined by the Hilbert order, we keep track of the number of spatial entities that fall inside. The spatial join or selection is then applied at the level of the grid, based on uniformity assumptions about the spatial distributions inside the cells. In addition, we assume independence with respect to the other query components. For example, for estimating the input cardinality of the right merge-join input at the plan of Figure 3.4, we multiply the selectivity of the $?s$ hosted $?o$ pattern with that of the WITHIN($?g$,"POLYGON (...)") filter. In practice, this gives good estimates if the spatial distribution of the entities that instantiate $?s$ is independent to the spatial distribution of all entities.

3.6.5 Runtime Optimizations

RDF-3X uses a lightweight Sideways Information Passing (SIP) mechanism for skipping redundant values when scanning the indexes [NW09]. Consider a merge join, which binds the values of a variable $?s$ coming from two inputs. If the join result is fed to another (upper) merge-join operator that binds $?s$, then the upper operator can use the next value v of its other input to notify the lower operator that $?s$ values less than v need not be computed.

In the case of spatial joins where at least one side comes from a scan in the R-tree (e.g., consider the plan shown in Figure 3.2a), SIP is not applicable since there is

no global order for the geometries in the 2D space. On the other hand, the SMJ algorithm proposed in Section 3.5.3 can use SIP to notify the operators below its left input which is the minimum ID value for the next entity e_l to pair with any entity buffered in B_R. For the spatial hash join, we can also use SIP, by creating a bloom filter for one input, similar to the one RDF-3X constructs for the traditional hash join, and use it to prune tuples from its other input, while scanning the B^+-tree index. A value is pruned if it is not included in the bloom filter.

3.7 Updates

The proposed encoding scheme requires significant changes in the update mechanism of RDF-3X [NW08, NW10a]. Inserting a new spatial entity is straight-forward and requires generating the appropriate ID based on the entity's geometry and the occupancy of the grid. On the other hand, removing or updating the geometry of a spatial entity requires additional care as it might trigger the re-encoding of other spatial entities besides the one being updated. Such re-encodings tend to improve the latency of spatial queries, since entities are "moved" to lower levels of the grid, but incur an overhead during updates because they result in additional triples to be removed and re-inserted with new IDs.

Insert and delete commands in RDF-3X (cf. Section 3.2) are given in batches and are processed in two phases. In the first phase, the triples to insert or delete are resolved via lookups in the dictionary, i.e. they are translated into triples of integer IDs used internally by the system. Updates are not applied directly to the database; instead, the affected triples are first resolved in memory for all updates in the batch using *differential indexes*, which are then synchronized with the base indexes in the second phase. This is a common technique in bulk update processing that aims to minimize I/Os and increase the system throughput. RDF-3X maintains six differential indexes (SPO, SOP, OPS, OSP, PSO, POS), one for each full base index, which are synchronized with both the full and the aggregated base indexes. For example, the SPO differential index is synchronized with the base SPO index, the binary aggregated index SP, and the unary aggregated index S.

SRX integrates the original update mechanism of RDF-3X with the encoding scheme of Section 3.4. To do that, it changes only the first update phase, whereas the index synchronization can be used as is. To simplify the presentation, we distinguish two cases: a) only inserts of new triples, i.e., the subject entity s of the input triple $\langle s, p, o\rangle$ does not exist in the dictionary, b) inserts and deletes of triples whose subject entity already exists in the data. The update process takes as input a batch B of triples annotated with *insert* or *delete*, and updates two in-memory sets of triples tI (to insert) and tD (to delete), which are used to build the differential indexes.

Inserts of new entities. The insertion to the triples set tI is performed similarly to the original RDF-3X update process, but IDs are generated using the modified function Generate-ID. Generate-ID takes as input the entity's URI and a boolean value, which indicates whether the new ID should be spatial ($true$) or not ($false$), i.e., whether the input triple introduces a geometry for the subject entity. Generate-ID is also responsible for updating the dictionary and for tracking the set of new IDs for the current batch B. The set new (initially empty for a batch) contains all IDs that do not exist in the database and is used in the second part of the update algorithm to avoid expensive lookups in the base indexes, as we explain later on. Since, the insertion of new triples only differs from the original RDF-3X process in the creation of the ID, we omit the pseudocode for the sake of brevity.

Updates on existing entities. The pseudocode for the updates on existing entities is given in Algorithm Updates on existing entities. This part handles triples with existing spatial and non-spatial subject entities, and is further split into three sub-parts: one for inserting triples that introduce a geometry for the non-spatial subject (*lines* 5-16), one for inserting triples that do not introduce a geometry (*lines* 17-23), and a last one for deleting triples (*lines* 24-34).

In the first sub-part, when a geometry is introduced for a non-spatial entity, the algorithm generates a new spatial ID s_{new} (*line* 8) and proceeds with updating the in-memory sets tI and tD accordingly. To do so, it first checks if the old subject ID (s_{id}) exists in the set of new IDs for the current batch; if yes, it simply updates the set new along with tI (*lines* 15-16), otherwise it retrieves all affected triples from the database and updates both tI and tD (*lines* 11-14 and 16). The update algorithm also ensures in this case that each entity is associated with *at most one* geometry but these additional checks are omitted here for the sake of brevity. The last two sub-parts of Updates on existing entities follow the original RDF-3X update logic and differ only in the use of new in *lines* 20 and 28 to avoid expensive lookups in the base indexes; these lookups are only performed as last steps in *lines* 22 and 30.

Spatial re-encoding is the task of re-assigning spatial IDs that get released (after geometry deletions) to spatial entities encoded at higher levels of the grid due to overflow. It is an iterative bottom-up process, from lower to higher levels of the grid, which takes place in *line* 34 of Updates on existing entities. The re-encoding function receives the spatial ID of an entity whose geometry is being deleted, replaces this ID with a non-spatial one (the next free even ID), and checks if there is a spatial entity from a higher level that can be re-encoded using the recently released spatial ID. If so, the re-encoding of the spatial entity releases another spatial ID, and the process cascades until no more re-encodings are possible.

Algorithm: UPDATES ON EXISTING ENTITIES
Input : Batch B of triples annotated with $op = \{insert, delete\}$
Output : Sets of triples tI (to insert) and tD (to delete)

```
1  let new be the set of new entity IDs for the current batch B;
2  while t = ⟨s,p,o,op⟩ = B.get_next() do
3      if s ∈ dictionary then
4          let s_id be the ID of s as found in the dictionary;
5          if s_id is not spatial and op = insert and p =
           "hasGeometry" then
               //A geometry is given for s
6              let p_id = FETCH_OR_GEN_ID(p, false);
7              let o_id = FETCH_OR_GEN_ID(o, false);
8              let s_new = GENERATE_ID(s, true);
9              tI = tI ∪ {⟨s_new, p_id, o_id⟩};
10             if s_id ∉ new then
11                 let affected be the set of triples in the
                   database containing s_id as subject or object;
12                 let replace = affected \ tD;
13                 tI = tI ∪ replace;
14                 tD = tD ∪ replace;
15             else new = new \ {s_id};
16             change s_id to s_new in all triples of tI;
17         else if op = insert and p ≠ "hasGeometry" then
               //Both for spatial and non spatial s_id
18             let p_id = FETCH_OR_GEN_ID(p, false);
19             let o_id = FETCH_OR_GEN_ID(o, false);
20             if {s_id, p_id, o_id} ∩ new ≠ ∅ then
21                 tI = tI ∪ {⟨s_id, p_id, o_id⟩};
22             else if ⟨s_id, p_id, o_id⟩ ∉ database then
23                 tI = tI ∪ {⟨s_id, p_id, o_id⟩};
24         else if op = delete and (s_id is spatial or p ≠
           "hasGeometry") then
               //For any valid delete operation
25             if p ∈ dictionary and o ∈ dictionary then
26                 let p_id be the ID of p as found in the
                   dictionary;
27                 let o_id be the ID of o as found in the
                   dictionary;
28                 if {s_id, p_id, o_id} ∩ new ≠ ∅ then
29                     tI = tI \ {⟨s_id, p_id, o_id⟩};
30                 else if ⟨s_id, p_id, o_id⟩ ∈ database then
31                     tD = tD ∪ {⟨s_id, p_id, o_id⟩};
32                 else continue;
33                 if s_id is spatial and p = "hasGeometry"
                   then
34                     re-encode spatial entities;
```

The overall process relies on two thresholds h_1, $h_2 \in [0, 1]$, which define a range $[h_1, h_2]$ on the ratio of assigned to total spatial IDs that a cell can accommodate (fill factor). In particular, a re-encoding process starts when the fill factor of a cell c drops below h_1, and continues as long as (i) there are entities from higher levels to re-encode in c, and (ii) c's fill factor remains below h_2. By the time at least one of these two conditions does not hold, the algorithm continues with examining the parent cells of c (at the next level), and so forth, until it reaches the top level. In the end, all spatial entities have been re-encoded at the lowest possible level such that each cell's fill factor is smaller than h_2. The two thresholds h_1 and h_2 are used to trade off the frequency of re-encodings with the overhead in processing updates, and we discuss the choice of their values in Section 3.8.

3.8 Experimental Evaluation

We compare SRX with the original RDF-3X system [NW08], the latest version of Strabon [KKK12]; version `3.3.2`, and the latest versions of two commercial triple stores with spatial data support, Virtuoso `7.2.5-rc1.3217-pthreads` [Vir] and GraphDB Free `8.6` [Gra] (the successor of OWLIM-SE that we used in [LMBT14]). We implemented SRX in C++ (g++ 8.2.0) and conducted all experiments on a machine with an i7-4930K CPU at 3.40 GHz, a 3.6Tb 7.2K rpm SATA-3 hard disk, and 64GB RAM running Linux Debian (4.18.0-1 amd64). For the Strabon database, we used PostgreSQL `11.2` and PostGIS `2.5` versions, while for the R-tree implementation, we used the open-source SaIL library [HHT05], which we also extended with support for incremental kNN computation (cf. Section 3.3).

3.8.1 Queries Setup

Datasets. We evaluate our system using two real datasets: LinkedGeoData[8] (LGD) and YAGO2s[9] (YAGO). LGD contains user-contributed content from OpenStreetMap project. YAGO is an RDF knowledge base, derived from Wikipedia, WordNet and Geonames. Table 3.2 shows statistics about the sizes of the datasets (including the dictionary and indexes) and the number of entities and geometries in them. The sizes of the input triple files are 2.4GB (LGD) and 18.1GB (YAGO). The R-trees (using 4KB nodes) occupy 160MB and 221MB, respectively. The size of the grid in both datasets is 1.5GB (89M cells in total for all levels). Note that, despite the aggressive indexing, in both cases, we end up with a database size having around double the

[8] https://tinyurl.com/yc4lxqdv
[9] https://tinyurl.com/y7ukhge3

Table 3.2: Characteristics of the real datasets.

Dataset	Triples	Entities	Points	Polygons	Linestrings	Multipoints
LGD (5.1 GB)	15.4M	10.6M	590K	264K	2.6M	0
YAGO (29.8 GB)	205.3M	108.5M	4M	0	0	780K

Table 3.3: Percentage (%) of geometries per grid level.

Level	0 (bottom)	1	2	3	4	5	6	≥ 7
LGD	28.5	21.6	16.9	12.7	8.7	5.4	3.0	3.2
YAGO	50.3	19.2	8.1	4.5	3.0	2.4	1.9	10.6

size of the input files. Regarding the spatial distribution of the entities they include, both datasets are highly skewed, as shown in the Appendix-Chapter 8.

Encoding. We used a grid of 8,192 × 8,192 cells at the bottom level, hence, the maximum number of bits used in an entity's ID to encode its cell-ID is 26. This means that we can have up to 14 levels of spatial approximation. This is the maximum granularity we can achieve when the IDs of the entities are 32-bit integers. Using 64-bit IDs for better spatial approximation is possible, but significantly increases the size of the triple indexes, thus, one should do this only when the total number of entities is greater than 2^{32}. Besides, the grid must be relatively small so that it resides in memory (for selectivity estimation purposes). In our case, the grid size is less than 2GB for both datasets. As shown in Table 3.3, all levels of the grid are used in the encoding, due to data skew and several geometry extents (polygons, linestrings, multipoints); in YAGO many multipoints are not cleaned and have very large MBRs.

Queries. All queries used in our experiments have two parts: (i) an RDF part that can be evaluated by a traditional SPARQL engine and (ii) a spatial part, i.e., a FILTER condition that includes a WITHIN predicate (for spatial range queries), a DISTANCE predicate (for spatial distance joins) or a kNN predicate (for spatial nearest neighbors). The range queries have similar structure to those depicted in Figure 3.1b; we divide them into four classes based on the selectivities of the two parts. Queries belonging to class SL have their RDF part more selective compared to their spatial part and the opposite holds for queries in class LS (S stands for small result, L for large). For queries in classes SS and LL, both parts roughly have the same selectivity. The characteristics of the spatial join queries (denoted by J) and the spatial kNN queries will be discussed in Section 3.8.2. All queries can be found in the Appendix-Chapter 8.

Comparison Measures. We evaluated each query 5 times (both with cold and warm cache) and report their average runtimes that include the query optimization cost (i.e., the time spent by the optimizer to apply the techniques of Section 3.6) and the time spent in the ID-to-string dictionary lookups for the output variables.

System Parameters. RDF-3X does not have its own data cache for the query results; instead, it relies entirely on the OS caching mechanism. The same architectural principle is also adopted in our implementation.[10] When a query is executed for a second time, its optimization and evaluation is performed from scratch, since there are no logs or cached results as in a typical database system. To illustrate the effect of OS caching in the overall response time of the system, we report query evaluation times on warm and cold caches separately.

3.8.2 Queries Comparison

Results on Range Queries. Table 3.4 shows response times for range queries on the LGD dataset. The first three columns of the table show the number of results of the RDF query component only, the spatial component only and the complete query (combined). We first focus on comparing our approach (Encoding) with the basic extension presented in Section 3.3 (Basic) and the original RDF-3X system (Baseline). Basic uses the R-tree to retrieve the entities falling in the given range only for queries where the spatial component is selective enough (LS, SS); in all other cases, it applies the same plan as Baseline, i.e. it evaluates the RDF part first and then applies the WITHIN filter to the tuples that qualify it. On the other hand, Encoding always chooses to evaluate the RDF part of the queries first and uses the spatial range filtering technique (see Section 3.5.1) to reduce the number of entities that have to be spatially verified. Encoding is superior in all queries. In specific, we avoid fetching a large percentage of exact geometries (96% on average for all range queries in both datasets), which Baseline obtains by random accesses to the dictionary. The cost differences between Encoding and Baseline is small only for SL queries, where the spatial filtering has little effect. In all other cases, Encoding is significantly faster than Baseline and Basic, especially in LS and SS queries and in queries involving entities with non-point geometries, denoted by a star (*), where the difference is up to one order of magnitude. In the case of warm caches, all runtimes are very low, so the cost of Encoding may exceed the cost of Baseline sometimes (e.g., see SL queries) due to the overhead of applying the spatial filter on all accessed entities in the evaluation of the RDF part of the query.

The difference in the optimization times (in parentheses) between warm and cold caches in all alternatives is because the reported numbers include the time spent for parsing the query, resolving the IDs of the URIs/strings in it, and finally building the optimal plan. Hence, when a query is issued for the first time, it requires some dictio-

[10]We only included a small separate cache of 40Kb for the R-tree. Since the OS caches R-tree pages, we used a small cache size in order to reduce the effect of double caching by the SaIL library.

Table 3.4: Spatial range queries on LGD; runtime in ms - optimizer time in ().

Query	Number of results			Strabon		GraphDB		Virtuoso		SRX					
										Baseline (RDF-3X)		Basic extension (Sec. 3.3)		Encoding	
	RDF	Spatial	Combined	Cold	Warm	Cold	Warm	Cold	Warm	Cold	Warm	Cold	Warm	Cold	Warm
LGD.SL1	524	2,537,757	411	64,581	12,791	6,960	136	74,645	83	3,880 (99)	35 (1)	3,333 (148)	54 (20)	2,334 (107)	78 (1)
LGD.SL2	215,355	2,943,209	186,302	168,099	20,129	20,957	14,045	78,568	76	4,495 (97)	272 (1)	3,644 (178)	330 (58)	3,009 (100)	323 (1)
LGD.SL3*	13,090	2,537,757	9,814	160,591	18,081	8,496	822	72,624	36	11,554 (97)	82 (1)	9,891 (147)	104 (20)	3,983 (100)	177 (1)
LGD.LS1	25,617	9,002	86	63,614	12,866	9,568	2,338	58,757	81	1,913 (95)	84 (1)	856 (124)	62 (15)	222 (109)	14 (1)
LGD.LS2	191,976	908	3	63,065	12,785	24,702	17,159	46,066	167	2,257 (97)	176 (2)	429 (117)	21 (15)	183 (91)	12 (2)
LGD.LS3*	5,791	908	9	63,251	12,694	16,065	410	45,317	183	14,305 (107)	52 (1)	484 (127)	20 (14)	174 (89)	2 (1)
LGD.SS1	8,621	9,002	69	63,403	13,271	8,118	829	58,658	51	1,696 (98)	65 (1)	932 (131)	63 (16)	211 (92)	14 (1)
LGD.SS2*	13,090	9,002	120	66,370	12,708	8,488	949	57,745	35	8,181 (97)	75 (1)	1,167 (137)	61 (15)	450 (100)	5 (1)
LGD.SS3*	5,791	9,002	7	66,275	12,750	16,479	410	57,251	22	14,308 (107)	53 (1)	934 (142)	53 (16)	350 (100)	3 (1)
LGD.LL1	191,976	350,405	13,416	89,097	13,900	24,868	17,178	53,714	120	2,694 (95)	183 (1)	2,562 (142)	200 (17)	815 (117)	55 (2)

Table 3.5: Spatial range queries on YAGO; runtime in ms - optimizer time in ().

Query	Number of results			GraphDB		Virtuoso		SRX					
								Baseline (RDF-3X)		Basic extension (Sec. 3.3)		Encoding	
	RDF	Spatial	Combined	Cold	Warm	Cold	Warm	Cold	Warm	Cold	Warm	Cold	Warm
YAGO.SL1*	11,547	364,992	891	23,689	2,823	66,017	9,053	10,610 (61)	61 (1)	10,342 (62)	61 (1)	6,119 (46)	48 (1)
YAGO.SL2*	6,030	31,260	69	32,091	1,816	59,802	1,318	8,984 (173)	70 (1)	8,654 (175)	70 (1)	3,783 (168)	43 (1)
YAGO.LS1*	2,226	138	0	4,817	232	19,276	19	2,769 (60)	61 (1)	2,661 (79)	64 (15)	772 (56)	37 (1)
YAGO.LS2*	285,613	41,945	4,471	182,118	9,657	77,759	1,274	17,590 (183)	696 (1)	16,471 (178)	697 (1)	8,692 (181)	161 (1)
YAGO.SS1*	6,030	8,440	3	30,249	1,853	51,155	459	8,375 (175)	70 (1)	12,019 (173)	275 (17)	3,201 (170)	41 (1)
YAGO.SS2*	7,074	7,042	2	11,131	547	36,008	325	4,641 (61)	62 (1)	11,286 (85)	245 (15)	2,319 (56)	46 (1)
YAGO.LL1*	285,613	184,743	10,454	188,015	13,465	66,381	5,040	19,882 (184)	701 (1)	18,688 (182)	699 (1)	10,978 (179)	173 (1)
YAGO.LL2*	152,693	107,625	88	82,420	10,880	55,230	3,123	6,262 (61)	2,971 (1)	5,999 (62)	2,993 (1)	5,302 (56)	1,921 (1)

nary lookups for resolving the IDs of the entities. With warm caches, the respective dictionary pages are already cached by the OS, thus, query optimization is always cheaper. Note that, in most cases, the time spent for query optimization by Encoding is similar to that of Baseline, meaning that the overhead of augmenting the query graph and using spatial statistics is negligible compared to the query optimization overhead of the original RDF-3X system. With warm caches, the overhead in query optimization by Encoding and Basic compared to Baseline (due to the use of spatial statistics) is more profound.

Similar results are observed for range queries on the YAGO dataset (see Table 3.5). All queries in this case involve entities that may have multipoint geometries (therefore they are marked by a star). Encoding always chooses to evaluate the RDF part of the queries first, as in LGD. Basic chooses the same plan as Baseline in all cases, except for LS1 and SS queries, where it opts to evaluate the spatial selection using the R-tree; on the other hand, the spatial part of LS2 is not considered very selective by the optimizer, preventing the use of R-tree for that query. Note that for YAGO the cost of Basic is high enough (even higher than Baseline for SS queries). After analysis, we found that this is due to the bad performance of the R-tree on this dataset; the range queries access roughly half of the R-tree nodes. The reason is that many multipoints in YAGO are dirty and have huge MBRs that cover most of the data space. Thus, the non-leaf R-tree entries have extremely large MBRs, causing a random query to access a large percentage of tree nodes.

Overall, with cold caches, the median speedup of Encoding over Baseline (resp. Basic) across all queries is 8.3× (resp. 2.6×) for LGD, and 2× (resp. 2×) for YAGO. When warm caches are used, the median speedups are 5.3× (resp. 4×) for LGD, and 1.6× (resp. 2.8×) for YAGO.

Table 3.6: Spatial distance join queries on LGD; runtime in ms - optimizer time in ().

Query	Spatial join threshold ϵ	Number of results		Strabon		GraphDB		SRX					
								Baseline (RDF-3X)		Basic extension (Sec. 3.3)		Encoding	
		RDF	Final	Cold	Warm	Cold	Warm	Cold	Warm	Cold	Warm	Cold	Warm
LGD.J1	0.003	12,145,200	6,831	> 5 min	> 5 min	> 5 min	> 5 min	111,208 (123)	109,295 (1)	3,936 (280)	188 (128)	2,854 (246)	566 (130)
LGD.J2	0.01	274,576	538	> 5 min	27,194	> 5 min	101,756	21,796 (133)	18,476 (2)	4,497 (326)	256 (188)	2,229 (314)	273 (196)
LGD.J3	0.02	13,423,300	8,742	> 5 min	> 5 min	> 5 min	> 5 min	> 5 min	> 5 min	5,412 (417)	433 (267)	3,952 (401)	712 (275)
LGD.J4*	0.05	171,348,000	795,322	> 5 min	> 5 min	> 5 min	> 5 min	> 5 min	> 5 min	106,856 (613)	97,426 (474)	30,841 (589)	21,593 (475)
LGD.J5*	0.01	15,564,000	2,782	> 5 min	> 5 min	> 5 min	> 5 min	59,468 (142)	49,528 (2)	13,530 (334)	355 (186)	10,976 (310)	1,161 (189)
LGD.J6.1*	0.0005	20,181,600	7	> 5 min	> 5 min	> 5 min	> 5 min	133,685 (141)	119,677 (2)	15,291 (243)	199 (88)	12,943 (208)	204 (91)
LGD.J6.2*	0.001	20,181,600	22	> 5 min	> 5 min	> 5 min	> 5 min	133,693 (139)	120,059 (2)	15,372 (240)	195 (89)	12,970 (208)	198 (91)
LGD.J6.3*	0.01	20,181,600	743	> 5 min	> 5 min	> 5 min	> 5 min	134,433 (137)	119,668 (2)	17,036 (341)	308 (187)	8,533 (297)	1,497 (189)

Table 3.7: Spatial distance join queries on YAGO; runtime in ms - optimizer time in ().

Query	Spatial join threshold ϵ	Number of results		GraphDB		SRX					
						Baseline (RDF-3X)		Basic extension (Sec. 3.3)		Encoding	
		RDF	Final	Cold	Warm	Cold	Warm	Cold	Warm	Cold	Warm
YAGO.J1*	0.1	6,245,000	2,635	-	-	118,992 (44)	103,626 (1)	14,738 (204)	445 (129)	11,795 (199)	684 (130)
YAGO.J2*	0.1	523,815,000	6,799,189	> 5 min	> 5 min	> 5 min	> 5 min	137,147 (205)	112,954 (129)	136,114 (275)	115,226 (204)
YAGO.J3*	0.1	16,528	832	142,545	9,732	8,994 (57)	162 (1)	10,547 (220)	264 (129)	9,425 (203)	279 (131)
YAGO.J4*	0.1	3,165	451	69,923	1,477	7,990 (52)	124 (1)	8,796 (209)	219 (128)	8,139 (204)	228 (130)
YAGO.J5*	0.1	565	113	-	-	2,836 (48)	95 (1)	3,547 (199)	164 (129)	3,406 (194)	168 (130)
YAGO.J6*	0.1	19,814,600	664,613	> 5 min	> 5 min	> 5 min	292,119 (2)	45,004 (375)	21,696 (130)	43,679 (356)	22,945 (205)
YAGO.J7*	0.1	544,771,000	4,204,184	> 5 min	> 5 min	> 5 min	> 5 min	40,454 (195)	21,169 (129)	16,721 (267)	1,831 (201)
YAGO.J8.1*	0.001	3,519,380	85,188	-	-	86,075 (48)	77,085 (1)	8,889 (185)	150 (115)	8,381 (189)	150 (115)
YAGO.J8.2*	0.01	3,519,380	86,222	-	-	87,701 (48)	77,093 (1)	9,117 (190)	201 (115)	8,535 (186)	202 (115)
YAGO.J8.3*	0.1	3,519,380	131,828	-	-	86,068 (48)	77,152 (1)	9,471 (205)	383 (128)	8,066 (206)	461 (130)

Results on Spatial Joins. Table 3.6 and Table 3.7 show the costs of spatial distance join queries on LGD and YAGO, respectively. The threshold 0.1 shown in the tables corresponds to a distance around 10km. In LGD, all queries have thresholds greater than the diagonal of a cell in our encoding except queries LGD.J6.1 and LGD.J6.2. In YAGO, threshold 0.1 is greater than the cell diagonal, but 0.01 is not. After performing experiments with various types of queries, we found that the SMJ and SHJ-ID algorithms should only be used when the spatial distance threshold is greater than the diagonal of the grid cell at the bottom level. Otherwise, they do not produce any verified results and, hence, they have similar or slightly worse performance compared to directly applying SHJ (as Basic would). We have added this simple rule of thumb in the optimizer of our system, hence, in all spatial join queries that have a distance threshold less than the cell diagonal, Encoding applies the same plans as Basic using the SHJ operator. In LGD, these queries are J6.1 and J6.2, while in YAGO, the respective queries are J8.1 and J8.2. For this reason, we focus mostly on queries where the distance threshold is greater than the cell diagonal.

All spatial join queries on the LGD dataset (Table 3.6) have a similar pattern: they include two disjoint RDF star-shaped parts with a spatial distance predicate between the geometries of their center nodes. This is the only type of queries we could define here since the LGD dataset includes a rather poor RDF part; besides the POI type, there are very few properties such as "label" and "name" which link the POIs with text attributes. For this type of queries, Baseline can only execute a bushy plan where the two stars are evaluated separately and then joined in a nested-loop fashion, applying the spatial distance filter. On the other hand, Basic may choose to apply an R-tree join first for retrieving the candidate pairs within distance ϵ or to first evaluate the RDF part of the query and follow-up with a spatial

hash join (SHJ) in the end (e.g., see the plans of Figure 3.2c and Figure 3.2d). In all queries we tested, Basic chose the SHJ algorithm and this is quite reasonable; in large datasets, the optimizer would prefer not to perform an expensive spatial self-join over the whole set of points. Encoding can choose between one of the previously mentioned methods and also try the algorithms of Section 3.5.3 and Section 3.5.4 on the augmented query graph. Since we have star-shaped queries and the IDs of the center nodes are coming sorted, SMJ was favored in all queries we present. Although Encoding is much faster than Baseline, we observe that for the case of warm caches, the former does not bring much benefit over Basic for most join queries on LGD. The main reason is that Encoding does not save any geometry lookups due to the particular data distribution; every entity from either of the two spatial join inputs participates in at least one non verified spatial join pair and therefore it cannot be pruned without fetching its geometry. In addition, Basic benefits from the fact that it buffers the complete join inputs before hashing them into the buckets of SHJ, thus, the geometry of each entity is processed only once. On the other hand, SMJ (used by Encoding) produces and verifies the join pair candidates on-the-fly, resulting in the processing of a given geometry multiple times. However, if the size of inputs is very large, Basic can become significantly slower than Encoding (see LGD.J4) because SHJ requires the allocation of a large hash table to accommodate a huge number of buffered geometries. Recall that SHJ, used by Basic, is a blocking operator which requires both inputs to be read as a whole before processing the join and, thus, can become a bottleneck if the inputs are too large.

The results for queries with spatial join components in YAGO are shown in Table 3.7. Depending on the type of the query and the selectivities of the two parts, our encoding-based approach uses either SMJ or SHJ-ID. Specifically, SMJ is used in queries J1 and J8.3, whereas SHJ-ID is used in J2, J6, and J7. In queries J8.1 and J8.2, Encoding follows the same plans as Basic. In the remaining queries (J3, J4 and J5), Basic and our encoding-based approach produced the same plans as Baseline; these queries include a single connected RDF graph pattern with a rather selective RDF part. As a result, the performance of Basic is similar to that of Encoding for queries J3, J4, J5, J8.1, and J8.2. For the remaining queries, Encoding is slightly faster than Basic with cold caches (the two techniques are comparable for warm caches), because Encoding selects a different plan based on the augmented query graph. A notable exception is YAGO.J7, where Encoding performs much better than Basic, because the spatial join inputs have a different spatial distribution and Encoding can prune many tuples using SHJ-ID.

Note that, for large inputs, SHJ might be slower than SMJ. This is reflected in the performance difference between queries LGD.J6.1, LGD.J6.2 (resp. YAGO.J8.1, YAGO.J8.2), where SRX applies the same plan as Basic using SHJ, and queries

LGD.J6.3 (resp. YAGO.J8.3), where SMJ is used.

Overall, with cold caches, the median speedup of Encoding over Baseline across all queries we used is 10.3× and 8.4× for LGD and YAGO. When warm caches are used, the respective median speedup is 136.5× for LGD and 82.1× for YAGO. Regarding spatial distance joins, Encoding and Basic have similar median performance for YAGO. For LGD with cold caches, Encoding has a median 1.3 speedup over Basic, whereas with warm caches Encoding shows a median 0.7 slowdown over Basic.

Results on Spatial kNN Queries. kNN queries in Tables 3.8-3.17 have been made from (and have the same names with) the range queries used in Tables 3.4-3.5. Each kNN query has the same RDF part with the respective range query along with a Filter kNN($?g$, "POINT (...)") clause, where "POINT (...)" is the middle point of "RECTANGLE (...)" in the Filter WITHIN($?g$, "RECTANGLE (...)") clause of the range query. Tables 3.8-3.17 provide results for $k = 5, 10, 20, 50$, and 100.

In both datasets, Basic follows the same plan as Baseline with only exceptions LGD.SL1 and YAGO.LS1, where Basic uses the R-tree. In these two queries, Basic employs the incremental kNN operator (cf. Section 3.3) followed by hash joins, which are favored by the optimizer because the RDF part of the query is selective enough and, as a result, the cost of the building phase of the respective hash tables is low. Such a plan achieves much better performance over Baseline in some cases (e.g. for LGD.SL1 and $k = 5$ with cold caches), however, our experiments demonstrate that Baseline is usually a better option than Basic, especially for $k > 20$. We attribute this behavior to the following reasons: (i) Baseline evaluates the RDF part of the query by leveraging efficient sequential scans over the compressed B$^+$-trees in combination with very fast merge joins, and (ii) LGD.SL1 and YAGO.LS1 have very selective RDF parts (the most selective for each dataset), therefore, the cost of the final dictionary lookups to fetch the geometries of the entities, as performed by Baseline, is low.

When cold caches are used, Unsorted and Sorted are significantly faster (due to filtering and fewer geometry lookups) than Baseline for all kNN queries except YAGO.LL2; in this case, Baseline is superior to both Unsorted and Sorted but for different reasons. First, Unsorted and Baseline use exactly the same plan to evaluate the RDF part of the query, and their only difference lies in the final verification phase where they must retrieve the actual geometries from the dictionary. We found that the result set of the RDF part of YAGO.LL2 contains many tuples carrying the same geometry, which amplifies the effects of caching and significantly reduces the cost of dictionary lookups. So, Baseline outperforms Unsorted due to the CPU overhead of the latter to maintain its priority queues. Yet, when Sorted is an option, the optimizer chooses a different plan for the RDF part, which leverages merge joins and outputs tuples in ascending order of their spatial IDs but shows poor performance.

Table 3.8: Spatial kNN queries on LGD for $k = 5$; runtime in ms - optimizer time in ().

Query	Number of results (RDF)	Strabon		GraphDB		Virtuoso		SRX							
								Baseline (RDF-3X)		Basic extension (Sec. 3.3)		Encoding (Unsorted)		Encoding (Sorted)	
		Cold	Warm	Cold	Warm	Cold	Warm	Cold	Warm	Cold	Warm	Cold	Warm	Cold	Warm
LGD.SL1	524	64,581	12,968	7,336	78	108,284	10	1,173 (86)	33 (1)	548 (121)	47 (12)	466 (69)	57 (1)	380 (89)	18 (1)
LGD.SL2	215,355	95,637	44,738	23,353	16,527	91,761	1,001	1,345 (77)	208 (1)	1,342 (76)	208 (1)	449 (69)	100 (1)	177 (79)	8 (1)
LGD.SL3*	13,090	69,479	15,453	9,070	1,289	N/A	N/A	7,122 (85)	77 (1)	7,103 (83)	77 (1)	701 (69)	65 (1)	564 (83)	31 (1)
LGD.LS1	25,617	68,845	16,722	10,099	2,682	98,572	85	1,296 (77)	87 (1)	1,283 (76)	87 (1)	525 (70)	74 (1)	426 (84)	60 (1)
LGD.LS2	191,976	93,550	41,670	26,857	20,171	95,581	325	1,542 (77)	195 (2)	1,541 (77)	191 (1)	530 (70)	102 (1)	185 (73)	25 (1)
LGD.LS3*	5,791	75,161	14,249	16,138	512	N/A	N/A	12,483 (83)	53 (1)	12,471 (79)	53 (1)	464 (69)	48 (1)	188 (73)	12 (1)
LGD.SS1	8,621	66,576	14,342	8,461	941	99,445	33	1,233 (88)	66 (1)	1,266 (87)	66 (1)	502 (70)	63 (2)	487 (90)	50 (1)
LGD.SS2*	13,090	69,496	15,540	9,015	1,248	N/A	N/A	7,174 (87)	77 (1)	7,122 (87)	77 (1)	599 (69)	65 (1)	511 (73)	52 (1)
LGD.SS3*	5,791	75,341	14,061	16,288	519	N/A	N/A	12,375 (87)	53 (1)	12,509 (87)	53 (1)	525 (68)	48 (1)	447 (82)	40 (1)
LGD.LL1	191,976	94,509	42,433	26,931	20,142	97,280	321	1,570 (77)	192 (1)	1,608 (76)	192 (1)	546 (68)	101 (1)	235 (72)	18 (1)

Table 3.9: Spatial kNN queries on LGD for $k = 10$; runtime in ms - optimizer time in ().

Query	Number of results (RDF)	Strabon		GraphDB		Virtuoso		SRX							
								Baseline (RDF-3X)		Basic extension (Sec. 3.3)		Encoding (Unsorted)		Encoding (Sorted)	
		Cold	Warm	Cold	Warm	Cold	Warm	Cold	Warm	Cold	Warm	Cold	Warm	Cold	Warm
LGD.SL1	524	64,720	12,941	7,340	80	108,416	12	1,174 (88)	33 (1)	876 (121)	72 (12)	504 (70)	57 (2)	504 (90)	27 (1)
LGD.SL2	215,355	95,608	45,125	23,354	16,536	92,213	1,001	1,327 (77)	208 (1)	1,329 (76)	212 (1)	452 (70)	100 (1)	176 (77)	8 (1)
LGD.SL3*	13,090	69,437	15,487	9,149	1,292	N/A	N/A	7,140 (87)	77 (1)	7,115 (74)	77 (1)	749 (69)	65 (1)	612 (92)	31 (1)
LGD.LS1	25,617	68,666	16,665	10,118	2,711	98,710	85	1,306 (77)	87 (1)	1,273 (76)	87 (1)	509 (70)	74 (1)	470 (84)	60 (1)
LGD.LS2	191,976	93,902	42,130	27,158	20,179	95,801	325	1,577 (77)	192 (1)	1,588 (77)	192 (1)	525 (70)	102 (1)	184 (73)	25 (1)
LGD.LS3*	5,791	75,219	14,073	16,200	519	N/A	N/A	12,483 (87)	53 (1)	12,461 (87)	53 (1)	485 (69)	49 (1)	223 (70)	23 (1)
LGD.SS1	8,621	66,535	14,388	8,473	942	99,528	33	1,217 (87)	66 (1)	1,240 (87)	66 (1)	492 (69)	62 (1)	472 (94)	50 (1)
LGD.SS2*	13,090	69,405	15,523	9,082	1,288	N/A	N/A	7,178 (87)	77 (1)	7,055 (87)	77 (1)	618 (73)	65 (1)	543 (92)	52 (1)
LGD.SS3*	5,791	75,315	13,970	16,302	544	N/A	N/A	12,421 (87)	54 (1)	12,475 (87)	53 (1)	667 (69)	49 (1)	575 (95)	56 (1)
LGD.LL1	191,976	94,205	42,670	27,043	20,148	97,809	322	1,620 (78)	192 (1)	1,634 (77)	192 (1)	544 (73)	101 (1)	252 (73)	19 (1)

Table 3.10: Spatial kNN queries on LGD for $k = 20$; runtime in ms - optimizer time in ().

Query	Number of results (RDF)	Strabon		GraphDB		Virtuoso		SRX							
								Baseline (RDF-3X)		Basic extension (Sec. 3.3)		Encoding (Unsorted)		Encoding (Sorted)	
		Cold	Warm	Cold	Warm	Cold	Warm	Cold	Warm	Cold	Warm	Cold	Warm	Cold	Warm
LGD.SL1	524	64,510	12,954	7,376	87	108,909	12	1,133 (88)	33 (1)	1,269 (121)	116 (12)	545 (70)	56 (1)	532 (92)	28 (1)
LGD.SL2	215,355	95,644	45,126	23,356	16,540	93,970	1,004	1,363 (79)	209 (1)	1,330 (77)	209 (1)	453 (69)	100 (1)	178 (75)	8 (1)
LGD.SL3*	13,090	69,274	15,584	9,150	1,306	N/A	N/A	7,164 (87)	77 (1)	7,168 (82)	77 (1)	750 (69)	65 (1)	608 (92)	30 (1)
LGD.LS1	25,617	68,805	16,686	10,214	2,725	99,406	85	1,302 (77)	88 (1)	1,281 (77)	87 (1)	519 (70)	74 (1)	472 (92)	60 (1)
LGD.LS2	191,976	93,585	41,657	27,164	20,180	95,925	327	1,598 (77)	192 (1)	1,615 (77)	192 (1)	528 (70)	102 (1)	182 (72)	26 (1)
LGD.LS3*	5,791	75,127	14,025	16,284	546	N/A	N/A	12,437 (87)	54 (1)	12,434 (86)	54 (1)	542 (69)	48 (1)	312 (78)	34 (1)
LGD.SS1	8,621	66,618	14,380	8,533	950	100,382	34	1,223 (88)	66 (1)	1,204 (86)	65 (1)	515 (70)	62 (1)	515 (94)	50 (1)
LGD.SS2*	13,090	69,536	15,699	9,094	1,300	N/A	N/A	7,170 (87)	77 (1)	7,149 (86)	77 (1)	608 (69)	65 (1)	551 (88)	52 (1)
LGD.SS3*	5,791	75,403	14,025	16,306	545	N/A	N/A	12,457 (87)	54 (1)	12,467 (87)	54 (1)	667 (69)	48 (1)	560 (83)	55 (1)
LGD.LL1	191,976	94,252	42,573	27,223	20,150	98,285	322	1,590 (77)	192 (1)	1,646 (77)	192 (1)	588 (69)	101 (1)	266 (72)	19 (1)

Table 3.11: Spatial kNN queries on LGD for $k = 50$; runtime in ms - optimizer time in ().

Query	Number of results (RDF)	Strabon		GraphDB		Virtuoso		SRX							
								Baseline (RDF-3X)		Basic extension (Sec. 3.3)		Encoding (Unsorted)		Encoding (Sorted)	
		Cold	Warm	Cold	Warm	Cold	Warm	Cold	Warm	Cold	Warm	Cold	Warm	Cold	Warm
LGD.SL1	524	64,803	13,097	7,399	110	110,023	13	1,139 (85)	33 (1)	3,686 (129)	265 (12)	668 (70)	56 (1)	653 (92)	32 (1)
LGD.SL2	215,355	95,515	44,992	23,359	16,584	94,177	1,005	1,335 (77)	208 (1)	1,324 (76)	210 (1)	459 (69)	100 (1)	177 (76)	9 (1)
LGD.SL3*	13,090	69,473	15,580	9,298	1,399	N/A	N/A	7,096 (87)	77 (1)	7,091 (87)	77 (1)	883 (69)	65 (1)	851 (94)	33 (1)
LGD.LS1	25,617	68,860	16,667	10,255	2,729	99,767	86	1,315 (77)	87 (1)	1,304 (77)	88 (2)	564 (71)	75 (1)	501 (84)	61 (1)
LGD.LS2	191,976	93,740	41,659	27,320	20,257	96,761	328	1,611 (77)	193 (2)	1,639 (78)	191 (1)	528 (69)	102 (1)	223 (82)	27 (1)
LGD.LS3*	5,791	75,280	13,946	16,333	592	N/A	N/A	12,423 (87)	54 (1)	12,463 (87)	54 (1)	617 (69)	49 (1)	388 (82)	41 (1)
LGD.SS1	8,621	66,514	14,341	8,556	973	100,768	34	1,222 (87)	66 (1)	1,159 (87)	65 (1)	534 (70)	62 (1)	523 (91)	50 (1)
LGD.SS2*	13,090	69,224	15,513	9,269	1,367	N/A	N/A	7,163 (87)	77 (1)	7,170 (86)	77 (1)	688 (69)	65 (1)	629 (85)	52 (1)
LGD.SS3*	5,791	75,301	14,037	16,517	574	N/A	N/A	12,479 (87)	54 (1)	12,351 (87)	54 (1)	791 (69)	48 (1)	752 (82)	60 (1)
LGD.LL1	191,976	93,971	42,339	27,360	20,280	98,525	323	1,633 (77)	192 (1)	1,573 (77)	192 (1)	638 (70)	101 (1)	303 (80)	22 (2)

Table 3.12: Spatial kNN queries on LGD for $k = 100$; runtime in ms - optimizer time in ().

Query	Number of results (RDF)	Strabon		GraphDB		Virtuoso		SRX							
								Baseline (RDF-3X)		Basic extension (Sec. 3.3)		Encoding (Unsorted)		Encoding (Sorted)	
		Cold	Warm	Cold	Warm	Cold	Warm	Cold	Warm	Cold	Warm	Cold	Warm	Cold	Warm
LGD.SL1	524	64,623	13,252	7,644	116	110,171	13	1,118 (87)	33 (1)	7,683 (127)	506 (12)	739 (70)	57 (1)	751 (92)	38 (1)
LGD.SL2	215,355	95,492	44,878	23,361	16,676	94,825	1,014	1,324 (77)	208 (1)	1,346 (77)	208 (1)	451 (69)	100 (1)	180 (76)	9 (1)
LGD.SL3*	13,090	69,496	15,557	9,455	1,470	N/A	N/A	7,156 (87)	77 (1)	6,981 (86)	77 (1)	1,059 (69)	65 (1)	1,109 (93)	50 (1)
LGD.LS1	25,617	68,781	16,618	10,342	2,759	101,913	87	1,298 (77)	87 (1)	1,300 (77)	87 (1)	630 (69)	75 (1)	578 (68)	73 (1)
LGD.LS2	191,976	93,874	41,536	27,716	20,369	96,912	330	1,562 (77)	192 (1)	1,583 (76)	191 (1)	540 (69)	102 (1)	233 (86)	27 (1)
LGD.LS3*	5,791	75,184	13,970	16,678	632	N/A	N/A	12,469 (87)	54 (1)	12,493 (87)	53 (1)	795 (69)	48 (1)	602 (83)	52 (1)
LGD.SS1	8,621	66,668	14,667	8,774	1,048	101,206	35	1,251 (87)	66 (1)	1,224 (87)	66 (1)	655 (70)	63 (2)	613 (91)	65 (1)
LGD.SS2*	13,090	69,620	15,798	9,332	1,484	N/A	N/A	7,183 (87)	77 (1)	7,170 (86)	77 (1)	764 (77)	65 (1)	734 (93)	53 (1)
LGD.SS3*	5,791	75,234	14,030	16,713	625	N/A	N/A	12,459 (87)	53 (1)	12,425 (87)	54 (1)	1,127 (69)	49 (1)	1,080 (82)	69 (1)
LGD.LL1	191,976	94,626	42,383	27,424	20,281	99,163	324	1,598 (79)	192 (1)	1,609 (77)	192 (1)	623 (69)	101 (1)	309 (84)	22 (1)

When warm caches are used, Unsorted performs better than Baseline for all kNN queries on LGD except LGD.SL1. This is reasonable since the Unsorted method

Table 3.13: Spatial kNN queries on YAGO for $k = 5$; runtime in ms - optimizer time in ().

Query	Number of results (RDF)	GraphDB		SRX							
				Baseline (RDF-3X)		Basic extension (Sec. 3.3)		Encoding (Unsorted)		Encoding (Sorted)	
		Cold	Warm	Cold	Warm	Cold	Warm	Cold	Warm	Cold	Warm
YAGO.SL1*	11,547	86,349	3,054	6,108 (51)	59 (1)	6,170 (51)	58 (1)	2,411 (72)	57 (1)	2,111 (86)	43 (1)
YAGO.SL2*	6,030	102,461	1,977	7,553 (120)	69 (1)	7,537 (124)	69 (1)	3,068 (169)	66 (1)	2,864 (228)	43 (1)
YAGO.LS1*	2,226	-	-	2,432 (53)	58 (1)	3,943 (110)	98 (16)	1,349 (80)	60 (1)	1,158 (82)	43 (1)
YAGO.LS2*	285,613	>5 min	137,117	13,340 (129)	715 (1)	13,253 (129)	717 (1)	6,009 (193)	720 (1)	5,567 (211)	676 (1)
YAGO.SS1*	6,030	101,674	1,977	7,530 (111)	69 (1)	7,526 (115)	69 (1)	3,096 (192)	66 (1)	2,803 (210)	40 (1)
YAGO.SS2*	7,074	52,999	683	4,100 (51)	60 (1)	4,106 (50)	60 (1)	2,305 (82)	59 (1)	1,850 (70)	21 (1)
YAGO.LL1*	285,613	>5 min	138,160	13,248 (139)	715 (1)	13,220 (127)	718 (1)	6,071 (185)	719 (1)	5,654 (226)	689 (1)
YAGO.LL2*	152,693	169,217	15,148	4,709 (50)	2,992 (1)	4,721 (51)	2,987 (1)	5,750 (75)	3,016 (1)	13,118 (83)	2,273 (1)

Table 3.14: Spatial kNN queries on YAGO for $k = 10$; runtime in ms - optimizer time in ().

Query	Number of results (RDF)	GraphDB		SRX							
				Baseline (RDF-3X)		Basic extension (Sec. 3.3)		Encoding (Unsorted)		Encoding (Sorted)	
		Cold	Warm	Cold	Warm	Cold	Warm	Cold	Warm	Cold	Warm
YAGO.SL1*	11,547	86,351	3,055	6,045 (50)	58 (1)	6,097 (50)	58 (1)	2,395 (66)	57 (1)	2,115 (86)	43 (1)
YAGO.SL2*	6,030	102,464	1,979	7,560 (115)	69 (1)	7,548 (121)	69 (1)	3,117 (190)	66 (1)	2,850 (228)	43 (1)
YAGO.LS1*	2,226	-	-	2,431 (51)	58 (1)	3,922 (91)	97 (16)	1,304 (77)	61 (1)	1,152 (82)	43 (1)
YAGO.LS2*	285,613	>5 min	137,120	13,284 (127)	716 (1)	13,208 (137)	716 (1)	5,983 (185)	721 (1)	5,547 (209)	674 (1)
YAGO.SS1*	6,030	101,675	1,979	7,544 (109)	69 (1)	7,574 (121)	69 (1)	3,112 (195)	67 (1)	2,804 (208)	40 (1)
YAGO.SS2*	7,074	53,002	684	4,117 (53)	59 (1)	4,111 (51)	60 (1)	2,327 (77)	59 (1)	1,844 (66)	22 (1)
YAGO.LL1*	285,613	>5 min	138,161	13,343 (127)	716 (1)	13,347 (131)	714 (1)	6,030 (179)	723 (1)	5,713 (227)	690 (1)
YAGO.LL2*	152,693	169,219	15,149	4,726 (51)	2,987 (1)	4,711 (50)	2,990 (1)	5,811 (82)	3,019 (1)	13,114 (86)	2,275 (1)

Table 3.15: Spatial kNN queries on YAGO for $k = 20$; runtime in ms - optimizer time in ().

Query	Number of results (RDF)	GraphDB		SRX							
				Baseline (RDF-3X)		Basic extension (Sec. 3.3)		Encoding (Unsorted)		Encoding (Sorted)	
		Cold	Warm	Cold	Warm	Cold	Warm	Cold	Warm	Cold	Warm
YAGO.SL1*	11,547	86,354	3,057	6,073 (50)	59 (1)	6,117 (50)	59 (1)	2,415 (72)	57 (1)	2,096 (68)	43 (1)
YAGO.SL2*	6,030	102,468	1,982	7,549 (114)	69 (1)	7,577 (122)	68 (1)	3,103 (195)	66 (1)	2,854 (228)	43 (1)
YAGO.LS1*	2,226	-	-	2,449 (51)	57 (1)	3,946 (105)	97 (16)	1,335 (80)	61 (1)	1,141 (78)	43 (1)
YAGO.LS2*	285,613	>5 min	137,122	13,345 (127)	718 (1)	13,308 (125)	716 (1)	6,017 (185)	722 (1)	5,589 (211)	676 (1)
YAGO.SS1*	6,030	101,678	1,980	7,543 (114)	69 (1)	7,542 (113)	69 (1)	3,092 (191)	67 (1)	2,829 (214)	40 (1)
YAGO.SS2*	7,074	53,006	686	4,098 (50)	60 (1)	4,098 (50)	59 (1)	2,293 (82)	59 (1)	1,838 (70)	23 (1)
YAGO.LL1*	285,613	>5 min	138,165	13,261 (123)	718 (1)	13,313 (129)	717 (1)	6,055 (191)	721 (1)	5,657 (226)	688 (1)
YAGO.LL2*	152,693	170,222	15,251	4,720 (55)	2,990 (1)	4,720 (51)	2,983 (1)	5,820 (77)	3,017 (1)	13,084 (86)	2,280 (1)

Table 3.16: Spatial kNN queries on YAGO for $k = 50$; runtime in ms - optimizer time in ().

Query	Number of results (RDF)	GraphDB		SRX							
				Baseline (RDF-3X)		Basic extension (Sec. 3.3)		Encoding (Unsorted)		Encoding (Sorted)	
		Cold	Warm	Cold	Warm	Cold	Warm	Cold	Warm	Cold	Warm
YAGO.SL1*	11,547	88,397	3,189	6,088 (51)	59 (1)	6,089 (50)	59 (1)	2,417 (74)	57 (1)	2,111 (72)	43 (1)
YAGO.SL2*	6,030	104,512	2,104	7,552 (115)	69 (1)	7,540 (113)	69 (1)	3,114 (194)	66 (1)	2,879 (230)	44 (1)
YAGO.LS1*	2,226	-	-	2,475 (51)	58 (1)	3,884 (89)	97 (16)	1,371 (82)	61 (1)	1,155 (82)	43 (1)
YAGO.LS2*	285,613	>5 min	137,227	13,337 (125)	716 (1)	13,245 (129)	715 (1)	5,993 (187)	725 (1)	5,589 (208)	677 (1)
YAGO.SS1*	6,030	104,722	1,996	7,543 (116)	69 (1)	7,536 (115)	69 (1)	3,084 (181)	67 (1)	2,831 (210)	40 (1)
YAGO.SS2*	7,074	54,011	753	4,096 (50)	60 (1)	4,096 (50)	60 (1)	2,311 (77)	59 (1)	1,876 (66)	23 (1)
YAGO.LL1*	285,613	>5 min	139,201	13,307 (123)	716 (1)	13,351 (131)	716 (1)	6,029 (177)	725 (1)	5,667 (204)	689 (1)
YAGO.LL2*	152,693	171,984	15,305	4,701 (51)	2,989 (1)	4,728 (51)	2,990 (1)	5,804 (79)	3,012 (1)	13,122 (86)	2,275 (1)

Table 3.17: Spatial kNN queries on YAGO for $k = 100$; runtime in ms-optimizer time in ().

Query	Number of results (RDF)	GraphDB		SRX							
				Baseline (RDF-3X)		Basic extension (Sec. 3.3)		Encoding (Unsorted)		Encoding (Sorted)	
		Cold	Warm	Cold	Warm	Cold	Warm	Cold	Warm	Cold	Warm
YAGO.SL1*	11,547	91,800	3,308	6,085 (50)	59 (1)	6,109 (58)	59 (1)	2,429 (74)	57 (1)	2,146 (70)	43 (1)
YAGO.SL2*	6,030	107,319	2,261	7,552 (115)	69 (1)	7,520 (113)	69 (1)	3,149 (195)	66 (1)	2,871 (228)	44 (1)
YAGO.LS1*	2,226	-	-	2,447 (51)	57 (1)	10,788 (98)	320 (16)	1,367 (78)	60 (1)	1,590 (70)	147 (1)
YAGO.LS2*	285,613	>5 min	137,529	13,344 (129)	715 (1)	13,258 (127)	717 (1)	6,009 (189)	725 (1)	5,557 (201)	680 (1)
YAGO.SS1*	6,030	107,657	2,211	7,545 (120)	69 (1)	7,541 (114)	69 (1)	3,135 (193)	66 (1)	2,850 (208)	40 (1)
YAGO.SS2*	7,074	55,145	878	4,118 (50)	59 (1)	4,096 (50)	60 (1)	2,363 (80)	59 (1)	1,879 (68)	24 (1)
YAGO.LL1*	285,613	>5 min	142,926	13,252 (129)	713 (1)	13,374 (137)	718 (1)	6,077 (185)	727 (1)	5,729 (227)	691 (1)
YAGO.LL2*	152,693	175,855	15,543	4,718 (53)	2,989 (1)	4,729 (50)	2,987 (1)	5,783 (80)	3,017 (1)	13,135 (86)	2,274 (1)

tends to perform fewer dictionary lookups than Baseline and, in queries with very selective RDF part, such as LGD.SL1, the benefits of Unsorted over Baseline are

negligible. In YAGO with warm caches, Unsorted performs similarly or slightly worse (e.g. for YAGO.LS2, YAGO.LL1, and YAGO.LL2) than Baseline for the same reason we mentioned before: many entities in the result of the RDF part of these queries have the same geometry, and the cost of the additional geometry lookups in Baseline is mitigated by caching. The only LGD queries where Baseline is slightly better than Sorted are LGD.SL1 for $k = 100$ and LGD.SS3 for all k values except $k = 5$. Note that, although LGD.LS3 has the same RDF part with LGD.SS3, Sorted is constantly better than Baseline for LGD.LS3 because its kNN predicate is different. Regarding YAGO, Sorted is better than Baseline in all queries apart from YAGO.LS1 for $k = 100$.

Finally, Sorted is superior to Unsorted in most cases. For LGD and warm caches, the only queries where Unsorted is better than Sorted are LGD.LS3, LGD.SS1 for $k = 100$, and LGD.SS3 for all k values except $k = 5$. Still, under cold caches, Sorted is better even in these cases. For YAGO, Sorted is better than Unsorted in all queries but YAGO.LS1 for $k = 100$, where Unsorted is superior under both warm and cold caches. Generally, Sorted is preferable over Unsorted and Baseline, as it tends to avoid a significant number of geometry retrievals. Yet, Unsorted is a good alternative since it can overcome the deficiencies of Sorted in the few cases where Baseline is better: LGD.SS3 for all k values except $k = 5$, and YAGO.LS1 for $k = 100$.

Overall, for LGD and with cold caches, Encoding Unsorted (resp. Sorted) has a median 2.9× (resp. 7.9×) speedup over Baseline whereas, for YAGO, the median speedup over Baseline is 2.2× for Unsorted and 2.3× for Sorted. For LGD queries with warm caches, the median speedups of Unsorted and Sorted over Baseline are 1.1× and 1.5× respectively. Last, for YAGO with warm caches, Unsorted and Baseline perform similarly whereas Sorted has a median 1.3× speedup over Baseline.

Comparison with Existing Systems. We compared SRX against three popular RDF stores with geospatial data support, namely Strabon, GraphDB, and Virtuoso. For Strabon, we only present results with LGD, as it could not load YAGO even after three days (and even when using the bulk loader we obtained from the authors of [KKK12]; this issue is also reported in [PGA14]).

We allowed each system to allocate the whole available memory of the machine and performed the experiments with cold and warm caches just like for our system. Since these systems have their own data caches, experiments with cold caches were conducted by clearing the OS cache and restarting the system. The symbol '-' in Tables 3.7, and 3.13-3.17 denotes empty or incorrect results. N/A (not applicable) is used in Tables 3.8-3.12, and 3.18 for Virtuoso because its internal function `bif:st_distance`, which is used in spatial join and kNN queries (cf. Appendix-Chapter 8), works only for point geometries. In fact, this is why there are no Virtuoso results in Tables 3.6-3.7 and Tables 3.13-3.17. Although queries J1, J2, and J3 in

Table 3.18: Median speedups of SRX over Strabon, GraphDB, Virtuoso for LGD and YAGO across all queries of each type.

Query Type	Strabon (LGD)		GraphDB (LGD)		GraphDB (YAGO)		Virtuoso (LGD)		Virtuoso (YAGO)	
	Cold	**Warm**	**Cold**	**Warm**	**Cold**	**Warm**	**Cold**	**Warm**	**Cold**	**Warm**
range	168.4	933.4	34.4	151.8	8.9	43.7	145.9	4.7	13.1	9.5
distance	31.2	339.8	31.2	397	8.5	13	N/A	N/A	N/A	N/A
unsorted kNN	130.9	264.6	22	20	33.3	30	192.9	2.1	N/A	N/A
sorted kNN	140.2	437.5	24.9	34.2	36.2	49.5	290	6.9	N/A	N/A

Table 3.6 involve only points, they are also not supported by Virtuoso, presumably because it tries to apply the DISTANCE predicate first between all types of geometries. Note that both GraphDB and Virtuoso compute the great-circle distance, whereas Strabon, Encoding, Baseline, and Basic compute the Euclidean distance. This does not prevent us from a fair comparison among GraphDB and Virtuoso since both distance functions have similar CPU cost.

Table 3.18 summarizes the median speedups of SRX over Strabon, GraphDB, and Virtuoso across all queries we used on both datasets. SRX is 8.5× faster (in the worst case) than the competitors in all cases except for the case of Virtuoso on LGD with warm caches, where SRX median speedups are lower. We cannot comment further on the performance of GraphDB and Virtuoso as they are not open-source systems. On the contrary, the performance of Strabon for range (Table 3.4), and kNN (Tables 3.8-3.12) queries is dominated by the time needed to fetch data from disk: $60s$ (resp. $12s$) with cold (resp. warm) caches on average in both range and kNN queries. We also observe that for these types of queries, the query time tends to increase with the size of the result for the RDF part of the query. Finally, distance join query times (Table 3.6) in Strabon are dominated by the CPU rather than the I/O time due to the large number of candidate pairs that need to be examined.

3.8.3 Updates Setup

In the experiments for updates we used the same encoding and R-tree configurations as for queries (cf. Section 3.8.1). Thresholds h_1 and h_2 used to trigger re-encodings (cf. Section 3.7) were set to 0.5 and 0.7 respectively. We also experimented with other thresholds (e.g. 0.35 and 0.5) but we did not notice any significant performance difference.

Datasets. The update benchmark relies on Deltas that we are extracted by calculating the difference of two versions of LGD and YAGO: LGD `2013_04_29` to `2015_11_02` [11], and YAGO `2.5.3` to `3.0.2` [12]. Details are presented in the Appendix-Chapter 8. In both datasets, each delta consists of a delete, an update, and an insert workload,

[11] https://tinyurl.com/ydbscsxf
[12] https://tinyurl.com/y7ukhge3

all measured in number of triples. The column 'HasGeo' shows the number of $\langle s, p, o \rangle$ triples with $p =$ "hasGeometry" whereas the numbers for the rest of the triples are given in column 'Other'. For the YAGO dataset, we encountered a small number of 'HasGeo' deltas between versions `2.5.3` and `3.0.2`; thus, only for this type of triples, we extracted the deltas using the last version of YAGO (`3.1`) instead of `3.0.2`. YAGO `3.1` contains many more 'Other' triples we did not consider here since they are not related to any spatial entities and, hence, they do not affect the performance of re-encoding. Finally, LGD and YAGO deltas have been extracted using only types of triples that appear in both the initial and final versions.

Update Workloads. To generate realistic update workloads we split deltas in batches of varying size (in number of triples). For the smaller LGD dataset, we present experiments for batch sizes of 1M, 2M, 4M, and 8M triples whereas, for YAGO, we use batch sizes of 1M, 16M, 32M, and 64M triples. Each batch is marked as *delete*, *update* or *insert* and contains randomly selected triples from the respective delta. For instance, to form the delete batches of a specific batch size b, we first collect all delete triples ('hasGeometry' and 'Other') included in the delete delta, we shuffle them, and group them in batches of size b each. In all experiments of the next section, the batches are applied in a particular order, simulating the transition from the initial to the final version of the dataset: first all deletions, then all updates, and finally all insertions. The update benchmark can be found in the Appendix-Chapter 8.

3.8.4 Updates Comparison

We compare SRX with Strabon, GraphDB, and Virtuoso. Results are given in Figure 3.9 and Figure 3.10 for LGD and YAGO respectively. Update experiments with Strabon (Figure 3.11) were feasible only on small subsets of LGD and are discussed later on. All reported times for SRX and RDF-3X reflect the total time needed to construct the in-memory differential indexes and synchronize them with the base indexes (i.e. the B^+-trees on disk).

Deletes. As shown in Figure 3.9 and Figure 3.10, the latency of processing a delete batch with RDF-3X and SRX shows a slight improvement across consecutive batches of the same size (left-most part of each plot) and tends to increase on average with the batch size. The slight improvement of delete latency over time is more apparent with YAGO and is reasonable since the overall database tends to get smaller. SRX latencies are in general higher than those of RDF-3X, and this is because SRX performs additional dictionary lookups and base index scans when trying to re-encode entities at lower levels of the grid. Overall, the median slowdown of SRX over RDF-3X across all delete batches is small: $0.5\times$ for LGD, and $0.8\times$ for YAGO. The slowdown is smaller for YAGO because the geometries in the delete batches of YAGO are almost

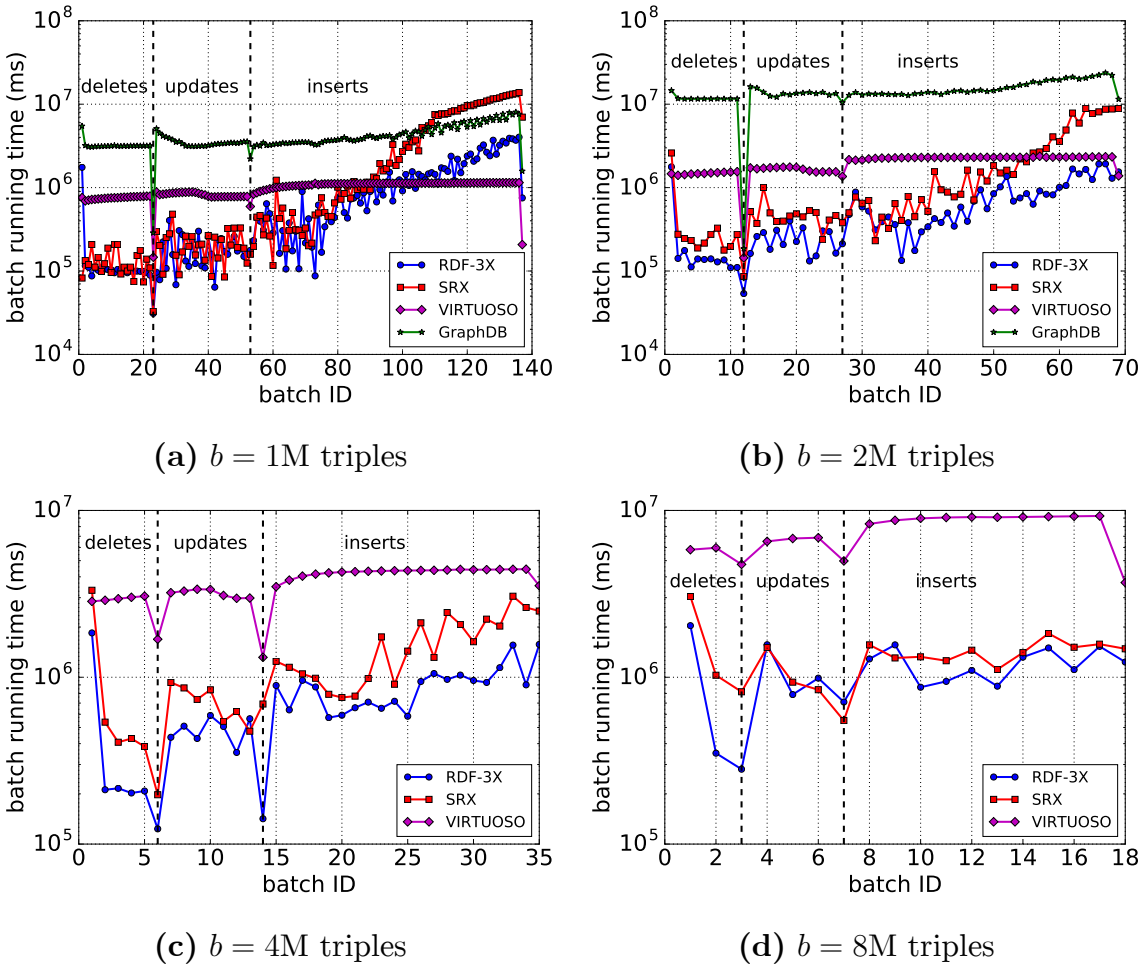

(a) $b = 1$M triples

(b) $b = 2$M triples

(c) $b = 4$M triples

(d) $b = 8$M triples

Figure 3.9: Latency (ms) of processing batches of size b on LGD.

half on average compared to LGD, hence, re-encoding is triggered less frequently. Note that the high processing latencies in the first delete batches of each experiment are due to some warm-up issues.

Inserts. The right-most part of each plot in Figure 3.9 and Figure 3.10 (labeled with "inserts") shows the performance of SRX and RDF-3X for inserts. In contrast to deletes, the latency of processing an insert batch tends to increase over time for both SRX and RDF-3X, although it appears more stable for larger batches, especially for LGD (Figure 3.9d). We attribute this both to the differential index construction and to the index synchronization phases (cf. Section 3.7).

During the differential index construction, SRX and RDF-3X perform a number of database scans to check whether an input triple is new or old[13]. Hence, when the database increases in size as more insert batches are processed, the cost of these scans

[13]This check was not included in the version of RDF-3X we had but we added it for consistency.

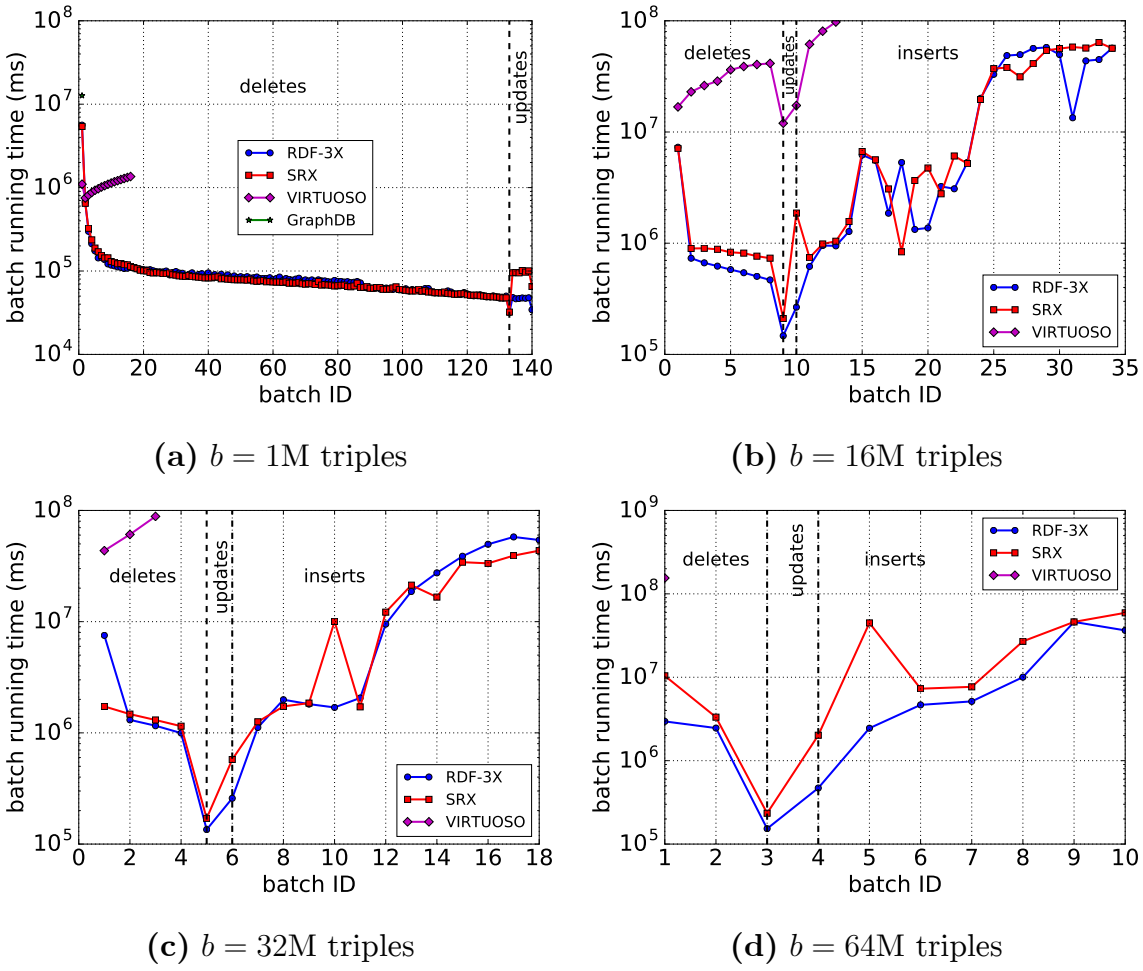

(a) $b = 1$M triples

(b) $b = 16$M triples

(c) $b = 32$M triples

(d) $b = 64$M triples

Figure 3.10: Latency (ms) of processing batches of size b on YAGO.

tends to increase. Second, and most important, whenever an index synchronization is performed and a leaf page of a base B$^+$-tree overflows, the system generates a new page for the additional triples but avoids tree compaction. This is a common technique that tries to minimize the update latency at the cost of redundant leaf pages, which are expected to be filled by subsequent updates or compacted periodically when the system is idle. The technique achieves better leaf page utilization when used for bulk inserts of large size but does not perform well for small frequent inserts like those in Figure 3.9a-b and Figure 3.10b-c. Applying many small insert batches one after the other results in a large number of almost empty leaf pages (hence, a large increase in I/Os), and the performance of the system degrades significantly. This is in fact the reason we do not present times for insert batches in Figure 3.10a; after some point in this experiment, the processing of each single insert batch started taking almost double the time of the previous batch and we had to stop it. The problem we described is exacerbated due to the extensive use of indexes in RDF-3X (all of

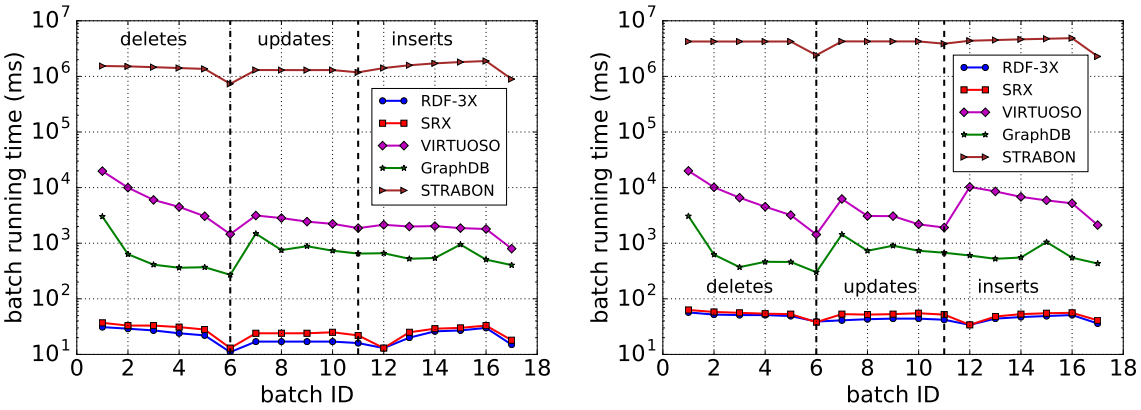

(a) initial base = 10K triples **(b)** initial base = 100K triples

Figure 3.11: Latency (ms) of processing batches of size 1K triples on two different subsets **(a)** and **(b)** of LGD; the former dataset is a subset of the latter.

which have to be updated with the new triples) and becomes even more profound in SRX due to the additional re-assigment of IDs when new geometries are introduced for existing entities (*lines* 6-16 in Updates on existing entities). The latter also explains why the difference in performance of inserts between SRX and RDF-3X is amplified over time in Figure 3.9a-c. Overall, the median slowdown of SRX over RDF-3X across all insert batches is 0.6× for both LGD and YAGO.

It should be noted, that SRX inherits its design from the last version of RDF-3X which targets read-intensive workloads and performs well under bulk inserts, but does not focus on Online transaction processing. There is some preliminary work on OLTP in [NW10b], but it has not been integrated to the current RDF-3X. We leave the efficient management of single triples and very small insert as future work.

Updates. The middle part of each plot in Figure 3.9 and Figure 3.10 (labeled with "updates") shows the performance of SRX and RDF-3X in processing update batches. Here, the latency fluctuates slightly but tends to remain stable in the long term. Since an update in SRX and RDF-3X is implemented as a delete followed by an insert, we attribute the reasons behind this behavior to the combined performance of delete and insert batches, as explained before. Overall, the median slowdown of SRX over RDF-3X is 0.7× for LGD and 0.3× for YAGO.

Comparison with Existing Systems. We also performed experiments with Strabon, GraphDB, and Virtuoso, which we allowed to use the whole available memory of our machine, as for queries. Results are shown in Figure 3.9 for LGD, in Figure 3.10 for YAGO, and in Figure 3.11 for the LGD subsets. In YAGO, both GraphDB and Virtuoso were quite slow, and so we stopped the respective experiment at the point where each system had been running for as long as SRX took to apply all delete,

update, and insert batches. Moreover, GraphDB did not perform updates for batch sizes 4M and 8M in LGD, and 16M, 32M, and 64M in YAGO, due to memory overflow. In the next, we first discuss the update results on LGD and YAGO, and we then explain the results on the LGD subsets that we generated specifically for Strabon.

For LGD and YAGO, SRX performs significantly better compared to GraphDB and Virtuoso in both datasets, especially for deletes and updates, even though it also applies spatial re-encoding of entities. For inserts, SRX is almost an order of magnitude faster (in the worst case) with large batches, and gets worse than GraphDB and Virtuoso only when using batch sizes of 1M and 2M in LGD. We have already explained the reasons behind SRX's performance degradation for inserts in the previous. Overall, the median speedup of SRX over GraphDB (resp. Virtuoso) for deletes, inserts, and updates is: 35.3×, 8.9×, and 22.6× (resp. 5.9×, 2.4×, and 4.1×) for LGD. For YAGO, the respective median speedup of SRX over Virtuoso is: 41.2×, 82.9×, and 9.2× (GraphDB was slow for YAGO and managed to apply only the first delete batch in Figure 3.10a).

The two datasets of Figure 3.11 are selected subsets from LGD, which we describe in the Appendix-Chapter 8. Overall, the median speedup of SRX over GraphDB (resp. Virtuoso) for deletes, inserts, and updates on both these datasets is: 12.4×, 16.2×, and 22.6× (resp. 132.1×, 91.9×, and 79.8×), while SRX performs very close to RDF-3X. Compared to results we get with LGD and YAGO, it is worth noticing that GraphDB performs better than Virtuoso with smaller datasets. Still, as for the case of queries, we cannot further comment on the performance of GraphDB and Virtuoso over all update experiments because they are not open-source systems.

Strabon is orders of magnitude slower than SRX and at least two orders of magnitude slower than Virtuoso because it does not support bulk updates; instead, each record in the update batch is treated as an individual database transaction. This approach has a high overhead in performance and cannot scale with frequent updates. As a side note, Strabon builds on the Sesame RDF store [BKvH01] and extends Sesame's query engine and optimizer, but not its transaction processing module.

3.9 Conclusion

In this chapter, we presented SRX, a system for spatial RDF data management built on top of the popular RDF-3X system. SRX employs a flexible scheme that encodes approximations of the geometries of the RDF entities into the entities' IDs. The encoding is based on a hierarchical decomposition of the 2D space and can be effectively exploited in the evaluation of SPARQL queries with various types of spatial filters (ranges, distance joins, kNNs). We did experiments with real datasets showing

that our approach minimizes the evaluation cost of the spatial component in all RDF queries, while incurring a small overhead during updates.

Chapter 4

Content Recommendation for Viral Social Influence

How do we create content that will become viral in a whole network after we share it with friends or followers? Significant research activity has been dedicated to the problem of strategically selecting a *seed set* of initial adopters so as to maximize a meme's spread in a network. This line of work assumes that the success of such a campaign depends solely on the choice of a *tunable* seed set of adopters, while the way users perceive the propagated meme is *fixed*. Yet, in many real-world settings, the opposite holds: a meme's propagation depends on users' perceptions of its *tunable* characteristics, while the set of initiators is *fixed*.

In this chapter, we address the natural problem that arises in such circumstances: Suggest content, expressed as a limited set of *attributes*, for a creative promotion campaign that starts out from a given seed set of initiators, so as to maximize its expected spread over a social network. To our knowledge, no previous work addresses this problem. We find that the problem is NP-hard and inapproximable. As a tight approximation guarantee is not admissible, we design an efficient heuristic, Explore-Update, as well as a conventional Greedy solution. Our experiments show that Explore-Update selects near-optimal attribute sets with real data, achieves 30% higher spread than baselines, and runs an order of magnitude faster than the Greedy solution.

4.1 Introduction

Online networking offers opportunities for new types of marketing. A prime example of such a new marketing technique is viral marketing, whereby organizations run promotion campaigns through word-of-mouth effects within online social networks. The *Influence Maximization* (IM) problem [KKT03], studied intensively during the last decade, aims to find well-chosen *seed nodes* from which to launch such campaigns so as to achieve good results.

Recent works [dVGL12, CM13] have focused on the parameters that define the popularity of a post, campaign, idea, or *meme* within a network. Such works were the first to study the question of how commercial brand posts engage online social network users, drawing from the theory of Uses & Gratifications [Kat59]; they examine post parameters such as *content type* (e.g., entertaining, informational), *media type* (e.g., vivid, interactive), *posting time* (e.g., workday, peak hours) and *valence of comments* (e.g., positive, negative). Interestingly, such studies have reached some ambivalent conclusions; for instance, [dVGL12] ascertains that entertaining content decreases the number of "likes", while [CM13] claims the exact opposite.

Concurrent research has studied the problem of *viral product design* [AW11, BB14], which calls for engineering products by incorporating viral attributes so as to generate peer-to-peer influence that encourages adoption within a network. Aral and Walker [AW11] study the question of viral attribute selection under randomized trials only; Barbieri and Bonchi [BB14] allude to the same problem as a complement to the standard IM problem of selecting a set of seed nodes that maximizes influence, but do not investigate it as a stand-alone problem in its own right. Conceptually, both these works pertain to attributes attached to products; they do not investigate the more general problem of choosing content, out of a set of eligible options, for any kind of *meme* spreading in a network, so as to make it viral.

In this chapter, we introduce and study the problem of selecting content that characterizes any type of *meme*, so as to maximize its expected spread through a network, starting out from a fixed set of initial adopters. For instance, an advertisement post may feature aspects such as *topics*, *people*, *locations* and *abstract themes*. We are particularly interested in those content aspects that are associated with specific *online social network pages*; we denote such aspects as **content attributes**. Fittingly, online social network users themselves are associated with such non-personal network pages: they express their preferences for specific brands, topics of interest, public persons, hobbies, or locations by subscribing to or "liking" such pages. Thereby, an attribute's popularity can be gauged via its number of subscribers or page "likes". For our purposes, we denote the pages that a user subscribes to or "likes" as **user attributes**. We contend that, the more content and user attributes overlap, the more likely that user is to propagate that post. We envisage an organization that aims to achieve high viral effect of a campaign initiated from its fixed set of subscribers. For example, assume $FlyFast$ airways wants to launch a promotion campaign in social media. $FlyFast$ already has a social network presence, and its page has a subscribers' set S fixed at a given moment, while it faces constraints related to its budget and people's attention span. In their design, $FlyFast$ consultants are interested to identify a set of k content attributes, out of a universe of eligible, mutually compatible options, that will maximize the expected network spread of a post starting out from its

subscribers' set S. Assume that, for $k = 4$, the optimal attribute set is {*"Best travel Accessories"*, *"Airline food guide"*, *"Hipster Europe"*, *"Backpacker tips"*}. Guided by this knowledge, $FlyFast$ can infuse its post with complementary content that appeals to users interested in those topics, e.g., promotions to backpackers, references to its hipster audience, and highlights on its food quality. Thereby, it can maximize its promotion's reach.

We are the first to study the *Influence Maximization* problem in which the seed is *given* and post content is *sought*. Our related contributions are as follows:

Problem Setting. We motivate the Influence Maximization problem in settings where the set of initial adopters is fixed, or even a single point of origin, and the content of a propagated meme can be tuned. We formulate the concept of *digital influence* as a special case of social influence.

Propagation Model. We devise a *content-aware* propagation model, whereby the probability of influence across edges depends on content. We show that, with this model: (i) the problem of choosing content attributes that maximize influence is NP-hard; (ii) the spread function is not submodular, hence no submodularity-based approximation algorithm applies; and (iii) it is NP-hard to approximate the optimal solution within a factor of $n^{1-\varepsilon}$ for $\varepsilon > 0$.

Algorithm. We design a fast algorithm, Explore-Update, which achieves higher influence spread than baselines; its effectiveness is based on the iterative estimation of the marginal spread achieved by each attribute, while its efficiency is gained by limiting such computations only to nodes within a probability-based distance threshold θ and attributes potentially affecting such nodes.

Experiments. We compare Explore-Update to two baselines and show that it always achieves better propagation results, while it is significantly faster than a naïve Greedy approach; we calculate the optimal solution on a reduced dataset with a small universe of attributes, showing Explore-Update can achieve optimality; last, we demonstrate the scalability of Explore-Update on seed set size.

4.2 Motivation

4.2.1 Idea Habitats

An *idea habitat* [BH05] is the set of environmental cues that make people think about an idea and pass it along. Regardless of how well an idea is encoded, it will persist and spread only if the environment cues people to retrieve it regularly. In other words, even if an idea *can* be easily recalled, if it is only rarely cued by the environment, it may remain rare and be forgotten. It follows that, for an idea to

spread, it should be not only well encoded and easily recalled, but also regularly retrieved. Promotion campaigns aim to assist the spread of any meme in the same way as idea habitats assist the spread of ideas. For instance, assume that *FlyFast* food is good and therefore memorable. Still, without a viral promotion, *FlyFast* will miss the spotlight, letting other airlines gain public attention.

4.2.2 Digital Influence

Social influence is defined based on peer behavior [Ara11], so as to distinguish it from confounding factors [GM04, dBL01, AMS09, Man93].

Definition 2. Social Influence *expresses the extent to which the behavior of one's peers changes the utility one expects to receive from engaging in a certain behavior, and hence the likelihood that one will engage in that behavior.*

This definition can be used to make an argument that, if we understand how behaviors spread from person to person, our society will be able to promote agreeable behaviors, such as physical exercise and financial responsibility, and limit disagreeable ones, such as violence and dirty needle sharing. By this definition, peer behaviors may relate to awareness, persuasiveness, imitation and social learning [Ara11]. We propose that *digital influence* can be seen as a case of awareness-related social influence, defined as follows:

Definition 3. Digital Influence *expresses the extent to which the content of a commercial digital posting changes the support one wants to provide to that posting, and thus the likelihood that one will propagate it.*

In online social networks, posts are propagated from user to user by means of actions such as *like*, *share*, or *repost* [ALB+15]. Without loss of generality, we group all these actions under the *like* action. What matters is whether users endorse and promote a post further by making it visible to their friends and followers. In our setting, we emphasize the importance of earning *likes* from users at large.

Nowadays, as online social network users are exposed to a plethora of posts, we can safely assume that they become selective on what they *like*. Therefore, a brand that fails to issue likable posts via its social network pages is unlikely to spread awareness of its activities and products. In the same vein, a brand that can estimate how viral a post will be and create appropriate digital content, stands good chances to succeed. We argue that such estimation can be based on the digital influence of content associated with a meme.

4.2.3 Distinctiveness

We emphasize three distinct elements of this work.

Problem Formulation. While our model takes into consideration the influence with regard to a post exercised by users themselves, we seek to maximize the influence exercised by the appeal and quality of a post's content within a network. To the best of our knowledge, we are the first to define this problem, which is distinct from, and cannot be treated by methods aiming at, user selection.

Nature of Attributes. In related works, attributes are configured as *general topics*; e.g., in [BB14] authors assign *tags*, conceived of as general topics, to the role of product attributes. By contrast, in our problem formulation and in our experimental study, an attribute corresponds to a topic of interest *identifiable via a non-personal social network page*. Thus, even a page on an abstract theme (e.g., *Psychology of Relations*) is a possible attribute in our setting: it has a specific commercial value (4,719,837 followers) that differentiates it from other pages on similar topics.

Use of Tags. The type of content attributes we investigate can hardly be articulated via tagging. Tags express highly idiosyncratic user impressions, focusing on arbitrary aspects of content; they are volatile as descriptors of content, whereas we need a stable ground truth to represent content. For example, a video post may relate to several specific topics of interest, yet it would be hard to identify these via user tagging. In consequence, past tagging does not offer valuable information in our problem setting.

4.3 Problem Statement

From the preceding discussion, we conclude that any brand would gain by maximizing the expected effectiveness of its product promotion campaigns within an online social network. We assume that there exists a certain set of *subscribers* to the brand's social network page, and a promotion campaign aims to influence the maximum number of *non-subscribers*; as we discussed, such users are associated with topics expressing their interests.

4.3.1 Content-Aware Cascade Model

We model an online social network as a directed graph $G = (V, E)$, where $V = \{v_1, v_2, ..., v_n\}$ is a set of nodes, each of which corresponds to an individual user, and $E \subset V \times V$ is a set of directed edges representing social relations among users. Each node v has a set of associated attributes $F_v = \{f_v^1, f_v^2, \ldots\}$, from a universe Φ, that define user preferences; we identify these attributes as the non-personal network pages

a user expresses interest in. A meme propagated through the network is associated with a set of attributes $F = \{f_{p_1}, f_{p_2}, \ldots, f_{p_K}\} \subseteq \Phi$; these content attributes, along with the user attributes F_v associated with the targeted node v, affect the probability of its propagation across a network edge e_{uv}.

Accordingly, we define the *Content-Aware Cascade* model (CAC) as a variant of the Independent Cascade model (IC), in which edge propagation probabilities depend on content and user attributes. A CAC diffusion process unfolds in steps, starting from an initial seed set of activated nodes. A node u activated at time step t has a single chance to activate its out-neighbors. The process is incremental, as nodes can alternate only from inactive to active states; the diffusion ends when there is no newly activated node at a given step. At any step, a newly activated node u activates its out-neighbor v with probability $p(u, v)$ equal to:

$$\begin{aligned} p_{uv} &= b_{uv} + q_{uv} \cdot h_{uv}(F_v, F), \quad b_{uv}, q_{uv} \in [0, 1] \\ h_{uv}(F_v, F) &= \min\left\{\tfrac{1-b_{uv}}{q_{uv}}, |F_v \cap F|\right\} \end{aligned} \tag{4.1}$$

where b_{uv} is a *base probability* on an edge and q_{uv} a *marginal probability* that indicates how much the probability on an edge increases for each selected attribute in F matching a preference of node v, as indicated by the transition function $h_{uv}(F_v, F)$, with a sanity bound of $\frac{1-b_{uv}}{q_{uv}}$. We stress that the marginal probability q_{uv} distinguishes among different user links, albeit not among different attributes for a given link; a more complex model could distinguish among different attributes, or even define a probability distribution function over the set of all attributes [BBM12], to be learned by historical logs. We choose to relegate the problem of defining and learning such probability distribution functions to future work, and now study the problem under the modeling assumption that each attribute has the same independent effect on the probability function. Yet, our simplified model forms a special case of any more complex model in which each attribute would have a different effect on the probability function; i.e., in this special case, such effects are rendered equal. So, our subsequent hardness and inapproximability results hold for any such more complex model as well. Furthermore, parameters q_{uv} and b_{uv} can be obtained from past data, as in [BBM12]; in our setting, we assume that such parameters have been obtained in advance.

Given a seed set S of subscribers, for every set of attributes F, we can obtain the total number of activated nodes after running several trials of the diffusion process from S [KKT03]. The *expected* number of activated nodes for a given seed set S and a selected set of attributes F is called *influence spread*, denoted as $\sigma(F|S)$, or, as S is fixed in our problem, just $\sigma(F)$. Thus, $\sigma(F)$ is the *expected* spread of the diffusion, which we can calculate using live-edge instances of the graph (i.e., instances

of activated-only edges [KKT03]) as:

$$\sigma(F) = \sum_{X} Prob[X] \cdot \sigma_X(F) \tag{4.2}$$

where $\sigma_X(F)$ is the influence spread in live-edge instance X.

4.3.2 Content-Aware Influence Maximization

We define the CAIM problem as follows:

Problem 1. *Given a directed graph $G = (V, E)$, where each node v is associated with user attributes $F_v = \{f_v^1, f_v^2, \ldots\}$ from a universe of eligible attributes Φ, a seed set of adopter nodes S, quantities q_{uv}, b_{uv} for each edge $e_{uv} \in E$, and a transition function $h_{uv}(F_v, F) = \min\left\{\frac{1-b_{uv}}{q_{uv}}, |F_v \cap F|\right\}$ for edge probabilities, select a set of k attributes $F \subset \Phi$ that maximizes the spread $\sigma(F|S)$ of a diffusion process with content attributes F starting from S.*

CAIM is a novel problem that aims to find out how one can maximize the benefits of a network promotion campaign with given points of departure. The motivation derives from the fact that, in the real world, brands want to exploit their own social network pages for marketing purposes. Instead of targeting the most influential initiators for a promotion, as in classical IM, one can judiciously invest in the creation of a post with lucrative content, under fixed initiators, guided by the content attributes provided by the CAIM solution. As promotions can be formed with a wide variety of content attributes, each possible attribute set F corresponds to a different probabilistic graph, on which we can compute the influence spread of the seed set S; the attribute set F that achieves maximum spread constitutes the CAIM solution. We emphasize that, due to the drastic difference between classical IM and CAIM in the way influence spread is achieved, *the solutions to these two problems cannot be qualitatively compared against each other.*

4.4 Hardness and Inapproximability

We now show the hardness of the CAIM problem and study the properties of influence spread function $\sigma(F)$. To calculate $\sigma(F)$, we first calculate edge probabilities with respect to the selected content attributes F and then estimate the expected spread on the graph starting from the given set of subscribed nodes S.

Theorem 1. *The CAIM problem with the CAC model is NP-hard.*

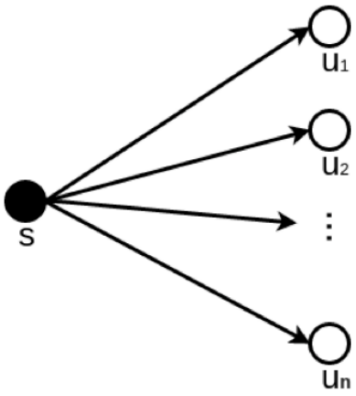

Figure 4.1: A graph instance demonstrating that the CAIM problem is NP-hard.

Proof. Consider an instance of the NP-complete *Set Cover* problem, defined by a collection of subsets $S_1, S_2, \ldots, S_m$, a universe of elements $U = \{u_1, u_2, \ldots, u_n\}$ and an integer k. We are asked whether there are k sets that will cover all elements in U. We show that *Set Cover* can be reduced to a *trivial* instance of CAIM as follows: We construct a bipartite graph with one activated node on the left side that connects to n nodes on the right side, as shown in Figure 4.1. We map each member u_i of universe U to a node on the right side and add an attribute f_j to set F_{u_i} if u_i belongs to subset S_j. We set $b_{uv} = 0$ and $q_{uv} = 1$ for all edges $(u, v) \in E$, i.e., a node v is influenced if at least one of its user attributes is selected. In this trivialized version of CAIM, the spread can be computed deterministically; there is no need for expected spread computations. Then, an algorithm that could optimally solve this trivial instance of CAIM, among others, would decide any instance of *Set Cover*: if we can target all nodes in the CAIM instance using k attributes, we can in effect cover all elements in U using k subsets in *Set Cover*. Otherwise, if the optimal spread in CAIM does not reach all nodes, it follows that there is no set of k subsets that covers all elements in *Set Cover*. Thus, by reduction from *Set Cover*, CAIM is at least as hard as any problem in NP. □

By Theorem 1, there is no polynomial-time algorithm to find an optimal set of attributes F, unless P=NP. We now proceed to study the properties of the influence spread function $\sigma(F)$.

A function $\sigma(F)$ is *submodular* if it follows a *diminishing returns* rule: the marginal gain from adding an element to a set F is at most as high as the marginal gain from adding the same element to a subset of F. That is, $\sigma(F_1 \cup \{f\}) - \sigma(F_1) \geq \sigma(F_2 \cup \{f\}) - \sigma(F_2)$, where $F_1 \subset F_2 \subset \Phi$, for any $f \in \Phi$.

We call a transition function $h_{uv}(F_v, F)$ *monotonic* on F if, for subsets of attributes $F_1 \subset F_2 \subset \Phi$, it holds that $h_{uv}(F_v, F_1) \leq h_{uv}(F_v, F_2)$, for any node v. If the transition function is not monotonic, then the influence spread function is neither

monotonic, nor submodular, because selecting more attributes may reduce probabilities $p(u, v)$ and thereby reduce the total influence spread. We assume that attributes have nonnegative effects on users, rendering the transition function $h_{uv}(\cdot)$ monotonic: edge probabilities can only increase if we add attributes to F, i.e. $h_{uv}(F_v, F) \leq h_{uv}(F_v, F + \{f\})$ for any $f \in \Phi$ and $v \in G$; hence $\sigma(F)$ is monotonic. We now examine whether $\sigma(F)$ is also submodular. This turns out to not be the case, even for a monotonic and submodular transition function, as the next counterexample shows.

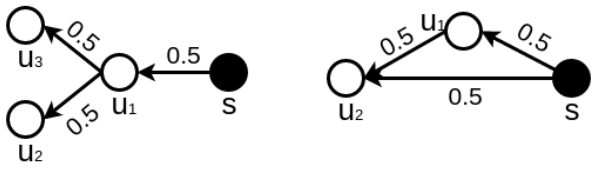

Figure 4.2: Increasing and decreasing marginal returns.

Example 2. *Consider the graph on the left-hand side in Figure 4.2, with a universe of attributes* $\Phi = \{A, B, C\}$*, sets of preferred attributes for each node be* $F_{v_1} = \{A\}$ *and* $F_{v_2} = F_{v_3} = \{A, B, C\}$*,* $b_{uv} = 0.5$*,* $q_{uv} = \frac{1}{2|F_v|}$ *on all edges, and one active node* s*. Then, consider two subsets of attributes* $F_1 = \emptyset$*,* $F_2 = \{B, C\}$*, where* $F_1 \subset F_2$*, and a attribute* $f = A \in \Phi \setminus F_2$*. The achieved spreads for each attributes subset, and the respective marginal gains obtained after adding attribute* f *to subsets* F_1 *and* F_2*, are calculated as follows. For subset attribute* F_1 *selected, we have:*

$$p_{sv_1} = \tfrac{1}{2}, \quad p_{v_1v_2} = p_{v_1v_3} = \tfrac{1}{2}$$
$$\sigma(F_1) = \tfrac{1}{2} + 2\tfrac{1}{4} = 1$$

whereas when $f = A$ *is added to* F_1*, we get:*

$$p_{sv_1} = 1, \quad p_{v_1v_2} = p_{v_1v_3} = \tfrac{2}{3}$$
$$\sigma(F_1 + \{A\}) = 1 + 2 \cdot \tfrac{2}{3} = \tfrac{7}{3}$$

Hence $\Delta_1 = \sigma(F_1 + \{A\}) - \sigma(F_1) = \frac{7}{3} - 1 = \frac{4}{3}$*. Similarly, for* F_2 *selected, we have:*

$$p_{sv_1} = \tfrac{1}{2}, \quad p_{v_1v_2} = p_{v_1v_3} = \tfrac{5}{6}$$
$$\sigma(F_2) = \tfrac{1}{2} + 2 \cdot \tfrac{5}{12} = \tfrac{4}{3}$$

while when $f = A$ *is added to* F_2*, we get:*

$$p_{sv_1} = 1, \quad p_{v_1v_2} = p_{v_1v_3} = 1$$
$$\sigma(F_2 + \{A\}) = 3$$

Hence $\Delta_2 = \sigma(F_2 + \{A\}) - \sigma(F_2) = 3 - \frac{4}{3} = \frac{5}{3}$*. Since* $\Delta_2 > \Delta_1$*, the submodularity of* $\sigma(F)$ *does not hold.*

Given this negative result, the influence function $\sigma(F)$ might have an *increasing returns* property (supermodularity), whereby it would hold that $\sigma(F_1 \cup \{f\}) - \sigma(F_1) \leq \sigma(F_2 \cup \{f\}) - \sigma(F_2)$, for $F_1 \subset F_2 \subset \Phi$ and any attribute $f \in \Phi$. The following counterexample shows that this property does not hold either.

Example 3. *Consider the right graph in Figure 4.2, with a universe of attributes $\Phi = \{A, B\}$, sets of preferred attributes per node $F_{v_1} = \{A, B\}$ and $F_{v_2} = \{A\}$, $b_{uv} = 0.5$ and $q_{uv} = \frac{1}{2|F_v|}$ on all edges, and one active node s. Consider two subsets of attributes $F_1 = \emptyset$ and $F_2 = \{B\}$. Then, for subset attribute F_1 selected, we have:*

$$p_{sv_1} = \tfrac{1}{2}, \quad p_{sv_2} = p_{v_1 v_2} = \tfrac{1}{2}$$
$$\sigma(F_1) = \tfrac{1}{2} + \left(1 - \left(1 - \tfrac{1}{4}\right)\tfrac{1}{2}\right) = \tfrac{9}{8}$$

whereas when $f = A$ is added to F_1 we get:

$$p_{sv_1} = \tfrac{3}{4}, \quad p_{sv_2} = p_{v_1 v_2} = 1$$
$$\sigma(F_1 + \{A\}) = \tfrac{3}{4} + 1 = \tfrac{7}{4}$$

Hence $\Delta_1 = \sigma(F_1 + \{A\}) - \sigma(F_1) = \frac{7}{4} - \frac{9}{8} = \frac{5}{8}$. Similarly, for F_2 selected, we have:

$$p_{sv_1} = \tfrac{3}{4}, \quad p_{sv_2} = p_{v_1 v_2} = \tfrac{1}{2}$$
$$\sigma(F_2) = \tfrac{3}{4} + \left(1 - \left(1 - \tfrac{3}{8}\right)\tfrac{1}{2}\right) = \tfrac{23}{16}$$

while when $f = A$ is added to F_2 we get:

$$p_{sv_1} = 1, \quad p_{sv_2} = p_{v_1 v_2} = 1$$
$$\sigma(F_2 + \{A\}) = 2$$

Hence $\Delta_2 = \sigma(F_2 + \{A\}) - \sigma(F_2) = 2 - \frac{23}{16} = \frac{9}{16}$. Since $\Delta_1 > \Delta_2$, the influence function $\sigma(F)$ is not supermodular either.

Eventually, we have established the following:

Theorem 2. *The spread function $\sigma(F)$ with a probability transition function $h_{uv}(F_v, F) = \min\left\{\frac{1-b_{uv}}{q_{uv}}, |F_v \cap F|\right\}$ is neither submodular nor supermodular.*

By Theorem 2, it follows that we cannot use a greedy algorithm with an approximation guarantee based on submodularity, as in [KKT03]. Moreover, in the following we show that it is NP-hard to approximate the optimal solution to CAIM.

Theorem 3. *It is NP-hard to approximate the optimal solution to the CAIM problem with the Content-Aware Cascade model within a factor $n^{1-\varepsilon}$ for any $\varepsilon > 0$.*

Proof. Consider an instance of the *Set Cover* problem, in which we need to decide whether we can cover all elements of a universe $U = \{u_1, u_2, \ldots, u_n\}$ by selecting at most k subsets out of a collection of $S_1, S_2, \ldots, S_m \subset U$.

We then construct a graph G for the CAIM problem with a single subscriber node s and nodes $u_1, u_2, \ldots, u_n$ corresponding to elements in U, connected so that u_{i-1} points towards u_i for all $i = 2 \ldots n$, and s is connected to u_1, and, for every subset S_j an element u_i belongs to, we add a attribute f_j to the preferred attributes of u_i. Next, for some integer c we add $\eta = n^c - n - 1$ more nodes $x_1, x_2, \ldots, x_\eta$ such that u_n has outgoing edges to them and each x_i has the same preferred attributes as u_n. Graph G, shown in Figure 4.3, has $N = n^c$ nodes. We set $b_{uv} = 0$ and $q_{uv} = 1$ for all edges, so that an edge becomes active if at least one of the attributes associated with its target node is selected. Then, if it is possible to select k subsets that cover all elements of universe U, we can also have $N = n^c$ activated nodes. Conversely, if there is no selection of k subsets that covers all U, then there is at least one node u_i that does not get activated, precluding influence spread to nodes $x_1, x_2, \ldots, x_\eta$. We can then only target at most n out of n^c nodes, a fraction of $n^{1-c} = N^{\frac{1}{c}-1}$. Thus, if we had a polynomial-time algorithm that approximated the optimal solution to CAIM within a factor of $N^{1-\varepsilon}$ for any $\varepsilon > 0$, then it would suffice to set $c = \lceil \frac{1}{\varepsilon} \rceil$ and use that algorithm so as to decisively distinguish between a case that accepts a solution activating all N nodes and one that does not, and thereby also decide *Set Cover*. Thus, by reduction from *Set Cover*, we have shown that it is NP-hard to approximate the optimal solution to CAIM within a reasonable factor. □

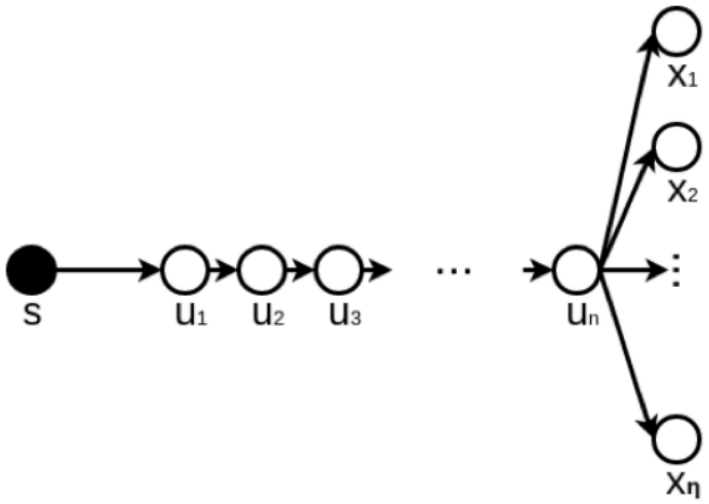

Figure 4.3: A graph instance demonstrating that it is NP-hard to approximate the optimal solution to the CAIM problem.

4.5 The Explore-Update Algorithm

As it is NP-hard to approximate the CAIM solution within a factor of $n^{1-\varepsilon}$ with the Content-Aware Cascade model, we proceed to design heuristic solutions therefor. We structure our exposition as follows: we first present a simple, yet time-consuming greedy heuristic; then, through a sequence of simplifying assumptions, we will generate a much more efficient algorithm called Explore-Update.

Our first proposal is a baseline greedy algorithm that selects the attribute of highest marginal gain to add at each iteration, shown in Algorithm Greedy. This is an adaptation of the *Local Update* algorithm in [BB14] to our problem. Intuitively, it is reasonable to greedily select the locally best attribute in each iteration, especially for small values of k. This kind of algorithm has been shown to achieve better quality than others in classical Influence Maximization [CWW10, CLC13, LKG+07].

Algorithm 1: Greedy(G, S, k)

```
1 F = ∅;
2 while |F| < k do
3 |   for every f ∈ Φ \ F do
4 |   |   calculate σ(F + {f}) using Monte Carlo simulations
5 |   F = F ∪ argmax_f {σ(F + {f})}
6 return F
```

Though simple and effective, Greedy is inefficient due to its calculation of influence spread by MC simulations. In a manner reminiscent of [CWW10], we can improve efficiency by considering *maximum influence paths* between nodes and the seed set. We call a path $P_{max} = \langle u = u_0, u_1, u_2, \ldots, v = u_m \rangle$ between vertices $u \in S$ and $v \in G$ *maximum influence path* (MIP) if this path is the most probable among all paths between u and v: $P_{max} = \text{argmax}_P \prod_{i=0}^{m-1} prob(u_i, u_{i+1})$. Under the *simplifying assumption* that influence is propagated only through MIPs, we can estimate influence spread in polynomial time as follows: For a threshold θ and a node v, we build a tree structure called *in-arborescence* $A_{in}(v)$, which includes all MIPs of probability higher than θ from any node to v: $A_{in}(v) = \{\mathsf{MIP}(u, v) \mid prob(\mathsf{MIP}(u, v)) > \theta, u \in G\}$. Then, given a node u, the seed set S, and an arborescence $A_{in}(v)$, Algorithm calculateAP recursively estimates the probability that u is activated in $A_{in}(v)$, i.e., its *activation probability* $ap(u, A_{in}(v))$.

Based on these calculations, for all nodes $u \in G$, we can calculate the influence spread $\sigma(F)$ as follows:

$$\sigma(F) = \sum_{u \in G} ap(u, A_{in}(u)) \tag{4.3}$$

Algorithm 2: calculateAP(u, $A_{in}(v)$, S)

1 **if** $u \in S$ **then**
2 $\quad ap(u, A_{in}(v)) = 1$
3 **else if** u *has no in-neighbors in* $A_{in}(v)$ **then**
4 $\quad ap(u, A_{in}(v)) = 0$
5 **else**
6 $\quad ap(u, A_{in}(v)) = 1 - \prod_{\omega \in N_{in}(u)} (1 - ap(\omega, A_{in}(v)) prob(\omega, u))$
7 **return** $ap(u, A_{in}(v))$

We can then employ Equation 4.3 so as to estimate influence spread in Algorithm Greedy, in lieu of MC simulations, deriving Algorithm Arb; at each iteration, we compute the in-arborescence of node u for a given threshold θ by converting each probability p_e on an edge e to $-\log p_e$ and employing an efficient implementation of Dijkstra's algorithm. If computing an arborescence takes time t, then Lines 4-6 take nt and the total time is $O(k|\Phi|nt)$.

Algorithm 3: Arb(G, S, θ, k)

1 $F = \emptyset$;
2 **while** $|F| < k$ **do**
3 $\quad$ **for** *every* $f \in \Phi \setminus F$ **do**
4 $\quad\quad$ **for** *every* $u \in G$ **do**
5 $\quad\quad\quad$ compute $A_{in}(u)$ with threshold θ
6 $\quad\quad\quad$ $ap(u, A_{in}(u))$ = calculateAP(u, $A_{in}(u)$, S)
7 $\quad\quad$ calculate $\sigma(F + f) = \sum_{u \in G} ap(u, A_{in}(u))$
8 $\quad F = F \cup \text{argmax}_f \{\sigma(F + \{f\})\}$
9 **return** F

We further reduce the runtime of Algorithm Arb by eschewing redundant iterations of the loops over nodes u and attributes f. First, we limit the calculation of in-arborescences and activation probabilities only to nodes whose in-arborescence under threshold θ reaches at least one node in S; only such nodes can yield non-zero estimated activation probability. To find out these nodes, we compute the out-arborescence of all nodes in S, $A_{out}(S)$, consisting of all MIPs of probability higher than θ from a node $v \in S$ to other nodes in G. Nodes in $A_{out}(S)$ yield non-zero activation probability estimates. Yet, the set of paths in $A_{out}(S)$ may contain directed loops, hence we cannot apply a recursive algorithm like Algorithm calculateAP directly on $A_{out}(S)$; we still need to obtain the in-arborescence $A_{in}(u)$ of each $u \in A_{out}(S)$; we do so while building $A_{out}(S)$, by adding MIP(v, u) to $A_{in}(u)$ for each $u \in A_{out}(v)$. Algorithm Explore illustrates this explore process.

Algorithm 4: Explore(G, F, S, θ)

```
A_out(S) = ∅
A_in(u) = ∅ for every u in G
for every v ∈ S do
    compute A_out(v) for given θ and F
    update A_in(u) for each u ∈ A_out(v)
return {A_in(u) ≠ ∅| for u ∈ G}
```

Then we can calculate influence spread $\sigma(F)$ using the union of such in-arborescences, A_{in}, by Algorithm Update.

Algorithm 5: Update(A_{in}, S)

```
for every u ∈ A_in do
    ap(u) = CalculateAP(u, A_in(u), S)
σ(F) = Σ_{u∈A_in} ap(u)
return σ(F)
```

Second, we limit the calculation of marginal gain in Algorithm Arb only to those attributes that can affect the influence spread. We call an edge in G *participating*, if at least one of its endpoints are in $A_{out}(S)$. Figure 4.4 presents a graph for a seed set S (and selected attributes set F) in the green area; the yellow area includes nodes in $A_{out}(S)$; the set of participating edges Π is shown in solid and dotted lines; dotted edges have only one endpoint in $A_{out}(S)$; non-participating edges are shown in dashed lines, in the gray area.

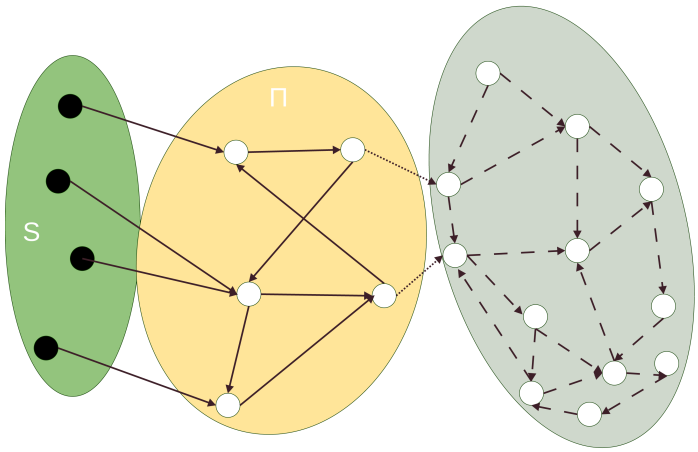

Figure 4.4: Participating and non-participating edges.

Non-participating edges cannot increase influence spread, regardless whether their probability is increased; only participating edges have such potential. We limit the attributes Algorithm Arb considers based on this observation. Let $E(f)$ be the set of edges that include attribute f among their preferred attributes, hence their probability is affected when adding f to F. Then, at any iteration, if *none* of the edges in $E(f)$ is a participating edge, i.e., $E(f) \cap \Pi = \emptyset$, then attribute f need not be examined as a candidate to be added to F; it bears no effect to influence function $\sigma(F + \{f\})$.

Putting together our enhancements to Algorithm Arb, we design the polynomial-time Algorithm Explore-Update. In a nutshell, at each iteration, Explore-Update selects the hitherto unselected attribute f affecting participating edges that brings about the largest increase of influence spread, using the Explore procedure for calculating in-arborescences and the Update procedure for calculating influence spread, while updating the set of participating edges Π at each iteration and using it to determine which attributes need to be examined at the next iteration.

Algorithm 6: Explore-Update(G, S, k, θ)

```
1  F = ∅
2  A_in = Explore(G, F, S, θ)
3  Π = {(u, v) ∈ G | u ∈ A_in or v ∈ A_in}
4  while |F| < k do
5      for f ∈ Φ \ F do
6          if E(f) ∩ Π ≠ ∅ then
7              A_in = Explore(G, F + {f}, S, θ)
8              Π_f = {(u, v) ∈ G | u ∈ A_in or v ∈ A_in}
9              σ(F + {f}) = Update(A_in, S)
10     f_max = argmax_f {σ(F + {f})}
11     F = F ∪ f_max
12     Π = Π_fmax
13 return F
```

Let the time complexity to calculate an out-arborescence for node in S be $t_{out\theta}$, then the Explore procedure takes $|S|t_{out\theta}$ and the Update procedure takes $O(n_{in\theta}n_{out\theta})$ time, where $n_{in\theta}$ is the number of nodes in in-arborescences, and $n_{out\theta}$ is the number of nodes in out-arborescence of S. Therefore, if we perform κ calculations of A_{in} per iteration, the total runtime is $O(k\kappa(|S|t_{out\theta} + n_{in\theta}n_{out\theta}))$. In effect, the Explore-Update algorithm is expected to perform well when the size of arborescences is small, and the number of updates κ per iteration is smaller than $|\Phi|$. As propagation probabilities on edges are usually small in real networks, the size of arborescences is indeed expected to be small. The number of updates depends on the structure of the network. In a large-diameter network where multiple hops are required to reach most nodes from S via a MIP, there is a good chance to reduce the number of computations significantly.

4.6 Experimental Study

This section presents an experimental study on the Greedy and Explore-Update algorithms we have introduced. All experiments were run on a 32GB Intel Core i5-2450M CPU machine @ 2.50GHz, while algorithms were implemented in C++.

As there is no previous work on the CAIM problem, we compare to basic baselines. Still, as we discussed, the previous work that comes closest to our problem is that by Barbieri and Bonchi [BB14]; yet that work solves primarily the problem of selecting a set of seed nodes, and secondarily a set of product attributes, so as to maximize product influence in a network. The best-performing algorithm for updating an attribute set in [BB14], *Local Update*, performs one addition or removal of an attribute to/from the current attribute set at each iteration; in effect, our Greedy algorithm can be considered as an adaptation of *Local Update* to our problem, where only additions of attributes are needed. Therefore, to the extent that a comparison to [BB14] is possible, *we conduct it via the comparison to the Greedy algorithm itself.* Another method for updating an attribute set proposed in [BB14], *Generic Update*, is a hard-to-tune genetic algorithm, which may lead to an unpredictable number of output attributes. Besides, as the experimental study in [BB14] shows, *Genetic Update* offers no qualitative advantage while it is much slower than *Local Update*, which is already by far the most time-consuming algorithm in our study. Therefore, we do not consider a genetic algorithm in our experimental study.

Diffusion models. In the Content-Aware Cascade model the probability on edge (u, v) is a linear function of product and base probabilities q_{uv} and b_{uv}. To assign these probabilities we use two techniques prevalent in previous work [CWW10].

- **Weighted Cascade model**: probability $\frac{1}{d_v}$ is assigned to edge (u, v), where d_v is the in-degree of node v. We use this model for the sake of compatibility with previous works, even while it may fit less to our problem setting.
- **Multivalency model**: the probability for edge (u, v) is drawn uniformly at random from a set of probabilities. We choose that set to be $[0.02, 0.04, 0.08]$.

Further, we calculate b_{uv} for every edge (u, v), and set $q_{uv} = \frac{b_{uv}}{|F_v|}$.

Algorithms. We compare the Explore-Update algorithm under different threshold θ values to three other algorithms:

- **Greedy**: This is Algorithm Greedy in this chapter, which is effectively an adaptation of *Local Update*, the best algorithm in [BB14]. A similar algorithm has been used extensively in the context of the Influence Maximization problem, and always demonstrated top performance in terms of spread, while being slower than other heuristics [CLC13]; it requires specifying the number of Monte-Carlo simulations to calculate influence spread, as we do in the following.

Table 4.1: Data characteristics.

Dataset	Gnutella	VK
Nodes	10,876	7,420
Edges	39,994	57,638
Average Clustering Coefficient	0.0062	0.28
Number of Triangles	934	168,284
Diameter	9	16
Attributes/Seed sets	151	3,882
Default Seed Size	34	15

- **Top-Nodes**: This algorithm measures each attribute's frequency among node preferences and selects the k most frequent ones.
- **Top-Edges**: This algorithm assigns to each edge $e = (u, v)$ the attribute preferences of node v, F_v, and selects the k most frequent attributes across all edges.
- **Brute-Force**: This algorithm finds all possible sets of attributes of size k, computes each one's influence spread using Monte-Carlo simulations, and opts for the best. Because the solution space is exponential, we use this method on reduced datasets.

Datasets. We run experiments in two real-world networks. The first network is a peer-to-peer file sharing directed network Gnutella[1], where nodes represent hosts and edges represent connections between the Gnutella hosts. Our second network is extracted by crawling the social network VK[2]; nodes are users and edges are friendships among them. Statistics are presented in Table 4.1.

Attribute assignment and seed selection. We utilize one general and one ad-hoc method for attribute preference assignment. In Gnutella, to assign an attribute preferences set F_v to node v, we find the block partitioning that minimizes the description length of the network by stochastic blockmodel ensemble; this technique is used to discover the block structure of empirical networks and results to block memberships for each node [KN11, Pei15]. We allow nodes to have overlapping memberships to different blocks. Each block β_i is associated with a distinct attribute f_i. The attribute preference set of a node v_j, F_{v_j} is the set of attributes of the blocks v_j belongs to. The returned partitioning consists of 151 blocks; the default seed set S is one of the blocks, of size 34. For VK, the data comes along with annotations of *groups* and *pages*, which allow us to derive both node attributes and seed sets. A *group* or *page* is a community of users that share content with each other and communicate about a topic of interest (e.g., football clubs or TV series). We use these group memberships to derive both node attributes and seed sets, consistently to our motivation. There are 3882 such groups; the default seed size is 15. Unless otherwise indicated, in our experiments we use the default seeds.

[1]https://snap.stanford.edu/data/p2p-Gnutella04.html
[2]https://vk.com/

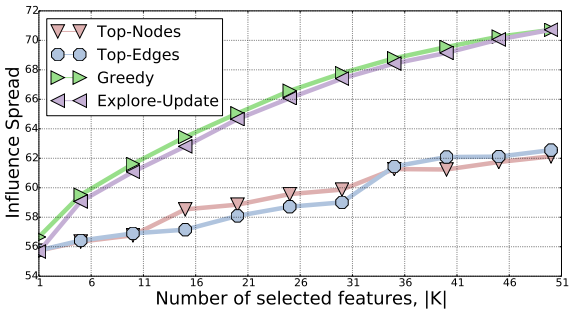

(a) Multivalency on Gnutella

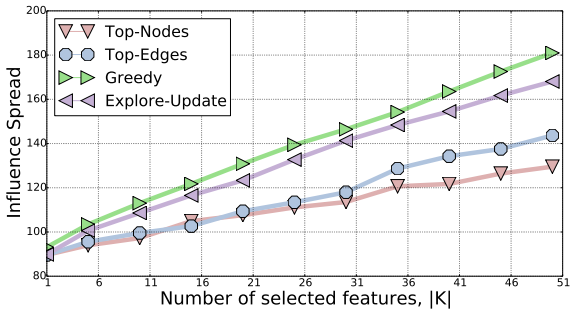

(b) Weighted Cascade on Gnutella

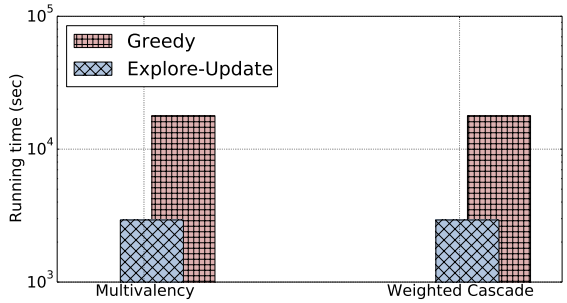

(c) Runtime on Gnutella, $k = 50$

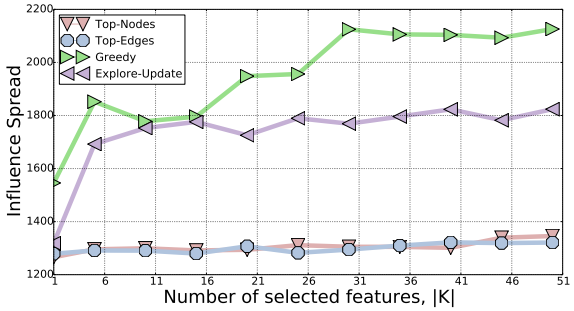

(d) Multivalency on VK

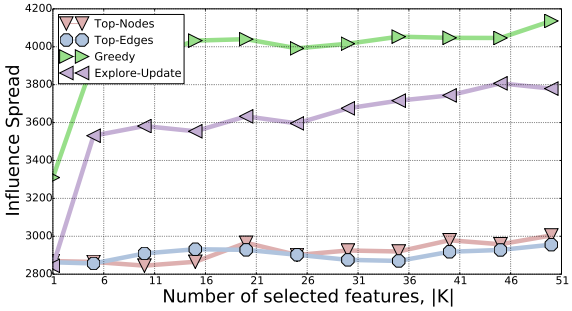

(e) Weighted Cascade on VK

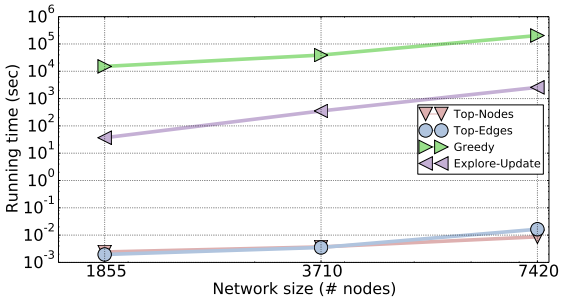

(f) Runtime on VK with Multivalency, $k = 20$

Figure 4.5: Influence spread and runtime results.

4.6.1 Influence spread

Figures 4.5a and 4.5b present our results on competing algorithms' influence spread[3] on the Gnutella network, varying number of selected attributes k from 1 to 51. We used 10000 MC simulations for Greedy, and $\theta = 1/320$ for Explore-Update. We observe that Explore-Update arrives just 1% and 5% below the performance of Greedy with the Multivalency and Weighted Cascade model, respectively. On the other hand, the Top-Edges and Top-Nodes algorithms reach only 88% and 85% of the spread of Explore-Update. Figures 4.5d and 4.5e present influence spread in VK network. Now Greedy used with just 500 Monte-Carlo simulations comfortably achieves 15%, 37%,

[3]We use 10000 Monte-Carlo simulations to compute the final spread of all solutions.

and 48% higher spread than Explore-Update with $\theta = 1/40$, Top-Nodes, and Top-Edges, respectively, in MV model. The picture is similar with the WC model, where Greedy achieves spread 9%, 38%, 40% higher than Explore-Update, Top-Nodes, and Top-Edges. Overall, our results confirm that Explore-Update achieves high influence spread for networks where the local neighborhood of the seed set has structure amenable to long distance arborescences.

4.6.2 Runtime

We now compare algorithms in terms of runtime. Figure 4.5c presents the results with Gnutella for $k = 50$; Explore-Update ($\theta = 1/320$) runs an order of magnitude faster than Greedy (10000 simulations); Top-Edges and Top-Nodes output a selected set in less than a second, hence we do not include them. Next, we investigate how the algorithms scale with increasing network size. We extract subnetworks of VK consisting of 1855, 3710, and 7420 nodes of the original network (i.e., 1/4, 1/2, and full network) and proportional edge density to the full network. In all cases, we compute the runtime on a seed set S of size 15, with the Multivalency model for $k = 20$, for Greedy (10000 simulations), Explore-Update ($\theta = 1/40$), and the Top-Edges and Top-Nodes heuristics. Figure 4.5f shows that runtime scales linearly in network size in all cases. Moreover, we ascertain that while Explore-Update fares no better than Greedy in terms of influence spread, it is much faster.

4.6.3 Effect of Seed Size

We now test the performance of Explore-Update for different sizes of the seed set S. We select different seed sets from size 21 (minimal size for the current block partition) to 101 with step 10 on Gnutella. Figures 4.6a and 4.6b present the influence spread for Explore-Update and Top-Edges for $k = 50$, as well as the runtime of Explore-Update, whereas Greedy is orders of magnitude slower for this setup, and Top-Nodes performs worse than Top-Edges. We note that Explore-Update always achieves better influence spread than Top-Edges. Interestingly, influence spread and runtime do not always grow with $|S|$. This is explicable by the fact that different seed sets induce different local structures.

4.6.4 Effect of θ

Next, we study the effect of the θ threshold, which controls the size of arborescences and thereby the influence spread achievable from seed set S. Figure 4.6c presents the influence spread and runtime with the Gnutella network for θ in $\{\frac{1}{10}, \frac{1}{20}, \ldots, \frac{1}{320}\}$, with the WC model for $k = 50$. The runtime of Explore-Update grows linearly in the

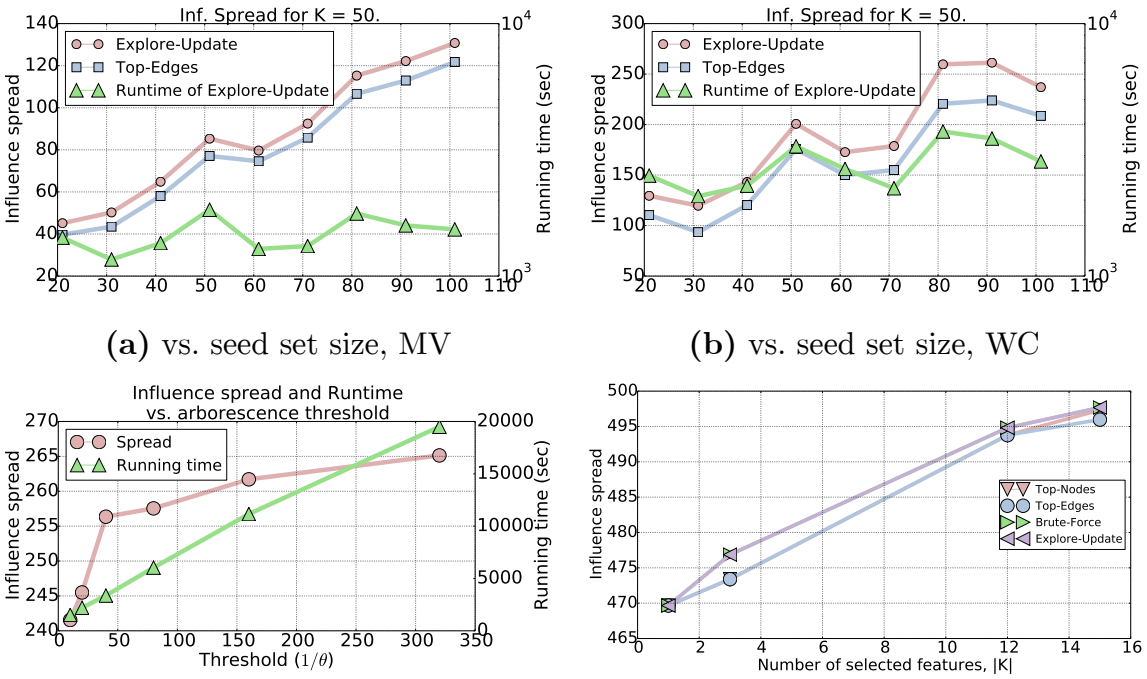

(a) vs. seed set size, MV

(b) vs. seed set size, WC

(c) vs. θ

(d) reduced network

Figure 4.6: Influence spread and runtime vs. seed set size and θ on Gnutella in **(a)**, **(b)**, and **(c)**. Influence spread on reduced network in **(d)**.

inverse threshold θ, while influence spread grows logarithmically in it. A good tradeoff between quality and runtime is found at the knee point in the influence spread curve for $\theta = \frac{1}{40}$.

4.6.5 Comparison to the Optimal Solution

By Theorem 3, we proved it is NP-hard to approximate the optimal solution to CAIM. Now, we compare the results of heuristics to the optimal solution obtained by brute force; we reduce the total number of attributes to 16 and use a reduced Gnutella network by selecting 2K nodes, yielding similar degree distribution properties to the original. Figure 4.6d shows the influence spread results, with the Multivalency model, for a random seed set of size 10. Remarkably, Explore-Update finds the optimal set of attributes with varying k.

Next, we select $k = 10$, yielding $\binom{16}{10} = 8008$ possible attribute sets, and calculate, with a new random seed set of size 428, the *rank* of each algorithm's solution among all possible attribute sets: for each attribute set, we compute its influence spread using 10000 MC simulations; we sort sets by their spread values, and identify the rank of the solution returned by each heuristic. Table 4.2 presents those ranks. Explore-Update selects the optimal solution, while Greedy with 500 parsimonious MC simulations

Table 4.2: Algorithm ranking with regards to optimal solution.

Algorithm	Rank	Spread
Explore-Update	1	34.592
Greedy	5	34.114
Top-Edges	113	33.592
Top-Nodes	113	33.592
...		
—	8008	27.82

yields the fifth best attribute set. The selected attribute sets differ from each other in 2 out of 10 attributes. We obtained similar results for other values of k, with Explore-Update always returning the optimal attribute set.

4.6.6 Real-World Examples

Last, we looked into the actual results - seed sets and selected attribute sets of our experiments, with special attention to the VK data set with the multivalency model, and inspected our results. One interesting observation was that those attributes that are liked by seed set users were rarely among the ones selected in the final solution; this fact indicates that our problem makes good practical sense, while a straightforward naive solution of sticking to what is liked by seed nodes does not yield good results. Nevertheless, selected attributes exhibited a remote, yet unpredictable, resemblance to the attributes liked by seed set nodes. For example, with a group titled "La vie et l'amour" as seed, the selected attributes in our VK network sample included "Home Comfort | Design | Interior Design | Style". With "Psychology of Relations" as seed, the selected attribute set included "Philosophy of Life". Such analogies between seed set and selected attributes, while retrospectively intuitive, would not be derived otherwise; they depend on the way nodes of diverse interests interact within the overall network structure. Such results vindicate our problem motivation.

We also checked how result sets change when we vary k. For example, we select 100 out of 431,374 subscribers of "Esoterica YOGA MEDITATION" as seed set. With $k = 3$, the selected attributes are {"MODA", "La vie et l'amour", "Blog for Men"}. As "Esoterica YOGA MEDITATION" targets primarily women, results such as "MODA" and "La vie et l'amour" are unsurprising. Nevertheless, interestingly, both Explore-Update and Greedy also return "Blog for Men" as a selected attribute, whereas the simple Top-Nodes and Top-Edges heuristics do not. This result shows that our algorithm can select non-trivial attributes.

4.7 Conclusion

In this chapter, we proposed the problem of content-aware influence maximization (CAIM). The goal is to select k attributes that characterize a propagated meme's content, such that its spread across a network from fixed points of departure is maximized, whereby different attribute sets yield different propagation probabilities across network edges. To our knowledge, there is no previous work on this problem. We formulated a content-aware cascade model and showed that the problem is NP-hard and inapproximable, while the influence function is neither submodular, nor supermodular. We developed an efficient algorithm for CAIM using bounded local arborescences to calculate influence spread. Our experimental study demonstrates that this Explore-Update algorithm selects topic sets that achieve high spread and is orders of magnitude faster than a conventional Greedy solution resembling algorithms developed for related problems. We also provide evidence that Explore-Update can achieve the optimal solution when the number of selected topics is small.

Chapter 5

Adaptive Content-Aware Influence Maximization through Online Learning to Rank with Business Analytics

How can we adapt the composition of a post by a *brand* agent over a series of rounds to make it more appealing in a social network? Techniques that progressively learn how to make a fixed post more influential over several rounds have been studied in the context of the *Influence Maximization* (IM) problem, which seeks a set of *seed users* that maximize a post's influence. However, to our knowledge, there is no work on progressively learning how a post's *features* affect its influence. In this chapter, we propose and study the problem of *Adaptive Content-Aware Influence Maximization* (ACAIM), which calls to find k features to form a post in each round so as to maximize the cumulative influence of those posts in a social network over all rounds. We solve ACAIM by applying, for the first time, an *Online Learning to Rank* (OLR) framework to IM purposes. We introduce the *Content-Aware TopRank Influence Dissemination* (CATRID) model, which expresses how posts disseminate in a social network using click probabilities and post visibility criteria, and develop a simulator that runs CATRID via a training-testing scheme based on VKontakte (VK) posts, so as to realistically represent the learning environment. We deploy three distinct learners that solve ACAIM in an online manner. We experimentally ascertain the practical suitability of our solutions via exhaustive experiments on diverse VK datasets, while the learner that achieves best performance is one that leverages user feedback along with a *transitive* data structure that determines the relative importance of post features to users.

5.1 Introduction

Consider stakeholders (henceforward, *brands*) that maintain social network pages[1] for advertising purposes and social network users who choose to *follow* pages they are interested in. After a user follows a page, she gets notified of relative posts and the page is added to her set of *user features* [ITTK17]. A brand may aim to build a *post* around a set of appealing *content features*, so that it spreads well in the network when shared with subscribers. This problem is called *Content-Aware Influence Maximization* (CAIM) [ITTK17]. Contrary to the problem of *Influence Maximization* (IM) [KKT03, LFWT18], CAIM seeks a set of features of a post propagated from a known set of initial adopters, rather than a set of initial adopters to promote a known post (or idea, belief, legend, behavior, etc.). Other works also utilize content to achieve influence in a social network [AW11, BBM12, BB14, CFL+15, LZT15], yet differ in terms of their targets, content type, and initial adopters.

A variation on IM is *adaptive* IM, whereby a brand diffuses a given post in many rounds and selects initial adapters in each round utilizing previous feedback, aiming to maximize the cumulative influence over all rounds. Some works study this problem under known network parameters [GK11, CK13, YT17, SHYC18, HTH+20], while others solve it aiming to simultaneously learn latent parameters [LMM+15, CWYW16, VLS16, VKW+17, WKVV17, WLW+19]. To our knowledge, no prior work addresses multi-round CAIM.

In this chapter, we study *Adaptive Content-Aware Influence Maximization* (ACAIM), which seeks content of a sequence of posts over several rounds, each first reaching a brand's subscriber set, aiming to maximize cumulative influence. We apply the TopRank Model (TRM), used to solve the *Online Learning to Rank* (OLR) problem [LKLS18], to model click probabilities per user and define a novel propagation model, *Content-Aware TopRank Influence Dissemination* (CATRID). We presume that users respond to specific post features; once a sufficient number of a user's friends likes a post, that post becomes visible to the user; user clicks on features of a propagated post denote the reasons for a user to like the post. We deploy a *simulator* that runs CATRID based on VK[2] data to obtain realistic feedback per round.

ACAIM addresses a real-world need; brands share *everyday* posts in their pages and wish to have appealing content. For instance, we solved ACAIM for a brand on "Olympic Games"; after feedback rounds of various content we found that the three most influential features for that brand in *ranked order* are the VK pages "Anonymous revelation stories", "Show business news", and "Funny & ridiculous jokes". These pages

[1] We consider that each *feature* corresponds to a specific social network page.
[2] `https://vk.com/`

serve as a repository for an advertiser to check posts shared therein and get ideas on how to form posts combining "Olympic Games" with the discovered features. The abundance of repository posts helps the advertiser create a different post each time; our simulator considers post uniqueness.

We summarize our main contributions as follows:

- **Problem.** We introduce the ACAIM problem, which seeks influential features in an adaptive setting, and solve it via Online Learning to Rank with the CATRID propagation model.
- **Simulator.** We deploy a simulator that runs CATRID to generate realistic feedback guided by real VK posts.
- **Learners.** We develop three learners for ACAIM: RANDOM, a baseline with non-trivial application semantics; *TopRank IM Classic* (TRIM_C), integrating TOPRANK [LKLS18]; and *TopRank IM Eliminator* (TRIM_E), which uses the same TRM click model as TRIM_C, but leverages clicks differently: TRIM_E eliminates features over rounds during *exploration* and further ranks them during *exploitation*, with impressive results.
- **Experiments.** We conduct a thorough experimental study to assess our solutions on multiple brands and VK datasets.

5.2 Problem Statement

We define ACAIM on a network $G = (V, E)$, where V is a set of nodes (users) and $E \subseteq V \times V$ is a set of directed edges (user relations).

5.2.1 TRM Click Model in Social Networks

Let L be the set of *features*, k the number of ranking positions with $|L| \geq k$, where each user $v \in V$ is associated with a feature set F_v capturing user preferences [ITTK17]. The set of $\frac{|L|!}{(|L|-k)!}$ k-permutations of L, $\mathcal{A}$, is a set of rankings, each corresponding to a *post* A_t, and defines the action space of a *learner* aiming to maximize the expected number of *likes* [ITTK17] over n rounds. By the learning process of [LKLS18], in each round t, the learner chooses a post $A_t \in \mathcal{A}$ and observes binary random variables $C^v_{t1}, \ldots, C^v_{tk}$ for each user $v \in V$, where $C^v_{tf} = 1$ if v clicked on feature f appearing in position i_f of A_t. Given feature f in position i_f in post A_t, the probability that user v clicks on f by the TRM click model [LKLS18] is:

$$v(A_t, i_f) = \mathbb{P}(C^v_{tf} = 1 \mid A_t) \tag{5.1}$$

We apply TRM as a position-based click model, where each A_t and each set F_v is a *weighted feature vector* of size $|L|$; the weight of feature f in A_t, $A_t(f)$, expresses the *portion degree* of f in A_t, while the weight of f in F_v, $F_v(f)$, expresses the *preference degree* of f in F_v; the sum of weights over features is equal to 1 in both A_t and F_v, while A_t has exactly k non-zero weights. We define:

$$\mathbb{P}(C^v_{tf} = 1 \mid A_t) = A_t(f) \cdot F_v(f) \tag{5.2}$$

By Equation 5.2, a user v clicks on feature f in A_t with probability equal to the inner vector product $A_t(f) \cdot F_v(f)$, which corresponds to the sum operand of a PBM click model [RDR07], where $A_t(f)$ holds *position-dependent examination* probabilities and $F_v(f)$ *item-dependent attraction* probabilities. We contend that if user v clicks on a feature f of A_t (i.e., if $C^v_{tf} = 1$), she is influenced by $A_t(f) \cdot F_v(f)$ value, otherwise (i.e., if $C^v_{tf} = 0$), f does not influence v. We argue that v ends up to *like* post A_t if she is sufficiently influenced by it. Semantically, each click of v on a feature f of A_t is interpreted as a positive impression of f on v that contributes to v liking A_t, and hence making it visible to her relations in G. For a post A_t to be visible to v, several friends of v should like it. Otherwise, v does not see A_t, hence she is not influenced by it. Thus, if a feature f of A_t is clicked by many users, it opens up many influence paths for A_t. We rewrite Equation 5.2 as:

$$\mathbb{P}(C^v_{tf} = 1 \mid A_t \textit{ is visible to } v) = A_t(f) \cdot F_v(f) \tag{5.3}$$

We integrate TRM (henceforward, depicted by Equation 5.3) in the CATRID propagation model, which we describe next.

5.2.2 CATRID Propagation Model

Parameters. The CATRID propagation model has four parameters: (i) post feature vector, A_t, (ii) user feature vector, F_v, (iii) user like threshold, lt_v, and (iv) post visibility fraction, vis_v. A_t and F_v define a user's TRM click model (Equation 5.3); lt_v defines how much a user v should be influenced to like A_t; and vis_v defines how many in-degree friends of v should like A_t to make it visible to v.

Execution. By CATRID, a post A_t propagates in discrete time steps. In the first step, all subscribers of the posting *brand* see A_t, apply TRM to possibly click on its features, and are influenced by the clicked features. A user v *likes* A_t when the *total influence* (the sum of separate influence incurred by each clicked feature) on v by A_t is not lower than lt_v. Activated subscribers comprise the first-step activated users. In each subsequent step, new non-subscribers are activated by A_t, where the vis_v of a user v is utilized to check whether A_t is visible to v and apply TRM in accordance

Table 5.1: The fixed parameters of CATRID, A_t and lt_v. Each X (Y) depicts the *weight* (*participation units*) of feature f in A_t.

k	3	4	5	Description
$A_t(f_1)$	0.5 (15)	0.4 (12)	0.33 (10)	f_1 denotes the 1st-ranked feature in A_t
$A_t(f_2)$	0.33 (10)	0.3 (9)	0.26 (8)	f_2 denotes the 2nd-ranked feature in A_t
$A_t(f_3)$	0.16 (5)	0.2 (6)	0.2 (6)	f_3 denotes the 3rd-ranked feature in A_t
$A_t(f_4)$	N/A	0.1 (3)	0.13 (4)	f_4 denotes the 4th-ranked feature in A_t
$A_t(f_5)$	N/A	N/A	0.06 (2)	f_5 denotes the 5th-ranked feature in A_t
lt_v	[0, 0.5]	[0, 0.4]	[0, 0.33]	lt_v is randomly selected from each range

with lt_v to determine whether v likes A_t. The propagation of A_t stops when no new user likes A_t. The next section provides more details.

Training. To tune the parameters of CATRID we introduce a training[3] phase that considers only posting *brands* as features, hence handles single-feature posts (*sp*). This training phase tunes the F_v and vis_v parameters of CATRID. We calculate $F_v(f)$ as $\frac{clicks\_on\_f}{sum\_of\_clicks}$, where the numerator depicts the number of times that v clicks on f and the denominator the total clicks by v, and vis_v as the average percentage of in-degree friends of v who liked *sp* before v liked it. The training process initializes values in each F_v uniformly to $\frac{1}{|L|}$ and also sets each vis_v to 10%. For each examined post *sp*, if user v liked *sp*, we consider that v clicked on *brand*, hence update counters for F_v and vis_v accordingly. We set parameters A_t and lt_v for each k as in Table 5.1. The weights in A_t relate to the *simulator* we present in next section; we select lt_v values independently at random from ranges based on the maximum value in A_t that denotes the maximum possible *total influence* of A_t on any v.

Knowledge. The training phase yields a *trained*CATRID known solely to our *simulator*, while each *learner* only knows that user clicks abide by the TRM click model. In the testing phase, a learner starts its execution knowing the same A_t and F_v as the simulator. We evaluate learners under real-world settings, where *partial knowledge* (i.e., the TRM click model) is available, but *complete knowledge* (i.e., the CATRID propagation model) is not. To enhance the realism of the testing phase, we apply the simulator's TRM using VK posts.

5.2.3 ACAIM Problem

Given a social network $G = (V, E)$, a feature universe L, a weighted feature set F_v of size $|L|$ capturing the preferences of each user v, a budget k, a *brand* corresponding to a feature in L and having a subscriber set S, a *simulator* representing the feedback environment based on a known *trained*CATRID, a set of testing posts, and a number of rounds n, build a *learner* that, selecting a post A_t of k features to

[3]In our experiments, the training phase covers the years 2010–2017 of VK (80% of data).

be propagated from S in each round t and evaluating its known TRM by random sampling, maximizes the cumulative influence spread (i.e., number of total likes) I_n in G over n rounds:

$$I_n = \max \sum_{t=1}^{n} \text{spread}(A_t \mid S) \tag{5.4}$$

As F_v is updated differently by simulator and learner in the testing phase, we depict their respective variants as F_v^s for the simulator's variant and F_v^l for the learner's variant. The set S is the starting point of the influence process, but is not taken for granted: A_t activates *some* users in S, and *brand* is always the top-ranked feature in A_t; we search for the remaining $k-1$ features.

We stress that ACAIM is the first IM-problem that benefits from OLR research. The motivation to use OLR was to build an IM-framework that provides *realistic feedback* in simulation. Previous IM works use *random sampling feedback* relative to the activation probabilities on the edges of G, and such kind of feedback is much less trustworthy for practical applicability to real world. Instead, the activation of users in CATRID relates with their click probabilities and not with probabilities on their edges. This fact enables the applicability of ACAIM to social networks, since we contend that it is much easier for a social network company to define which features of a post attract the users (gain their clicks) than finding which of their friends influenced them for that post, as the number of features in a post is much less than the number of user friends.

5.3 CATRID Simulator

Function SimCATRID presents our *simulator*.

Function SimCATRID

Input : A_t, S, $testingPosts$, CATRID_t
Output : $\mathcal{I}_t$, CATRID_t

Load sp posts from $testingPosts[f]$ to $clickPosts[f]$ for each $f \in A_t$;
Activate S in first step (no vis_v) and Activate a different $V \setminus S$ in next steps (with vis_v);
for *each user* $v \in S$ *or* $v \in V \setminus S$ *who sees* A_t, *her activation is evaluated as follows* **do**
    $I_{\tau v} = 0$; // init the *total influence* of A_t on v
    for *each feature* $f \in A_t$ **do** // TRM applicability
        if v *liked at least* 1 *post* $sp \in clickPosts[f]$ **then** // v clicked on f
            $I_{\tau v} = I_{\tau v} + A_t(f) \cdot F_v^s(f)$; Update $F_v^s(f)$; // CATRID_t updated
    if $I_{\tau v} \geq lt_v$ **then** $\mathcal{I}_t$.insert(v); // v gets activated by A_t
Update vis_v for each user $v \notin S$ who sees A_t; // CATRID_t updated
return $\mathcal{I}_t$, CATRID_t;

Given a post A_t, a *brand*'s subscriber set S, the posts of testing phase $testingPosts$, and the CATRID model tuned up to round t, the simulator outputs the set of users $\mathcal{I}_t$ activated by A_t along with the CATRID model updated by processing of A_t.

SimCATRID runs the CATRID propagation model to produce realistic output when called by the learners, to be discussed in next section. To do so, simulator considers complete knowledge of any post sp published during testing[4] phase involving any feature in L; $testingPosts[f]$ contains all sp posts by posting $brand$ f in increasing chronological order. For each feature in A_t, simulator first loads (Line 1) a number of posts equal to the proportional *participation units* of f in A_t (Table 5.1). E.g., if SimCATRID is called for first time with $k = 4$ and f is the 3rd feature in A_t, then $clickPosts[f]$ includes the first 6 posts published by f in the testing phase. We load posts progressively over calls to SimCATRID; in the rare case that no more posts exist for some feature, we randomly pick one over all testing years. To clarify the logic of sp posts loading in Line 1, we stress that simulator approximates each real post A_t that cannot accurately be found due to the ambiguities of post tagging [ITTK17], by considering real sp posts for which it has knowledge of.

After loading posts, simulator proceeds to the activation of users in discrete time steps (Line 2). First, activation mentions to subscribers (S), then activation pertains to a *different* set of non-subscribers ($V \setminus S$) up until no new user likes A_t. Subscribers always see A_t but non-subscribers should use vis_v to check if A_t is visible to them, while the activation process is the same for each user v who sees A_t (Lines 3–8). On each such user v (Line 3), simulator applies the TRM click model based on the sp posts associated to the features in A_t and computes the *total influence* $I_{\tau v}$ of A_t on v; if that is not less than lt_v, then v is activated by A_t. Note that CATRID_t is updated by F_v^s changes due to v clicked on f (Line 7), as also by vis_v changes of non-subscribers who see A_t (Line 9).

SimCATRID in effect follows a TRM click pattern by the condition in Line 6, since the more prominently a feature f appears in a post (higher $A_t(f)$) and the more it attracts the interest of user v (higher $F_v(f)$), the more likely it is that v *likes* at least one of the sp posts associated with f and so to precisely infer that v *clicks* on f. To achieve that, simulator requires a good tuning of A_t and F_v, ensured in training. Besides A_t and F_v, the *like* of a user to a post also depends on latent factors (e.g., how popular the post's features are at that time, how often a user likes posts) that our simulator implicitly considers, and that enhances further its realistic responses.

[4]In our experiments, the testing phase covers the years 2018–2019 of VK (20% of data).

5.4 ACAIM Learners

In this section, we present our ACAIM learners, which utilize a known input (G, L, F_v^l) and an unknown input ($trained$CATRID, $testingPosts$), leveraged by the simulator. Associated with the known input are the brand feature $brand$, the subscriber set S, the number of features per post k, and the number of rounds n; Trim_C has an additional clicks threshold parameter θ. The output of all learners is the cumulative influence spread I_n and the modified CATRID (CATRID_n) over n rounds of learning. For all learners, the top-ranked feature for each A_t is $brand$, hence we consider $brand$ as chosen by default.

5.4.1 The Learner Random

The learner Random constitutes a baseline to solve ACAIM. In each round t, it forms the post A_t by uniformly at random selecting $k-1$ features out of L and defining their rank to A_t. Then, it uses SimCATRID to find activated users ($\mathcal{I}_t$) to update I_n and also updates CATRID. After processing all n rounds, it returns the cumulative influence spread I_n and the associated CATRID_n. Despite the trivial operation of Random, its randomly picked $k-1$ features for each A_t could express an arbitrary human selection in the real world.

5.4.2 The Learner Trim_C

Algorithm Trim_C presents the *classic* learner Trim_C, which represents an adaptation of TopRank learner in [LKLS18] to IM purposes.

Trim_C has an *exploration* and *exploitation* stage. In *exploration*, a relation R is filled in each round t to maintain an *order* among disjoint feature blocks of L, noted as $B_{t1}, \ldots, B_{td}$, where their union forms L and mentioned as a *partition* of L. Each *block* is located at a separate *level* in the order of R; features residing in blocks of higher levels compete to participate in higher-ranked positions of A_t than features of blocks in lower levels. The entries of R are feature pairs. Adding a feature pair (f_2, f_1) to R denotes that Trim_C has collected enough evidence to infer that f_2 is less influential (collected sufficiently less clicks) than f_1 and technically this means that f_1, f_2 were previously in the same level, yet henceforward f_2 is to be located at a lower level than f_1. Features of same level are equal candidates for selection to participate in the associated-to-level ranks of A_t, but as learning rounds proceed, Trim_C applies R to find a *winner* feature for each rank in A_t that hereafter permanently occupies the respective rank of A_t. The *exploration* ends when A_t comprises a winner feature for each rank apart from the last rank, for which no winner can be found since two

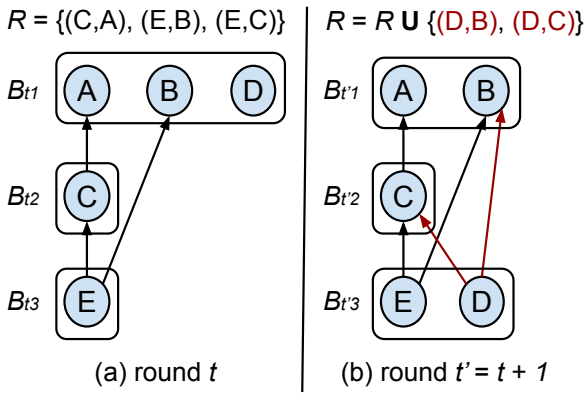

Figure 5.1: Flow of TRIM_C for $|L| = 5$ and $k = 4$.

features cannot participate in a single rank for comparison. Then, the *exploitation* stage starts, in which all formed posts may differ only on the feature in last rank since there are no updates on R, hence no new partitions of L.

Therefore, the logic of TRIM_C is to continuously (over rounds) downgrade features from higher levels to lower levels and selecting k features to form posts by following a priority order per level, while randomizing its selections for features of same level where there is not yet found a dominance relationship among them. For instance, Figure 5.1 presents an execution flow of TRIM_C over two consecutive rounds (t and $t' = t + 1$) for 5 features (A till E) and $k = 4$. In round t, the first three ranks in A_t will contain features from $B_{t1} = \{A, B, D\}$ but with random order, while in the fourth rank will be C. Assume that the feedback of A_t showed that D is less influential than B and C, so R is properly updated to be used in next round t'. In this round, TRIM_C randomly selects A and B to place them in first two ranks of $A_{t'}$, C is now placed in third rank, while the learner randomizing between D and E for the fourth rank.

Given $B_{t1}, \ldots, B_{td}$, the action space $\mathcal{A}$ of TRIM_C in round t is:

$$\mathcal{A}(B_{t1}, \ldots, B_{td}) = \{b_{t1} \| \ldots \| b_{td}, \forall\ b_{tc} \text{ of } B_{tc} \mid c \leq d\} \tag{5.5}$$

where b_{tc} denotes a permutation of block B_{tc} and $\forall\ b_{tc}$ denotes all permutations of that block; the symbol $\|$ denotes concatenation. Thus, $\mathcal{A}(B_{t1}, \ldots, B_{td})$ represents the set of all the block permutation concatenations of the partition $B_{t1}, \ldots, B_{td}$. As a learner selects $k - 1$ out of L features for its posts, for the last block B_{td} in Equation 5.5, $\forall\ b_{td}$ denotes the set of k'-permutations of B_{td} with cardinality $\frac{|B_{td}|!}{(|B_{td}|-k')!}$ where $k' = (k-1) - |\cup_{c<d} B_{tc}|$.

Regarding the complete execution of TRIM_C, in each round t, it starts by creating a partition of L using the relation R (Line 3); if R did not change in the previous round then partition remains the same. After partitioning L, TRIM_C proceeds depending on the value of k; for $k < 5$, the action space $\mathcal{A}$ is computed in reasonable time and

Algorithm TRIM_C

```
   Input     : G, L, F_v^l, trainedCATRID, testingPosts
   Output    : I_n, CATRID_n // cumulative influence spread and CATRID over n rounds
   Param.    : brand, S, k, n, θ
1  A_t[1] = brand; I_n = 0; CATRID_n = trainedCATRID; R = ∅; // init
2  for t = 1, ..., n do
3      Create a partition of L (B_t1, ..., B_td) only if R updated in previous round;
4      if k < 5 then // computation of A is practical
5          Compute A(B_t1, ..., B_td) as in Eq. 5 and randomly select a post for A_t;
6      else // computation of A costs too much and so is avoided
7          Randomly define the permutations b_t1, ..., b_td and merge them for A_t;
8      I_t, CATRID_n = SimCATRID(A_t, S, testingPosts, CATRID_n); I_n = I_n + |I_t|;
9      Apply TRM (Eq. 3) based on random sampling to guess clicks for each user in I_t;
10     Update F_v^l(f) in case v clicked on f and collect all clicks for each such f;
11     Update aggregated click deltas Δ_{f1 f2} for every features f1, f2 ∈ B_tc | c ≤ d;
12     Update R with (f2, f1) if the aggregated click delta Δ_{f1 f2} ≥ θ;
13 return I_n, CATRID_n;
```

the learner forms A_t by selecting a post from $\mathcal{A}$ uniformly at random (Lines 4–5). For larger k, the computation of $\mathcal{A}$ is too expensive, so the learner forms A_t by uniformly at random defining a permutation for each block and concatenating the features appearing in those permutations (Lines 6–7). After creating A_t, TRIM_C uses SimCATRID to find activated users ($\mathcal{I}_t$) to update I_n and also updates CATRID (Line 8). For each activated user v, TRIM_C applies the TRM click model based on *random sampling* to guess to which features of A_t the user v clicked on, updates F_v^l for clicked features, and collects all the clicks of users associated with each feature of A_t (Lines 9–10). So, each feature has collected a number of aggregated clicks up to round t and based on such values, TRIM_C updates the *clicks difference* ($\Delta_{f_1 f_2}$) for every features f_1, f_2 residing in the same block (Line 11) to possibly update R with the respective entry (f_2, f_1) in case its $\Delta_{f_1 f_2}$ is no less than the threshold θ (Line 12).

The time complexity of TRIM_C for *exploration* is $\mathcal{O}(k|L|(|P_L| + |\mathcal{A}|))$ for $k < 5$ and $\mathcal{O}(k|L||P_L|)$ for larger k, where $|P_L|$ and $|\mathcal{A}|$ denote the *average* time of creating a partition-of-L and $\mathcal{A}$ when R changes. The worst case is R to change $|L|$ times to find a winner feature for each one of k levels. The space complexity is $\mathcal{O}(\frac{|L|!}{(|L|-k)!} + k|L|)$; the first term matches to maximum entries in $\mathcal{A}$, the second term to maximum entries in R that represent the worst case.

Although TRIM_C learns what k features form influential posts, to achieve that in practice, it needs several rounds to complete learning (finish *exploration*) as can be shown in our experiments. This happens for three main reasons. First, features residing in levels that are not examined for the forming of posts (e.g., E in Fig. 5.1a) do

not yield any new knowledge in R until there will may be a time to be examined again; we call this waiting period as *non-examination* time. Second, such non-examined features do not help at all to downgrade any examined features, and so there is a remarkable *examination* time for R to be updated with examined features. Third, examination time is aggravated further by the threshold θ that requests aggregated click values for comparison pertaining to several rounds. Note that all mentioned problems worsen as L increases. Therefore, high non-examination and examination times significantly delay the enrichment of R and so the speedup of learning.

5.4.3 The Learner TRIM_E

To handle the drawbacks of TRIM_C, we need a learner that in each round can yield *knowledge* (dominance relationships among features) from *each* feature of L, and not halting the examination of *large* portions in L. Also, we want to *reason* on the derived knowledge to make it more dense for achieving an even faster learning, and this can happen only when a learner is able to exploit all the possible feature connections over L. Finally, when a learner compares the clicks of two features to infer an evidence of dominance, we want more *flexible* thresholds associated with the ranking of A_t, and not an aggregated *fixed* threshold irrespective of ranking. To achieve all such things, we deploy the *eliminator* learner TRIM_E that also uses the TRM click model as TRIM_C, but its logic is different.

In a nutshell, TRIM_E follows a policy of double-checking elimination. When it finds evidence that a feature is less influential than another, TRIM_E records the former as suspect; upon receiving a second piece of evidence corroborating the suspicion (either by full repetition or by providing an alternative inference path), it eliminates the suspect. Yet, it may also render a once-suspect feature non-suspect upon contrary evidence. Figure 5.2 presents an execution flow of TRIM_E based on evidence. The logic of TRIM_E is to find multiple connections among features so as to faster eliminate them and complete the learning with the k features that survived.

TRIM_E leverages a *transitive structure* $\mathcal{T}$ and a *participation structure* $\mathcal{P}$. The transitive structure $\mathcal{T}$ stores *suspicion paths* where a path's *source* feature is *suspect to be less influential than* (henceforward, *slit*) its *destination* feature. Each path encodes a *suspicion* among its source and destination features. E.g., consider features f_1, f_2, f_3; if f_1 is *slit* f_2 and f_2 is *slit* f_3 then $\mathcal{T}$ has the paths $\{\langle f_1, f_2\rangle, \langle f_2, f_3\rangle, \langle f_1, f_2, f_3\rangle\}$. A feature may be connected with any other feature in $\mathcal{T}$ via only one path; in case a *new path* (either *repetitive* as step 9 in Fig. 5.2 or *alternative* as step 7 in Fig. 5.2) arises among connected features, then the source feature is eliminated. We discuss technical details about $\mathcal{T}$ later. The participation structure $\mathcal{P}$ stores the *average* independent contribution of each feature that participates in posts. The *independent*

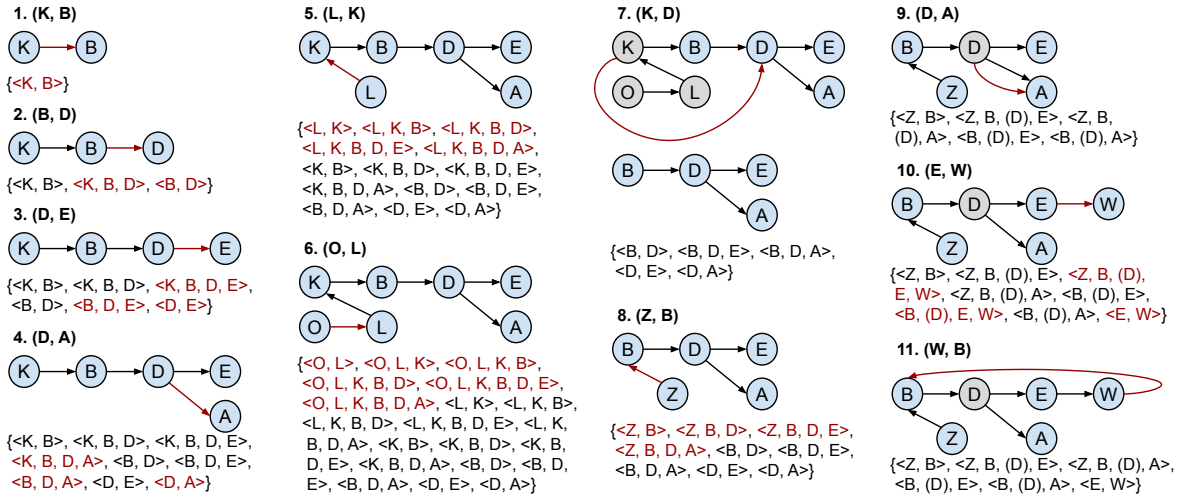

Figure 5.2: Flow of TRIM_E. Each step digests new evidence (feature path, red); in step 7, (K, D) eliminates features in grey; in step 9, the eliminated D remains as intermediate; in step 11, the cycle caused by (W, B) cancels paths containing subpath <B, (D), E, W>.

contribution (*score*) of a feature f is the difference of the clicks achieved by f and the total clicks achieved by other features in a propagated post A_t.

Algorithm TRIM_E presents the *eliminator* learner TRIM_E. In each round t, TRIM_E may eliminate features of L utilizing $\mathcal{T}$. It stores all features eliminated over rounds in $elimF$ and keeps track of features not yet eliminated in $liveF$, computed as the set difference between L and $elimF$ (Line 4). Feature elimination stops when the size of $liveF$ is $k-1$; whence the *exploitation* stage of TRIM_E commences, whereas preceding rounds constitute its *exploration* stage. During *exploration*, TRIM_E forms a post A_t as RANDOM, using $liveF$ instead of L (Lines 5–6). During *exploitation*, it applies a *score*-aware majority rule of $\mathcal{P}$ to form A_t (Lines 7–8). After creating A_t, it uses SimCATRID to find activated users ($\mathcal{I}_t$) to update I_n and also updates CATRID (Line 9). Then, it applies TRM on each user $v \in \mathcal{I}_t$ to guess her clicks on each feature $f \in A_t$ to possibly update $F_v^l(f)$ and collects all clicks of users on such f (Lines 10–11).

In *exploration*, for each ranked feature pair (f'_1, f'_2) (Line 12), TRIM_E computes its normal range (NR) and clicks *ratio* using the posts and clicks, respectively, associated with those features (Lines 13–14). If *ratio* is no less than the upper limit of NR, then it calls function ElimWithT to potentially eliminate features due to f'_2 being *slit* f'_1 (Lines 15–16). Yet, if *ratio* is no more than the lower limit of NR, then ElimWithT induces eliminations due to f'_1 being *slit* f'_2 (Lines 17–18). Lastly, in *exploration* and *exploitation*, A_t updates $\mathcal{P}$ based on derived clicks and eliminations in t (Line 19).

ElimWithT takes as input two features f_1, f_2 where f_1 is *slit* f_2 without intermediate features, updates $\mathcal{T}$ and $elimF$, and uses the auxiliary functions FwdCheck and BwdCheck, where the former checks whether f_1 is already *slit* f_2, while the latter

Algorithm TRIM_E

Input : G, L, F_v^l, $trained$CATRID, $testingPosts$
Output : I_n, CATRID_n // cumulative influence spread and CATRID over n rounds
Param. : $brand, S, k, n$

1 $A_t[1] = brand$; $I_n = 0$; CATRID_n = $trained$CATRID; // init
2 $\mathcal{T} = \emptyset$; $elimF = \emptyset$; $\mathcal{P}[i_f][f] = 0, \forall f \in L \wedge i_f = 2, \ldots, k$; // init
3 **for** $t = 1, \ldots, n$ **do**
4 $liveF = L \setminus elimF$; // non-eliminated features
5 **if** $|liveF| > k - 1$ **then** // elimination is not over
6 Randomly select $k - 1$ features of $liveF$ and define their rank to form A_t;
7 **else if** $|liveF| = k - 1$ **then** // elimination is over
8 Apply the majority rule of $\mathcal{P}$ to form A_t;
9 $\mathcal{I}_t$, CATRID_n = SimCATRID($A_t, S, testingPosts$, CATRID_n); $I_n = I_n + |\mathcal{I}_t|$;
10 Apply TRM (Eq. 3) based on random sampling to guess clicks for each user in $\mathcal{I}_t$;
11 Update $F_v^l(f)$ in case v clicked on f and collect all clicks for each such f;
  // This **loop** is executed only when elimination is not over
12 **for** *each feature pair* $(f_1', f_2') \in A_t : f_1', f_2' \neq brand \wedge rank(f_1') < rank(f_2')$ **do**
  // spPostsN means number Of sp Posts; f_1'_sp takes #sp of one-rank-higher f_1'
13 f_1'_sp = spPostsN($rank(f_1') - 1, k$); f_2'_sp = spPostsN($rank(f_2'), k$);
14 NR = range($1, f_1'$_$sp \div f_2'$_sp); $ratio = f_1'$_$clicks_t \div f_2'$_$clicks_t$;
15 **if** $ratio \geq$ *upper limit of* NR **then** // f_2' is *slit* f_1'
16 $\mathcal{T}, elimF$ = ElimWithT($f_2', f_1', \mathcal{T}, elimF$);
17 **else if** $ratio \leq$ *lower limit of* NR **then** // f_1' is *slit* f_2'
18 $\mathcal{T}, elimF$ = ElimWithT($f_1', f_2', \mathcal{T}, elimF$);
19 Update $\mathcal{P}$ based on collected clicks in t and delete its t-eliminated feature entries;
20 **return** I_n, CATRID_n;

checks the opposite. Both functions return a flag denoting whether the respective condition is satisfied, $multiElim$ is a flag indicating whether the elimination of a feature may incur further feature eliminations, and $newPath$ (repetitive or alternative) is a path that carries new suspicion knowledge for $\mathcal{T}$; $newPath$ is never stored in $\mathcal{T}$.

FwdCheck operates as follows. Let ϕ_1 be the source feature and ϕ_2 the destination feature of $newPath$ (Line 1). If a suspicion path from ϕ_1 to ϕ_2 already exists (Line 2), the consideration of $newPath$ denotes that ϕ_1 is twice *slit* ϕ_2, hence ϕ_1 should be eliminated by policy. The eliminated ϕ_1 is added to $elimF$ and all paths where ϕ_1 is source or destination are deleted from $\mathcal{T}$ (Line 8). Since $multiElim$ may be activated (Line 3), to manage a possible feature elimination domino (*ed*) induced by the elimination of ϕ_1, FwdCheck needs the info of ϕ_1 in $\mathcal{T}$, hence eliminates ϕ_1 at the end of *ed*. An *ed* happens when the existing path from ϕ_1 to ϕ_2 is alternative to $newPath$ (Lines 4–5), hence two alternative paths to ϕ_2 are also trodden by each other feature $prv\phi$ that already has a path to ϕ_1 and ϕ_2, hence each such $prv\phi$ is eliminated (Lines 6–7).

Function FwdCheck

```
   Input      : newPath, multiElim, 𝒯, elimF
   Output     : 1 (satisfied) or 0 (not satisfied)
1  ϕ1 = newPath.first(); ϕ2 = newPath.last();
2  if 𝒯.hasPath(ϕ1, ϕ2) then // ϕ1 is already slit ϕ2
       // ϕ1 is 2-times slit ϕ2, so ϕ1 will be eliminated
3      if multiElim = 1 then
           // ϕ1 elimination may incur elimination domino (ed)
4          existingPath = 𝒯.getPath(ϕ1, ϕ2);
5          if existingPath ≠ newPath then // ed happens
6              for each prvϕ : 𝒯.hasPath(prvϕ, ϕ1) ∧ 𝒯.hasPath(prvϕ, ϕ2) do
7                  elimF.insert(prvϕ); 𝒯.erase(𝒯.outAndinPaths(prvϕ));
8      elimF.insert(ϕ1); 𝒯.erase(𝒯.outPaths(ϕ1)); 𝒯.erase(𝒯.inPaths(ϕ1));
9      return 1;
10 else return 0;
```

Function BwdCheck

```
   Input      : newPath, 𝒯
   Output     : 1 (satisfied) or 0 (not satisfied)
1  ϕ1 = newPath.first(); ϕ2 = newPath.last();
2  if 𝒯.hasPath(ϕ2, ϕ1) then // ϕ2 is already slit ϕ1
       // A cycle occurs among ϕ1 and ϕ2; the newPath cancels the existingPath and
          all the superpaths of newPath and existingPath from 𝒯
3      existingPath = 𝒯.getPath(ϕ2, ϕ1); 𝒯.erase(existingPath);
4      𝒯.erase(𝒯.subPath(existingPath)); 𝒯.erase(𝒯.subPath(newPath));
5      return 1;
6  else return 0;
```

In BwdCheck, ϕ_1 and ϕ_2 are still the source and destination features of $newPath$ (Line 1), but now if there exists a path from ϕ_2 to ϕ_1, then $newPath$ induces a cycle (Line 2). By policy, TRIM_E resolves a suspicion cycle by canceling the two paths that form the cycle and deleting from $\mathcal{T}$ any path containing them (Lines 3–4).

Let us resume our focus on ElimWithT. This function sequentially executes three steps for given features f_1, f_2.

In the first step, it checks the early termination cases (Lines 1–2). If FwdCheck finds that f_1 is already *slit* f_2, then it updates $elimF$ and deletes from $\mathcal{T}$ all relative *elimination* info (Line 1). Yet, if BwdCheck finds that f_2 is already *slit* f_1, hence it deletes from $\mathcal{T}$ all relative *cycle* info (Line 2). If no early termination happens, ElimWithT updates $\mathcal{T}$ with the suspicion that f_1 is *slit* f_2 (Line 3).

In the second step, ElimWithT checks the outpaths of f_2 to update $\mathcal{T}$ (Line 4). For each destination feature $nxtf_2$ of f_2, a *path* is formed from f_1 to $nxtf_2$ to search for new suspicion knowledge among f_1 and $nxtf_2$ to insert to $\mathcal{T}$ (Lines 5–6). In case f_1 is eliminated through FwdCheck, ElimWithT stops checking the outpaths of f_2, as f_1

Function ElimWithT

```
   Input     : f1, f2, T, elimF
   Output    : T, elimF
1  if FwdCheck(⟨f1, f2⟩, 1, T, elimF) = 1 then return T, elimF;
2  if BwdCheck(⟨f1, f2⟩, T) = 1 then return T, elimF;
3  T.insert(⟨f1, f2⟩); // insert to T the fact that f1 is slit f2
4  if T.outPaths(f2) ≠ ∅ then // T is updated with all the slit knowledge derived from f2
5      for each feature nxtf2 : T.hasPath(f2, nxtf2) do
6          path = ⟨f1⟩||T.getPath(f2, nxtf2);
7          if FwdCheck(path, 1, T, elimF) = 1 then break;
8          if BwdCheck(path, T) = 1 then continue;
9          T.insert(path);
10 if T.inPaths(f1) ≠ ∅ then // T is updated with all the slit knowledge derived from f1
11     for each feature prvf1 : T.hasPath(prvf1, f1) do
12         prefix = T.getPath(prvf1, f1)||⟨f2⟩;
13         if FwdCheck(prefix, 0, T, elimF) = 1 then continue;
14         if BwdCheck(prefix, T) = 1 then continue;
15         T.insert(prefix);
16         Repeat Lines 4–9 with the difference that now FwdCheck(path, 0, T, elimF)
           and path = prefix.allButLast()||T.getPath(f2, nxtf2);
17 return T, elimF;
```

is permanently deleted from $\mathcal{T}$ (Line 7). Else, if FwdCheck is not satisfied, BwdCheck examines whether $path$ yields a cycle; if so, $path$ is invalidated, hence we proceed with the next outpath of f_2 (Line 8), otherwise we insert $path$ to $\mathcal{T}$ (Line 9).

In the third step, ElimWithT checks the inpaths of f_1 to update $\mathcal{T}$ (Line 10). For each source feature $prvf_1$ of f_1, a path $prefix$ is formed from $prvf_1$ to f_2 to gauge new suspicions (Lines 11–12); an elimination of $prvf_1$ via FwdCheck does not affect the examination of other inpaths of f_1, since f_1 itself is not eliminated (Line 13). The $multiElim$ flag is not activated when the source feature of $newPath$ in FwdCheck is $prvf_1$, since the possible elimination of a feature depending on the elimination of $prvf_1$ is already considered by examining each $prvf_1$ in Line 11. If FwdCheck is not satisfied, BwdCheck checks if $prefix$ creates a cycle, to invalidate it and proceed with the next inpath of f_1 (Line 14); if no such cycle exists, we insert $prefix$ to $\mathcal{T}$ (Line 15). Lastly, a $path$ is formed from $prvf_1$ to $nxtf_2$ to update $\mathcal{T}$ with the suspicion knowledge derived from the second and third steps of ElimWithT (Line 16).

Technical Details of $\mathcal{T}$. We implement $\mathcal{T}$ using indexes src and dst. For a given path, src maps the path source to path destination, whereas dst maps the path destination to the whole path ignoring its destination. E.g., if $\mathcal{T}$ includes the paths $\{\langle f_1, f_2\rangle, \langle f_2, f_3\rangle, \langle f_1, f_2, f_3\rangle\}$, then $src[f_1] = \{f_2, f_3\}$ and $src[f_2] = \{f_3\}$, while $dst[f_2] = \{\langle f_1\rangle\}$ and $dst[f_3] = \{\langle f_2\rangle, \langle f_1, f_2\rangle\}$. As only one path exists in $\mathcal{T}$ among any connected features, $\mathcal{T}$ is a space saving structure that provides efficient data access to

its associated functions `hasPath`, `getPath`, `outPaths`, `inPaths`, `erase`, `insert`, and `subPath`. We design $\mathcal{T}$ so that it retains dense suspicion knowledge despite *eliminations* or *cycles*, to facilitate the fast completion of *exploration* stage of Trim_E, as such retention causes beneficial *ed*s. Thus, when a feature is eliminated, its outpaths and inpaths are deleted from $\mathcal{T}$, yet that feature may exist as a path intermediate feature in $\mathcal{T}$. Besides, when two paths form a cycle and are canceled, all their superpaths are deleted from $\mathcal{T}$, yet all their subpaths remain stored in $\mathcal{T}$. Lastly, $\mathcal{T}$ is scalable and memory efficient, as it is gradually constructed via size increases and decreases, but in the long term its size diminishes.

The time complexity of Trim_E relative to *exploration* is $\mathcal{O}(k|L||\mathcal{T}|)$ for $k > 3$ and $\mathcal{O}(kn|\mathcal{T}|)$ for smaller k, where $|\mathcal{T}|$ denotes the *average* time of updating $\mathcal{T}$. In each round, k features may update $\mathcal{T}$; for $k > 3$, number of rounds is $|L|$ instead of n due to fast eliminations. The space complexity is $\mathcal{O}(|L|^2 + k|L|)$; the first term matches to maximum entries in $\mathcal{T}$, the second term to maximum entries in $\mathcal{P}$. Yet, $|L|^2$ is very unlikely in practice due to frequent eliminations.

5.5 Experimental Evaluation

We wrote code in C++ and ran experiments on an Intel Xeon CPU E7-4830 @ 2.13 GHz machine with 252GB RAM running Linux Debian (4.9.0-13-amd64). For graph operations we used the open-source graph library Lemon [DJK11].

5.5.1 Setup

Datasets. To evaluate our learners for the ACAIM problem, we created two big VK data that we often call data $\mathbb{A}$ and data $\mathbb{B}$. Since VK has in total 27 categories, by selecting the 10 ($\mathbb{A}$) and 20 ($\mathbb{B}$) most popular pages from each category, we formed a feature set $|L| = 270$ and $|L| = 540$ in each case; the popularity of a page was measured by the number of its subscribers. In particular, both $\mathbb{A}$ and $\mathbb{B}$ operate as a cluster that includes three, scalable to network size, datasets that we call A1, A2, and A3 in $\mathbb{A}$ and B1, B2, and B3 in $\mathbb{B}$. Our experimental evaluation is done on these six datasets. The requested preprocessing to form the mentioned datasets consists of two stages; Tables 5.2 and 5.3 present the first and second stage respectively. In first stage, we subsequently (i) collected all the VK users until August 2019, (ii) removed the blocked users (deactivated, private, or empty profile), (iii) applied a *feature-pruning* to filter out any user who did not like at least one post published from a feature in L, as that user does not contribute at all neither in training (years 2010-2017) nor in testing (years 2018-2019) phases of ACAIM for our selected L, and

Table 5.2: First Preprocessing to prune VK users for $|L| = 270$ and $|L| = 540$.

VK Users	After Removing Blocked Users	Feature-Pruning		Testing-Pruning	
		$\|L\| = 270$	$\|L\| = 540$	$\|L\| = 270$	$\|L\| = 540$
500M	348.4M	91.1M	99.9M	43.8M	48.3M

Table 5.3: Second Preprocessing to create three, scalable to network size, VK datasets respectively for data $\mathbb{A}$ ($|L| = 270$) and data $\mathbb{B}$ ($|L| = 540$).

Dataset	$\mathbb{A}$:A1	$\mathbb{A}$:A2	$\mathbb{A}$:A3	$\mathbb{B}$:B1	$\mathbb{B}$:B2	$\mathbb{B}$:B3
hop1_out_avg	94.48	94.48	94.48	98.76	98.76	98.76
increase factor (%)	200K	150K	100K	200K	150K	100K
increased_hop1_out_avg	189K	141.8K	94.5K	197.6K	148.2K	98.8K
influential_users	10	20	39	16	31	53
influenced_users	1.9M	2.7M	3.7M	2.8M	3.9M	4.8M
hop1_in_influential_users	6.6K	7.7K	15.7K	7.1K	9.5K	17.9K
hop2_in_influential_users	1.5M	1.8M	3M	1.7M	2.3M	3.6M
Nodes	3.3M	4.4M	6.2M	4.4M	5.9M	7.8M
Edges	320.8M	417.2M	669.7M	434.6M	596.5M	879M

(iv) applied a *testing-pruning* to further exclude any user who did not like at least one post of L in testing phase, as the evaluation of learners depends on a feedback during testing. In second stage, we created the described six datasets with a top-to-bottom process as presented in Table 5.3. The logic here is first to find the average out-degree (*hop1_out_avg*) of previous 43.8M and 48.3M users, and to increase it by a different factor for each dataset so as to create a network size scalability. Then, each user that has an out-degree equal or higher than *increased_hop1_out_avg* is considered an *influential_user*, while each user that can be directly influenced by an *influential_user* is considered an *influenced_user*. Further, to enhance the probability that a propagation reaches an *influential_user*, we also considered users who contribute to that via one-hops or two-hops. The union of *influential_users*, *influenced_users*, *hop1_in_influential_users*, and *hop2_in_influential_users* yields the nodes of respective dataset along with their accompanied edges. We stress that our preprocessing approach gives as maximum a realistic enough three-hop influence connectivity for an *influenced_user* that represents the target for IM problems, while any pruned user incurred unnecessary memory overhead for the proof-of-concept purposes of our work. Last, we note that in training phase we used 9.5M (resp. 18.4M) *sp* posts for $\mathbb{A}$ (resp. $\mathbb{B}$) and the total available *sp* posts to simulator in testing phase are 2.8M for $\mathbb{A}$ and 5.6M for $\mathbb{B}$.

Metrics. We use the metrics of *reliability* and *scalability* to measure the performance of our learners. In ACAIM, the most *reliable* learner is the learner that consistently achieves the highest influence in most cases for separate brands in different datasets, while the most *scalable* learner is the learner that remains most valuable for a *brand*

as the network size grows. We highlight that in this work we are not interested to measure the scalability of an unreliable learner.

Runs. All *reliability* results are averaged over 10 runs, while all *scalability* results are stemmed from 1 run. The former experiments relate with ordinary brands where their execution time is affordable and so we used 10 runs to reduce randomness, while the latter experiments mention to highly popular brands and their execution time is as expected very high to allow multiple runs. For that, we used nine different brands for scalability experiments to derive a general conclusion for scalability from 9 runs instead of just 1 run. Note also that each run relates with a different lt_v for CATRID.

Notation. We use the symbols $\mathcal{E}_1$ for *exploration* and $\mathcal{E}_2$ for *exploitation*. Also, in all our figures, *llr* means last learning round of $\mathcal{E}_1$, *fte* means remaining features to eliminate, *influence spread* is the cumulative influence spread over rounds, and *min* measures the total execution time over rounds in minutes excluding the input loading time of each round. The number of considered rounds is logically set to 2000, and we depict each *brand* by using its ID in VK (see Table 5.7 in Section 5.5.4).

5.5.2 Reliability

To measure the *reliability* of ACAIM learners, we select six brands belonging to different categories for maximum diversification; three brands for datasets A1, A2, and A3 and three brands for datasets B1, B2, and B3. In all cases, we selected the *brand* whose number of subscribers is closest to the average number of subscribers over all brands for respective dataset; we argue that this is a fair selection policy that expresses the majority of brands in VK in terms of their subscription numbers. Figures 5.3 and 5.4 present the reliability results for data $\mathbb{A}$ and data $\mathbb{B}$ respectively.

In Figure 5.3, the first three plots relative to A1 depict the influence spread of a *brand* belonging to "Products, stores" category for $k = 3$, 4, and 5; the next three plots relative to A2 of a *brand* belonging to "Auto, motor" category and the last three plots relative to A3 of a *brand* belonging to "Food, recipes" category. In all cases, TRIM_E achieves the best performance due to its faster $\mathcal{E}_1$ that also enables a really influential $\mathcal{E}_2$; TRIM_E has the second fastest $\mathcal{E}_1$ only for $k = 3$ in Figures 5.3a and 5.3d, but even in these two cases, its derived $\mathcal{E}_2$ is more effective than others. TRIM_C with $\theta = 5$ is the second best solution, while a choice of $\theta = 10$ yields a slightly better performance in Figures 5.3b, 5.3f, and 5.3i; these figures denote that a slower $\mathcal{E}_1$ of a higher θ can induce a more influential $\mathcal{E}_2$ compared to a lower θ. This is a sound result as a stricter θ is theoretically more reliable. Yet, overall, we observe in practice that the more TRIM_C increases its θ the more close it performs with RANDOM, which is the worst learner of all. The reason is that the clicks collected over a logical number

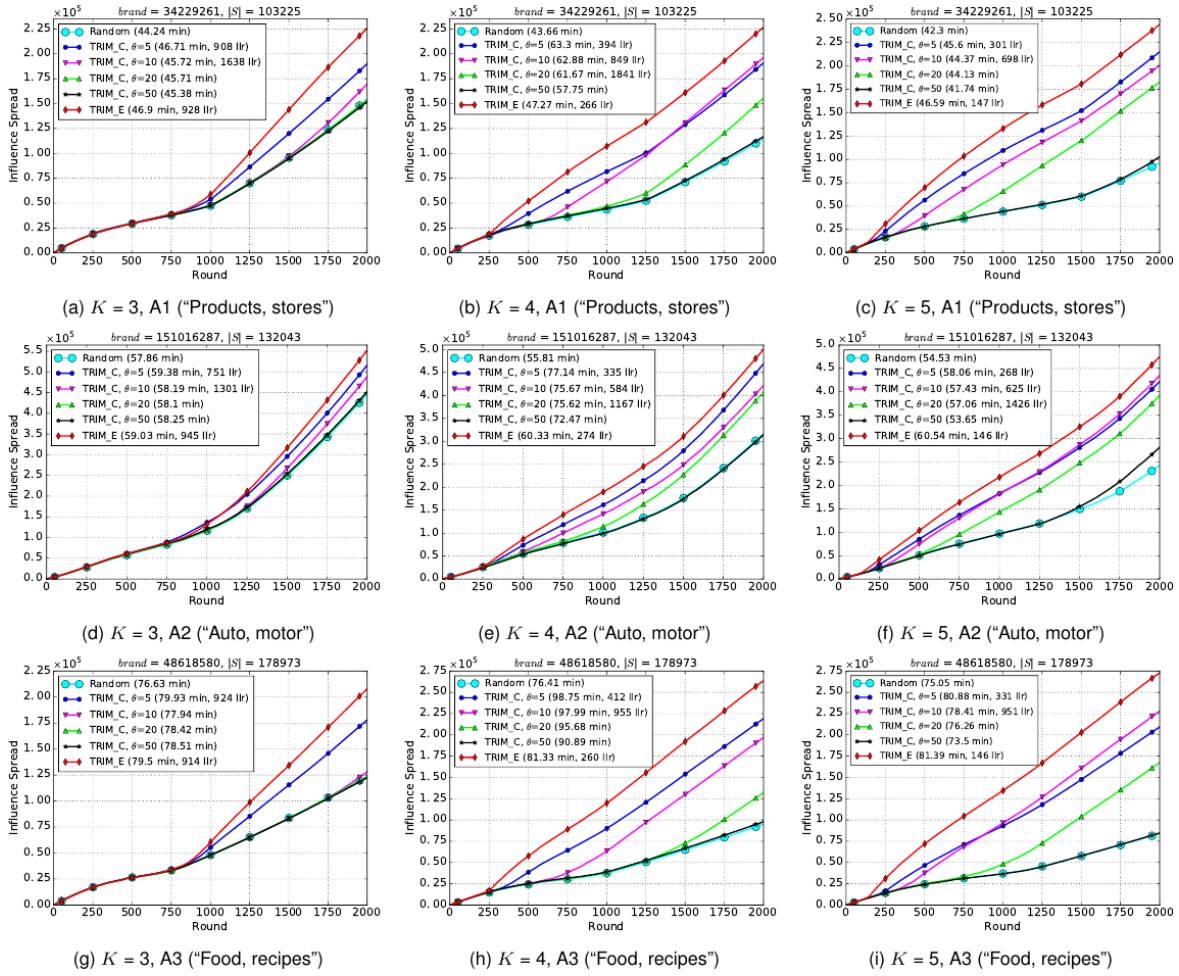

(a) K = 3, A1 ("Products, stores") (b) K = 4, A1 ("Products, stores") (c) K = 5, A1 ("Products, stores")

(d) K = 3, A2 ("Auto, motor") (e) K = 4, A2 ("Auto, motor") (f) K = 5, A2 ("Auto, motor")

(g) K = 3, A3 ("Food, recipes") (h) K = 4, A3 ("Food, recipes") (i) K = 5, A3 ("Food, recipes")

Figure 5.3: Reliability results of RANDOM, TRIM_C, and TRIM_E in datasets A1, A2, and A3 for $k = 3$, 4, and 5.

of rounds do not easily permit an aggregated computed clicks delta among features to early surpass a high θ, and that incurs a slow $\mathcal{E}_1$ for such θ cases. Note that in real world and as our CATRID simulator also successfully captures, the subscribers of an ordinary *brand* do not like so often its posts and that usually prevents a high propagation collecting a large number of clicks. So, a lower θ is more beneficial for TRIM_C, which is a deficiency in its operation due to the loose ranking of features. Yet, there is no other alternative, especially if one notice that TRIM_C has high θ cases that incur a too much slow $\mathcal{E}_1$ (for $\theta = 10$ in Figure 5.3a and $\theta = 20$ in Figure 5.3b) or an unfinished $\mathcal{E}_1$ (for $\theta = 10$ in Figure 5.3g, $\theta = 20$ in Figures 5.3a, 5.3c, 5.3d, 5.3g, 5.3h, and 5.3i, and $\theta = 50$ in all plots of Figure 5.3). In the worst-case scenario, where $\theta = 50$, TRIM_C performs similarly to RANDOM since during $\mathcal{E}_1$ it scarcely manages to surpass θ, and so it selects posts under very common settings with RANDOM.

In Figure 5.4, the first three plots relative to B1 depict the influence spread of a *brand* belonging to "Cities, countries" category for $k = 3$, 4, and 5; the next three

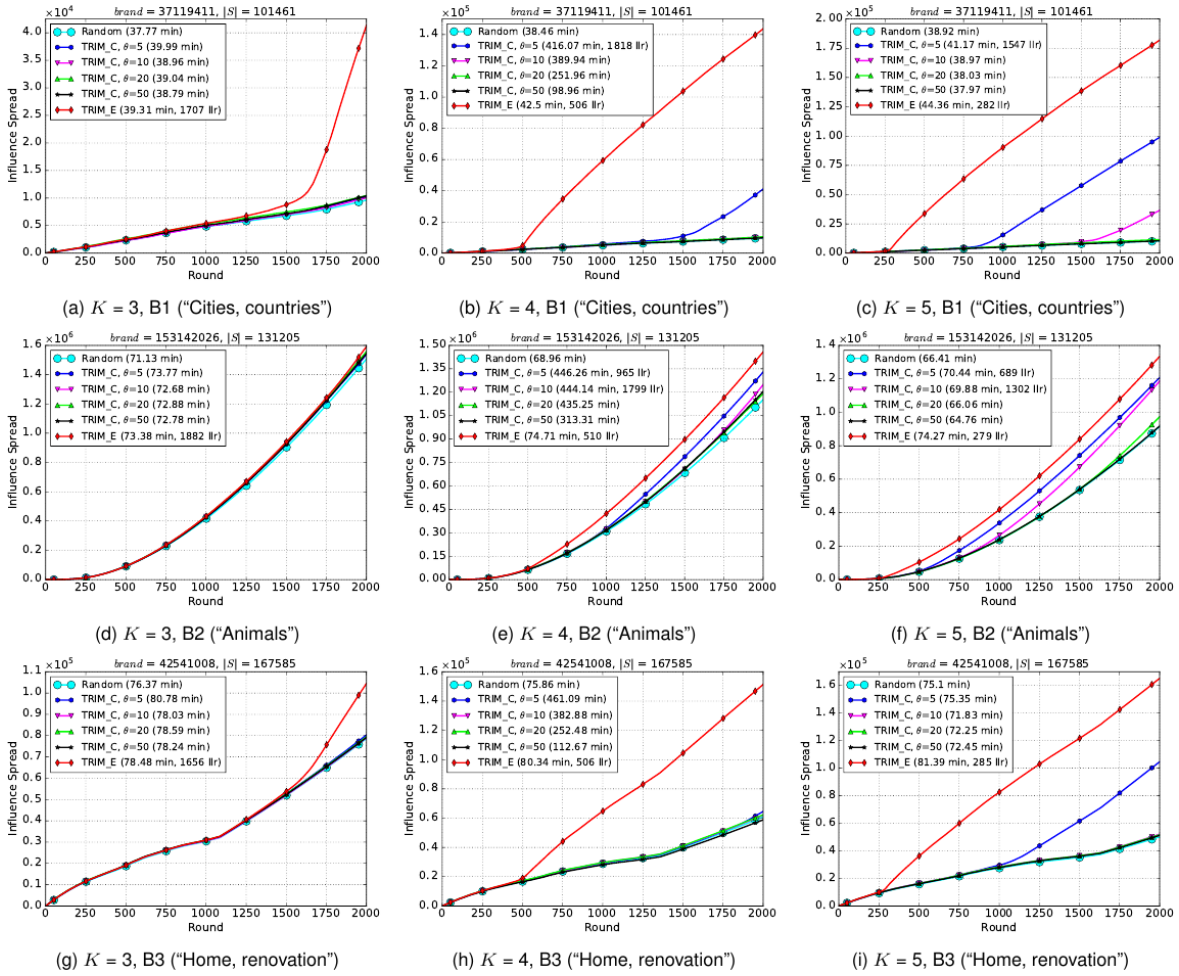

(a) K = 3, B1 ("Cities, countries") (b) K = 4, B1 ("Cities, countries") (c) K = 5, B1 ("Cities, countries")

(d) K = 3, B2 ("Animals") (e) K = 4, B2 ("Animals") (f) K = 5, B2 ("Animals")

(g) K = 3, B3 ("Home, renovation") (h) K = 4, B3 ("Home, renovation") (i) K = 5, B3 ("Home, renovation")

Figure 5.4: Reliability results of RANDOM, TRIM_C, and TRIM_E in datasets B1, B2, and B3 for $k = 3$, 4, and 5.

plots relative to B2 of a *brand* belonging to "Animals" category and the last three plots relative to B3 of a *brand* belonging to "Home, renovation" category. In all cases, TRIM_E outperforms TRIM_C and RANDOM, it is also the only learner that always has a finite $\mathcal{E}_1$, while its superiority is really impressive in several cases (Figures 5.4a, 5.4b, 5.4c, 5.4h, and 5.4i). Again, RANDOM achieves the worst performance, whereas TRIM_C is remarkably less competitive in data $\mathbb{B}$ compared to data $\mathbb{A}$ due to the much bigger effect of θ on its performance, even when θ is low. That is explained by the larger L in data $\mathbb{B}$ which entails a significantly broader distribution of clicks on its features. This deficiency of TRIM_C shows that its efficacy is not scalable to the feature size.

Moreover, in both Figures 5.3 and 5.4 the $\mathcal{E}_1$ of TRIM_E and TRIM_C finishes sooner as k increases with some exceptions (for $\theta = 10$ in Figure 5.3f and $\theta = 20$ in Figures 5.3c and 5.3f). This happens because a larger k enables a more frequent participation of a feature in propagated posts, and so more chances for it to be compared with other features based on its collected clicks. Yet, a faster $\mathcal{E}_1$ of a larger k may lead

Table 5.4: Percentages (%) depicting how much *influence better* TRIM_C (with most influential θ) and TRIM_E are over RANDOM for data $\mathbb{A}$ and data $\mathbb{B}$.

Algorithm	RANDOM (A1, B1)			RANDOM (A2, B2)			RANDOM (A3, B3)			**Average**		
	$k=3$	$k=4$	$k=5$	$k=3$	$k=4$	$k=5$	$k=3$	$k=4$	$k=5$	$k=3$	$k=4$	$k=5$
TRIM_C ($\mathbb{A}$)	23.3	71.2	123.9	15.6	48.1	78.9	43.7	130.5	171.1	27.5	83.2	124.6
TRIM_C ($\mathbb{B}$)	8.6	320.9	849.7	3.3	15.3	32	2.1	6.2	108.6	4.6	114.1	330.1
TRIM_E ($\mathbb{A}$)	46.5	97.9	154.3	23.6	58.1	95.4	67.9	177.3	224.4	46	111.1	158
TRIM_E ($\mathbb{B}$)	329	1372.9	1646.9	5.6	26.5	45.8	32.9	148.9	229.4	122.5	516.1	640.7

Table 5.5: Percentages (%) depicting how much *influence better* TRIM_E is over TRIM_C (with most influential θ) for data $\mathbb{A}$ and data $\mathbb{B}$.

Algorithm	TRIM_C (A1, B1)			TRIM_C (A2, B2)			TRIM_C (A3, B3)			**Average**		
	$k=3$	$k=4$	$k=5$	$k=3$	$k=4$	$k=5$	$k=3$	$k=4$	$k=5$	$k=3$	$k=4$	$k=5$
TRIM_E ($\mathbb{A}$)	18.8	15.5	13.5	6.9	6.7	9.2	16.8	20.3	19.6	14.1	14.1	14.1
TRIM_E ($\mathbb{B}$)	294.7	249.9	83.9	2.1	9.6	10.4	30.1	134.3	57.8	108.9	131.2	50.7

Table 5.6: Percentages (%) depicting how much *learning faster* TRIM_E is over TRIM_C (with most influential θ) for data $\mathbb{A}$ and data $\mathbb{B}$.

Algorithm	TRIM_C (A1, B1)			TRIM_C (A2, B2)			TRIM_C (A3, B3)			**Average**		
	$k=3$	$k=4$	$k=5$	$k=3$	$k=4$	$k=5$	$k=3$	$k=4$	$k=5$	$k=3$	$k=4$	$k=5$
TRIM_E ($\mathbb{A}$)	-2.2	219.1	104.7	-25.8	22.2	328	1.1	58.4	551.3	-8.9	99.9	328
TRIM_E ($\mathbb{B}$)	>17.1	259.2	448.5	>6.2	89.2	146.9	>20.7	>295.2	>601.7	>14.6	>214.5	>399

to a lower influence for both TRIM_E and TRIM_C as it is shown in Figures 5.3d, 5.3e, and 5.3f for A2 and in Figures 5.4d, 5.4e, and 5.4f for B2. How k affects the influence of a *brand* depends on how loyal are its subscribers. Namely, if the subscribers of a *brand* like often its posts, then they create the chances for a good influence in the network, and so the learner should choose a small k to give more focus on the *brand*. Yet, there is a loyalty tradeoff as we observe in the next section, since a highly adopted *brand* may perform better with a larger k instead of a smaller one. Regarding RANDOM, we notice that its performance constantly deteriorates as k increases except for B1 (Figures 5.4a, 5.4b, and 5.4c) where it hardly improves. The reason is that the power of RANDOM lies mostly on *brand*, so by giving a less focus on it with a larger k, we boost the uncertain influence of arbitrary features that accompany the *brand*.

Overall, for both data $\mathbb{A}$ and data $\mathbb{B}$, Table 5.4 presents the influence comparison of TRIM_C and TRIM_E with RANDOM, Table 5.5 compares the influence among TRIM_E and TRIM_C, while Table 5.6 compares the learning speed of previous learners; for TRIM_C we selected its most influential θ version in each case. In all Tables, each single column after *Algorithm* and before *Average* includes the results for each dataset that stems from the intersection with the respective row. For instance, Table 5.4 denotes that TRIM_C is 123.9% influence better than RANDOM for $k=5$ in A1 and TRIM_E is 148.9% influence better than RANDOM for $k=4$ in B3.

We observe in *Average* column of Table 5.4 that both TRIM_C and TRIM_E out-

perform more RANDOM as k increases, that difference in performance becomes more intense in data $\mathbb{B}$, and also that RANDOM is obviously more competitive to TRIM_C than TRIM_E. As previously explained for ordinary brands, RANDOM performs better with a small k while the other two learners are often more influential with a larger k. In addition, the more features that exist in data $\mathbb{B}$ aggravate further the performance of RANDOM as its arbitrary selections are increased. Yet, the interesting point here is that although TRIM_C has severe scalability issues in data $\mathbb{B}$ (e.g., TRIM_C is just 4.6% influence better than RANDOM for $k = 3$ in data $\mathbb{B}$), it manages to amplify its average influence over RANDOM in regards to data $\mathbb{A}$ for $k = 4$ and $k = 5$.

The *Average* column of Table 5.5 shows that TRIM_E is 14.1% influence better than TRIM_C for each k in data $\mathbb{A}$, while TRIM_E is 108.9%, 131.2%, and 50.7% influence better than TRIM_C for $k = 3$, 4, and 5 in data $\mathbb{B}$. Since TRIM_C is not scalable to the feature size, it needs a large enough k to be competitive to TRIM_E and slightly achieves that for $k = 5$. Additionally to the influence comparison, in *Average* column of Table 5.6 we remark that TRIM_E is -8.9%, 99.9%, and 328% learning faster than TRIM_C for $k = 3$, 4, and 5 in data $\mathbb{A}$, whereas TRIM_E is at least 14.6%, 214.5%, and 399% learning faster than TRIM_C for $k = 3$, 4, and 5 in data $\mathbb{B}$. The $\mathcal{E}_1$ of TRIM_C is faster than the one of TRIM_E only for $k = 3$ in A1 and A2, while in all other cases it is slower and actually emphatically slower in most times. Both Figures 5.3 and 5.4 demonstrate that the learning speed of a learner crucially defines its influence spread, and that connection becomes even more dependent when that speed is accompanied by an effective learning. This connection is highly satisfied by TRIM_E and that explains its remarkable superiority over TRIM_C, especially in data $\mathbb{B}$. The most representative case is for $k = 4$ in data $\mathbb{B}$ where TRIM_E is at least 214.5% learning faster and 131.2% influence better than TRIM_C.

Regarding the running time of learners, RANDOM is the most fast solution in data $\mathbb{A}$ and data $\mathbb{B}$ for $k = 3$ and $k = 4$, while it usually comes second after TRIM_C with $\theta = 50$ for $k = 5$; in the latter case TRIM_C is a little faster due to a gradually smaller randomized feature set induced after exceeding θ. These results are expected due to the low overhead and influence spread of mentioned learners. The noteworthy point for TRIM_E is that besides its much higher influence than RANDOM, its execution time remains very close to RANDOM in all cases, which highlights the efficient, flexible, and compact implementation of $\mathcal{T}$. Last, note the remarkably costly execution of TRIM_C for $k = 4$, especially in data $\mathbb{B}$, which relates with the expensive computation of $\mathcal{A}$; for $k = 3$ the cost of $\mathcal{A}$ is much more affordable, whereas for $k = 5$ the computation of $\mathcal{A}$ is avoided.

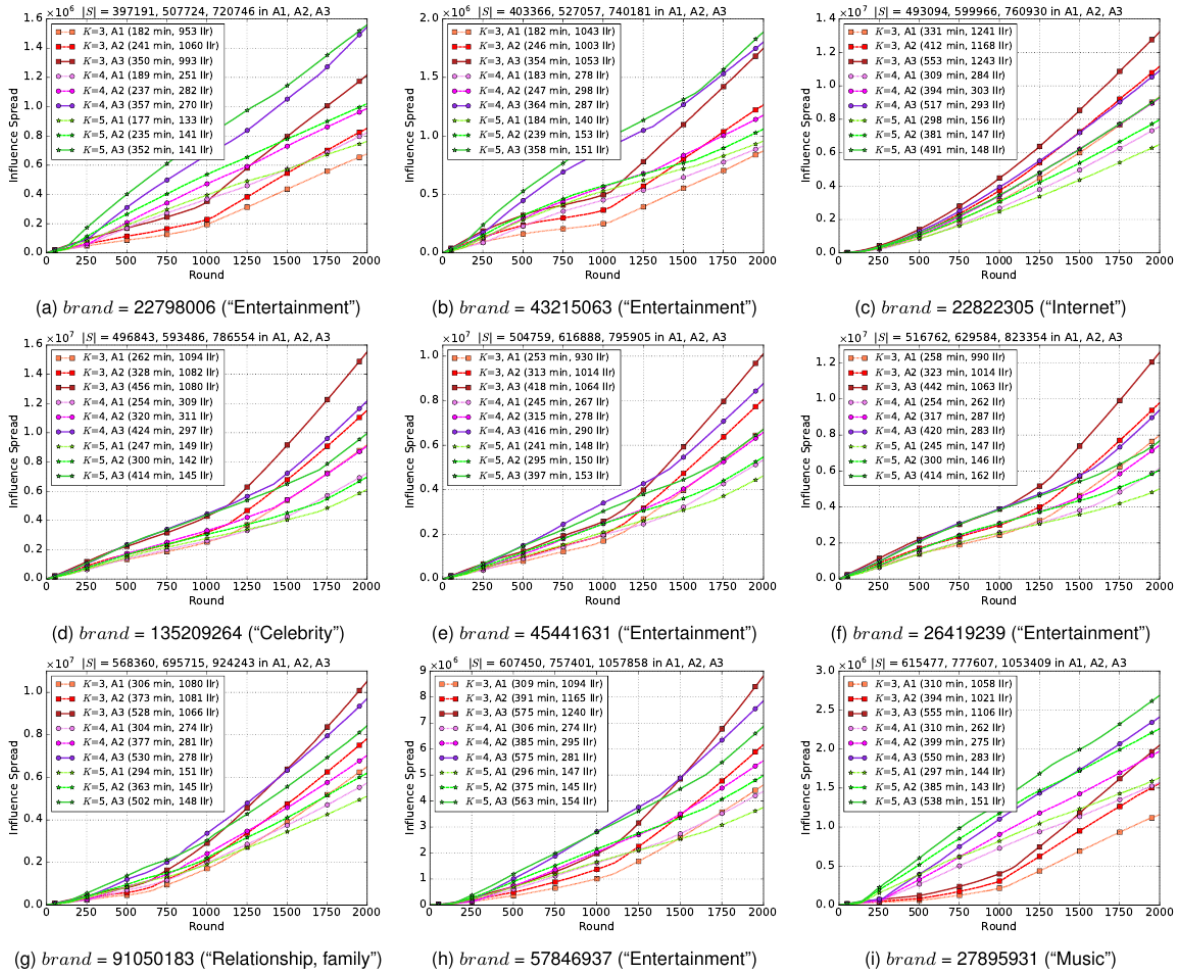

Figure 5.5: Scalability results of TRIM_E for the nine most popular VK brands (depicted in increasing $|S|$) in datasets A1, A2, and A3 for $k = 3$, 4, and 5.

5.5.3 Scalability

In previous section, we have experimentally proved the superiority of TRIM_E over RANDOM and TRIM_C by evaluating the *reliability* of all learners for separate brands in different datasets. In this section, we check if TRIM_E also enables the *scalability* of a *brand* to network size; the other two learners are ignored due to their much inferior reliability. To measure the scalable performance of TRIM_E under the most demanding settings, we selected the nine most popular brands of VK, where the popularity is interpreted by the number of subscribers. In Figure 5.5, we present the scalability results of selected brands for $k = 3$, 4, and 5 in datasets A1, A2, and A3, while Figure 5.6 shows the respective results in datasets B1, B2, and B3.

In both Figures 5.5 and 5.6, we observe that for all brands, TRIM_E is highly scalable to network size since under any fixed k and as the dataset grows, TRIM_E not only manages to complete its learning but also it achieves a constantly higher

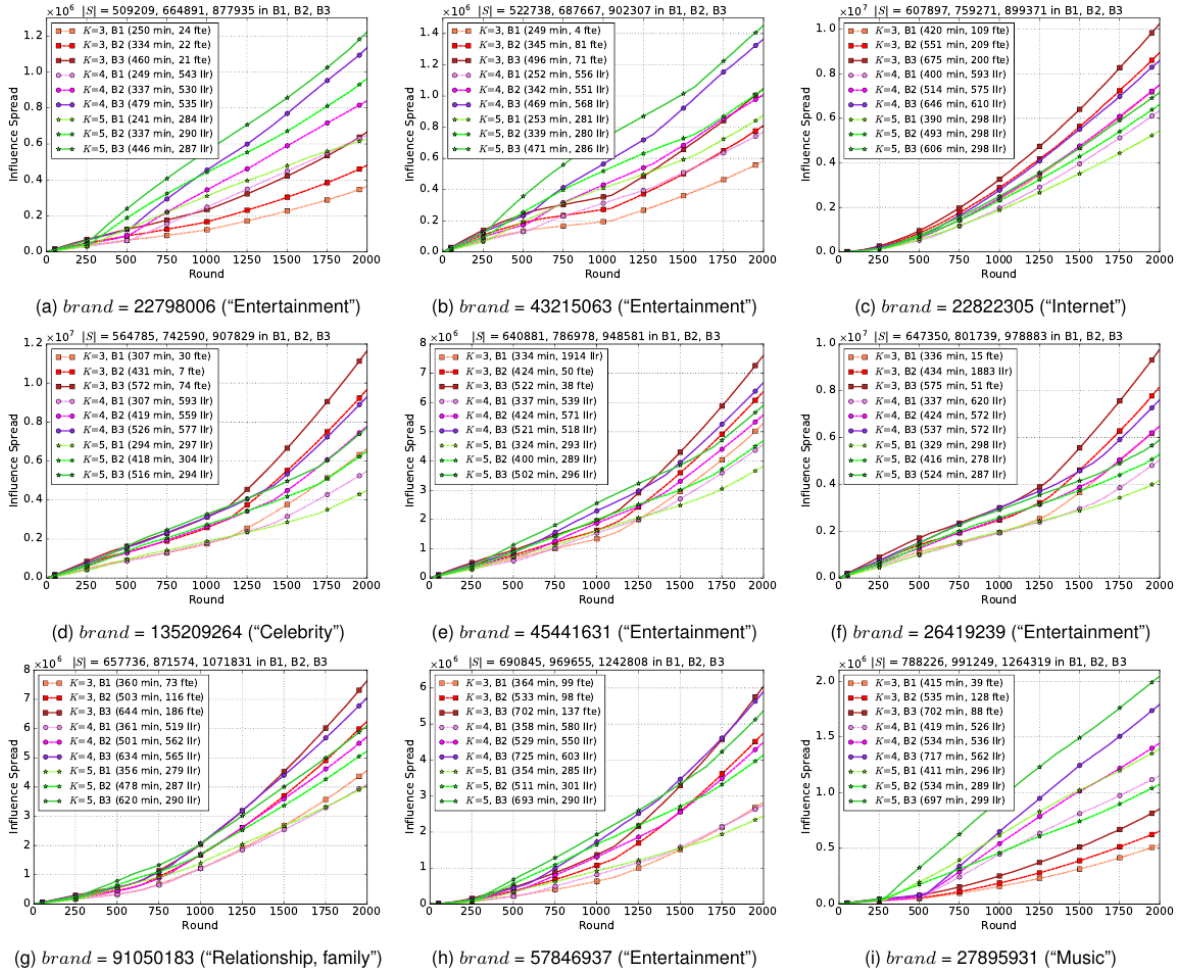

Figure 5.6: Scalability results of TRIM_E for the nine most popular VK brands (depicted in increasing $|S|$) in datasets B1, B2, and B3 for $k = 3$, 4, and 5.

influence accompanied by logically higher execution times. Regarding influence, the only exception takes place in Figure 5.6i where TRIM_E is more influential for $k = 5$ in B1 compared to $k = 5$ in B2, while regarding incomplete learning, the sole exceptions happen for $k = 3$ in Figure 5.6 when *fte* replaces *llr*. The *fte* cases show an obvious difficulty of TRIM_E to provide a finite $\mathcal{E}_1$, but even in these special cases, its efficacy remains highly scalable to network size.

As in previous section, we verify that TRIM_E still learns faster as k grows, as also that the choice of the proper k relates with the subscription loyalty of a *brand*. In the most cases of both Figures 5.5 and 5.6, we remark that a smaller k is more beneficial for a highly popular *brand*, yet there is a loyalty tradeoff that clearly demonstrates the opposite for some brands (Figures 5.5a, 5.5b, 5.5i, 5.6a, 5.6b, and 5.6i).

5.5.4 Business Applicability

In Table 5.7 we present all the features (L) we used in this work according to the 27 VK categories they belong to.

The Tables 5.8 and 5.9 enhance the *business applicability* of this work by presenting the ACAIM results of TRIM_E for thirty worldwide-familiar VK brands for $k = 4$ and $k = 5$ respectively. For illustration, we selected the highest k values and the biggest dataset we used in this work (B3) to more representatively capture the most common application scenarios in social networks.

We observe that in all cases TRIM_E manages to early finish its learning (depicted by llr) and significantly improve the influence spread per round among *exploration* and *exploitation*. That improvement accordingly increases the execution time per round while simultaneously satisfies the real-time needs of ACAIM.

Regarding the found features, we generally remark that a feature relative to "revelation" or "humor" is very popular in VK as it is part of most solutions. Further, we observe that in several cases there is an interesting *semantic connection* among brands and found features that can be characterized as (i) *expected* (e.g., "E-squire magazine" with "A celebrity magazine" for $k = 4$ and "A taxi order service" with "Taxi TaxovichkoF" for $k = 4$), (ii) *non-trivial* (e.g., "Great Britain" with "Football Europe" for $k = 5$ and "Shakira" with "Between us girls" for $k = 4$), (iii) *profound* (e.g., "Tools & garden equipment" with "Kontinental Hockey League (KHL)" for $k = 5$ and "Doctor Komarovsky" with "Believe Orthodoxy" for $k = 4$ and 5), (iv) *opposite* (e.g., "Real Madrid CF" with "FC Barcelona" for $k = 4$ and 5, and "Moto" with "Auto" for $k = 5$), and (v) *unexpected* (e.g., "Pharmaceutical products" with "Dating jokes" for $k = 5$ and "Helsinki airport" with "Modern mom" for $k = 5$).

Table 5.7: The IDs of brands (features in L) belonging to 27 categories of VK we considered in experiments. The first part of each category presents its 10 most popular brands in VK (depicted in decreasing $|S|$) and by aggregating all such first parts we form the $|L| = 270$ of data $\mathbb{A}$. Similarly, both parts of each category correspond to the 20 most popular brands in VK and totally yield the $|L| = 540$ of data $\mathbb{B}$. The VK social network page of each *brand* is publicly available to registered users just by using the ID of *brand* as follows: `https://vk.com/publicID` . In case of visit, we recommend using the Google Chrome browser so as to translate the content of pages since they mostly use the Russian language.

Animals	Auto, motor	Beauty, health	Celebrity	Cities, countries	Communication Services	Consumer Services	Culture, art	Education
32015300	23783750	39728801	135209264	20845272	34243323	170175796	147845620	12648877
110065937	151016287	45064245	45588871	127925490	44345402	173437170	38634441	25346844
65320054	29196806	28627911	35930308	127925061	52602834	171825683	142754704	33338722
34964358	38472666	34757875	104052041	27042171	24862387	35356518	99464023	149500863
33621085	148411246	28646177	41623203	37119411	18970929	49688236	19589874	34305040
35806476	39236729	46509740	139740824	31516466	149499917	49054793	143826157	36959676
32375815	31128331	23245066	41734504	69518720	28722213	41155241	66687279	44759043
29188817	40679923	35486195	26211015	66232651	41676683	166344567	180103132	149653328
23530818	133712630	36085261	134533652	34274053	33341280	46664792	31554488	33842750
59227775	51362846	23164653	225666	69547083	47786809	103075639	102090470	42307767
153142026	159415165	126100310	123675921	36338110	133310139	25198495	148230634	74595166
33798093	38894284	32922940	23546772	33156709	274672	39659800	40137153	61912980
36168102	90060110	107019848	174163184	88229325	20194367	98749490	47551578	28938560
30262661	125649823	16945011	44257435	40901026	49381792	81115275	61744518	72985232
82141367	43387535	125770269	23482802	36086936	38875560	41637433	122195630	40167434
43228812	23983339	49591829	3113588	144260965	114022615	25811852	74641828	29599237
35850395	163406855	34981365	95470601	32258596	1590042	66222045	37537193	45688121
105229582	24444828	126100569	46688098	37169648	126999658	168454811	26270763	103027469
159858626	153344099	29686754	30314549	32182751	66177799	82417135	26610299	46603834
50336153	37735548	26614831	94334686	33025155	161848270	96734258	96794207	142977738

Entertainment	Finance and Insurance	Food, recipes	Hobbies	Home, renovation	Internet	Job search	Media	Medicine	Music	Products, stores
57846937	22522055	43879004	55662720	36184135	22822305	12248221	29246653	133726577	27895931	36941068
26419239	124002407	39009769	29559271	32439535	28477986	31154183	48512305	55122354	45703770	24098496
45441631	34638472	48946342	31976785	38379853	2158488	29046529	29573241	29716377	34384434	34229261
43215063	84244100	32194285	34118551	42541008	162729615	44490261	22079806	27885374	35983383	30559917
22798006	43978738	18464856	24713873	32228890	35145657	78800961	18496184	149732802	22866546	28556858
58170807	166850908	46117626	79483347	41002749	23688663	48020228	9693056	43540875	28905875	35114569
12382740	38182092	40020627	43688579	90730773	79525017	34116496	101982925	49119584	29078047	80345103
31836774	20225241	48618580	34215577	137793489	139732885	56292539	15755094	51431740	29258893	39513007
23064236	73260851	47118092	23390361	123474518	72982321	23315499	108468	47591566	23180464	34483558
56106344	102218499	34451036	41883468	1792796	550910	85115964	29534144	42852777	105999460	10362317
40567146	140864751	83935640	76314525	36326284	31273955	36188056	24199209	160966228	48713061	40020304
26750264	144847188	42092461	43772432	64392368	41154660	40527789	73247559	45377300	34001496	96457590
460389	34980638	42025607	26776509	70275937	153766591	127560216	25380626	149401625	64977560	28673372
43776215	79995162	32509740	25397178	106277494	22884714	117282915	152992737	64964821	43335937	23616160
36164349	181526312	138816943	68229174	134655935	26456494	4808406	20035339	45251830	74653596	165599758
30179569	68349832	32231484	147720339	124764538	442	53809539	36792820	37875518	52599708	48210134
26669118	154346076	49694199	56048543	66630509	72378974	72355306	55264762	121816651	42440233	125303834
48319873	35144827	94216909	47679753	124303122	72866026	127738547	89493	49517102	26515827	34168005
38683579	104669972	28565318	23170931	42689002	40182105	63740509	24565142	48383801	27338836	24698811
33769500	75905130	34889014	23337480	136958443	43001537	82020695	16775977	36456996	33898099	49840023

Professional Services	Relationship, family	Restaurants	Social and public organizations	Sport	Tourism and Leisure	Transportation Services
111499611	91050183	30637940	71729358	71474813	346191	74611457
19542789	40498005	130641709	36166073	137451337	14897324	79459310
31577711	28890647	165062392	32194500	128350290	133668394	108040038
1163441	68114884	172149046	133180305	48940689	34543413	70228347
5425797	32432151	123287849	26307864	30428125	150802579	142153191
49690338	68895020	104616476	34137285	23693281	25117353	96196967
61796383	28293246	166652899	27794994	22746750	22558194	70270286
50512447	27470044	172231135	68016956	51812607	38363244	104141529
130698013	32651025	61879718	42701798	15326149	33445697	59131740
25276999	36318299	170513366	40587282	8722610	42763042	40738724
33301261	23758942	25300817	33382046	16202769	69580110	151316183
182438388	35555977	164409488	46987089	86224065	41053835	91708214
354372	20249656	53484080	31976441	12637219	21352492	26690472
27570276	34378420	59415411	54391852	23403635	63731512	170878251
57950162	55074079	99296079	38630769	64098698	30975621	53639653
57409266	24036559	49440926	36606428	30111136	133799113	153050613
87610407	24722253	87945351	39881081	23471538	26127512	66775477
31424891	68519692	78995926	31727306	28639294	54365037	82297106
30786950	44786979	164782094	25539323	138649060	146744120	45078595
38000521	24985591	127265072	50406378	40586683	35806721	93511310

Table 5.8: The ACAIM results of TRIM_E in regards to 30 selected brands for $k = 4$ in dataset B3 of data $\mathbb{B}$. The first table presents the found most influential features for each *brand* when *exploration* of TRIM_E ends; the second table shows the influence spread and execution time per round for each *brand* before and after *exploration* as also their cumulative values. All results are derived from 1 run of TRIM_E over 2000 rounds for each *brand*.

brand (id | category | name)	**2nd-ranked feature** (id | category | name)	**3rd-ranked feature** (id | category | name)
354372 | Professional Serv. | "A recruiting platform" **4th-ranked feature** (id | category | name)	34215577 | Hobbies | "Anonymous human revelation" 12382740 | Entertainment | "Epicenter of humor"	29534144 | Media | "Humoristic information blog"
16202769 | Sport | "Kontinental Hockey League (KHL)" **4th-ranked feature** (id | category | name)	26419239 | Entertainment | "Laugh to tears" 135209264 | Celebrity | "The best Bot on VK"	12382740 | Entertainment | "Epicenter of humor"
21352492 | Tourism and Leisure | "Great Britain" **4th-ranked feature** (id | category | name)	34215577 | Hobbies | "Anonymous human revelation" 22746750 | Sport | "FC Barcelona"	56106344 | Entertainment | "Anonymous revelation stories"
22522055 | Finance and Insurance | "Sberbank" **4th-ranked feature** (id | category | name)	26419239 | Entertainment | "Laugh to tears" 12382740 | Entertainment | "Epicenter of humor"	135209264 | Celebrity | "The best Bot on VK"
22558194 | Tourism and Leisure | "USA" **4th-ranked feature** (id | category | name)	56106344 | Entertainment | "Anonymous revelation stories" 135209264 | Celebrity | "The best Bot on VK"	34215577 | Hobbies | "Anonymous human revelation"
23403635 | Sport | "Real Madrid CF" **4th-ranked feature** (id | category | name)	22746750 | Sport | "FC Barcelona" 26419239 | Entertainment | "Laugh to tears"	12382740 | Entertainment | "Epicenter of humor"
24098496 | Products, stores | "E-squire magazine" **4th-ranked feature** (id | category | name)	34215577 | Hobbies | "Anonymous human revelation" 40498005 | Relationship, family | "Relationship psychology"	66687279 | Culture, art | "A celebrity magazine"
24565142 | Media | "National Geographic" **4th-ranked feature** (id | category | name)	34215577 | Hobbies | "Anonymous human revelation" 66687279 | Culture, art | "A celebrity magazine"	12382740 | Entertainment | "Epicenter of humor"
27570276 | Professional Serv. | "Tools & garden equipment" **4th-ranked feature** (id | category | name)	79525017 | Internet | "Sweepstakes" 123474518 | Home, renovation | "Builder"	31976785 | Hobbies | "Science & Technology"
30559917 | Products, stores | "Business Strategy" **4th-ranked feature** (id | category | name)	34215577 | Hobbies | "Anonymous human revelation" 56106344 | Entertainment | "Anonymous revelation stories"	29246653 | Media | "Sarcastic and funny news"
36184135 | Home, renovation | "Interior design ideas" **4th-ranked feature** (id | category | name)	34215577 | Hobbies | "Anonymous human revelation" 460389 | Entertainment | "Fresh memes uncensored"	56106344 | Entertainment | "Anonymous revelation stories"
36941068 | Products, stores | "AliExpress" **4th-ranked feature** (id | category | name)	34215577 | Hobbies | "Anonymous human revelation" 12382740 | Entertainment | "Epicenter of humor"	460389 | Entertainment | "Fresh memes uncensored"
37119411 | Cities, countries | "Moscow" **4th-ranked feature** (id | category | name)	34215577 | Hobbies | "Anonymous human revelation" 56106344 | Entertainment | "Anonymous revelation stories"	460389 | Entertainment | "Fresh memes uncensored"
37537193 | Culture, art | "Couple relationships" **4th-ranked feature** (id | category | name)	29599237 | Education | "Believe Orthodoxy" 29246653 | Media | "Sarcastic and funny news"	56106344 | Entertainment | "Anonymous revelation stories"
40679923 | Auto, motor | "Moto" **4th-ranked feature** (id | category | name)	26419239 | Entertainment | "Laugh to tears" 12382740 | Entertainment | "Epicenter of humor"	135209264 | Celebrity | "The best Bot on VK"
43001537 | Internet | "Apple" **4th-ranked feature** (id | category | name)	12382740 | Entertainment | "Epicenter of humor" 22746750 | Sport | "FC Barcelona"	26419239 | Entertainment | "Laugh to tears"
44257435 | Celebrity | "Shakira" **4th-ranked feature** (id | category | name)	22746750 | Sport | "FC Barcelona" 36166073 | Social and public organizations | "Between us girls"	34215577 | Hobbies | "Anonymous human revelation"
48383801 | Medicine | "Pharmaceutical products" **4th-ranked feature** (id | category | name)	79525017 | Internet | "Sweepstakes" 30179569 | Entertainment | "Slaughter humor"	34215577 | Hobbies | "Anonymous human revelation"
48940689 | Sport | "Olympic Games" **4th-ranked feature** (id | category | name)	56106344 | Entertainment | "Anonymous revelation stories" 45441631 | Entertainment | "Funny & ridiculous jokes"	73247559 | Media | "Show business news"
49119584 | Medicine | "Doctor Komarovsky" **4th-ranked feature** (id | category | name)	34215577 | Hobbies | "Anonymous human revelation" 29599237 | Education | "Believe Orthodoxy"	56106344 | Entertainment | "Anonymous revelation stories"
53484080 | Restaurants | "Dodo Pizza" **4th-ranked feature** (id | category | name)	26419239 | Entertainment | "Laugh to tears" 34215577 | Hobbies | "Anonymous human revelation"	56106344 | Entertainment | "Anonymous revelation stories"
53639653 | Transportation Serv. | "A suburban passenger company" **4th-ranked feature** (id | category | name)	135209264 | Celebrity | "The best Bot on VK" 34215577 | Hobbies | "Anonymous human revelation"	89493 | Media | "A dance radio station"
66775477 | Transportation Serv. | "Helsinki airport" **4th-ranked feature** (id | category | name)	34215577 | Hobbies | "Anonymous human revelation" 32015300 | Animals | "A paradise for cat lovers"	29534144 | Media | "Humoristic information blog"
74611457 | Transportation Serv. | "A taxi order service" **4th-ranked feature** (id | category | name)	12382740 | Entertainment | "Epicenter of humor" 70270286 | Transportation Serv. | "Taxi TaxovichkoF"	79525017 | Internet | "Sweepstakes"
103075639 | Consumer Serv. | "A clothing & footwear care product" **4th-ranked feature** (id | category | name)	29534144 | Media | "Humoristic information blog" 66687279 | Culture, art | "A celebrity magazine"	79525017 | Internet | "Sweepstakes"
104052041 | Celebrity | "Natalia Oreiro" **4th-ranked feature** (id | category | name)	26419239 | Entertainment | "Laugh to tears" 12382740 | Entertainment | "Epicenter of humor"	34215577 | Hobbies | "Anonymous human revelation"
126100569 | Beauty, health | "Hairstyles & Haircuts" **4th-ranked feature** (id | category | name)	56106344 | Entertainment | "Anonymous revelation stories" 26419239 | Entertainment | "Laugh to tears"	34215577 | Hobbies | "Anonymous human revelation"
139732885 | Internet | "Joom" **4th-ranked feature** (id | category | name)	73247559 | Media | "Show business news" 26419239 | Entertainment | "Laugh to tears"	56106344 | Entertainment | "Anonymous revelation stories"
151316183 | Transportation Serv. | "Lufthansa" **4th-ranked feature** (id | category | name)	34215577 | Hobbies | "Anonymous human revelation" 24098496 | Products, stores | "E-squire magazine"	29534144 | Media | "Humoristic information blog"
165599758 | Products, stores | "Xiaomi" **4th-ranked feature** (id | category | name)	26419239 | Entertainment | "Laugh to tears" 56106344 | Entertainment | "Anonymous revelation stories"	460389 | Entertainment | "Fresh memes uncensored"

brand (id | $\lvert S\rvert$)	**llr**	**avg. spread per round until llr**	**avg. spread per round after llr**	**spread**	**avg. time per round until llr**	**avg. time per round after llr**	**time**
354372 | 59821	508	4.96	51.19	78909	0.83 sec	1 sec	32.28 min
16202769 | 138344	501	105.36	385.14	630119	1.95 sec	2.62 sec	82.68 min
21352492 | 20036	474	11.02	42.26	69724	0.27 sec	0.34 sec	11.11 min
22522055 | 222795	547	60.61	369.24	569672	3.43 sec	3.94 sec	127.9 min
22558194 | 53809	513	45.29	157.87	257993	0.79 sec	1.1 sec	34.4 min
23403635 | 107830	504	253.57	390.34	711751	1.7 sec	1.99 sec	64.57 min
24098496 | 317643	535	443.39	780.91	1381252	4.88 sec	5.68 sec	184.2 min
24565142 | 139134	505	56.28	170.92	283960	1.9 sec	2.32 sec	74.72 min
27570276 | 44052	474	9.72	86.79	137056	0.63 sec	0.87 sec	27.49 min
30559917 | 201038	544	34.99	99.6	164063	2.68 sec	3.08 sec	100.01 min
36184135 | 449805	536	75.14	314.6	500855	6.1 sec	7.21 sec	232.57 min
36941068 | 304871	535	21.17	160.86	246994	4.15 sec	4.87 sec	157.6 min
37119411 | 175994	517	18.22	193.26	296033	2.19 sec	2.46 sec	80.7 min
37537193 | 50057	471	14.89	38.17	65381	0.65 sec	0.82 sec	26.5 min
40679923 | 89837	519	99.91	161.59	291184	1.24 sec	1.34 sec	44.51 min
43001537 | 128777	523	22.73	79.77	129725	1.69 sec	1.93 sec	62.99 min
44257435 | 33375	502	112.88	326.16	545261	0.56 sec	0.76 sec	24.14 min
48383801 | 22067	450	6.34	129.87	204158	0.29 sec	0.57 sec	17.2 min
48940689 | 213802	542	133.42	418.75	682860	3.38 sec	3.99 sec	128.67 min
49119584 | 49144	444	16.45	62.18	104060	0.72 sec	0.83 sec	27.33 min
53484080 | 69289	492	29.26	154.05	246718	1.07 sec	1.22 sec	39.89 min
53639653 | 3077	409	1.99	10.61	17707	0.04 sec	0.05 sec	1.93 min
66775477 | 4121	409	3.92	16.52	27892	0.06 sec	0.08 sec	2.71 min
74611457 | 28455	457	14.18	77.89	126671	0.4 sec	0.62 sec	19.23 min
103075639 | 9314	425	5.77	39.28	64324	0.12 sec	0.2 sec	6.51 min
104052041 | 43913	522	222.62	620.62	1033487	0.98 sec	1.35 sec	42.47 min
126100569 | 245088	536	95.61	207.92	355646	3.28 sec	3.76 sec	122.11 min
139732885 | 204755	518	42.4	218.15	345276	2.96 sec	3.29 sec	107.88 min
151316183 | 6271	450	13.58	51.4	85795	0.09 sec	0.15 sec	4.81 min
165599758 | 312288	504	94.89	530.24	841075	4.85 sec	5.37 sec	176.24 min

Table 5.9: The ACAIM results of TRIM_E in regards to 30 selected brands for $k = 5$ in dataset B3 of data $\mathbb{B}$. The first table presents the found most influential features for each *brand* when *exploration* of TRIM_E ends; the second table shows the influence spread and execution time per round for each *brand* before and after *exploration* as also their cumulative values. All results are derived from 1 run of TRIM_E over 2000 rounds for each *brand*.

brand (id | category | name)	**2nd-ranked feature** (id | category | name)	**3rd-ranked feature** (id | category | name)
354372 | Professional Serv. | "A recruiting platform"	34215577 | Hobbies | "Anonymous human revelation"	460389 | Entertainment | "Fresh memes uncensored"
4th-ranked, 5th-ranked feature (id | category | name)	28477986 | Internet | "Unbelievable humoristic news"	12382740 | Entertainment | "Epicenter of humor"
16202769 | Sport | "Kontinental Hockey League (KHL)"	26419239 | Entertainment | "Laugh to tears"	22746750 | Sport | "FC Barcelona"
4th-ranked, 5th-ranked feature (id | category | name)	12382740 | Entertainment | "Epicenter of humor"	45441631 | Entertainment | "Funny & ridiculous jokes"
21352492 | Tourism and Leisure | "Great Britain"	73247559 | Media | "Show business news"	22746750 | Sport | "FC Barcelona"
4th-ranked, 5th-ranked feature (id | category | name)	23693281 | Sport | "Football Europe"	31976785 | Hobbies | "Science & Technology"
22522055 | Finance and Insurance | "Sberbank"	26419239 | Entertainment | "Laugh to tears"	45441631 | Entertainment | "Funny & ridiculous jokes"
4th-ranked, 5th-ranked feature (id | category | name)	56106344 | Entertainment | "Anonymous revelation stories"	135209264 | Celebrity | "The best Bot on VK"
22558194 | Tourism and Leisure | "USA"	56106344 | Entertainment | "Anonymous revelation stories"	22746750 | Sport | "FC Barcelona"
4th-ranked, 5th-ranked feature (id | category | name)	66687279 | Culture, art | "A celebrity magazine"	135209264 | Celebrity | "The best Bot on VK"
23403635 | Sport | "Real Madrid CF"	22746750 | Sport | "FC Barcelona"	12382740 | Entertainment | "Epicenter of humor"
4th-ranked, 5th-ranked feature (id | category | name)	31836774 | Entertainment |"Cool tricks for fun"	12637219 | Sport | "European Football"
24098496 | Products, stores | "E-squire magazine"	34215577 | Hobbies | "Anonymous human revelation"	40498005 | Relationship, family | "Relationship psychology"
4th-ranked, 5th-ranked feature (id | category | name)	26307864 | Social and public organizations | "The art of reality"	28477986 | Internet | "Unbelievable humoristic news"
24565142 | Media | "National Geographic"	34215577 | Hobbies | "Anonymous human revelation"	56106344 | Entertainment | "Anonymous revelation stories"
4th-ranked, 5th-ranked feature (id | category | name)	29559271 | Hobbies | "Science"	66687279 | Culture, art | "A celebrity magazine"
27570276 | Professional Serv. | "Tools & garden equipment"	25397178 | Hobbies | "Male thoughts"	12382740 | Entertainment | "Epicenter of humor"
4th-ranked, 5th-ranked feature (id | category | name)	31976785 | Hobbies | "Science & Technology"	16202769 | Sport | "Kontinental Hockey League (KHL)"
30559917 | Products, stores | "Business Strategy"	34215577 | Hobbies | "Anonymous human revelation"	12382740 | Entertainment | "Epicenter of humor"
4th-ranked, 5th-ranked feature (id | category | name)	56106344 | Entertainment | "Anonymous revelation stories"	460389 | Entertainment | "Fresh memes uncensored"
36184135 | Home, renovation | "Interior design ideas"	34215577 | Hobbies | "Anonymous human revelation"	460389 | Entertainment | "Fresh memes uncensored"
4th-ranked, 5th-ranked feature (id | category | name)	56106344 | Entertainment | "Anonymous revelation stories"	36164349 | Entertainment | "Satirical humor"
36941068 | Products, stores | "AliExpress"	34215577 | Hobbies | "Anonymous human revelation"	26419239 | Entertainment | "Laugh to tears"
4th-ranked, 5th-ranked feature (id | category | name)	135209264 | Celebrity | "The best Bot on VK"	79525017 | Internet | "Sweepstakes"
37119411 | Cities, countries | "Moscow"	34215577 | Hobbies | "Anonymous human revelation"	91050183 | Relationship, family | "A dating Bot"
4th-ranked, 5th-ranked feature (id | category | name)	66687279 | Culture, art | "A celebrity magazine"	29534144 | Media | "Humoristic information blog"
37537193 | Culture, art | "Couple relationships"	29599237 | Education | "Believe Orthodoxy"	56106344 | Entertainment | "Anonymous revelation stories"
4th-ranked, 5th-ranked feature (id | category | name)	460389 | Entertainment | "Fresh memes uncensored"	33338722 | Education | "Vocabulary"
40679923 | Auto, motor | "Moto"	135209264 | Celebrity | "The best Bot on VK"	133712630 | Auto, motor | "Auto Blog"
4th-ranked, 5th-ranked feature (id | category | name)	26419239 | Entertainment | "Laugh to tears"	23783750 | Auto, motor | "Auto"
43001537 | Internet | "Apple"	73247559 | Media | "Show business news"	29573241 | Media | "NR.Music"
4th-ranked, 5th-ranked feature (id | category | name)	12382740 | Entertainment | "Epicenter of humor"	26419239 | Entertainment | "Laugh to tears"
44257435 | Celebrity | "Shakira"	56106344 | Entertainment | "Anonymous revelation stories"	34215577 | Hobbies | "Anonymous human revelation"
4th-ranked, 5th-ranked feature (id | category | name)	22746750 | Sport | "FC Barcelona"	73247559 | Media | "Show business news"
48383801 | Medicine | "Pharmaceutical products"	79525017 | Internet | "Sweepstakes"	34215577 | Hobbies | "Anonymous human revelation"
4th-ranked, 5th-ranked feature (id | category | name)	28477986 | Internet | "Unbelievable humoristic news"	44786979 | Relationship, family | "Dating jokes"
48940689 | Sport | "Olympic Games"	12382740 | Entertainment | "Epicenter of humor"	56106344 | Entertainment | "Anonymous revelation stories"
4th-ranked, 5th-ranked feature (id | category | name)	34215577 | Hobbies | "Anonymous human revelation"	31836774 | Entertainment |"Cool tricks for fun"
49119584 | Medicine | "Doctor Komarovsky"	34215577 | Hobbies | "Anonymous human revelation"	56106344 | Entertainment | "Anonymous revelation stories"
4th-ranked, 5th-ranked feature (id | category | name)	29599237 | Education | "Believe Orthodoxy"	29246653 | Media | "Sarcastic and funny news"
53484080 | Restaurants | "Dodo Pizza"	26419239 | Entertainment | "Laugh to tears"	45441631 | Entertainment | "Funny & ridiculous jokes"
4th-ranked, 5th-ranked feature (id | category | name)	135209264 | Celebrity | "The best Bot on VK"	31976785 | Hobbies | "Science & Technology"
53639653 | Transportation Serv. | "A suburban passenger company"	43540875 | Medicine | "Humoristic medicine"	135209264 | Celebrity | "The best Bot on VK"
4th-ranked, 5th-ranked feature (id | category | name)	460389 | Entertainment | "Fresh memes uncensored"	133799113 | Tourism and Leisure | "Civilization cemetery"
66775477 | Transportation Serv. | "Helsinki airport"	79525017 | Internet | "Sweepstakes"	36959676 | Education | "Interesting facts"
4th-ranked, 5th-ranked feature (id | category | name)	135209264 | Celebrity | "The best Bot on VK"	55074079 | Relationship, family | "Modern mom"
74611457 | Transportation Serv. | "A taxi order service"	79525017 | Internet | "Sweepstakes"	12382740 | Entertainment | "Epicenter of humor"
4th-ranked, 5th-ranked feature (id | category | name)	29246653 | Media | "Sarcastic and funny news"	23783750 | Auto, motor | "Auto"
103075639 | Consumer Serv. | "A clothing & footwear care product"	135209264 | Celebrity | "The best Bot on VK"	29534144 | Media | "Humoristic information blog"
4th-ranked, 5th-ranked feature (id | category | name)	29573241 | Media | "NR.Music"	34215577 | Hobbies | "Anonymous human revelation"
104052041 | Celebrity | "Natalia Oreiro"	29246653 | Media | "Sarcastic and funny news"	26419239 | Entertainment | "Laugh to tears"
4th-ranked, 5th-ranked feature (id | category | name)	56106344 | Entertainment | "Anonymous revelation stories"	460389 | Entertainment | "Fresh memes uncensored"
126100569 | Beauty, health | "Hairstyles & Haircuts"	56106344 | Entertainment | "Anonymous revelation stories"	34215577 | Hobbies | "Anonymous human revelation"
4th-ranked, 5th-ranked feature (id | category | name)	26419239 | Entertainment | "Laugh to tears"	31836774 | Entertainment |"Cool tricks for fun"
139732885 | Internet | "Joom"	26419239 | Entertainment | "Laugh to tears"	23482802 | Celebrity | "Egor Kreed"
4th-ranked, 5th-ranked feature (id | category | name)	45441631 | Entertainment | "Funny & ridiculous jokes"	12382740 | Entertainment | "Epicenter of humor"
151316183 | Transportation Serv. | "Lufthansa"	34215577 | Hobbies | "Anonymous human revelation"	40567146 | Entertainment | "Worldwide entertaining news"
4th-ranked, 5th-ranked feature (id | category | name)	29534144 | Media | "Humoristic information blog"	26419239 | Entertainment | "Laugh to tears"
165599758 | Products, stores | "Xiaomi"	135209264 | Celebrity | "The best Bot on VK"	12382740 | Entertainment | "Epicenter of humor"
4th-ranked, 5th-ranked feature (id | category | name)	26419239 | Entertainment | "Laugh to tears"	56106344 | Entertainment | "Anonymous revelation stories"

brand (id | $\|S\|$)	**llr**	**avg. spread per round until llr**	**avg. spread per round after llr**	**spread**	**avg. time per round until llr**	**avg. time per round after llr**	**time**
354372 | 59821	285	5.87	60.57	105556	0.76 sec	1 sec	32.55 min
16202769 | 138344	289	89.29	320.32	573875	1.95 sec	2.54 sec	82.73 min
21352492 | 20036	267	11.64	35.01	63791	0.25 sec	0.33 sec	10.97 min
22522055 | 222795	283	51.92	363.06	638083	3.24 sec	3.84 sec	126.32 min
22558194 | 53809	297	42	127.44	229517	0.76 sec	1.01 sec	32.93 min
23403635 | 107830	290	227	331.61	632901	1.64 sec	1.82 sec	60.59 min
24098496 | 317643	301	447.29	620.99	1189713	4.91 sec	5.56 sec	183.99 min
24565142 | 139134	291	52.68	167.02	300769	1.83 sec	2.33 sec	76.04 min
27570276 | 44052	263	8.96	32.15	58218	0.58 sec	0.72 sec	23.74 min
30559917 | 201038	305	36.29	117.61	210425	2.68 sec	2.98 sec	98.86 min
36184135 | 449805	312	99.02	339.02	603175	6.04 sec	7.1 sec	233.3 min
36941068 | 304871	300	25.23	178.22	310548	3.96 sec	4.99 sec	162.78 min
37119411 | 175994	285	20.77	190.02	331822	2.14 sec	2.53 sec	83.44 min
37537193 | 50057	265	15.32	32.06	59688	0.64 sec	0.79 sec	26.01 min
40679923 | 89837	277	100.12	154.91	294655	1.22 sec	1.42 sec	47.02 min
43001537 | 128777	282	28.66	105.29	188976	1.7 sec	1.93 sec	64.06 min
44257435 | 33375	287	57.79	265.5	471388	0.48 sec	0.71 sec	23.16 min
48383801 | 22067	257	7.48	143.44	251944	0.27 sec	0.55 sec	17.6 min
48940689 | 213802	290	76.34	353.2	626113	3.04 sec	3.64 sec	119.58 min
49119584 | 49144	268	12.88	52.47	94346	0.67 sec	0.82 sec	26.94 min
53484080 | 69289	295	20.68	171.54	298579	1 sec	1.22 sec	39.98 min
53639653 | 3077	239	0.64	7.43	13247	0.04 sec	0.05 sec	1.86 min
66775477 | 4121	241	1.22	12.65	22550	0.05 sec	0.08 sec	2.97 min
74611457 | 28455	267	10.1	82.24	145232	0.36 sec	0.63 sec	20.06 min
103075639 | 9314	241	2.95	32.13	57240	0.11 sec	0.17 sec	5.85 min
104052041 | 43913	305	142.09	524.15	931774	0.79 sec	1.3 sec	41.55 min
126100569 | 245088	298	103.14	203.05	376331	3.25 sec	3.64 sec	120.7 min
139732885 | 204755	292	32.59	199.6	350442	2.85 sec	3.34 sec	110.06 min
151316183 | 6271	264	9.35	43.6	78166	0.1 sec	0.16 sec	5.25 min
165599758 | 312288	281	73.75	528.8	929742	4.63 sec	5.39 sec	177.87 min

5.6 Conclusion

In this chapter, we proposed the ACAIM problem and realistically solve it on several VK datasets. In particular, we utilized for first time an OLR framework for IM purposes, we introduced the CATRID propagation model to enable OLR for ACAIM, we deployed a simulator to express a real feedback environment based on VK posts, we developed three learners to solve ACAIM, and we presented a thorough experimental evaluation that illustrates the importance of ACAIM to social network industry. A detailed business applicability study is also included which, by considering worldwide known brands, it further stresses the suitability of ACAIM in real world.

Chapter 6

A Content Recommendation Policy for Gaining Subscribers

How can we recommend content for a *brand* agent to use over a series of rounds so as to gain new subscribers to its social network page? The *Influence Maximization* (IM) problem seeks a set of k users, and its content-aware variants seek a set of k post features, that achieve, in both cases, an objective of expected influence in a social network. However, apart from raw influence, it is also relevant to study gain in subscribers, as long-term success rests on the subscribers of a brand page; classic IM may select k users from the subscriber set, and content-aware IM starts the post's propagation from that subscriber set. In this chapter, we propose a novel *content recommendation policy* to a brand agent for *Gaining Subscribers by Messaging* (GSM) over many rounds. In each round, the brand agent messages a fixed number of social network users and invites them to visit the brand page aiming to gain their subscription, while its most recently published content consists of features that intensely attract the preferences of the invited users. To solve GSM, we find, in each round, which content features to publish and which users to notify aiming to maximize the cumulative subscription gain over all rounds. We deploy three GSM solvers, named Random, Scan, and Substitute, and we experimentally evaluate their performance based on VKontakte (VK) posts by considering different user sets and feature sets. Our experimental results show that Substitute provides the best solution, as it is significantly more efficient than Scan with a minor loss of efficacy and clearly more efficacious than Random with competitive efficiency.

6.1 Introduction

The problem of *Influence Maximization* (IM) [LFWT18] is relevant and useful to stakeholders (henceforward, *brands*) that pursue viral marketing campaigns in social

networks. The classic IM [KKT03] seeks k users that maximize the influence of a *fixed* post in a network; the inverse variant of IM [ITTK17] seeks k content *features*[1] to form a viral post that starts its diffusion from a *fixed* set of initial adopters.

Nowadays, most brands maintain social network pages for advertising purposes, since social network users *follow* pages they are interested in; these followers are the *subscribers* of a brand. Yet, in the IM literature, subscribers are usually *taken for granted* [ITTK17, KLK20] or *ignored* [KKT03, LFWT18]. In the former case, it is lucrative for the content-aware IM techniques to apply in practice only when several subscribers exist; yet, *new* brands having zero or limited subscribers cannot benefit from such techniques. So, we provide a concrete way for such brands to gain subscribers and take advantage of works in [ITTK17, KLK20]. In the latter case, the classic IM problem applies independently of subscribers but their loyalty capabilities are not explored. For instance, it is more feasible and economic for a brand to motivate k influential loyal subscribers for promoting its posts than searching for k agnostic adopters that may not be supporters of the brand and contribute loosely to its promotion. So, even *established* brands with several subscribers, can benefit from our gaining subscribers method so as to find even more influential loyal users for classic IM purposes [KKT03, LFWT18]. Further, in the real world, the network topology is usually not known on its whole [SS13, HS15, LCCM19], whereas subscribers are always known, even if that knowledge requires explicit on-demand retrieval. Therefore, the need arises to focus on subscribers and study how brands can gain subscribers.

In this chapter, we propose a novel multi-round *content recommendation policy* that a brand agent/advertiser can use to *Gain Subscribers by Messaging* (GSM). As the GSM problem takes place over many rounds, we deploy three algorithms that solve GSM in a non-adaptive way (beforehand) for all rounds. Our solutions recommend to the advertiser, in each round, which k content features to publish and which m non-subscriber users to notify of those k features so as to maximize chances to gain the subscription of those m users. The notification is done by messaging (e.g., a short message acting like an invitation to visit the brand page), and each user is notified once; that user is never notified again for any reason. The best GSM solver is the one that achieves the maximum *subscription gain* over all rounds. We define subscription gain (henceforward, SG) as a weighted sum depicting the aggregate preference of m users for k features. For any two (k, m) solutions that achieve similar SG, we consider the cumulative (no duplicates allowed) *reach* of their respective m users to select the (k, m) solution with the maximum reach; the reach (henceforward, R) of a user is equal to her out-degree. R acts as a second filter (when needed) that helps to the selection of most influential new subscribers.

[1] We consider that each *feature* corresponds to a specific social network page.

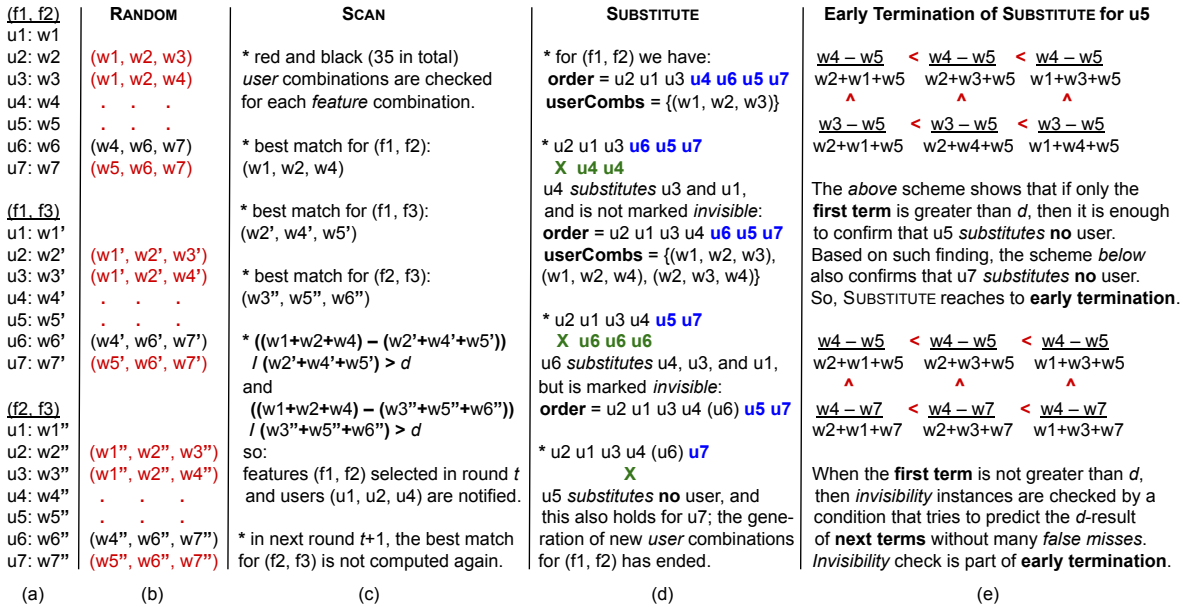

Figure 6.1: An example that shows the basic execution components of GSM solvers for $k = 2$ features and $m = 3$ users.

GSM naturally applies to social networks, such as VK[2], which constitutes the Russian version of Facebook in terms of usability and scale. In social networks, the pages to which a user subscribes, form the features (preferences) of user and in this work we consider real VK posts to fine-tune with different weights such features for our experiments. Moreover, VK strictly allows 20 messages per 12 hours to any user who has a VK account and wishes to send a message to any other non-friend VK user. Thus, each message is valuable for the advertiser and constitutes a single chance to attract the attention of notified user. By solving GSM, the advertiser prioritizes the publishing (as each round has priority over the next round) of the right k-size content for the right m users to maximize the gain of subscribers. If, alternatively, the advertiser were to apply a random messaging policy, then she would gain subscribers at a lower pace, and also face the danger of losing access to her page for some period due to spam reports sent by notified users to the VK company; a user invited to visit a page of no interest may report spamming.

To make motivation clear, we present the following example:

Example: Consider Figure 6.1. If advertiser has no algorithm to solve GSM, then she randomly selects m users (e.g., v_4, v_6, v_7) and k features (e.g., f_1, f_3); this is a trivial approach and we do not use it in this work. Yet, if she uses RANDOM algorithm, then for the selected m users (e.g., same as previous) she finds the k features that give the maximum SG (e.g., f_1, f_2 with $SG = w_4 + w_6 + w_7$), where w_4 equals to the weighed sum of v_4 in regards to f_1 and f_2. Lastly, if she uses SCAN or SUBSTITUTE algorithm, then

[2] https://vk.com/

Algorithm RANDOM

```
   Input     : G, L, F_v
   Output    : SG, R // cumulative subscription gain and reach over n rounds in GSM
   Param.    : k, m, d, n // d is not used here
1  SG = 0; R = 0; deletedV = ∅;
2  for t = 1, ..., n do
3      roundBest.users = ∅; roundBest.features = ∅; roundBest.SG = 0;
       roundBest.R = 0; // initialize the best solution for round t
4      Randomly select m users from G.V to form roundBest.users such as
       |roundBest.users| = m and none of these m users is included in deletedV;
5      roundBest.R = computeReach(roundBest.users, G);
6      for each feature combination c_f from k feature combinations of L do
7          c_f.SG = computeSG(roundBest.users, c_f, F_v);
8          if c_f.SG > roundBest.SG then
9              roundBest.SG = c_f.SG; roundBest.features = c_f;
10     SG = SG + roundBest.SG; R = R + roundBest.R;
11     for each user v ∈ roundBest.users do deletedV.insert(v);
12 return SG, R;
```

she finds a (k, m) solution with much higher SG due to considering all possible (k, m) combinations to optimally solve GSM instead of depending on random selections. A higher SG expresses a higher probability[3] that some of m invited users will become subscribers to brand's page. Algorithms in Figure 6.1 will be gradually discussed.

We summarize our contributions as follows: (1) we propose the GSM problem that applies to any social network; (2) we deploy three GSM solvers, named RANDOM, SCAN, and SUBSTITUTE; and (3) we provide a rich experimental evaluation that verifies the superiority of SUBSTITUTE over other solvers; to the best of our knowledge, the problem of gaining subscribers using content has not been studied previously.

6.2 GSM Solvers

We define the GSM problem as follows: Given a social network $G = (V, E)$ with $|V|$ users and $|E|$ edges, a feature universe L, a weighted feature set F_v of size $|L|$ capturing the preferences of each user v, a budget k, a limited number of m notification messages, a similarity threshold d, and a number of rounds n, find in each round t what k content features to publish and which m users to notify so as to maximize the cumulative subscription gain SG over n rounds:

$$SG = \max \sum_{t=1}^{n} SG_t(k, m)$$

[3]The sum of weights over features for each user equals to 1. So, the maximum SG value equals to m and each SG value divided by m belongs to range $[0, 1]$.

6.2.1 The Solver Random

Algorithm Random presents a baseline that solves GSM. In each round t, Random uniformly at random selects m users from V not chosen in previous rounds and focuses on selecting features (Lines 3–5). In more detail, Random searches for the k-size feature set that yields the maximum gain in round t ($roundBest.SG$) with regard to the selected m users, and increases the cumulative SG and reach R (Lines 6–10). Lastly, it keeps track of all notified users (Line 11) to avoid messaging them again.

In Figure 6.1b, Random selects the users $v4, v6, v7$ and so it compares only the 3 black user combinations to find which k features are the best match (yield the highest SG) for selected users. Note that Random overlooks all the red user combinations and that depicts its crucial deficiency.

6.2.2 The Solver Scan

Algorithm Scan presents the solver Scan. In a nutshell, Scan computes and stores in each round t the best match (the m-size user combination that yields the maximum SG) for each k-size feature combination by examining all possible m-size user combinations, so as to find the $roundBest$ for t, and skips in next rounds any feature combinations that do not need to be processed again.

We indicate the algorithm's workflow by marking three execution steps with bold numbers above Line 7, Line 20, and Line 23. In the first step (Lines 7–19), if all users notified in the previous round are *not* contained in the best match for current feature set c_f, then the best match for c_f does not change and it is used again to possibly update $roundBest$ based on similarity threshold d. If the first step is not executed (condition in Line 7 is false), then we move to the second step (Lines 20–22). This step is the most costly part of Scan as it examines all sets of m users sequentially to find the best match for c_f. After this processing, the third step (Line 23) possibly updates $roundBest$ by using the found best match for c_f.

In Figure 6.1c, Scan compares 35 m-size user combinations for each one of (f_1, f_2), (f_1, f_3), and (f_2, f_3) so as to find their best matches. Then, Scan compares those three best matches and finds that the best match of (f_1, f_2) yields the higher SG over others, and so the features f_1, f_2 and users v_1, v_2, v_4 are selected in current round. Note that in next round, the best match of (f_2, f_3) remains unchanged since it does not overlap with notified users of previous round.

6.2.3 The Solver Substitute

Algorithm Substitute presents the solver Substitute. This solver addresses the main bottleneck of Scan, which is the examination of all user combinations in its

Algorithm SCAN

```
   Input     : G, L, F_v
   Output    : SG, R // cumulative subscription gain and reach over n rounds in GSM
   Param.    : k, m, d, n
   // Each entry of fC maps k features to the m users who yield the maximum SG
1  for each feature combination c_f from k feature combinations of L do fC[c_f] = ∅;
   // Each entry of uC maps m users to their reach R as computed in G
2  for each user combination c_u from m user combinations of V do uC[c_u] = −1;
3  SG = 0; R = 0; deletedV = ∅;
4  for t = 1, ..., n do
5      roundBest.users = ∅; roundBest.features = ∅; roundBest.SG = 0;
       roundBest.R = 0; // initialize the best solution for round t
6      for each feature combination c_f ∈ fC do
           // 1. Check to may skip computation of fC[c_f] and Update roundBest
7          if all users in deletedV are not contained in fC[c_f] then
8              c_f.SG = computeSG(fC[c_f], c_f, F_v);
9              if roundBest.SG ≥ c_f.SG then
10                 diff = (roundBest.SG − c_f.SG) ÷ c_f.SG;
11                 if diff > d then continue;
12             else
13                 diff = (c_f.SG − roundBest.SG) ÷ roundBest.SG;
14                 if diff > d then
15                     if uC[fC[c_f]] = −1 then
16                         uC[fC[c_f]] = computeReach(fC[c_f], G);
17                     roundBest.users = fC[c_f];
                       roundBest.features = c_f; roundBest.SG = c_f.SG;
                       roundBest.R = uC[fC[c_f]]; continue;
18             Repeat lines 15-16 to compute uC[fC[c_f]];
19             if uC[fC[c_f]] > roundBest.R or (uC[fC[c_f]] = roundBest.R
               and c_f.SG > roundBest.SG) then Update roundBest as in line 17;
               // continue is executed either the condition in if is true or false
           // 2. Compute fC[c_f] with the examination of each c_u ∈ uC (loop here!)
20         Let crnt_c_u be the current best user combination stored in fC[c_f];
21         Let next_c_u be the next c_u ∈ uC for examination to may update fC[c_f];
22         Compare crnt_c_u with next_c_u by following a similar process to lines 8-19
           so as to may update fC[c_f] and crnt_c_u with next_c_u;
           // 3. Update roundBest
23         Repeat lines 8-19 to update roundBest;
24     SG = SG + roundBest.SG; R = R + roundBest.R;
25     deletedV = ∅; for each user v ∈ roundBest.users do deletedV.insert(v);
26     Delete each c_u ∈ uC that contains at least one user v ∈ deletedV;
27 return SG, R;
```

second step. In particular, SUBSTITUTE adds an intermediate step (Lines 10–31) that creates only the necessary m-size user combinations to find the best match for current feature set c_f. To do that, it utilizes the structure $selV$ (initialized in Lines 2–4) that stores for each c_f a set of pairs corresponding to users associated with their achieved SG in c_f, organized in descending order by their SG values.

Algorithm SUBSTITUTE

Input : G, L, F_v
Output : SG, R // cumulative subscription gain and reach over n rounds in GSM
Param. : k, m, d, n
// Each entry of fC maps k features to the m users who yield the maximum SG
1 **for** *each feature combination* c_f *from* k *feature combinations of* L **do** $fC[c_f] = \emptyset$;
2 **for** *each feature combination* $c_f \in fC$ **do**
3 $v.SG$ = computeSG(v, c_f, F_v); $allV[c_f]$.insert($(v, v.SG)$); // $v.SG$ desc sort
4 Form $selV[c_f]$ by taking the first $m * n$ pairs of $allV[c_f]$; // plus d-extensions
5 $SG = 0$; $R = 0$; $deletedV = \emptyset$;
6 **for** $t = 1, \ldots, n$ **do**
7 $roundBest.users = \emptyset$; $roundBest.features = \emptyset$; $roundBest.SG = 0$;
$roundBest.R = 0$; // initialize the best solution for round t
8 **for** *each feature combination* $c_f \in fC$ **do**
// **1.** Check to may skip computation of $fC[c_f]$ and Update $roundBest$
9 Repeat lines 7-19 of SCAN with only difference that now $c_f.R$ = computeReach($fC[c_f]$, G) is used and so $c_f.R$ replaces $uC[fC[c_f]]$;
// **2.** Create only the necessary m-size user combinations (uC) for c_f
10 Form the first c_u by taking the first m pairs of $selV[c_f]$ and set $uC[c_u] = -1$; // each c_u is a set of pairs $(v, v.SG)$ here
11 $offset = m$; $c_f.invisible = \emptyset$; // it contains each invisible $v \in selV[c_f]$
12 **for** $e2 = selV[c_f].get(m+1), \ldots, selV[c_f].last()$ **do**
13 $subs = \emptyset$; $invis = 0$; $travs = 0$;
14 **for** $e1 = selV[c_f].get(offset), \ldots, selV[c_f].first()$ **do**
15 **if** $e1.v \in c_f$.invisible **then** { $invis++$; $travs++$; **continue**; }
16 $e1\_comb = \emptyset$; $e2\_comb = \emptyset$; $denom.SG = e2.v.SG$;
17 **for** $ei = selV[c_f].first(), \ldots, selV[c_f].get(m)$ **do**
18 **if** $ei = e1$ **then continue**;
19 $e1\_comb$.insert($ei.v$); $e2\_comb$.insert($ei.v$);
20 $denom.SG = denom.SG + ei.v.SG$;
21 After $m-1$ loop executions **break**;
22 $diff = (e1.v.SG - e2.v.SG) \div denom.SG$;
23 **if** $diff > d$ **then break**; **else** $subs$.insert($e1$); // $e2$ can sbst $e1$
24 $e1\_comb$.insert($e1.v$); $e1.R$ = computeReach($e1\_comb, G$);
25 $e2\_comb$.insert($e2.v$); $e2.R$ = computeReach($e2\_comb, G$);
26 $e1\_out = G$.outEdges($e1.v$); $e2\_out = G$.outEdges($e2.v$);
27 **if** ($e1.R \geq e2.R$ **and** $|e1\_out| \geq |e2\_out|$) **then** $invis++$;
28 $travs++$; // traversal of $selV[c_f]$ proceeds with its previous $e1$
29 **if** $|subs| = 0$ **then break**; // termination; no more uC are created
30 $offset++$; **if** $travs = invis$ **then** $c_f.invisible$.insert($e2.v$) and **continue**; // $e2$ marked as invisible for all traversed $e1$; no uC for $e2$
31 For each $e1 \in subs$ and for each $c_u \in uC$ where $e1 \in c_u$, replace $e1$ with $e2$ to form $c_{u'}$ and set $uC[c_{u'}] = -1$; // each $c_{u'}$ is a new uC
// **3.** Compute $fC[c_f]$ with the examination of **each** $c_u \in uC$ (**loop** here!)
32 Repeat lines 20-22 of SCAN; // $c_f.R$ in place of $uC[fC[c_f]]$ as in line 9
// **4.** Update $roundBest$
33 Repeat line 23 of SCAN; // $c_f.R$ in place of $uC[fC[c_f]]$ as in line 9
34 $SG = SG + roundBest.SG$; $R = R + roundBest.R$;
35 $deletedV = \emptyset$; **for** *each user* $v \in roundBest.users$ **do** $deletedV$.insert(v);
36 Delete from each $selV[c_f]$ all pairs that contain a user $v \in deletedV$;
37 **return** SG, R;

Specifically, the first m entries of $selV[c_f]$ form the first user combination (Line 10). Then, we compare each entry $e2$ (Line 12) having a position greater than m in $selV[c_f]$ with each previous entry $e1$ of $selV[c_f]$ (Line 14) to check whether $e2$ can *substitute* $e1$. If a substitution happens (Line 23), there may exist a better solution for c_f having $e2$ in place of $e1$. Otherwise, if $e2$ cannot substitute the first compared $e1$, then $e2$ cannot substitute any $e1$, and also this holds for any next $e2$, resulting in *early termination* (Line 29). This termination is beneficial for two reasons: first, there is no need to compare more $(e2, e1)$ pairs to find a better solution for c_f, and second, it ends the generation of new user combinations for c_f thereby incurring less overhead in third step (Line 32). To further enhance that termination, we add a condition in Line 27 that counts instances of *invisibility*. A case of invisibility occurs when the current combination that includes $e1$ has no less reach than the same combination with $e2$ in place of $e1$, and also the atomic reach of $e1$ is no less than the atomic reach of $e2$; then, in most cases $e1$ is a better option than $e2$. If such evidence is observed for all the $e1$ to which we compare $e2$, then we mark $e2$ as invisible henceforward (Line 30). Intuitively, the invisibility of $e2$ means that it is very likely that no user combination derived by replacing any $e1$ with $e2$, would constitute a better solution for c_f, so we opt to ignore them.

Figure 6.1d presents the execution logic of Substitute for $c_f = (f_1, f_2)$. The *order* represents $selV$ and $userCombs$ includes the m-size user combinations for c_f that can be seen as a gradually constructed *knowledge base* to find the best match for c_f. With blue color we depict the not yet examined entries of $selV$, while with green color we capture its currently examined entries for substitution; the symbol X denotes no substitution after checking, and when no green mark exists, it means no checking at all of respective $(e2, e1)$ pair. In more detail, the first entry of $userCombs$ comprises users v_1, v_2, v_3. Then, $e2 = v_4$ is compared with all black $e1$ that also they totally did not mark it as invisible, but v_4 does not substitute $e1 = v_2$, so $userCombs$ extends with combinations derived after the substitution of v_4 with v_3 and v_1 to its current entries. After that, $e2 = v_6$ can achieve three substitutions, but throughout checking, it marked as invisible and so it does extend at all $userCombs$. Finally, $e2 = v_5$ compares only with $e1 = v_4$ and since it cannot substitute it, it leads to early termination as it is sure that v_5 cannot substitute any $e1$ and this also holds for any entry after v_5 (here, v_7). So, although Scan examines 35 user combinations to find the best match for (f_1, f_2), Substitute finds that best match by only examining 3 user combinations; the same logic applies for (f_1, f_3) and (f_2, f_3).

Figure 6.1e justifies why the aforementioned early termination is possible when v_5 cannot substitute v_4. Since the *first term* is greater than d, namely $\frac{w_4 - w_5}{w_2 + w_1 + w_5} > d$, depicting the comparison result of user combinations (v_2, v_1, v_4) and (v_2, v_1, v_5), and showing that v_5 cannot substitute v_4, we prove early termination based on red *less*

symbols. In the first (top) scheme, we show that each *next term*, capturing a different d-comparison among v_5 and v_4 (first row) and among v_5 and v_3 (second row), is even greater than d if *first term* is greater than d; this also holds inductively for respective terms relative to v_1 and v_2. In the second (bottom) scheme, we apply a similar logic and show that each *next term* of second row that captures a different d-comparison among v_7 and v_4 is also greater than d if *first term* is greater than d, and so v_7 cannot substitute v_4 as also no other user based on the inductive logic of first scheme.

In practice, for an entry $e2$ to generate winner-candidate user combinations for c_f in Line 31, it must substitute at least one $e1$ and it must not be marked as invisible. The performance of Substitute relies on the fact that only a few $e2$ pass the two mentioned checks, and that fast leads to an occurrence of early termination (Line 29). Since it makes sense to compare reach only for really similar (k, m) candidates (d is small), any *false misses* due to the condition in Line 27 would have a negative impact on efficacy only in rare cases where early termination takes too long to take effect.

6.3 Experimental Evaluation

We wrote code in C++ and ran experiments on an AMD Ryzen 5 4600U CPU @ 2.1 GHz machine with 16GB RAM running Linux Ubuntu 20.04.3 LTS 64-bit. For graph operations we used the open-source graph library Lemon [DJK11].

6.3.1 Setup

Datasets. As VK comprises 27 categories, we select the 1 and 2 most popular pages from each category, to form sets of 27 and 54 features. We uniformly at random select 10 different groups of 80 users for $|L| = 27$ and $|L| = 54$ (same groups for both L), and 10 different groups of 100 users for $|L| = 27$ and $|L| = 54$ (same groups for both L); there is no relation among groups of 80 and 100 users. So, all the experimental results in our figures are averaged by 10.

Tuning. For each selected user, we realistically tune her $F_v(f)$ value for each feature $f \in L$ by taking the average of her *like* responses in all posts of the years 2010-2017 of VK; as f we considered only the *brand* that published the relative post where user liked it. The feature weight sum of each $F_v(f)$ equals to 1, and for any f where no *like* found, we initialized $F_v(f)$ with a dummy value.

Parameters. The number of content features (k) is examined until $k = 3$, as higher k values were costly for Scan. The other parameters are fixed; the number of m invited users is 3, the similarity threshold d is 0.001, and the number of n rounds is 20.

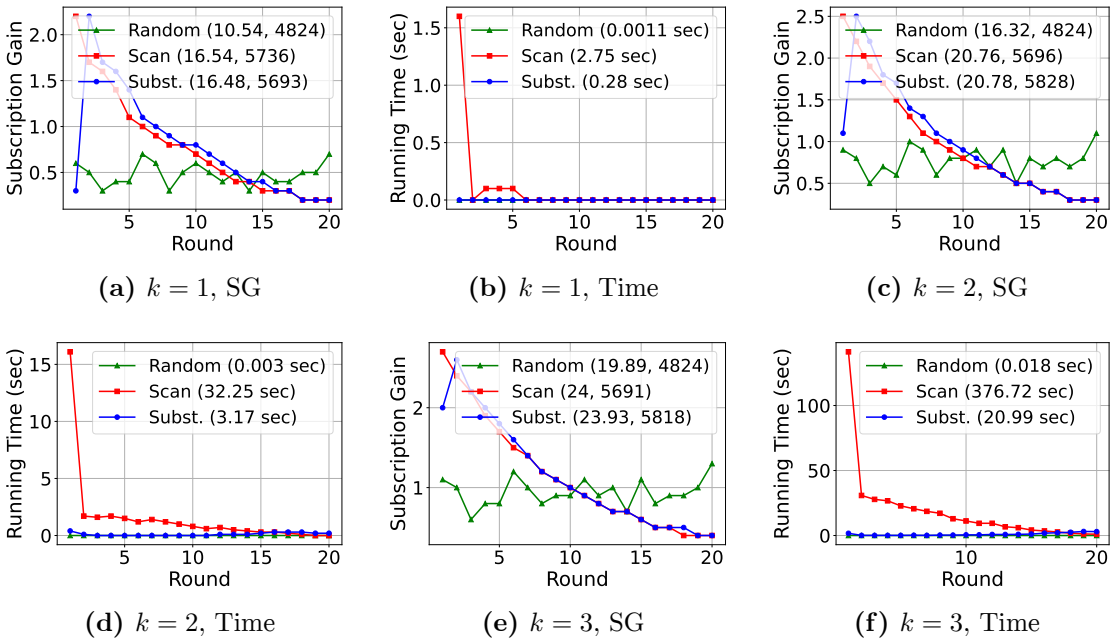

(a) $k = 1$, SG **(b)** $k = 1$, Time **(c)** $k = 2$, SG

(d) $k = 2$, Time **(e)** $k = 3$, SG **(f)** $k = 3$, Time

Figure 6.2: SG per round and Time per round results of RANDOM, SCAN, and SUBSTITUTE for $|L| = 27$, $|V| = 80$, and $k = 1, 2$, and 3.

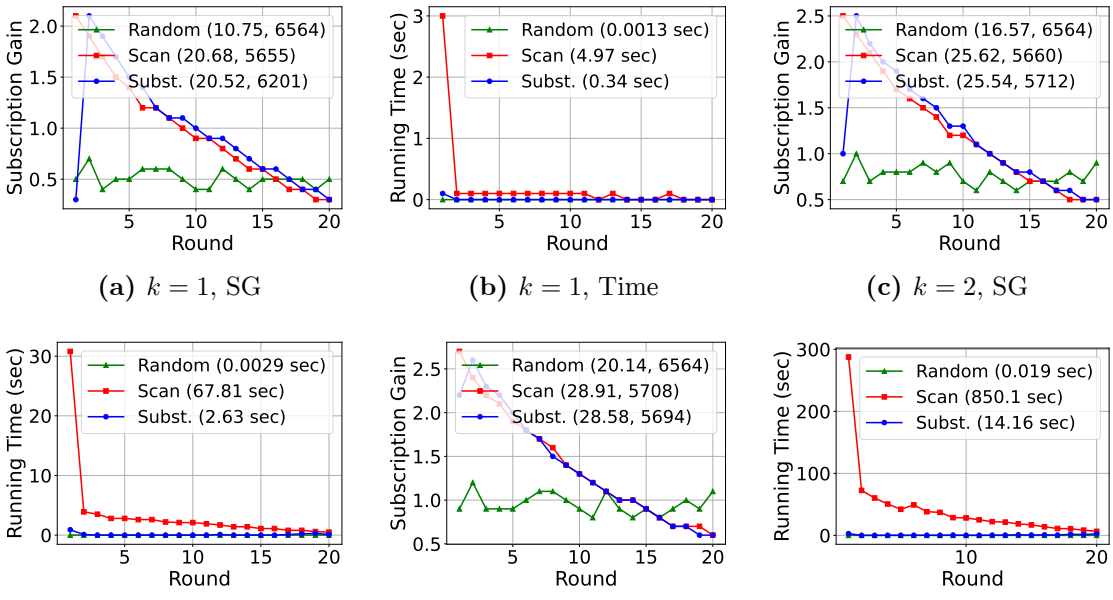

(a) $k = 1$, SG **(b)** $k = 1$, Time **(c)** $k = 2$, SG

(d) $k = 2$, Time **(e)** $k = 3$, SG **(f)** $k = 3$, Time

Figure 6.3: SG per round and Time per round results of RANDOM, SCAN, and SUBSTITUTE for $|L| = 27$, $|V| = 100$, and $k = 1, 2$, and 3.

6.3.2 Results

Figure 6.2 presents the subscription gain (SG) and running time (measured in seconds) results per round of RANDOM, SCAN, and SUBSTITUTE for $k = 1, 2$, and 3, and for

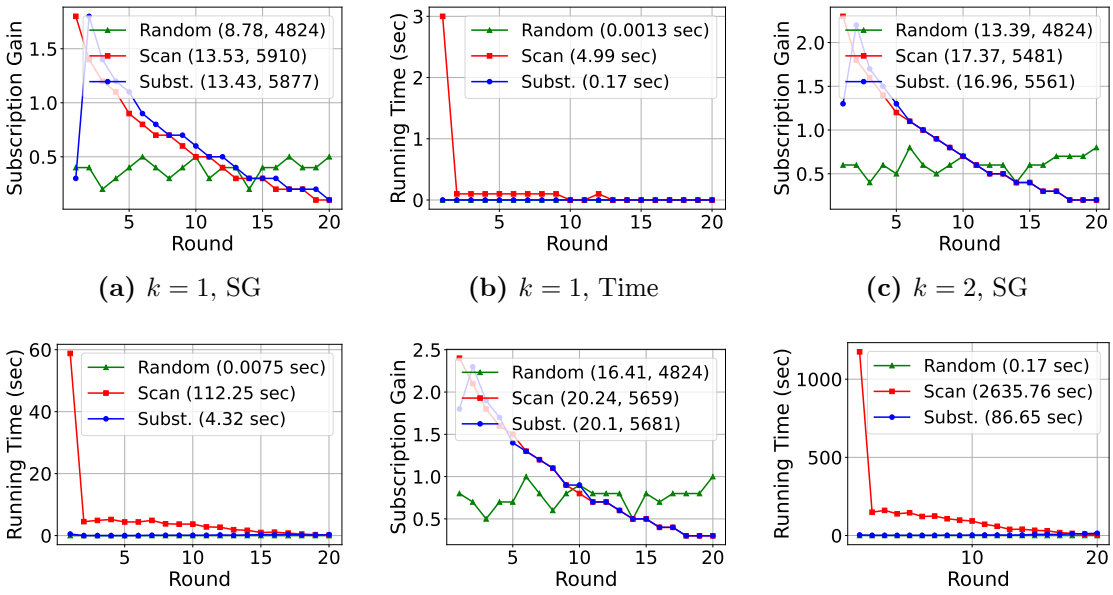

(a) $k = 1$, SG **(b)** $k = 1$, Time **(c)** $k = 2$, SG

(d) $k = 2$, Time **(e)** $k = 3$, SG **(f)** $k = 3$, Time

Figure 6.4: SG per round and Time per round results of RANDOM, SCAN, and SUBSTITUTE for $|L| = 54$, $|V| = 80$, and $k = 1, 2$, and 3.

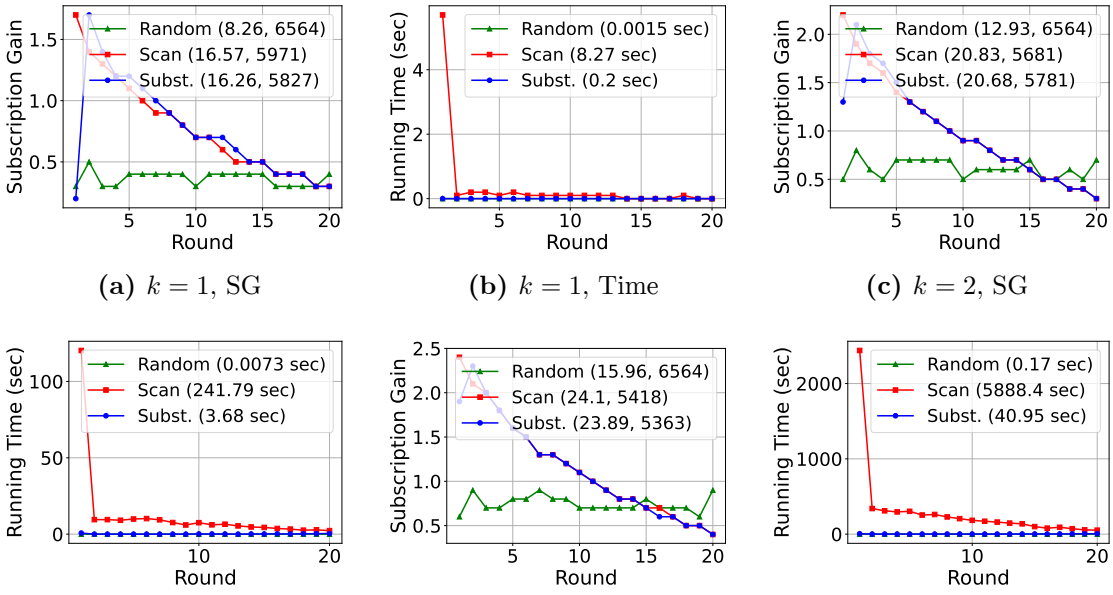

(a) $k = 1$, SG **(b)** $k = 1$, Time **(c)** $k = 2$, SG

(d) $k = 2$, Time **(e)** $k = 3$, SG **(f)** $k = 3$, Time

Figure 6.5: SG per round and Time per round results of RANDOM, SCAN, and SUBSTITUTE for $|L| = 54$, $|V| = 100$, and $k = 1, 2$, and 3.

$|L| = 27, |V| = 80$; Figure 6.3 for $|L| = 27, |V| = 100$, Figure 6.4 for $|L| = 54, |V| = 80$, and Figure 6.5 for $|L| = 54, |V| = 100$. Besides the per round results, in each SG figure

there is in legend for each solver a pair (X, Y), where X is the cumulative SG and Y is the cumulative reach R[4] over all rounds. Similarly, in each time figure, the legend mentions for each solver the cumulative running time over all rounds.

We observe that the general trend is the same in all figures; Substitute is almost equally effective to Scan and competitively efficient to Random. It is evident that Substitute achieves a slightly less cumulative SG in regards to Scan due to the poor SG result it achieves in first round; that behavior depends on aggressive false misses derived from true evaluation of condition in Line 27, but as rounds evolve such false misses reduce due to skipping of each c_f having an unaffected best solution (Line 9). Except for first round, the SG of both solvers is very close and diminishes as rounds grow because promising subscription candidates are messaged from the beginning. Yet, the SG of Random is the lowest and can be seen as fixed across rounds, as it does not apply messaging with priority as previous solvers. Regarding running time, Substitute is slower than Random but constant, while Scan performs better as rounds evolve but has a clear scalability issue when any of V, L, or k increases.

Moreover, we remark that in all figures as k grows all solvers achieve higher efficacy (SG) and lower efficiency (time). This is logical as a higher k yields a higher feature weight sum of m users to k features, but also it incurs more feature combinations for processing. Another interesting result is to see what happens when V increases over a fixed L, and what happens when L increases over a fixed V. In the former case, by comparing the Figures 6.2 and 6.3, as also the Figures 6.4 and 6.5, we note that the SG of Random is constant, while the SG of other two solvers clearly improves; a larger selection pool of users is always more beneficial for prioritized solvers. Yet, with more candidate user combinations present for processing, only Substitute improves its performance on running time (e.g., see Figures 6.2f, 6.3f, and Figures 6.4f, 6.5f), whereas Scan heavily deteriorates its performance; more users offer more chances for early termination cases to occur in Line 29 of Substitute since it is more likely that some users clearly separate over others. In the latter case, by comparing Figures 6.2 and 6.4, as well as Figures 6.3 and 6.5, we observe that both the efficacy and efficiency of all solvers worsen. The SG deteriorates as a heavier feature weight segmentation in F_v (due to larger L) decreases the feature weights of each user and so incurs lower feature weight sums of m users to k features. Further, a more intense segmentation strengthens the similarity of feature weights in F_v, and so increases the (k, m) candidates not filtered by threshold d. Lastly, the inferior running time is expected due to processing a larger pool of candidate feature combinations.

[4]We present R results for the sake of completeness; their analysis is not critical for GSM.

6.4 Conclusion

In this chapter, we proposed that brands can use a *content recommendation policy* to gain subscribers to their social network pages via messaging. We deployed three algorithms, Random, Scan, and Substitute to this task using a realistic tuning of VK posts. Our thorough experimental study on different user and feature sets verified that Substitute outperforms other solvers. To our knowledge, this is the first work to study how brands can gain subscribers using content.

Chapter 7

Conclusion

7.1 Summary

In this thesis, we studied important social and spatial data problems applied on graphs. In spatial domain, we deployed the SRX system that supports spatial RDF data management operations, while in social domain we examined three novel problems relative to content-aware recommendation applied to social networks.

To efficiently solve spatial RDF problems, we built the SRX system by extending the popular RDF-3X store [NW08] with a novel spatial encoding grid-scheme to support WITHIN, DISTANCE, and kNN queries, as also Updates of spatial RDF entities; the grid-scheme approximates the geometries of the spatial RDF entities inside their integer IDs and is used along with several introduced operators and optimizations. We evaluated SRX on LinkedGeoData (LGD) [LGD] and YAGO [YAG] RDF datasets and compared its performance with the latest versions of Virtuoso [Vir], GraphDB [Gra], and Strabon [KKK12]. The results show SRX's superior performance over the competitors; in regards to RDF-3X, SRX improves its performance for queries with spatial predicates while incurring little overhead during updates.

The first problem we analyzed and studied in social domain was the *Content-Aware Influence Maximization* (CAIM) problem. CAIM asks for the k features (or attributes) that can form a post so as to make it viral in a social network, starting its diffusion from the subscribers of the brand's social network page. We proved that the CAIM problem is NP-hard and inapproximable, and so we deployed an efficient heuristic, Explore-Update, which uses bounded local arborescences to calculate influence spread. Our experimental results on Gnutella[1] and VK[2] datasets show that Explore-Update selects near-optimal feature sets, achieves 30% higher spread than baselines, and runs an order of magnitude faster than the classic Greedy solution.

[1] https://snap.stanford.edu/data/p2p-Gnutella04.html
[2] https://vk.com/

We also analyzed CAIM under adaptive settings, and so we studied the *Adaptive Content-Aware Influence Maximization* (ACAIM) problem for online applicability to social networks. ACAIM seeks for k features to form a post in each round so as to maximize the cumulative influence of those posts over all rounds. To solve ACAIM, we utilized an *Online Learning to Rank* (OLR) framework for IM purposes, we introduced the *Content-Aware TopRank Influence Dissemination* (CATRID) propagation model to enable OLR for ACAIM, we deployed a simulator to express a real feedback environment for learners based on VK posts, and we developed three ACAIM learners evaluated on several VK datasets. Our experimental results show the practical value and suitability of ACAIM to social network industry.

The last problem we studied around social networks was to propose a *content recommendation policy* to a brand agent/advertiser for *Gaining Subscribers by Messaging* (GSM) over many rounds. To solve GSM, we find in each round, what content features to publish and which users to notify of those features aiming to maximize the cumulative subscription gain over all rounds. We deployed three GSM solvers, named RANDOM, SCAN, and SUBSTITUTE and tested their performance on VK datasets. Our experimental evaluation show that SUBSTITUTE clearly outperforms other solvers.

7.2 Future Work

In regards to SRX work, we plan to extend our update mechanism to support online updates in the spirit of [NW10b] and extend our query optimizer to consider the spatial distribution of entities that support a *characteristic set* [NM11]. A promising research direction that we also plan to pursue is to investigate how our encoding-based techniques can be adapted to distributed spatial analytics systems, such as those in [PKNK18], to improve their performance.

In social domain around content-aware recommendation, for CAIM we plan to study other propagation models and investigate the parallelization of Explore-Update, for ACAIM our main target is to extend it further for *loyalty marketing* purposes (e.g., gaining new subscribers over rounds), and for GSM we intend to apply our solutions on larger user and feature sets and develop better solvers for such cases.

Also, there is a number of new spatio-social problems that we can analyze and study based on the contributions of this thesis. For instance, we can solve ACAIM focusing on brands that have physical stores (e.g., Starbucks, Zara), having as target to maximize the influence over users for which we estimate that move around those stores. The same spatial dimension can also be considered for the GSM problem where the nearby users to the stores of brand will be notified earlier than more distant ones.

Lastly, another interesting direction is how to diversify the content we recommend to brands so as to solve ACAIM and GSM with more fairness and naturalness.

Chapter 8

Appendix

Here, we present the Appendix of this thesis. It provides detailed information on the datasets and benchmarks used in the experimental evaluation of Chapter 3. The material is provided for reproducibility purposes and consists of three parts. First, we give the spatial distribution of geometries in the two real datasets we used for query evaluation. Second, we provide the exact queries for each system, including Virtuoso, GraphDB, and Strabon. Third, we elaborate on the deltas extracted between different versions of the two datasets, which we used to generate update workloads.

To the best of our knowledge, the benchmark we present here is the first one for spatial RDF stores on real data. It includes: (i) a large collection of queries with different spatial predicates and selectivities, and (ii) a configurable update workload based on real changes in the two datasets over time.

8.1 Spatial distribution of geometries

Figures 8.1 and 8.2 show the density plots for the spatial distribution of geometries in the following two datasets, which have been used in Section 3.8.2:

1. LinkedGeodata (LGD), as retrieved from https://tinyurl.com/yc4lxqdv.
2. YAGO2s 2.5.3 (YAGO), as retrieved from https://tinyurl.com/y7ukhge3.

8.2 Queries

We describe the exact range, join, and kNN queries used in Section 3.8.2. Each query is uniquely identified by a QueryID, as used in this chapter. All queries can be found at: https://web.imsi.athenarc.gr/SRX.

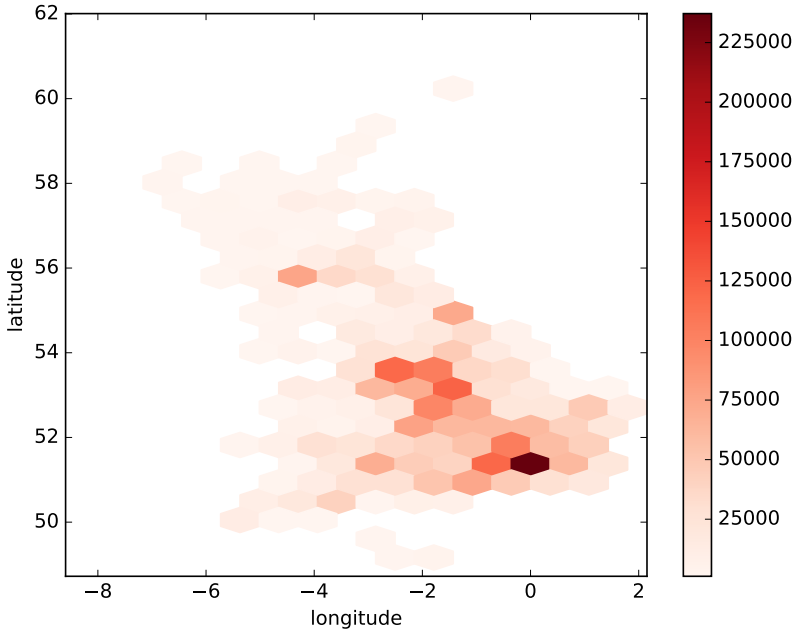

Figure 8.1: Spatial distribution of geometries in LGD. LGD contains geometries for entities in the United Kingdom with highest density in the area around London.

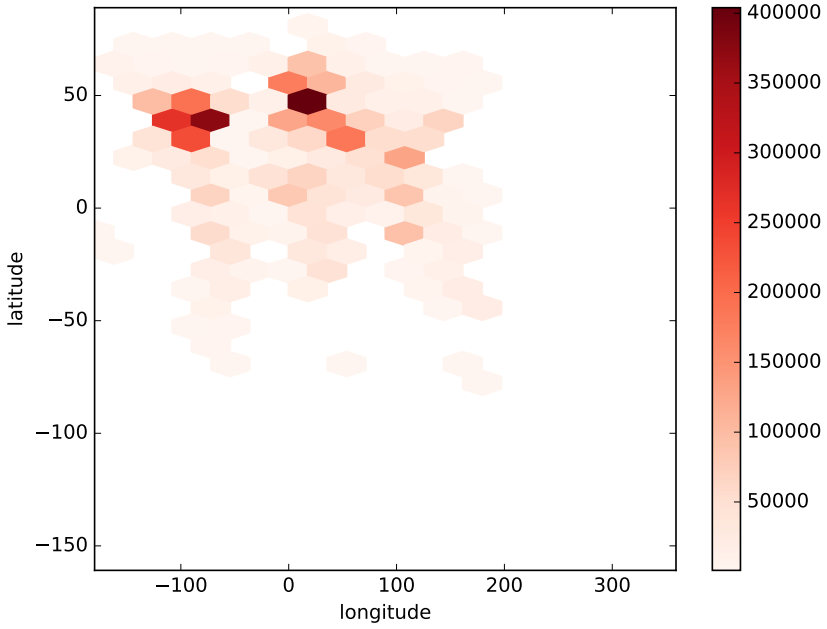

Figure 8.2: Spatial distribution of geometries in YAGO. YAGO's geometries spread all over the globe with highest density in North America and Europe.

8.2.1 Spatial range queries

The spatial range queries for LGD follow the template:

Select $?s$
Where $?s$ name $?n$. $?s$ label $?l$.
$?s$ type **[TYPE]** . $?s$ hasGeometry $?g$.
Filter WITHIN($?g$, "RECTANGLE(**[MBR]**)")

where **[TYPE]** and **[MBR]** are instantiated for each query as follows:

QueryID	[TYPE]	[MBR]
LGD.SL1	police	-5,50,0,55
LGD.SL2	bus_stop	-10,50,0,60
LGD.SL3*	park	-5,50,0,55
LGD.LS1	pub	-5,45,0,50
LGD.LS2	bus_stop	-10,45,-5,50
LGD.LS3*	road	-10,45,-5,50
LGD.SS1	restaurant	-5,45,0,50
LGD.SS2*	park	-5,45,0,50
LGD.SS3*	road	-5,45,0,50
LGD.LL1	bus_stop	-5,55,0,60

The spatial range queries for YAGO are given in Table 8.1:

Table 8.1: Spatial range queries for YAGO.

YAGO.SL1* Select $?gn$ $?fn$ $?pr$ Where $?p$ hasGivenName $?gn$. $?p$ hasFamilyName $?fn$. $?p$ hasWonPrize $?pr$. $?p$ diedIn $?c$. $?c$ hasGeometry $?g$. Filter WITHIN($?g$, "RECTANGLE(-100, 20, -80, 40)")	**YAGO.SL2*** Select $?gn$ $?fn$ Where $?p$ hasGivenName $?gn$. $?p$ hasFamilyName $?fn$. $?p$ a Wordnet_scientist_110560637 . $?p$ wasBornIn $?c$. $?c$ hasGeometry $?g$. Filter WITHIN($?g$, "RECTANGLE(-95, 40, -90, 45)")
YAGO.LS1* Select $?p$ $?w$ Where $?p$ hasAcademicAdvisor $?a$. $?a$ worksAt $?w$. $?w$ isLocatedIn $?l$. $?l$ hasGeometry $?g$. Filter WITHIN($?g$, "RECTANGLE(-160, -50, -150, -40)")	**YAGO.LS2*** Select $?e$ $?c$ Where $?e$ happenedIn $?l$. $?l$ a $?c$. $?c$ subClassOf Wordnet_city_108524735 . $?l$ hasGeometry $?g$. Filter WITHIN($?g$, "RECTANGLE(-130, 40, -120, 50)")
YAGO.SS1* Select $?gn$ $?fn$ Where $?p$ hasGivenName $?gn$. $?p$ hasFamilyName $?fn$. $?p$ a Wordnet_scientist_110560637 . $?p$ wasBornIn $?c$. $?c$ hasGeometry $?g$. Filter WITHIN($?g$, "RECTANGLE(-105, 45, -100, 50)")	**YAGO.SS2*** Select $?p$ $?w$ Where $?p$ graduatedFrom $?u$. $?p$ worksAt $?w$. $?u$ isLocatedIn $?l$. $?l$ hasGeometry $?g$. Filter WITHIN($?g$, "RECTANGLE(-110, 50, -100, 60)")
YAGO.LL1* Select $?e$ $?c$ Where $?e$ happenedIn $?l$. $?l$ a $?c$. $?c$ subClassOf Wordnet_city_108524735 . $?l$ hasGeometry $?g$. Filter WITHIN($?g$, "RECTANGLE(-90, 30, -80, 40)")	**YAGO.LL2*** Select $?p$ Where $?p$ hasArea $?a$. $?p$ isLocatedIn $?l$. $?l$ hasGeometry $?g$. Filter WITHIN($?g$, "RECTANGLE(-100, 30, -90, 40)")

8.2.2 Spatial distance join queries

The spatial distance join queries for LGD are given in Table 8.2:

The spatial distance join queries for YAGO are given in Table 8.3:

Table 8.2: Spatial distance join queries for LGD.

LGD.J1 (point-point) Select ?$s1$?$s2$ Where ?$s1$ type hotel . ?$s1$ hasGeometry ?$g1$. ?$s2$ type hotel . ?$s2$ hasGeometry ?$g2$. Filter DISTANCE(?$g1$,?$g2$) < "0.003"	**LGD.J2** (point-point) Select ?$s1$?$s2$?$l1$?$l2$ Where ?$s1$ name ?$l1$. ?$s1$ label ?$b1$. ?$s1$ type police . ?$s1$ hasGeometry ?$g1$. ?$s2$ name ?$l2$. ?$s2$ label ?$b2$. ?$s2$ type police . ?$s2$ hasGeometry ?$g2$. Filter DISTANCE(?$g1$,?$g2$) < "0.01"
LGD.J3 (point-point) Select ?$s1$?$s2$ Where ?$s1$ name ?$l1$. ?$s1$ label ?$b1$. ?$s1$ type pub . ?$s1$ hasGeometry ?$g1$. ?$s2$ name ?$l2$. ?$s2$ label ?$b2$. ?$s2$ type police . ?$s2$ hasGeometry ?$g2$. Filter DISTANCE(?$g1$,?$g2$) < "0.02"	**LGD.J4*** (polygon-polygon) Select ?$s1$?$s2$ Where ?$s1$ type park . ?$s1$ hasGeometry ?$g1$. ?$s2$ type park . ?$s2$ hasGeometry ?$g2$. Filter DISTANCE(?$g1$,?$g2$) < "0.05"
LGD.J5* (point-polygon) Select ?$s1$?$s2$ Where ?$s1$ label ?$b1$. ?$s1$ type police . ?$s1$ hasGeometry ?$g1$. ?$s2$ label ?$b2$. ?$s2$ type park . ?$s2$ hasGeometry ?$g2$. Filter DISTANCE(?$g1$,?$g2$) < "0.01"	**LGD.J6*** (point-line), **[EPS]** $\in \{0.01,0.001,0.0005\}$ Select ?$s1$?$s2$ Where ?$s1$ label ?$b1$. ?$s1$ type hotel . ?$s1$ hasGeometry ?$g1$. ?$s2$ label ?$b2$. ?$s2$ type road . ?$s2$ hasGeometry ?$g2$. Filter DISTANCE(?$g1$,?$g2$) < "**[EPS]**"

Table 8.3: Spatial distance join queries for YAGO.

YAGO.J1* Select ?$c1$?$c2$ Where ?$a1$ hasAirportCode ?$c1$. ?$a1$ hasGeometry ?$g1$. ?$a2$ hasAirportCode ?$c2$. ?$a2$ hasGeometry ?$g2$. Filter DISTANCE(?$g1$,?$g2$) < "0.1"	**YAGO.J2*** Select ?$p1$?$p2$ Where ?$p1$ hasGivenName ?$gn1$. ?$p1$ hasFamilyName ?$fn1$. ?$p1$ hasWonPrize ?$pr1$. ?$p1$ wasBornIn ?$c1$. ?$c1$ hasGeometry ?$g1$. ?$p2$ hasGivenName ?$gn2$. ?$p2$ hasFamilyName ?$fn2$. ?$p2$ hasWonPrize ?$pr2$. ?$p2$ wasBornIn ?$c2$. ?$c2$ hasGeometry ?$g2$. Filter DISTANCE(?$g1$,?$g2$) < "0.1"
YAGO.J3* Select ?p ?$c1$?$c2$ Where ?p hasGivenName ?gn . ?p hasFamilyName ?fn . ?p actedIn ?m . ?m isLocatedIn ?$c1$. ?$c1$ hasGeometry ?$g1$. ?p wasBornIn ?$c2$. ?$c2$ hasGeometry ?$g2$. Filter DISTANCE(?$g1$,?$g2$) < "0.1"	**YAGO.J4*** Select ?$p1$?$p2$ Where ?$p1$ hasFamilyName ?$fn1$. ?$p1$ wasBornIn ?$c1$. ?$c1$ hasGeometry ?$g1$. ?$p1$ isMarriedTo ?$p2$. ?$p2$ wasBornIn ?$c2$. ?$c2$ hasGeometry ?$g2$. Filter DISTANCE(?$g1$,?$g2$) < "0.1"
YAGO.J5* Select ?p Where ?p hasFamilyName ?fn . ?p livesIn ?$c1$. ?$c1$ hasGeometry ?$g1$. ?p worksAt ?$c2$. ?$c2$ hasGeometry ?$g2$. Filter DISTANCE(?$g1$,?$g2$) < "0.1"	**YAGO.J6*** Select ?$p1$?$p2$ Where ?$p1$ hasGivenName ?$gn1$. ?$p1$ hasFamilyName ?$fn1$. ?$p1$ a Wordnet_scientist_110560637 . ?$p1$ wasBornIn ?$c1$. ?$c1$ hasGeometry ?$g1$. ?$p2$ hasGivenName ?$gn2$. ?$p2$ hasFamilyName ?$fn2$. ?$p2$ a Wordnet_scientist_110560637 . ?$p2$ diedIn ?$c2$. ?$c2$ hasGeometry ?$g2$. Filter DISTANCE(?$g1$,?$g2$) < "0.1"
YAGO.J7* Select ?$p1$?$p2$ Where ?$p1$ graduatedFrom ?$u1$. ?$u1$ hasGeometry ?$g1$. ?$p2$ actedIn ?$m2$. ?$m2$ isLocatedIn ?$l2$. ?$l2$ hasGeometry ?$g2$. Filter DISTANCE(?$g1$,?$g2$) < "0.1"	**YAGO.J8***, **[EPS]** $\in \{0.1,0.01,0.001\}$ Select ?$p1$?$p2$ Where ?$p1$ worksAt ?$w1$. ?$w1$ hasGeometry ?$g1$. ?$p2$ worksAt ?$w2$. ?$w2$ hasGeometry ?$g2$. Filter DISTANCE(?$g1$,?$g2$) < "**[EPS]**"

8.2.3 Spatial kNN queries for Encoding, Baseline, and Basic

The spatial kNN queries for LGD have the following template:

Select ?s
Where ?s name ?n . ?s label ?l .
?s type **[TYPE]** . ?s hasGeometry ?g .

Filter kNN($?g$, "POINT(**[COORDS]**)", k)

where $k \in \{5, 10, 20, 50, 100\}$, and **[TYPE]**, **[COORDS]** are instantiated for each query as follows:

QueryID	[TYPE]	[COORDS]
LGD.SL1	police	-2.5, 52.5
LGD.SL2	bus_stop	-5, 55
LGD.SL3*	park	-2.5, 52.5
LGD.LS1	pub	-2.5, 47.5
LGD.LS2	bus_stop	-7.5, 47.5
LGD.LS3*	road	-7.5, 47.5
LGD.SS1	restaurant	-2.5, 47.5
LGD.SS2*	park	-2.5, 47.5
LGD.SS3*	road	-2.5, 47.5
LGD.LL1	bus_stop	-2.5, 57.5

The spatial kNN queries for YAGO, where $k \in \{5, 10, 20, 50, 100\}$, are given in Table 8.4:

Table 8.4: Spatial kNN queries for YAGO.

YAGO.SL1*	**YAGO.SL2***
Select $?gn$ $?fn$ $?pr$ Where $?p$ hasGivenName $?gn$. $?p$ hasFamilyName $?fn$. $?p$ hasWonPrize $?pr$. $?p$ diedIn $?c$. $?c$ hasGeometry $?g$. Filter kNN($?g$, "POINT(-90, 30)", k)	Select $?gn$ $?fn$ Where $?p$ hasGivenName $?gn$. $?p$ hasFamilyName $?fn$. $?p$ a Wordnet_scientist_110560637 . $?p$ wasBornIn $?c$. $?c$ hasGeometry $?g$. Filter kNN($?g$, "POINT(-92.5, 42.5)", k)
YAGO.LS1*	**YAGO.LS2***
Select $?p$ $?w$ Where $?p$ hasAcademicAdvisor $?a$. $?a$ worksAt $?w$. $?w$ isLocatedIn $?l$. $?l$ hasGeometry $?g$. Filter kNN($?g$, "POINT(-155, -45)", k)	Select $?e$ $?c$ Where $?e$ happenedIn $?l$. $?l$ a $?c$. $?c$ subClassOf Wordnet_city_108524735 . $?l$ hasGeometry $?g$. Filter kNN($?g$, "POINT(-125, 45)", k)
YAGO.SS1*	**YAGO.SS2***
Select $?gn$ $?fn$ Where $?p$ hasGivenName $?gn$. $?p$ hasFamilyName $?fn$. $?p$ a Wordnet_scientist_110560637 . $?p$ wasBornIn $?c$. $?c$ hasGeometry $?g$. Filter kNN($?g$, "POINT(-102.5, 47.5)", k)	Select $?p$ $?w$ Where $?p$ graduatedFrom $?u$. $?p$ worksAt $?w$. $?u$ isLocatedIn $?l$. $?l$ hasGeometry $?g$. Filter kNN($?g$, "POINT(-105, 55)", k)
YAGO.LL1*	**YAGO.LL2***
Select $?e$ $?c$ Where $?e$ happenedIn $?l$. $?l$ a $?c$. $?c$ subClassOf Wordnet_city_108524735 . $?l$ hasGeometry $?g$. Filter kNN($?g$, "POINT(-85, 35)", k)	Select $?p$ Where $?p$ hasArea $?a$. $?p$ isLocatedIn $?l$. $?l$ hasGeometry $?g$. Filter kNN($?g$, "POINT(-95, 35)", k)

8.2.4 Spatial kNN queries for Virtuoso

Virtuoso `7.2.5-rc1.3217-pthreads` does not support nearest neighbor queries per se, yet, some of these queries can be expressed using a combination of distance filters and ordering. The spatial kNN queries we used for Virtuoso involve only point queries as other geometries are not supported by the distance function in this version of the system. In Virtuoso's query language these queries for LGD follow the template:

Select $?s$ DISTANCE($?g$, "POINT(**[COORDS]**)")
Where $?s$ name $?n$. $?s$ label $?l$.
$?s$ type **[TYPE]** . $?s$ hasGeometry $?g$.

Filter WITHIN(?g, "POINT(**[COORDS]**)", **[RANGE]**)
Order By ASC 2
Limit k

where $k \in \{5, 10, 20, 50, 100\}$, and **[TYPE]**, **[COORDS]** are instantiated for each query as in Section 8.2.3 of this chapter. **[RANGE]** is measured in kilometers and is the minimum distance so that each query returns 100 results. **[RANGE]** is set for each query as follows:

QueryID	[RANGE]
LGD.SL1	110
LGD.SL2	20
LGD.LS1	170
LGD.LS2	190
LGD.SS1	180
LGD.LL1	80

8.2.5 Spatial kNN queries for GraphDB and Strabon

Similarly to Virtuoso, GraphDB `Free 8.6` and Strabon `3.3.2` do not support nearest neighbor queries per se, however, both systems can express them using a combination of distance filters and ordering. The spatial kNN queries for LGD in GraphDB's and Strabon's query language follow the same template:

Select ?s
Where ?s name ?n . ?s label ?l .
?s type **[TYPE]** . ?s hasGeometry ?g .
Order By ASC
DISTANCE(?g, "POINT(**[COORDS]**)")
Limit k

where $k \in \{5, 10, 20, 50, 100\}$, and **[TYPE]**, **[COORDS]** are instantiated for each query as in Section 8.2.3 of this chapter.

The spatial kNN queries for YAGO in GraphDB's query language are given in Table 8.5 with $k \in \{5, 10, 20, 50, 100\}$:

8.3 Deltas between different dataset versions

Here, we provide the exact differences (in number of triples) between versions:

1. `2013_04_29` and `2015_11_02` of LGD, as retrieved from https://tinyurl.com/ydbscsxf.

Table 8.5: Spatial kNN queries for YAGO in GraphDB.

YAGO.SL1*	**YAGO.SL2***
Select $?gn$ $?fn$ $?pr$ Where $?p$ hasGivenName $?gn$. $?p$ hasFamilyName $?fn$. $?p$ hasWonPrize $?pr$. $?p$ diedIn $?c$. $?c$ hasGeometry $?g$. Order By ASC DISTANCE($?g$, "POINT(-90, 30)") Limit k	Select $?gn$ $?fn$ Where $?p$ hasGivenName $?gn$. $?p$ hasFamilyName $?fn$. $?p$ a Wordnet_scientist_110560637 . $?p$ wasBornIn $?c$. $?c$ hasGeometry $?g$. Order By ASC DISTANCE($?g$, "POINT(-92.5, 42.5)") Limit k
YAGO.LS1*	**YAGO.LS2***
Select $?p$ $?w$ Where $?p$ hasAcademicAdvisor $?a$. $?a$ worksAt $?w$. $?w$ isLocatedIn $?l$. $?l$ hasGeometry $?g$. Order By ASC DISTANCE($?g$, "POINT(-155, -45)") Limit k	Select $?e$ $?c$ Where $?e$ happenedIn $?l$. $?l$ a $?c$. $?c$ subClassOf Wordnet_city_108524735 . $?l$ hasGeometry $?g$. Order By ASC DISTANCE($?g$, "POINT(-125, 45)") Limit k
YAGO.SS1*	**YAGO.SS2***
Select $?gn$ $?fn$ Where $?p$ hasGivenName $?gn$. $?p$ hasFamilyName $?fn$. $?p$ a Wordnet_scientist_110560637 . $?p$ wasBornIn $?c$. $?c$ hasGeometry $?g$. Order By ASC DISTANCE($?g$, "POINT(-102.5, 47.5)") Limit k	Select $?p$ $?w$ Where $?p$ graduatedFrom $?u$. $?p$ worksAt $?w$. $?u$ isLocatedIn $?l$. $?l$ hasGeometry $?g$. Order By ASC DISTANCE($?g$, "POINT(-105, 55)") Limit k
YAGO.LL1*	**YAGO.LL2***
Select $?e$ $?c$ Where $?e$ happenedIn $?l$. $?l$ a $?c$. $?c$ subClassOf Wordnet_city_108524735 . $?l$ hasGeometry $?g$. Order By ASC DISTANCE($?g$, "POINT(-85, 35)") Limit k	Select $?p$ Where $?p$ hasArea $?a$. $?p$ isLocatedIn $?l$. $?l$ hasGeometry $?g$. Order By ASC DISTANCE($?g$, "POINT(-95, 35)") Limit k

2. `2.5.3` and `3.0.2` of YAGO, as retrieved from https://tinyurl.com/y7ukhge3.

which we used to generate the update workloads of Section 3.8.4 of this chapter. The workloads can be found at: https://web.imsi.athenarc.gr/SRX.

Table 8.6: Deltas between LGD versions `2013_04_29` (14.7GB) and `2015_11_02` (21.6GB) used for the update benchmark.

Category	Deleted triples		Updated triples		Inserted triples	
	HasGeometry	**Other**	**HasGeometry**	**Other**	**HasGeometry**	**Other**
AerialwayThing_Nodes	2,265	19,761	12,640	61,878	22,799	198,796
AerialwayThing_Ways	1,126	15,329	9,419	38,345	9,486	94,979
AerowayThing_Nodes	7,860	95,947	7,366	53,177	18,488	174,201
AerowayThing_Ways	7,972	84,099	41,772	131,235	87,970	816,948
Amenity_Nodes	411,396	4,694,204	383,260	3,126,323	1,958,451	20,917,360
Amenity_Ways	168,547	2,381,609	465,889	1,913,576	1,705,501	19,771,641
Craft_Nodes	571	8,322	831	6,477	19,720	220,220
Craft_Ways	333	8,973	1,070	5,709	9,483	134,084
EmergencyThing_Nodes	4,996	107,124	9,631	197,532	369,059	4,031,998
EmergencyThing_Ways	3,002	62,098	9,412	42,782	26,342	442,821
HistoricThing_Nodes	11,783	241,258	20,013	191,571	170,642	1,459,176
HistoricThing_Ways	5,703	98,317	16,870	94,209	89,578	1,211,885
MilitaryThing_Nodes	472	5,968	583	6,345	11,282	147,547
MilitaryThing_Ways	732	12,412	2,155	9,376	10,062	122,245
Place_Nodes	72,941	10,117,063	183,472	5,211,302	930,603	10,494,621
Place_Ways	21,435	337,257	67,907	433,830	169,437	1,932,685
Shop_Nodes	79,362	948,495	115,006	999,194	678,149	7,271,373
Shop_Ways	21,683	1,300,070	59,325	205,847	242,059	906,075
TourismThing_Nodes	47,322	523,433	62,653	466,938	375,669	4,065,277
TourismThing_Ways	14,438	238,691	35,340	178,622	121,136	1,741,557
Total	**883,939**	**21,300,430**	**1,504,614**	**13,374,268**	**7,025,916**	**76,155,489**

Table 8.7: Deltas between YAGO versions `2.5.3` (18.1GB) and `3.0.2` (33.4GB) used for the update benchmark.

Category	Deleted triples		Updated triples		Inserted triples	
	HasGeometry	**Other**	**HasGeometry**	**Other**	**HasGeometry**	**Other**
yagoDBpediaClasses	0	381,887	0	0	0	500,640
yagoDBpediaInstances	0	85,949	0	0	0	2,637,748
yagoFacts	0	1,198,399	0	325	0	2,379,436
yagoGeonamesClasses	0	585	0	0	0	586
yagoGeonamesClassIds	0	0	0	0	0	1
yagoGeonamesData	473,999	6,661,873	1,693,055	0	2,973,857	21,919,394
yagoGeonamesEntityIds	0	106,133	0	0	0	117,579
yagoGeonamesGlosses	0	0	0	0	0	1
yagoImportantTypes	0	2,723,628	0	0	0	0
yagoLabels	0	6,941,073	0	1,601,561	0	36,642,854
yagoLiteralFacts	0	2,533,216	0	650	0	1,584,304
yagoMetaFacts	0	820,616	0	0	0	2,295,716
yagoMultilingualClassLabels	0	0	0	0	0	1
yagoMultilingualInstanceLabels	0	8,164,316	0	0	0	0
yagoSchema	0	10	0	24	0	133
yagoSimpleTaxonomy	0	5,670	0	0	0	474,817
yagoSimpleTypes	0	4,334,474	0	0	0	15,824,332
yagoSources	0	61,838,095	0	0	0	190,482,753
yagoStatistics	0	7	0	88	0	5
yagoTaxonomy	0	381,893	0	0	0	500,645
yagoTransitiveType	0	11,145,280	0	0	0	45,085,647
yagoTypes	0	8,274,938	0	0	0	16,182,189
yagoWikipediaInfo	0	16,347,220	0	0	0	36,167,000
yagoWordnetDomains	0	172	0	0	0	1
yagoWordnetIds	0	0	0	0	0	1
Total	**473,999**	**131,945,434**	**1,693,055**	**1,602,648**	**2,973,857**	**372,795,783**

Columns "HasGeometry" in Tables 8.6 and 8.7 show the numbers of $\langle s, p, o \rangle$ triples where p = "hasGeometry". These triples contain entity geometries as objects. The respective numbers for the rest of the triples are given in columns "Other".

For the update experiments with Strabon, which we present in Figure 3.11 of chapter, we created two different subsets of LGD (`2013_04_29`) that we used in Table 8.6. The first one corresponds to the initial base of Figure 3.11a, while the second is a superset of the first and corresponds to the initial base of Figure 3.11b.

To form the initial base **(a)** in Figure 3.11a, we initially took the first 250 point (*Nodes*) and 250 linestring (*Ways*) 'HasGeometry' triples, including all their related 'Other' triples, from each of the deleted, updated, and inserted LGD deltas in Table 8.6. These are the `deltas_a` to apply on base **(a)** in Figure 3.11a. Then, we kept from the initial version of LGD (`2013_04_29`) only the triples related to any spatial entities found in `deltas_a`, and we formed the base **(a)** that contains 10K triples.

The initial base **(b)** in Figure 3.11b contains 100K triples, and is created similarly. In this case, we picked the first 2500 point (*Nodes*) and 2500 linestring (*Ways*) 'HasGeometry' triples, including all their related 'Other' triples, from each of the LGD deltas.

Bibliography

[ABBBY14] C. Aslay, N. Barbieri, F. Bonchi, and R. A. Baeza-Yates. Online topic-aware influence maximization queries. In *EDBT*, pages 295–306, 2014.

[ACZH10] Medha Atre, Vineet Chaoji, Mohammed J. Zaki, and James A. Hendler. Matrix "Bit" loaded: A scalable lightweight join query processor for RDF data. In *WWW*, 2010.

[AGR17] Akhil Arora, Sainyam Galhotra, and Sayan Ranu. Debunking the myths of influence maximization: An in-depth benchmarking study. In *SIGMOD*, pages 651–666, 2017.

[ALB+15] C. Aslay, W. Lu, F. Bonchi, A. Goyal, and Laks V.S. Lakshmanan. Viral marketing meets social advertising: Ad allocation with minimum regret. *Proc. VLDB Endow.*, 8(7):814–825, 2015.

[AMMH07] Daniel J. Abadi, Adam Marcus, Samuel Madden, and Katherine J. Hollenbach. Scalable semantic web data management using vertical partitioning. In *VLDB*, 2007.

[AMS09] S. Aral, L. Muchnik, and A. Sundararajan. Distinguishing influence-based contagion from homophily-driven diffusion in dynamic networks. *Proc. of the National Academy of Sciences of the U.S.A.*, 106(51):21544–21549, 2009.

[Ara11] S. Aral. Commentaty-Identifying social influence: A comment on opinion leadership and social contagion in new product diffusion. *Marketing Science*, 30(2):217–223, 2011.

[ATOR] Christopher R. Aberger, Susan Tu, Kunle Olukotun, and Christopher Ré. Old techniques for new join algorithms: A case study in RDF processing. In *ICDE Workshops, 2016*.

[ATOR16] Christopher R. Aberger, Susan Tu, Kunle Olukotun, and Christopher Ré. Emptyheaded: A relational engine for graph processing. In *SIGMOD*, 2016.

[AW11] S. Aral and D. Walker. Creating social contagion through viral product design: A randomized trial of peer influence in networks. *Management Science*, 57(9):1623–1639, 2011.

[BAA11] Ceren Budak, Divyakant Agrawal, and Amr El Abbadi. Limiting the spread of misinformation in social networks. In *WWW*, pages 665–674, 2011.

[BB14] N. Barbieri and F. Bonchi. Influence maximization with viral product design. In *SDM*, 2014.

[BBCL14] C. Borgs, M. Brautbar, J. T. Chayes, and B. Lucier. Maximizing social influence in nearly optimal time. In *SODA*, pages 946–957, 2014.

[BBM12] N. Barbieri, F. Bonchi, and G. Manco. Topic-aware social influence propagation models. In *ICDM*, pages 81–90, 2012.

[BDK+13] Mihaela A. Bornea, Julian Dolby, Anastasios Kementsietsidis, Kavitha Srinivas, Patrick Dantressangle, Octavian Udrea, and Bishwaranjan Bhattacharjee. Building an efficient RDF store over a relational database. In *SIGMOD*, 2013.

[BH05] J. A. Berger and C. Heath. Idea Habitats: How the prevalence of environmental cues influences the success of ideas. *Cognitive Science*, 29(2):195–221, 2005.

[BK12] R. Battle and Dave Kolas. Enabling the geospatial semantic web with parliament and geosparql. *Semantic Web*, 3(4):355–370, 2012.

[BKS93] Thomas Brinkhoff, Hans-Peter Kriegel, and Bernhard Seeger. Efficient processing of spatial joins using R-trees. In *SIGMOD*, 1993.

[BKvH01] J. Broekstra, A. Kampman, and F. van Harmelen. Sesame: An architecture for storing and querying RDF data and schema information. In *Semantics for the WWW*. MIT Press, 2001.

[BNM10] Andreas Brodt, Daniela Nicklas, and Bernhard Mitschang. Deep integration of spatial query processing into native RDF triple stores. In *GIS*, 2010.

[CDES05] Eugene Inseok Chong, Souripriya Das, George Eadon, and Jagannathan Srinivasan. An efficient SQL-based RDF querying scheme. In *VLDB*, 2005.

[CFL+15] S. Chen, J. Fan, G. Li, J. Feng, K.-L. Tan, and J. Tang. Online topic-aware influence maximization. *Proc. VLDB Endow.*, 8(6):666–677, 2015.

[CK13] Yuxin Chen and Andreas Krause. Near-optimal batch mode active learning and adaptive submodular optimization. In *ICML*, pages 160–168, 2013.

[CLC13] Wei Chen, Laks V. S. Lakshmanan, and Carlos Castillo. *Information and Influence Propagation in Social Networks*. Morgan & Claypool Publishers, 2013.

[CLY14] W. Chen, T. Lin, and C. Yang. Efficient topic-aware influence maximization using preprocessing. *CoRR*, abs/1403.0057, 2014.

[CM13] I. P. Cvijikj and F. Michahelles. Online engagement factors on facebook brand pages. *Social Network Analysis and Mining*, 3(4):843–861, 2013.

[CMdR15] Aleksandr Chuklin, Ilya Markov, and Maarten de Rijke. *Click Models for Web Search*. Morgan and Claypool Publishers, 2015.

[CMPL15] Richard Combes, Stefan Magureanu, Alexandre Proutiére, and Cyrille Laroche. Learning to rank: Regret lower bounds and efficient algorithms. In *SIGMETRICS*, pages 231–244, 2015.

[CPL12] Y. -C. Chen, W. -C. Peng, and S. -Y. Lee. Efficient algorithms for influence maximization in social networks. *Knowl. Inf. Syst.*, 33(3):577–601, 2012.

[CSH+14] S. Cheng, H. Shen, J. Huang, W. Chen, and X. Cheng. IMRank: influence maximization via finding self-consistent ranking. In *SIGIR*, pages 475–484, 2014.

[CWW10] W. Chen, C. Wang, and Y. Wang. Scalable influence maximization for prevalent viral marketing in large-scale social networks. In *KDD*, pages 1029–1038, 2010.

[CWY13] Wei Chen, Yajun Wang, and Yang Yuan. Combinatorial multi-armed bandit: General framework, results and applications. In *ICML*, pages 151–159, 2013.

[CWYW16] Wei Chen, Yajun Wang, Yang Yuan, and Qinshi Wang. Combinatorial multi-armed bandit and its extension to probabilistically triggered arms. *JMLR*, 17(1):1746–1778, 2016.

[CYZ10] W. Chen, Y. Yuan, and L. Zhang. Scalable influence maximization in social networks under the linear threshold model. In *ICDM*, pages 88–97, 2010.

[CZTR08] Nick Craswell, Onno Zoeter, Michael Taylor, and Bill Ramsey. An experimental comparison of click position-bias models. In *WSDM*, pages 87–94, 2008.

[dBL01] C. Van den Bulte and G. L. Lilien. Medical innovation revisited: Social contagion versus marketing effort. *Am. J. Sociol.*, 106(5):1409–1435, 2001.

[DJK11] Balázs Dezső, Alpár Jüttner, and Péter Kovács. Lemon – an open source c++ graph template library. *ENTCS*, 264(5):23–45, 2011.

[DR01] P. Domingos and M. Richardson. Mining the network value of customers. In *KDD*, pages 57–66, 2001.

[dVGL12] L. de Vries, S. Gensler, and Peter S.H. Leeflang. Popularity of brand posts on brand fan pages: An investigation of the effects of social media marketing. *Journal of Interactive Marketing*, 26(2):83–91, 2012.

[EM16] Ahmed Eldawy and Mohamed F. Mokbel. The era of big spatial data: A survey. *Foundations and Trends in Databases*, 6(3-4):163–273, 2016.

[GBL11] A. Goyal, F. Bonchi, and L. V. S. Lakshmanan. A data-based approach to social influence maximization. *PVLDB*, 5(1):73–84, 2011.

[GCM+15] Artem Grotov, Aleksandr Chuklin, Ilya Markov, Luka Stout, Finde Xumara, and Maarten de Rijke. A comparative study of click models for web search. In *CLEF*, pages 78–90, 2015.

[GK11] Daniel Golovin and Andreas Krause. Adaptive submodularity: Theory and applications in active learning and stochastic optimization. *JAIR*, 42(1):427–486, 2011.

[GM04] D. Godes and D. Mayzlin. Using online conversations to study word-of-mouth communication. *Marketing Science*, 23(4):545–560, 2004.

[Gra] GraphDB. http://graphdb.ontotext.com.

[Gut84] Antonin Guttman. R-trees: A dynamic index structure for spatial searching. In *SIGMOD*, 1984.

[GZZ+13] Jing Guo, Peng Zhang, Chuan Zhou, Yanan Cao, and Li Guo. Personalized influence maximization on social networks. In *CIKM*, pages 199–208, 2013.

[HD10] L. Hong and B. D. Davison. Empirical study of topic modeling in twitter. In *SOMA*, pages 80–88, 2010.

[HHT05] Marios Hadjieleftheriou, Erik G. Hoel, and Vassilis J. Tsotras. Sail: A spatial index library for efficient application integration. *GeoInformatica*, 9(4):367–389, 2005.

[HS15] Thibaut Horel and Yaron Singer. Scalable methods for adaptively seeding a social network. In *WWW*, pages 441–451, 2015.

[HSCJ12] Xinran He, Guojie Song, Wei Chen, and Qingye Jiang. Influence blocking maximization in social networks under the competitive linear threshold model. In *SDM*, pages 463–474, 2012.

[HTH+20] Keke Huang, Jing Tang, Kai Han, Xiaokui Xiao, Wei Chen, Aixin Sun, Xueyan Tang, and Andrew Lim. Efficient approximation algorithms for adaptive influence maximization. *VLDBJ*, 29(6):1385–1406, 2020.

[ITTK17] Sergei Ivanov, Konstantinos Theocharidis, Manolis Terrovitis, and Panagiotis Karras. Content recommendation for viral social influence. In *SIGIR*, pages 565–574, 2017.

[Kat59] E. Katz. Mass communications research and the study of popular culture: An editorial note on a possible future of this journal. *Studies in Public Communication*, 2:1–6, 1959.

[KK10] Manolis Koubarakis and Kostis Kyzirakos. Modeling and querying metadata in the semantic sensor web: The model stRDF and the query language stSPARQL. In *ESWC*, 2010.

[KKK12] Kostis Kyzirakos, Manos Karpathiotakis, and Manolis Koubarakis. Strabon: A semantic geospatial DBMS. In *ISWC*, 2012.

[KKSW16] Sumeet Katariya, Branislav Kveton, Csaba Szepesvári, and Zheng Wen. DCM bandits: Learning to rank with multiple clicks. In *ICML*, pages 1215–1224, 2016.

[KKT03] D. Kempe, J. Kleinberg, and E. Tardos. Maximizing the spread of influence through a social network. In *KDD*, 2003.

[KLK20] Ansh Khurana, Alvis Logins, and Panagiotis Karras. Selecting influential features by a learnable content-aware linear threshold model. In *CIKM*, page 635–644, 2020.

[KN11] Brian Karrer and M. E. J. Newman. Stochastic blockmodels and community structure in networks. *Phys. Rev. E*, 83:016107, Jan 2011.

[KSWA15] Branislav Kveton, Csaba Szepesvári, Zheng Wen, and Azin Ashkan. Cascading bandits: Learning to rank in the cascade model. In *ICML*, pages 767–776, 2015.

[KWAS15] Branislav Kveton, Zheng Wen, Azin Ashkan, and Csaba Szepesvári. Combinatorial cascading bandits. In *NeurIPS*, pages 1450–1458, 2015.

[LCCM19] Paul Lagrée, Olivier Cappé, Bogdan Cautis, and Silviu Maniu. Algorithms for online influencer marketing. *TKDD*, 13(1):1–30, 2019.

[LCXZ12] Bo Liu, Gao Cong, Dong Xu, and Yifeng Zeng. Time constrained influence maximization in social networks. In *ICDM*, pages 439–448, 2012.

[LFWT18] Yuchen Li, Ju Fan, Yanhao Wang, and Kian-Lee Tan. Influence maximization on social graphs: A survey. *TKDE*, 30(10):1852–1872, 2018.

[LGD] Linkedgeodata. http://linkedgeodata.org/About.

[LKG+07] J. Leskovec, A. Krause, C. Guestrin, C. Faloutsos, J. M. VanBriesen, and N. S. Glance. Cost-effective outbreak detection in networks. In *KDD*, pages 420–429, 2007.

[LKLS18] Tor Lattimore, Branislav Kveton, Shuai Li, and Csaba Szepesvári. TopRank: A practical algorithm for online stochastic ranking. In *NeurIPS*, pages 3949–3958, 2018.

[LLS19] Shuai Li, Tor Lattimore, and Csaba Szepesvári. Online learning to rank with features. In *ICML*, pages 3856–3865, 2019.

[LMBT14] John Liagouris, Nikos Mamoulis, Panagiotis Bouros, and Manolis Terrovitis. An effective encoding scheme for spatial RDF data. *Proc. VLDB Endow.*, 7(12):1271–1282, 2014.

[LMM+15] Siyu Lei, Silviu Maniu, Luyi Mo, Reynold Cheng, and Pierre Senellart. Online influence maximization. In *KDD*, pages 645–654, 2015.

[LR96] Ming-Ling Lo and Chinya V. Ravishankar. Spatial hash-joins. In *SIGMOD*, 1996.

[LVC16] Paul Lagrée, Claire Vernade, and Olivier Cappé. Multiple-play bandits in the position-based model. In *NeurIPS*, pages 1605–1613, 2016.

[LWZC16] Shuai Li, Baoxiang Wang, Shengyu Zhang, and Wei Chen. Contextual combinatorial cascading bandits. In *ICML*, pages 1245–1253, 2016.

[LZT15] Y. Li, D. Zhang, and K.-L. Tan. Real-time targeted influence maximization for online advertisements. *Proc. VLDB Endow.*, 8(10):1070–1081, 2015.

[Mam11] Nikos Mamoulis. *Spatial Data Management*. Morgan & Claypool Publishers, 2011.

[Man93] C. F. Manski. Identification of endogenous social effects: The reflection problem. *The Review of Economic Studies*, 60(3):531–542, 1993.

[MHP05] Kyriakos Mouratidis, Marios Hadjieleftheriou, and Dimitris Papadias. Conceptual partitioning: An efficient method for continuous nearest neighbor monitoring. In *SIGMOD*, 2005.

[MP03] Nikos Mamoulis and Dimitris Papadias. Slot index spatial join. *TKDE*, 15(1):211–231, 2003.

[NDT16] Hung T. Nguyen, Thang N. Dinh, and My T. Thai±. Cost-aware targeted viral marketing in billion-scale networks. In *IEEE International Conference on Computer Communications*, pages 1–9, 2016.

[NM11] Thomas Neumann and Guido Moerkotte. Characteristic sets: Accurate cardinality estimation for RDF queries with multiple joins. In *ICDE*, 2011.

[NVDV18] Panagiotis Nikitopoulos, Akrivi Vlachou, Christos Doulkeridis, and George A. Vouros. DiStRDF: Distributed spatio-temporal RDF queries on Spark. In *EDBT/ICDT*, 2018.

[NW08] Thomas Neumann and Gerhard Weikum. RDF-3X: A RISC-style engine for RDF. *Proc. VLDB Endow.*, 1(1):647–659, 2008.

[NW09] Thomas Neumann and Gerhard Weikum. Scalable join processing on very large RDF graphs. In *SIGMOD*, 2009.

[NW10a] Thomas Neumann and Gerhard Weikum. The RDF-3X engine for scalable management of RDF data. *VLDB J.*, 19(1):91–113, 2010.

[NW10b] Thomas Neumann and Gerhard Weikum. x-RDF-3X: Fast querying, high update rates, and consistency for RDF databases. *Proc. VLDB Endow.*, 3(1-2):256–263, 2010.

[Ö16] M. Tamer Özsu. A survey of RDF data management systems. *Front. Comput. Sci.*, 10(3):418–432, 2016.

[Par] Parliament. http://parliament.semwebcentral.org.

[Pei15] Tiago P. Peixoto. Model selection and hypothesis testing for large-scale network models with overlapping groups. *Phys. Rev. X*, 5, 2015.

[PGA14] Kostas Patroumpas, Giorgos Giannopoulos, and Spiros Athanasiou. Towards geospatial semantic data management: Strengths, weaknesses, and challenges ahead. In *GIS*, 2014.

[PKNK18] Varun Pandey, Andreas Kipf, Thomas Neumann, and Alfons Kemper. How good are modern spatial analytics systems? *Proc. VLDB Endow.*, 11(11):1661–1673, 2018.

[RD02] M. Richardson and P. Domingos. Mining knowledge-sharing sites for viral marketing. In *KDD*, pages 61–70, 2002.

[RDR07] Matthew Richardson, Ewa Dominowska, and Robert Ragno. Predicting clicks: Estimating the click-through rate for new ads. In *WWW*, pages 521–530, 2007.

[SHYC18] Lichao Sun, Weiran Huang, Philip S. Yu, and Wei Chen. Multi-round influence maximization. In *KDD*, pages 2249–2258, 2018.

[SS13] Lior Seeman and Yaron Singer. Adaptive seeding in social networks. In *FOCS*, pages 459–468, 2013.

[TWTD17] Guangmo Tong, Weili Wu, Shaojie Tang, and Ding-Zhu Du. Adaptive influence maximization in dynamic social networks. *IEEE/ACM Transactions on Networking*, 25(1):112–125, 2017.

[TXS14] Y. Tang, X. Xiao, and Y. Shi. Influence maximization: near-optimal time complexity meets practical efficiency. In *SIGMOD*, pages 75–86, 2014.

[Vir] Virtuoso. http://virtuoso.openlinksw.com.

[VKW+17] Sharan Vaswani, Branislav Kveton, Zheng Wen, Mohammad Ghavamzadeh, Laks V.S. Lakshmanan, and Mark Schmidt. Model-independent online learning for influence maximization. In *ICML*, pages 3530–3539, 2017.

[VLS16] Sharan Vaswani, Laks V.S. Lakshmanan, and Mark Schmidt. Influence maximization with bandits, 2016.

[WFLT17] Yanhao Wang, Qi Fan, Yuchen Li, and Kian-Lee Tan. Real-time influence maximization on dynamic social streams. *PVLDB*, 10(7):805–816, 2017.

[WKB08] Cathrin Weiss, Panagiotis Karras, and Abraham Bernstein. Hexastore: Sextuple indexing for semantic web data management. *Proc. VLDB Endow.*, 1(1):1008–1019, 2008.

[WKC12] Chih-Jye Wang, Wei-Shinn Ku, and Haiquan Chen. Geo-store: A spatially-augmented sparql query evaluation system. In *GIS*, 2012.

[WKVV17] Zheng Wen, Branislav Kveton, Michal Valko, and Sharan Vaswani. Online influence maximization under independent cascade model with semi-bandit feedback. In *NeurIPS*, pages 1–24, 2017.

[WLW+19] Qingyun Wu, Zhige Li, Huazheng Wang, Wei Chen, and Hongning Wang. Factorization bandits for online influence maximization. In *KDD*, pages 636–646, 2019.

[WSKR03] Kevin Wilkinson, Craig Sayers, Harumi A. Kuno, and Dave Reynolds. Efficient RDF storage and retrieval in Jena2. In *SWDB*, 2003.

[WZF+13] Dong Wang, Lei Zou, Yansong Feng, Xuchuan Shen, Jilei Tian, and Dongyan Zhao. S-store: An engine for large RDF graph integrating spatial information. In *DASFAA*, 2013.

[YAG] YAGO. https://en.wikipedia.org/wiki/YAGO_(database).

[YLL12] Mao Ye, Xingjie Liu, and Wang-Chien Lee. Exploring social influence for recommendation: A generative model approach. In *SIGIR*, pages 671–680, 2012.

[YLW+13] Pingpeng Yuan, Pu Liu, Buwen Wu, Hai Jin, Wenya Zhang, and Ling Liu. TripleBit: A fast and compact system for large scale RDF data. *Proc. VLDB Endow.*, 6(7):517–528, 2013.

[YT17] Jing Yuan and Shaojie Tang. No time to observe: Adaptive influence maximization with partial feedback. In *IJCAI*, page 3908–3914, 2017.

[YWZ+09] Ying Yan, Chen Wang, Aoying Zhou, Weining Qian, Li Ma, and Yue Pan. Efficient indices using graph partitioning in RDF triple stores. In *ICDE*, 2009.

[ZMC+11] Lei Zou, Jinghui Mo, Lei Chen, M. Tamer Özsu, and Dongyan Zhao. gStore: Answering SPARQL queries via subgraph matching. *Proc. VLDB Endow.*, 4(8):482–493, 2011.

[ZNS+16] Shi Zong, Hao Ni, Kenny Sung, Nan Rosemary Ke, Zheng Wen, and Branislav Kveton. Cascading bandits for large-scale recommendation problems. In *UAI*, pages 835–844, 2016.

[ZTG+17] Masrour Zoghi, Tomas Tunys, Mohammad Ghavamzadeh, Branislav Kveton, Csaba Szepesvári, and Zheng Wen. Online learning to rank in stochastic click models. In *ICML*, pages 4199–4208, 2017.

[ZYW+13] Kai Zeng, Jiacheng Yang, Haixun Wang, Bin Shao, and Zhongyuan Wang. A distributed graph engine for web scale RDF data. *Proc. VLDB Endow.*, 6(4):265–276, 2013.